

MODELLING OF REINFORCED CONCRETE IN THE SERVICEABILITY LIMIT STATE

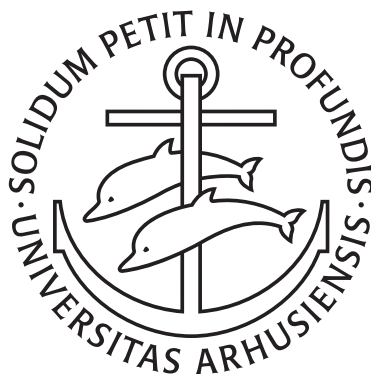
A STUDY OF CRACKING, STIFFNESS AND DEFLECTION IN FLEXURAL MEMBERS

PH.D. THESIS

ANNETTE BEEDHOLM RASMUSSEN

SUPERVISOR

LARS GERMAN HAGSTEN



AARHUS UNIVERSITY
DEPARTMENT OF ENGINEERING

APRIL 2019

ISBN: 978-87-7507-452-5
DOI: 10.7146/aui.329.223

ABSTRACT

The objective of the present thesis is to advance the understanding of the behaviour related to cracking in reinforced concrete, as well as improve modelling of flexural members in the serviceability limit state. This should create a stronger connection between modelling of the two limit states of design, and lead to better utilisation of both concrete and reinforcement.

One of the main issues within the subject of reinforced concrete in the serviceability limit state, addressed in this thesis, is that focus has for many years primarily been on investigations concerning the ultimate limit state. Research within the serviceability limit state thus lags behind, where models lack physical transparency and are merely conservative estimates. Furthermore, the different aspects of the serviceability limit state, namely the estimation of crack widths, stiffness, and deformation are not coherently modelled with a general way of interpreting the physical behaviour. This particularly concerns the effect of tension-stiffening on the flexural stiffness, which is addressed empirically or sometimes even ignored.

The thesis proposes an approach to evaluate all the important aspects of the serviceability limit state which was developed from one requirement; that both crack widths, flexural stiffness, and deflection, can be estimated from coherent physical considerations of how flexural members behave, analogue to the models for designing reinforced concrete in the ultimate limit state. This requirement resulted in an approach based on the knowledge of one single parameter; the crack spacing. The approach assumes that *all deformation takes place solely in the cracks, which means that crack widths can be estimated from the crack spacing and the mean strain in the reinforcement.*

Since the crack spacing is the foundation of the entire approach, it was considered crucial to gain as much knowledge as possible about this parameter. This is achieved, firstly, through a thorough literature review and, secondly, a comprehensive empirical study of crack spacings in 142 tensile tests and 462 flexural tests from the literature which are treated statistically. To minimise the influence of the randomness associated with cracking in concrete, a large amount of data was required. From the ambition of establishing a database of comparable data and to avoid subjectivity, all crack spacings have been collected in the same manner; by consistently measuring them from photos of the crack patterns.

For regression analysis of the crack spacings, the beams are grouped into two categories; laboratory beams, smaller than 300mm in effective depth, and structural beams, larger than 300mm. From both the empirical study and the results of a series of conducted tests, the two categories are observed to behave differently with respect to the crack patterns and crack spacings. Both categories of beams are analysed with respect to two different types of cracks; the secondary cracks and the primary cracks which individual crack spacings are measured at the level of the reinforcement and at mid-height of the members, respectively. The results of the regression analysis showed that only one type of crack develops in the laboratory beams with a spacing controlled primarily by the bond parameter; ϕ_s/ρ_s . However, a large random scatter is associated with the crack spacing in laboratory beams, whereas the conclusions for the structural beams is much clearer. In these beams, the primary crack spacing is found to be linearly proportional to the effective depth, while the secondary crack spacing showed dependency on both the cover and the ϕ_s/ρ_s -ratio. Nevertheless, these two parameters are found to largely describe the same variation in the crack spacing and their relation is therefore investigated further.

The proposed approach is seen to agree well with the test results of beams subjected to four-point-bending as well as it shows slightly better results than the Eurocode model for predicting deflections. From these positive results of the approach, a potential for future studies is seen in using the same fundamental assumptions for modelling other aspects of the behaviour of reinforced concrete.

RESUME

Målet med denne afhandling er dels at forbedre vores forståelse for armeret betons opførelse under revnedannelse og dels at forbedre modellering af bøjningspåvirkede emner i anvendelsesgrænsetilstanden. Dette skal skabe en stærkere forbindelse mellem modellering af de to forskellige grænsetilstande, og lede til bedre udnyttelse af både beton og armering.

En af udfordringerne ved armeret beton i anvendelsesgrænsetilstanden, som er behandlet i denne afhandling er, at der i mange år hovedsagligt har været fokus på forskning indenfor emner relateret til brudgrænsetilstanden og at forskning indenfor anvendelsesgrænsetilstanden derfor halter bagud. Dette betyder, at modellerne ikke understøtter den fysiske virkemåde og primært kun er konservative overslag. Ydermere er de forskellige aspekter af anvendelsesgrænsetilstanden; revnevidder, stivhed og deformationer, ikke beregnet ud fra en sammenhængende måde at betragte den fysiske virkemåde. Dette vedrører særligt tension-stiffening og dens effekt på bøjningsstivheden, som ofte er behandlet empirisk eller sårar ignoreret.

Denne afhandling præsenterer en model, hvorpå alle de vigtige aspekter af anvendelsesgrænsetilstanden kan evalueres. Modellen er udviklet ud fra én forudsætning, nemlig at både revnevidde, bøjningstivhed og nedbøjning kan beregnes ud fra de samme fysiske betragtninger af bjælkers opførelse, hvilket er analog til de modeller, der repræsenterer brudgrænsetilstanden. Denne forudsætning har resulteret i en model, som er baseret på kendskab til én parameter; revneafstanden. I modellen antages det, at *al deformation sker i revnerne og at revnevidder derfor kan estimeres ud fra kendskab til revneafstanden og middeltøjningen i armeringen.*

Da revneafstanden er fundamental for hele modellen, anses det at være afgørende at vide så meget så mulig om denne parameter. Derfor er revneafstanden undersøgt, først ved hjælp af et grundigt litteraturstudie, og derefter igennem et omfattende empirisk studie af revneafstande fra forsøg af 142 trækpåvirkede emner og 462 bøjningspåvirkede emner, som er fundet i litteraturen og behandlet statistisk. For at minimere indflydelsen af den naturlige variation, der er forbundet med revnedannelse i beton, var det nødvendigt at betragte en stor mængde data. Med hensigten om at etablere en database af sammenlignelige data og at undgå subjektivitet, er alle revneafstande blevet indsamlet på samme måde; ved systematisk at måle dem på billeder af revnemønstrene.

Til brug i en regressionsanalyse af revneafstandene er bjælkerne i databasen opdelt i to kategorier; laboratoriebjælker, med en effektiv højde på mindre end 300mm, og konstruktionsbjælker, større end 300mm. På baggrund af det empiriske studie, samt resultater fra udførte forsøg, er det konkluderet, at de to kategorier af bjælker opfører sig forskelligt med hensyn til revnemønstre og revneafstande. Begge bjælkekategorier er analyseret i forhold til to forskellige revnetyper; sekundære revner og primære revner med hver deres revneafstand målt hhv. i samme niveau som den langsgående armering og midt på bjælakens højde. Regressionsanalysen viser, at der kun dannes en type revner i laboratoriebjælkerne, som primært er styret af bond-parameteren; ϕ_s/ρ_s , men at der også er mange usikkerheder forbundet med disse bjælker. Konklusionerne for konstruktionsbjælker er derimod meget klare, hvor de primære revner udviser lineære proportionalitet med den effektive højde, mens de sekundære revner viser afhængighed af både dæklaget og ϕ_s/ρ_s -forholdet. Disse to parametre viser sig dog også at beskrive næsten den samme variation i revneafstanden, hvorfor deres relation er undersøgt yderligere.

Modellen viser gode resultater ved sammenligning med forsøgsresultater for bjælker påvirket til fire-punkts-bøjning, desuden er dens resultater en smule bedre end Eurocode modellen for beregning af nedbøjningen. På baggrund af disse positive resultater er der set potentiale i at benytte de fundamentale forudsætninger fra modellen til at udvikle modeller til beskrivelse af andre problemstillinger ved armeret beton.

PREFACE AND ACKNOWLEDGEMENTS

The present Ph.D. thesis *Modelling of reinforced concrete in the serviceability limit state - A study of cracking, stiffness and deflection in flexural members* is submitted in partial fulfilment of the requirements for obtaining a Ph.D. degree, during the period May 2014 to April 2019, in the Department of Engineering, Graduate School of Science and Technology, Aarhus University.

Firstly, I would like to express my gratitude to my supervisor Professor Lars German Hagsten for giving me the opportunity to study for my Ph.D. under his supervision. I sincerely thank him for giving highly competent guidance and support throughout my studies and for being dedicated to guiding me both academically and concerning the process.

I would also like to give a special thank to my colleagues. Among them, I would like to mention Associate Professor, Ph.D. Jakob Fisker for always showing interest in my research, for his many suggestions which have kept me on my feet and improved my research a great deal and, lastly, for sharing experiences from his own time as a Ph.D. student. I would also like to acknowledge Ph.D. Lise Kjær Andersen for being a great support as both a fellow student and a friend. Finally, also a thanks to my colleague Christian Svarre for, among other things, supporting me with great Matlab advice.

Next, I wish to express my gratitude to Professor Alejandro Pérez Caldentey for welcoming me as a visiting researcher in the Structural Concrete Laboratory at the Universidad Politécnica de Madrid from October 2018 to December 2018. I give my greatest appreciation to Professor Alejandro Pérez Caldentey for taking the time to discuss cracking in concrete with me and sharing some of his comprehensive knowledge on the subject. In this context, I would also like to thank Leonardo Todisco and Sarah Navarro-Lacroix for making my stay in Madrid enjoyable and for the fun and interesting discussions about structural engineering as well as other serious and less serious matters.

I would also like to thank former Associate Professor, Ph.D. Frede A. Christensen for always showing interest in my research, guiding me while I tackled various different statistical theories, and taking the time to discuss the relevance of my research as well as research in a broader sense.

I also wish to thank my brother Torben for the many like-minded conversations about the matter of being a Ph.D. student but also for the discussions about the statistical treatment of my data and for providing a different perspective on my research from the eyes a physicist.

Last, but not least, I would like to thank my boyfriend for taking care of me as well as my parents, my sister, my brother and all of my dear friends for having supported me unconditionally, cheering endlessly and for accepting my absence during the final time.

Annette Beedholm Rasmussen

Aarhus University, April 2019

Contents

1	Introduction	1
1.1	Subject of research	1
1.2	Initial hypothesis	3
1.3	Objective and limitations	5
1.4	Reading guide	7
2	Literature review	9
2.1	Plain concrete in tension	9
2.1.1	Studies of stress-strain behaviour	9
2.1.2	Modelling plain concrete in tension	13
2.1.3	Strength determination	14
2.2	Cracking in uni-axial tensile members	17
2.2.1	Studies of tests	17
2.2.2	Modelling of cracking in tensile members	26
2.2.3	Model tendencies	36
2.3	Cracking in flexural members	40
2.3.1	Studies of tests	40
2.3.2	Modelling of cracking in flexural members	64
2.3.3	Model tendencies	69
2.4	Stiffness and deformation of flexural members	73
2.4.1	Modelling the deflection including tension-stiffening	73
3	Experimental investigation of flexural cracking with respect to member depth	75
3.1	Introduction to the test	75
3.2	Results	76
3.2.1	System of cracks	76
3.2.2	Development of crack height	77
3.2.3	Variation of crack width	78
3.2.4	Sum of crack widths	79
4	Empirical study of crack spacings	81
4.1	Introduction	81
4.1.1	Categorisation of beams with respect to dimensions	81
4.1.2	Aim of study	81
4.1.3	Consistent method of collecting crack spacing data	82
4.2	Statistical toolbox	83
4.2.1	Test of normality	83
4.2.2	Correlation	84
4.2.3	Multi-variable linear regression	84
4.3	Tensile members	87
4.3.1	Introduction to the database	87

4.3.2	Analysis of crack spacing	91
4.3.3	Comparison of existing models and tests	98
4.4	Flexural members	102
4.4.1	Introduction to the database	102
4.4.2	Analysis of primary flexural crack spacing	108
4.4.3	Comparison of existing models and tests for the primary crack spacing	123
4.4.4	Analysis of secondary crack spacing	125
4.4.5	Comparison of existing models and tests for the secondary crack spacing	136
4.5	Investigation of stabilised crack systems	141
4.6	Comparison of crack spacings in tensile members and flexural members	142
4.7	Discussion and conclusions	144
4.7.1	Tensile members	144
4.7.2	Flexural members	145
4.7.3	Tension and flexural members	149
5	The approach for estimation of crack widths, stiffness, and deflection in flexural members	151
5.1	Identification of the system of cracks	151
5.2	Distribution of strains in-between cracks	152
5.3	Estimation of crack widths	154
5.4	Estimation of flexural stiffness	155
5.4.1	The effect of tension-stiffening	155
5.4.2	Flexural stiffness	155
5.4.3	Smearred flexural stiffness including tension-stiffening	157
5.5	Deflection analysis on the basis of the flexural stiffness	160
5.6	Analysis of statically indeterminate beams on the basis of the flexural stiffness	161
5.7	Conclusions	163
6	Application of approach	164
6.1	A coherent design of serviceability limit state	164
6.2	Exemplification of approach	166
6.2.1	Essential parameters	166
6.2.2	Crack width	167
6.2.3	Flexural stiffness	167
6.2.4	Deflection	168
6.3	Comparison of test and model	169
6.3.1	Introduction to test	169
6.3.2	Crack spacings	171
6.3.3	Essential parameters	172
6.3.4	Force-deflection response	173
6.3.5	Investigation of the location of maximum crack width	176
6.3.6	Development of crack width with increasing deflection	177
6.3.7	Force-crack width response	178
7	Conclusion	181
7.1	Further application and future studies	186
	References	188

Appendices	197
A Notations	198
B Paper 1: Cracking in flexural reinforced concrete members	204
C Paper 2: Investigation of reinforced concrete beams in serviceability limit state	213
D Paper 3: An experimental study of crack development in flexural reinforced concrete members	222

1 INTRODUCTION

1.1 Subject of research

Modelling of reinforced concrete in the serviceability limit state is first and foremost about ensuring the health and durability of the structure its whole life time. In general, this fact means controlling deformations and limiting crack widths.

It is well-known that the strength of concrete in tension is very limited and the associated failure is brittle. Cracking is, therefore, inherent in most reinforced concrete structures and an important part of the intended behaviour of this composite material. To be able to control the crack development, reinforcement is placed where concrete structures are subjected to tension, thereby, ensuring multiple, distributed and narrow cracks instead of few and wide cracks. Because even though we welcome cracks, there are several reasons to control their development and to keep the width of them restricted. One of the most important reasons is to ensure protection against corrosion of the reinforcement. Keeping the appearance of the structure safe and aesthetic is another reason, yet not structurally performance-based.

Traditionally, when doing a complete design of reinforced concrete structures, the focus often initially lies on the ultimate limit state, ensuring the strength. Hereafter, the serviceability limit state is considered, where requirements concerning crack widths and deformations are to be met. This often leads to modifications in the reinforcement design determined to ensure the strength in the ultimate limit state, which involves an increase in the amount of reinforcement. Part of why it sometimes requires more reinforcement to meet the serviceability requirements is because of the fact, as mentioned earlier, that crack development is highly affected by the arrangement of the reinforcement and the reinforcement is, therefore, the most important component in being able to control cracking. The choices made when first designing the ultimate limit state, thus, have a large effect on the forming cracks and their width in the serviceability limit state. This connection between the two limit states also goes the other way; the structural behaviour in the ultimate limit state is, to a large extent governed by the early crack formation initiated under service loads.

The focus on the ultimate limit state is not only seen in connection with the design procedure of structures but also within the field of research, where, over the past decades, the focus has, for the greater part, been about investigating issues concerning failure. Therefore, research within the serviceability limit state lags behind and, as a consequence, many models are empirical or lack physical transparency resulting in far less accurate models than models for the ultimate limit state. Furthermore, in the most practised methods, the different aspects of the serviceability limit state, namely the estimation of crack widths, stiffness, and deformation, are not coherently designed with respect to a general way of interpreting the physical behaviour under service loads. The models for predicting the various aspects are controlled by different and inconsistent parameters. Moreover, they often represent conservative estimates, where the influence of certain mechanisms is ignored.

Tension-stiffening is a mechanism sometimes ignored with regard to the design of the serviceability limit state, where the intact concrete between adjacent cracks is still able to carry tension. The concrete areas in tension increases the stiffness of the structure compared to the fully cracked stiffness, where it is assumed that the concrete carries no tension at all. The phenomenon is well defined and has been subject to a fair amount of research which investigates the effect of tension-stiffening. However, the models describing the effect do not hold a coherent physical explanation. Neither do they have any connection to models describing cracking even though it is a large part of the phenomenon, because it is the concrete between cracks that adds stiffness to an otherwise fully cracked member.

An examination of tests found in the existing literature shows that investigations addressing the behaviour of reinforced concrete in the serviceability limit state are mainly from members subjected to uni-axial tension, whereas, only a few tests are found which are dedicated to investigating cracking in beams subjected to flexure. This situation means that, while a large number of tests exist that hold useful information about the serviceability limit state, the experimental work originally had another focus.

With respect to the models for designing flexural members in the serviceability limit state, they are often derived from observations of the behaviour of tensile members without being validated against tests of flexural members. Furthermore, existing research regarding the process of cracking and determination of crack spacings and crack widths, in both tensile and flexural members, consists of contradictory explanations and interpretations of which parameters are governing for the cracking behaviour. In broad terms, there are two different approaches with respect to which mechanisms control the spacing between load-induced cracks. The two different and conflicting approaches are termed the no-slip and the bond-slip theories.

On the one hand, the formation of cracks is affected by various parameters that we can control and manipulate, which are related to the reinforcement arrangement, the interaction between concrete and reinforcement, the type of loading, support conditions and the geometry of the structure. On the other hand, a certain level of randomness is also associated with cracking owing to the inhomogeneous nature of concrete as a composite material. Hence, the formation of cracks can be difficult to put in an exact formula because it will always be influenced by factors that are beyond our control which adds a level of uncertainty to our predictions of crack spacings and crack widths. There are also other reasons for large variations in results when dealing with cracks, beside the concrete's inhomogeneity, which, among other things, could be cracking that is not related to the permanent loading situation such as transportation and construction, micro cracking during casting and curing of the concrete owing to temperature differences in the member, or restraint shrinkage-induced cracks.

The above-described issues concerning modelling of reinforced concrete in the serviceability limit state form the basis of the present research and can be summarised through the following four main subjects:

1. The initial focus on the ultimate limit state in terms of the design of structures, instead of a concurrent design of the two limit states, often results in additional reinforcement to meet serviceability limit state requirements.
2. Research within the field of the serviceability limit state, with respect to the estimation of crack widths, stiffness and deformations, lags behind when compared to research on the ultimate limit state.

Firstly, this issue concerns the existing tests addressing these subjects, which mainly consist of members subjected to uni-axial tension, whereas only a few tests are dedicated to investigating the behaviour of flexural members, with respect to cracking and deformation under service loads.

Secondly, the lack of research within these subjects means that the models for predicting crack widths, stiffness, and deformation are often empirical and conservative estimates. Furthermore, the models for flexural members are derived from mechanisms observed to be controlling for the behaviour of uni-axial tensile members without necessarily validating whether the same parameters govern members subjected to flexure.

Thirdly, the phenomenon of tension-stiffening and its effect on the stiffness is disconnected from the other aspects of the serviceability limit state, namely, crack spacings and crack widths, with respect to the physical interpretation of how reinforced concrete behaves under service loads. In addition, most models describing the effect of tension-stiffening lack physical considerations of the mechanisms controlling the phenomenon.

3. Existing models for predicting crack spacings in tensile and flexural members generally rest on two different and contradictory assumptions concerning which parameters control the distribution of stresses between cracks and, thus, the distance between one crack and the area where the next crack can form.
4. Due to the fact that cracking in reinforced concrete structures is associated with certain randomness a level of uncertainty is added to our prediction of crack spacings and crack widths. A larger amount of test results are thus needed to validate models when compared to the number of tests needed for validating other models or for validating the behaviour of other more homogeneous materials.

1.2 Initial hypothesis

One of the fundamental issues in the above-listed subjects regards the lack of physical coherency across all aspects of the serviceability limit state and this thesis, therefore, proposes an approach to overcome this shortfall. In order to connect cracking to the deflection of flexural members and describe all aspects of the serviceability limit state with the same physical assumptions, a hypothesis is proposed, which is;

The deformation of flexural members can, with reason, be assumed to take place solely in the cracks and, thereby, the deformation of the concrete can be neglected. Furthermore, the width of cracks is assumed to be related to the crack spacing and the variation of the strain in the reinforcement.

The hypothesis means that the mean strain in the concentrated tensile reinforcement, ϵ_{sm} , can be determined from the crack width, w , and the mean crack spacing, S_{rm} , which are illustrated for a beam subjected to four-point-bending in Fig. 1.1:

$$\epsilon_{sm} = \frac{w}{S_{rm}} \quad (1.1)$$

The curvature of the beam can then be found from the mean strain in the reinforcement and the height of the crack:

$$\kappa = \frac{\epsilon_{sm}}{d - x_{cr}} \quad (1.2)$$

where x_{cr} is the height of the compression zone for a cracked cross-section with an elastic distribution of strains.

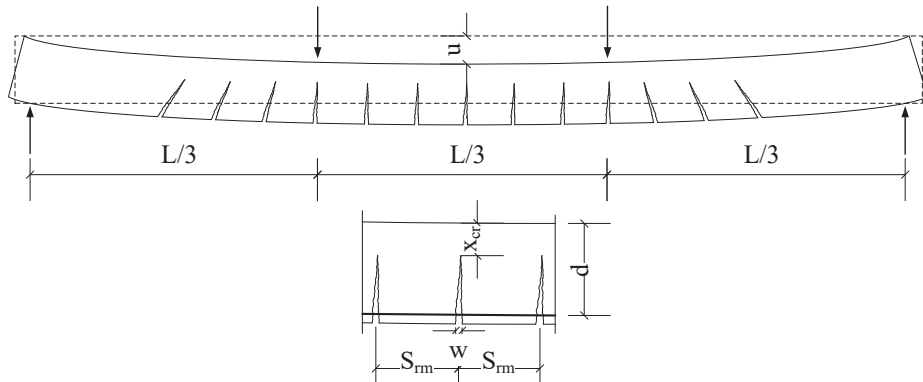


Figure 1.1: Idealised illustration of deflection and cracking in a beam subjected to four-point-bending

Putting Eq. (1.1) and (1.2) together, the curvature of the beam can be described from the crack spacing, the crack width, and the height of the crack:

$$\kappa = \frac{w}{S_{rm}(d - x_{cr})} \quad (1.3)$$

The deflection of a beam can generally be expressed as:

$$u = g \frac{M}{EI} L^2 \quad (1.4)$$

where g is a constant depending on the type of loading and the static system of the beam while EI is the flexural stiffness.

For a beam with a specific static system, the deflection can now be determined from the expression for the curvature, which accounts for the cracks that have formed with a distance of S_{rm} . With the use of the constitutive relations between the bending moment and the curvature $EI = \frac{M}{\kappa}$, the deflection at mid-point of the beam subjected to four-point-bending is:

$$u = \frac{23}{216} \kappa L^2 \quad (1.5)$$

where $M = \frac{1}{3}PL$

To test the hypothesis, the deflection is estimated from Eq. (1.5) with the use of the curvature in Eq. (1.3) and compared to two different series of tests from the literature by Kenel and Marti[1] and Gilbert and Nejadi[2], respectively. The two test series each consists of four flexural members subjected to four-point-bending, which will be thoroughly described in Chapter 6 of this thesis. The result of the comparison is illustrated in Fig. 1.2.

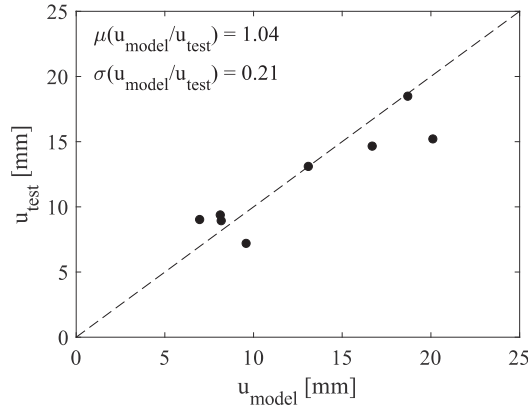


Figure 1.2: Comparison of test results and estimated deflection at mid-point of the beam in four-point-bending

The comparisons in the figure show a reasonable agreement between the deflections measured from the test, u_{test} , and the modelled deflections with the used of the hypothesis, u_{model} , with a mean value of the ratio u_{model}/u_{test} of 1.04 and a standard deviation of 0.21.

1.3 Objective and limitations

The preliminary investigation of the hypothesis, in the latter section, indicates that it is possible to describe the deflection of flexural members in the serviceability limit state from the knowledge of the spacing of cracks, S_{rm} and the strain variation in the reinforcement. This assumption, therefore, forms the basis for continuing the development of an approach to design all aspects of the serviceability limit state for flexural members, which will be the main focus throughout this thesis.

The proposed approach and the accompanying research is substantial for the design of flexural reinforced concrete members in the serviceability limit state, regarding crack control, flexural stiffness, and deflection. Improving the understanding of the behaviour of cracking as well as improving the modelling of the behaviour will allow for more accurate estimates, which can lead to better utilisation of both concrete and reinforcement. A wider knowledge of cracking in flexural members can also be beneficial with respect to the modelling of reinforced concrete in the ultimate limit state, where the structural behaviour, to a large extent, is governed by the development of cracks during service loads.

The above knowledge is gained through the following main objectives of the research project:

- Creating a coherent approach for the design of flexural members in the serviceability limit state based on the proposed initial hypothesis. The approach should include the estimation of both crack widths, flexural stiffness, and deflection from the knowledge of the crack spacing and should, thus, connect all aspects of the serviceability limit state by using the same assumptions as opposed to the existing models where this connecting is not the case. In that way, the proposed approach will be analogue to the design methods of the ultimate limit state and form basis for a relationship between the models connected to the ultimate limit state and the models connected to the serviceability limit state, which could create a concurrent and coherent design of the two limit states.
- The crack spacing is regarded as the most fundamental part of the proposed approach, and it is, therefore, considered crucial to gain as much knowledge about this parameter as possible. This gain is achieved by:
 1. Studying the existing literature on the subject of cracking in both tensile and flexural members.
 2. Conducting a series of tests which allows to study the development of cracks experimentally and to investigate some of the questions that arise from the review of the literature.
 3. A thorough empirical study of crack spacings with the use of a large database of 142 tested tensile members and 462 tested flexural members including a series of eight flexural tests and four tensile tests conducted at Aarhus University as part of the current research project. A large part of the existing tests found in the literature, although originally having a different focus, contain a substantial amount of valuable information with respect to crack patterns and crack spacings, which have not been analysed before.

All crack spacings in the database of the test members is to be collected in a consistent manner; from measuring on photos of the crack patterns. Therefore, only tests where photos exist of the crack pattern are included in the database. This important prerequisite is established in an attempt to avoid subjectivity and to create comparable data resting on the same basis. Furthermore, the method excludes several uncertainties related to crack spacings given in the experimental reports.

With the large size of the database, it will be possible to analyse the crack spacings statistically, minimising the influence of the randomness associated with cracking. The database of experimental results of the crack spacing should make it possible to investigate the influence of various parameters on the crack spacing and establish which of the parameters are of significance to the

variation of the crack spacing. Furthermore, the database should be used to investigate the accuracy of existing models and compare the performance, in an objective manner, of the two generally different and conflicting theories, mentioned earlier.

The empirical study also allows for a comparison of the cracking behaviour in tensile and flexural members, which can address the earlier discussed issue of whether the behaviour is related or controlled by completely different mechanisms.

- The proposed approach is to be validated by comparison with two test series of beams subjected to four-point-bending where the variation of both the crack spacing, the crack widths and the deflection have been measured with respect to increasing applied load. In the present research, the comparison of the proposed approach is, thus, limited to flexural member subjected to short-term loading.

1.4 Reading guide

Chapter 1 - Introduction Firstly, an introduction to the field of research is given, followed by a summary of the main issues addressed in the present thesis. The chapter, subsequently, introduces an initial hypothesis which is tested and concluded to be a sound basis for the development of a design approach for flexural members in the serviceability limit state. Lastly, the chapter contains the main objectives of the research project.

Chapter 2 - Literature review The chapter reviews the existing literature on the subjects that are considered fundamental to the serviceability limit state, namely; 1. Plain concrete in tension, 2. Cracking in reinforced concrete in uni-axial tension 3. Cracking in reinforced concrete in flexure and 4. Stiffness and deformation of flexural members. Even though the research primarily aims to improve the knowledge of flexural members, it is found natural to study plain concrete and tensile members beforehand because flexural cracking is seen as an extension of the other two subjects.

All subjects treated in the literature review are structured in the same way. Firstly, the physical behaviour related to the specific subject is described through experimental observations. Subsequently, a selection of existing models, attempting to predict the observed behaviour, are reviewed. The chapter also contains a brief parameter study of the selected models describing crack spacing in both tensile and flexural members, which reveals the models' behaviour with respect to the variation of various parameters.

Chapter 3 - Experimental investigation of flexural cracking with respect to member depth

The results are presented of a test series of eight beams conducted at Aarhus University as part of the present research project. The tests were carried out in order to clarify some of the unresolved questions about the behaviour of flexural members that arose from the literature review as well as to support some already stated conclusions in the literature review.

The test series consisted of beams of two different heights which proves to act quite differently with respect to the following elements; the appearance of the system of cracks, the development of the height of the cracks, and the variation of the crack widths within a single crack. Meanwhile, when the sum of crack widths in the beams are estimated, the beams with different heights act similarly.

Chapter 4 - Empirical study of crack spacings The chapter presents a comprehensive empirical analysis of the measured crack spacings in both tensile and flexural members. The database consists of 142 tensile tests and 462 flexural tests, where crack spacings are measured single-handedly from photos of the crack patterns in 85 of the tensile members and all the flexural members. An operation that was carried out in an attempt to avoid subjectivity and to create comparable data.

The chapter handles tensile members and flexural members separately, although in the same manner, where the following is sought to be investigated: 1) which parameters control the crack spacing, 2) what is the relations between extreme and mean crack spacings, and 3) which of the selected existing models are most accurate when compared to the database.

The crack spacing in tensile members and the crack spacing at the level of the tensile reinforcement in flexural members are compared in an attempt to answer the question of whether there is a similarity. For flexural members it is also investigated whether beams behave differently with respect to cracking depending on the height of the beam and whether a stabilised system of cracks can be identified with respect to a stress level to which no more cracks form.

The chapter is ended by summarising and discussing the conclusions found throughout the analysis.

Chapter 5 - The approach for estimation of crack widths, stiffness, and deflection of flexural members

The chapter presents the approach proposed based on the hypothesis investigated in the introduction. The approach satisfies the ambition that all aspects of the serviceability limit state can be estimated from the knowledge of the crack spacing and coherent physical considerations.

The five steps of the approach are described, which are: 1) the identification of the system of cracks and estimation of crack spacings, 2) the estimation of strains in the tensile reinforcement, 3) the prediction of crack widths from the summation of reinforcement strains, 4) the estimation of the flexural stiffness from the crack spacing and crack width, and 5) the deflection analysis with the use of the flexural stiffness.

The stiffness, including the tension-stiffening effect, is found to be dependent on the static system and type of loading. The influence of tension-stiffening is, therefore, investigated, with respect to both crack spacing and the static system, to identify when the tension-stiffening effect is significant and, thus, should be included with respect to the estimation of deflection. Furthermore, the effect of tension-stiffening on the redistribution of forces in statically indeterminate beams is investigated.

Chapter 6 - Application of approach This chapter concerns the application of the theory established in Chapter 5. Firstly, an overview of the approach is presented where the course of action for designing flexural members in the serviceability limit state is illustrated. Secondly, the approach is exemplified on a beam subjected to four-point-bending. Lastly, the approach is applied to two different test series, and compared to the test results. The following estimated results and test results are compared; crack spacings, force-deflection response and force-crack width response. Furthermore, the initial hypothesis, presented in the Introduction in Chapter 1, is investigated further by studying the relations between the maximum crack width and maximum crack spacing in each member and examining the development of the crack width with respect to increasing deflection.

Chapter 7 - Conclusion The final chapter concludes the thesis and suggests further applications of the proposed approach as well as possible future studies.

Appendices The following four documents are appended to this thesis:

A: A list of the notations used in the thesis

B, C, and D: Three conference papers published during the Ph.D. study

2 LITERATURE REVIEW

This chapter is the result of a thorough literature review of the main research areas concerning reinforced concrete in the serviceability limit state. The primary objective of the review is to gain more knowledge of flexural members both concerning 1) what existing tests have shown regarding load-induced cracking during the elastic stage and 2) how researchers have modelled this behaviour. To be able to reach that objective, it was necessary to, initially, study two other topics; 1) plain concrete in tension and 2) reinforced concrete uni-axial tensile members. The study of flexural members then came as a natural extension of these two. The first part of this chapter, therefore, consists of three main sections; section 2.1 on plain concrete in tension, and sections 2.2 and 2.3 on reinforced concrete subjected to tension and bending, respectively. The first three sections are followed by a section concerning the other main topic of serviceability, namely stiffness and deformation. Here, the behaviour and modelling of flexural members are reviewed. All subjects treated in the literature review are structured the same way. Before looking into how a certain phenomenon can be modelled, the physical behaviour, related to the subject, is described through experimental observations. Subsequently, the existing models are reviewed.

2.1 Plain concrete in tension

It is well known that the tensile strength of concrete is very limited compared to its compressive strength. In addition, the tensile strength is unreliable and hard to predict because of the brittle failure of concrete. In the design context, it is common to assume that concrete has no tensile strength. Though, when dealing with the development of cracks because of loading, it is necessary to study how concrete reacts to tension. In other cases, such as determination of minimum reinforcement, knowledge of the tensile strength is also relevant.

2.1.1 Studies of stress-strain behaviour

In Fig. 2.1a, the stress-strain response of concrete in tension is illustrated for three different specimens cured for different number of days. The tests are one of the first tests where the descending branch after the peak was measured. They were conducted by Evens and Marathe and referred to by van Mier[3]. Fig. 2.1b shows an idealised curve of the same response illustrating the two overall phenomenons affecting the response; micro cracking and tensile softening/macro cracking.

Micro cracking

Micro cracks are defined as so small in width and length that they are only visible through a microscope.[4] There are several different types of micro cracks, caused by different phenomenons. Some micro cracks are present even before any loading is applied. According to Hsu et al.[5] the micro cracks that exist prior to loading are mainly bond cracks at the interface between coarse aggregates and cement paste. The forming of bond cracks is most often owed to conditions during curing such as hydration of the cement paste and drying shrinkage. Fig. 2.2a shows a cut in a cylinder prior to any loading where a significant amount of micro cracks (marked with bold lines) around aggregates can be seen. The amount and size of micro cracks will grow when tension is applied.

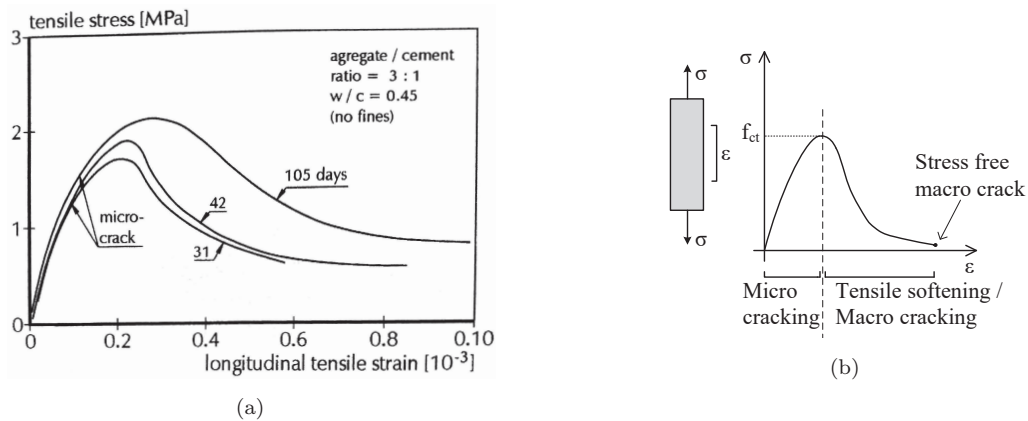


Figure 2.1: (a) Stress-strain diagram of concrete in uni-axial tension by Evans and Marathe, reprint from [3], (b) Idealised stress-strain diagram

Tensile softening

To study the increase of micro cracks into the forming a macro crack, van Mier[3] conducted a series of direct tension tests on prisms with a single edge notch. The growth of micro cracks in front of the stress-free preformed macro crack was studied with respect to different levels of applied uni-axial tension. In Fig. 2.2c an example is shown of a specimen of 16mm normal concrete. The specimen has already reached the peak stress but can still carry some tension. Thus, it is somewhere on the descending branch. Here the crack is not continuous through the specimen. Instead, it has two branches one on each side of an aggregate. The two branches overlap, which means that the section is actually fully cracked but not by one coherent crack.

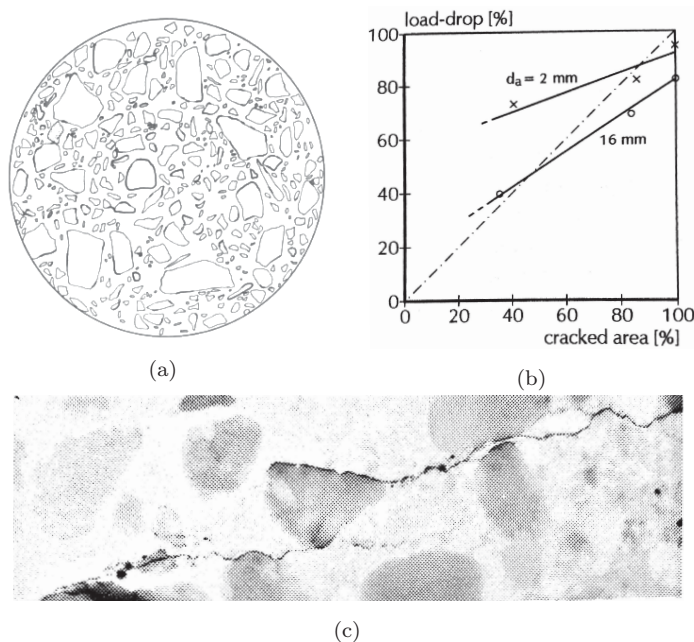


Figure 2.2: (a) Micro cracks at aggregate-cement-interface formed prior to loading, tests by Hsu et al., reprint from [5], (b) Load-drop after peak in relations to cracked area, tensile tests by van Mier, reprint from [3], (c) Example of overlapping cracks, tensile tests by van Mier, reprint from [3]

In Fig. 2.2b the area of the crack relative to the cross-sectional area is plotted against the load-drop relative to the peak load. The relations is plotted for both a 16mm normal concrete and a 2mm mortar. The plot reveals that the relative cracked area is larger than the load-drop. For the 16mm normal strength concrete, 80% of the cross-section is cracked while the load has only decreased 60%. Moreover, both specimens still carried load at 100% cracked area. The main explanation for why the specimens can still carry tension when they are cracked through the whole section is what van Mier refers to as crack-face bridging. The phenomenon is, as shown in Fig. 2.2c, where individual cracks approach each other without joining but instead overlap in two different levels. This phenomenon is also illustrated in Fig. 2.3a where it is seen how the two concrete blocks on each side of the cracking region are still connected through the aggregate. The stress finally drops to zero when the two cracks join as shown in Fig. 2.3b.

The crack-face bridging and the existence of coarse aggregates in concrete is the reason why the stress-strain response do not suddenly drop to zero after peak but decrease slowly in stress with increasing crack opening. This property of the material is known as the tensile softening. Although, crack-face bridging is not the only mechanism causing the softening behaviour of concrete in tension. Another reason is the sliding friction present between aggregates and cement paste when a crack opens, and the aggregates are being pulled out of the cement paste. Hordijk called this mechanism interlocking [6].



Figure 2.3: Crack-face bridging: (a) Overlapping cracks with load transfer through the aggregate, (b) Failure due to joining of cracks, reprint from [3]

The two-part diagram

The tensile response is often shown as a two-part diagram as illustrated in Fig. 2.4, which, for example, Hordijk[6] and Nielsen[7] did. A stress-strain response is used for the pre-peak behaviour while a stress-crack opening response characterises the post-peak behaviour because deformation happens locally in a crack post peak. The peak value of the response and the crack width to which the crack is stress-free depends on the concrete composition, the size of aggregates, and the curing conditions[3], which will be described further in the following.

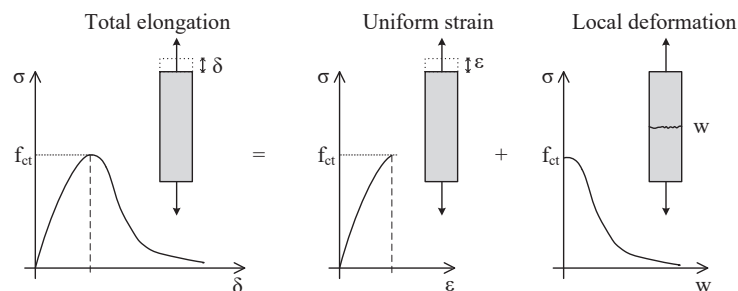


Figure 2.4: To part diagram explaining concrete in tension

Influence of aggregate size

In Fig. 2.5a, van Mier has explained the effect of aggregate size on an idealised response of concrete in tension. The figure illustrates how the stress level in the post-peak response increases with the increase

in aggregate size. Thus, the tensile softening effect increases. The branching of cracks becomes more pronounced because the areas (aggregates), connecting two concrete blocks on each side of a crack branch, are larger. Through a comparison of uni-axial tests with different maximum aggregate size, Hordijk [6] also concluded that the softening effect increased with increase in d_{max} . The reason for the increase can not only be owed to crack-face bridging, but also to a mechanism like interlocking, which must be more pronounced for large aggregates, because the crack-face becomes more uneven (provided that the crack runs through the cement paste and not the aggregates).

However, the increase in aggregate size does not necessarily mean an increase in the softening effect. The difference in the toughness of the aggregates and the cement paste is also of importance. When the concrete strength is increased, the difference in toughness decreases. When the aggregates and the cement paste have a similar toughness, the work needed for a crack to run through the aggregates is no longer more than to run through the cement paste. Thereby, the effects of crack-face bridging, and, thus, the tensile-softening, decreases with an increase in concrete strength.

Cornelissen et al. [8] also came to the above-stated conclusions about the influence of aggregate size in an experimental study. The overall behaviour of the post-peak curves and crack surfaces was compared with respect to the properties of aggregate sizes in light and normal weight concrete. Double notched specimens were unloaded and reloaded in the post-peak stage by three different unloading processes; unloading to a small tension level and loading to two different levels of compression. For the normal weight concrete, the specimens could transfer tensile stresses at higher crack openings than lightweight concrete could, hence, the softening effect was more pronounced for the normal weight concrete. This difference in softening effect can be explained by the larger aggregates and, thus, a coarser crack surface. Concerning to the cyclic loading, the crack surface, and, thus, the stiffness of the normal concrete was not damaged during unloading to tension. On the other hand, when unloading to compression, it caused a decrease in stiffness and damage to the crack surface.

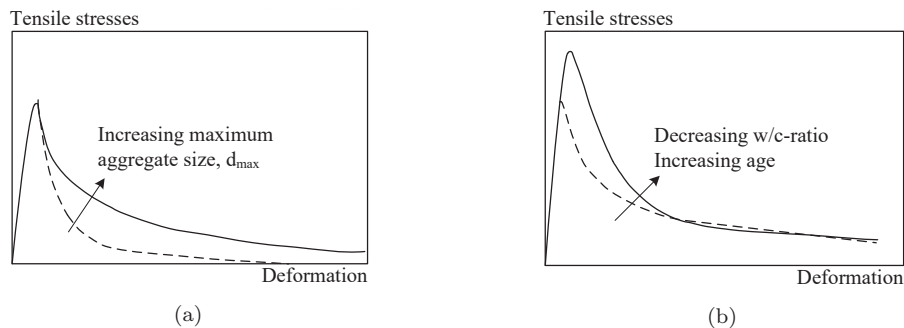


Figure 2.5: Idealised representation of: (a) The influence of aggregate size, (b) The influence of the w/c ratio and age, reprint from [3]

Influence of the water-cement ratio

In Fig. 2.5b, van Mier has illustrated the effect of decrease in water-cement ratio. The porosity of the concrete has a large negative effect on the strength in both compression and tension. High porosity comes from high w/c ratios because the capillary pores develop from the excess water remaining after hydration of the cement. The larger the size and greater the number of pores, the larger porosity and the smaller strength.[4] Hence, an increase in the w/c ratio decreases the concrete strength. According to van Mier[3], porosity will decrease over time because the degree of hydration increases. Increase of age, therefore, has the same effect on the concrete strength as a decrease in w/c ratio.

Influence of curing conditions

Humidity- and thermal- differences between a specimen and the surrounding atmosphere affect the tensile strength of concrete and can cause preformed cracks. When the moisture content in the cement decreases, the material will start to shrink. This process will initiate in the material in contact with/closest to the surrounding air. Because of a progressed shrinkage of the surface material, compared to the core, internal stresses develop. As shown in Fig. 2.6a, tensile stresses will occur at the surface, changing to compression at the centre. These eigen-stresses will, in some cases, exceed the tensile strength of the concrete and, therefore, cause cracking.[3]

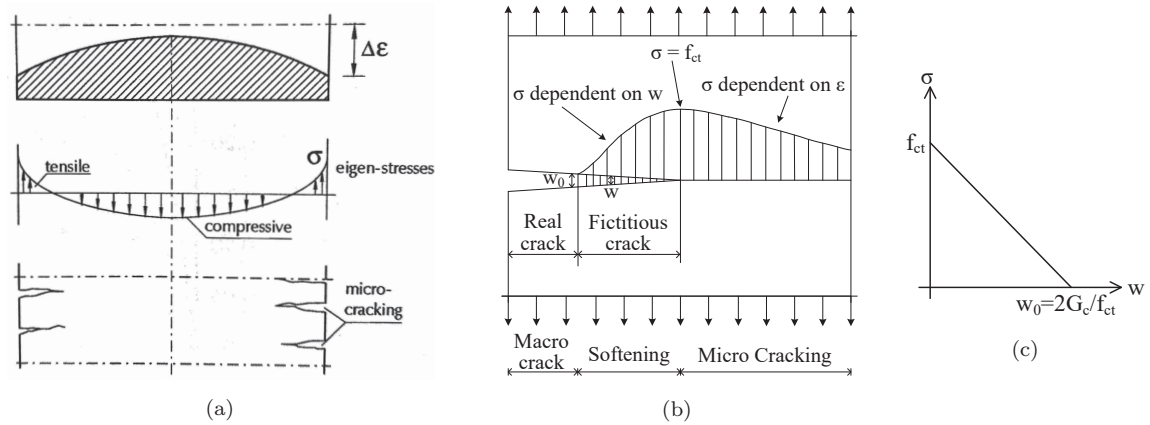


Figure 2.6: (a) Non-uniform drying causing eigen-stresses in concrete, reprint from [3], (b) The fictitious crack tip by Hillerborg, modified from [9], (c) Relations between crack width and stress during softening

2.1.2 Modelling plain concrete in tension

In the following section, models describing concrete in tension are presented. Firstly, a model describing the stress-crack width relations is presented, and the following sections explain some methods to determine the uni-axial and flexural tensile strength of concrete.

Stress-crack width relations

Several models exist to describe the response of concrete in tension which rests on different assumptions for the post-peak behaviour and how to accommodate the fact that stresses can still occur in the concrete after a crack has initiated. One model, often referred to, is proposed by Hillerborg[9] in 1976 and can be used to describe both the formation of a new crack and the growth of an existing crack.

A crack is said to start forming when the stresses at a free edge reach the uni-axial tensile strength, f_{ct} . When the crack starts to open, under increasing applied stress, the stresses will act across the crack until the crack has reached a certain width, denoted w_0 . Hillerborg assumed that this stress would decrease proportionally to the increase of crack width as illustrated in 2.6c. As Fig. 2.6b shows, the stresses in a single crack, therefore, varies from f_{ct} at the crack tip to zero where the width has become too large to transfer the stresses through aggregates. The stress-free crack represents the phase where crack-face bridging has been degraded.

Crack energy

The part of the crack in Fig. 2.6b, where stresses exist, can be associated with the phase of interface bridging. When going from the phase of uncracked concrete to a stress-free crack of the width w_0 , by applying stress, an amount of energy is released. The amount of energy, G_c , released per unit area of crack

surface, to overcome the stresses in the crack, is equal to the area under the $\sigma - w$ curve of the post-peak behaviour. Here, Hillerborg proposed a linear decrease of stress with the increase of crack width as in Fig. 2.6c. The crack energy, G_c , is, thus:

$$G_c = \int_0^{w_0} \sigma dw \Rightarrow w_0 = 2 \frac{G_c}{f_{ct}} \quad (2.1)$$

The size of the width w_0 , identifying a stress-free crack, therefore, becomes a variable dependent on the tensile strength of the concrete, f_{ct} , and the amount of energy, G_c , released per unit area of stress-free crack. These two material parameters are dependent on the concrete composition, the size of the aggregates, the quality of the aggregates, and the curing conditions.

2.1.3 Strength determination

The uni-axial tensile strength can, in general, be determined in two ways; namely by indirect or direct determination. Testing of the uni-axial tensile strength, as illustrated in Fig. 2.7a, can involve difficulties ensuring that the test member is subjected to pure tension without introducing any bending from asymmetric crack propagation. These difficulties were among others addressed by Hordijk[6]. Several other methods are, therefore, also developed to determine the tensile strength, where the uni-axial tensile strength are approximated from the results of these tests. The most known types of tests used for direct determination are:

- **Splitting test:** A cylinder, like the one used for compression tests, is loaded, as shown in Fig. 2.7b. From the failure load, P , the tensile stress, σ , can be determined as the uniformly distributed splitting stress along a vertical section, $\sigma = 2P/\pi\phi l$. The failure mechanism involves sliding of the concrete surface, because the loading of a uniform compression line-load on the cylinder, which increases the tensile strength, compared to the uni-axial strength.[4]

Nielsen's[7] compared test results of splitting tests and uni-axial tensile tests, which showed that the splitting tensile strength was 1.6 times larger than the uni-axial tensile strength: $f_{ts} = 1.6f_{ct}$

- **Flexural test:** The estimation of the flexural tensile strength involves a beam of plain concrete loaded to four-point-bending as illustrated in Fig. 2.7c. The flexural stress at failure is expressed by the bending moment at mid-point of the beam: $\sigma = M/\frac{1}{6}bh^2$. [4]

The flexural tensile strength of concrete is larger than the uni-axial because the tensile stresses vary within the cross-section. In the elastic stage, stresses are assumed to be linearly distributed, as in Fig. 2.7d. The uni-axial tensile strength can, therefore, be reached in the outermost fibres without it being reached closer to the neutral axis. Moreover, as described earlier, stresses are assumed still to be transferred across a crack until a certain crack width is reached. In bending, the stress within a crack will decrease from the outermost tensile fibres of the beam first, as in Fig. 2.7e [7].

Nielsen's[7] comparison of flexural and uni-axial tensile test results showed that the flexural tensile strength was 1.7 times larger than the uni-axial tensile strength: $f_{tb} = 1.7f_{ct}$

Because of the difficulties associated with the direct determination of the tensile strength, as well as the fact that it is often assumed to be non-existent in design contexts, several empirical expressions have been developed relating the tensile strength to the compressive strength of concrete. One of the most commonly used formulas for indirect determination of the uni-axial tensile strength is:

$$f_{ct} = 0.3f_c^{2/3} \quad (2.2)$$

for concrete grades \leq C50. The formula is used in both the Eurocode[10] and the fib Model Code 2010[11].

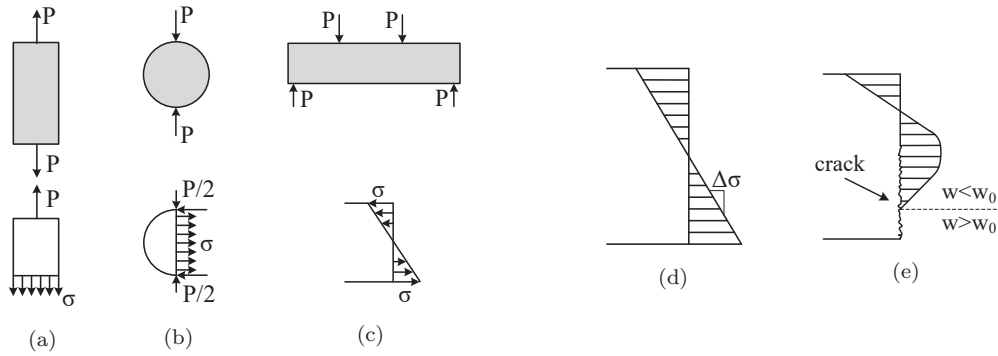


Figure 2.7: (a) Uni-axial tensile test, (b) Splitting test, (c) Flexural test, (d) Stress distribution in uncracked section, (e) Stress distribution in cracked section

Influence of casting and curing conditions

The tensile strength is considered to be dependent on the composition of the concrete and how the concrete is treated under casting and curing as well as during construction. Preformed micro cracks will affect the strength negatively, for example, because of eigen-stresses developed from shrinkage, as mentioned earlier. Furthermore, several tensile tests, treated by Nielsen[7], show that the tensile strength is affected significantly by the moisture conditions during curing. The tests indicate that when members are cured in water for the whole period of 28 days their strength could be approximated by Eq. (2.2) but if they are instead cured in a mixture of water and air, their tensile strength is reduced. The modified empirical formula deduced by Nielsen is:

$$f_{ct} = 0.35\sqrt{f_c} \approx \sqrt{0.1f_c} \quad (2.3)$$

In Fig. 2.8, the difference between the two estimates is shown where the reduction in strength because of poorer curing conditions can be seen to increase with increasing compressive strength. The formula $\sqrt{0.1f_c}$ can also be interpreted as a lower bound value while interpreting $0.3f_c^{2/3}$ as an upper bound value for the tensile strength.

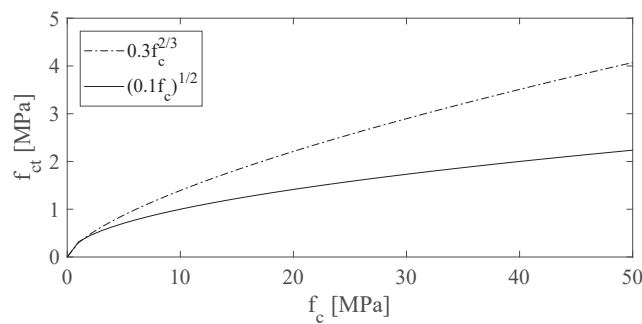


Figure 2.8: Comparison of two different expressions for the tensile strength expressed by the compressive strength of concrete

Size effect

The flexural tensile strength is found to vary with the size of the member, which is mainly due to the difference in stress variation in a cross-section. For a shallow beam, the gradient of the stress variation, in Fig. 2.7d, will be steeper than for a tall beam. Hence, the stresses will decrease much faster, towards the neutral axis, for a shallow beam than for a tall beam. In addition, for a cracked cross-section, tensile

stresses will exist across a relatively larger length of the crack in a shallow beam than in a tall beam. The flexural tensile strength, therefore, decreases with the height of the member. [7] [4]

Due to the above-stated fact, a size effect needs to be accounted for to be able to find the flexural tensile strength for members of any size. The size effect can be approximated by a Weibull formula describing the relations between the strength of the concrete for members with two different heights [7]:

$$\frac{f_{tb1}}{f_{tb2}} = \frac{h_2^{\frac{3}{m}}}{h_1} \quad (2.4)$$

where h_1 and h_2 are the height of the members in millimetres, m is an empirical factor determined by tests, and f_{tb1} and f_{tb2} are the tensile strengths. Nielsen[7] defines the factor $m = 11$ according to tests done by C. Forsell. The height of a cylinder tested in the laboratory is proposed to be $100mm$, which means that the flexural strength of a member of any other height can be determined with the factor:

$$s(h) = \frac{h^{-0.27}}{100} \quad (2.5)$$

The expression for the flexural tensile strength becomes:

$$f_{tb} = 1.7f_{ct}s(h) \quad (2.6)$$

As an example, the relations in $s(h)$ expresses that if the height of a member is increased tenfold, the strength is reduced to one half.

2.2 Cracking in uni-axial tensile members

The following presents a review of cracking in uni-axial tensile members, where, firstly, a study of existing experimental observations is used to describe the cracking behaviour with respect to crack pattern, crack types and stress distributions in cracked members. Secondly, selected models describing these crack types, their crack spacings and their crack widths, are reviewed. Lastly, a summary is included of how the European Code and the FIB Model Code handles tensile members in the serviceability limit state.

2.2.1 Studies of tests

The studies of tests involve, first, identification of different crack types. Then, stress distributions in the reinforcement of cracked members are illustrated from measurements of strains along reinforcement embedded in concrete cylinders. Lastly, three different parameters' influence on the cracking behaviour is discussed. The three parameters are:

- **The reinforcement layout** The parameter is studied because its influence gives a clear picture of why reinforcement is important and how the right layout contributes to achieving multiple cracking. When multiple cracking is ensured, the deformation is distributed across more cracks with minor width instead of few cracks with a large width.
- **The type of reinforcement** The influence of the type of reinforcement is studied because many models estimating the crack spacing rest on the assumption that the bond between concrete and reinforcement is a controlling parameter. The effect of bond quality is studied through comparison of crack spacings in members with plain reinforcement to members with deformed reinforcement.
- **The cover size** This parameter is also greatly influential in many existing models for estimating crack spacing and crack width. Therefore, this effect is studied through tests.

Each study concerning a certain parameter is closed with a summary of the most evident findings. Other parameters that could have been studied as well, because of their involvement in models, are the reinforcement diameter, ϕ_s and the tensile strength of the concrete. The main reason that they are not included here is because tests focusing on the variation of these parameters have not been found in the literature.

Crack pattern and the different type of cracks

The crack pattern developing in uni-axial tensile members has been described by several of researchers, e.g. Broms[12], Illston[13], Leonhardt[14], and Nielsen[7]. In 1971 Goto[15] described the crack pattern through a series of tests where the characteristics of crack types were analysed with respect to the type of reinforcement used; plain versus deformed reinforcement bars.

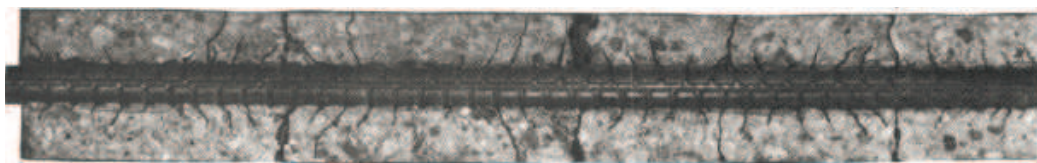


Figure 2.9: Cracks formed in concrete around deformed tension bars, reprint from [15]

Each member in this test series had one single reinforcement bar embedded centrally in the concrete. After loading, the members were injected with red ink along the reinforcement. Then the members were cut in

two equal parts, longitudinally along the reinforcement. On the cut surfaces, it was now possible to study the internal cracks. A photo of one of the tensile tests with deformed reinforcement is shown in Fig. 2.9. To limit shrinkage strains, and, thereby, eliminate preformed cracks, the members were tested in moist conditions.

Primary cracks Fig. 2.10 illustrates the two different types of cracks formed in the tension members with deformed reinforcement. One is the so-called primary cracks penetrating through the whole concrete section perpendicular to the reinforcement bar. The width of these cracks was observed increasing with the distance from the reinforcement, being largest at the surface of the concrete. This observation was seen more significant in the members with deformed reinforcement than for members with plain bars.

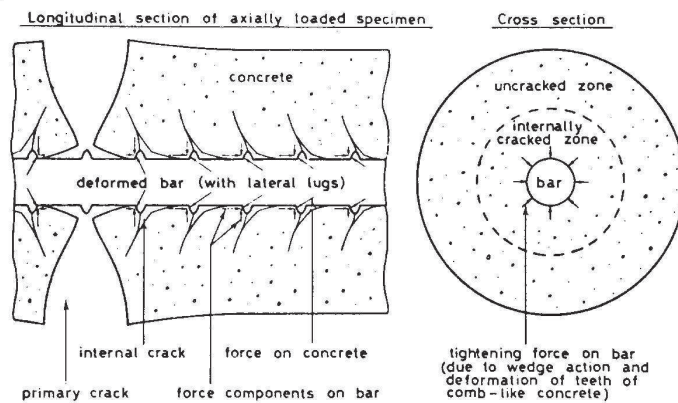


Figure 2.10: Principle illustration of crack types, reprint from [15]

Secondary cracks The other type of cracks, only observed in the members with deformed reinforcement, were named the secondary cracks or the internal cracks. At each rib of the reinforcement, a cone-like crack was formed, originating from the rib with a direction towards the nearest primary crack. The first secondary cracks developed adjacent to the primary cracks. With the increase in external tensile force, cracks were also formed at the ribs further away, one by one. Hence, the number of secondary cracks were dependent on the stress level in the reinforcement. At reinforcement stresses around 300MPa , the secondary cracks were seen to have developed to extent that some appeared at the inner face of a primary crack or even at the surface of the member. The angle of the secondary cracks was in the direction of the reinforcement from 45° to 80° with a mean value around 60° . At 300MPa , ink was observed along the reinforcement closest to the primary cracks indicating a loss of adhesion between the concrete and the reinforcement.

Stress distributions in reinforcement and concrete

In the following section, stress distributions are illustrated through measurements of strain variations along a deformed reinforcement bar embedded in concrete. In tests by Masukawa [16], a reinforced concrete cylinder, like the one shown in Fig. 2.11a, was equipped with strain gauges inside the reinforcement with an individual distance of 16.4mm . To be able to place the strain gauges, the bar was first cut in half, then strain gauges were placed in milled grooves, and finally, the bar was put back together with epoxy resin. This specific technique, developed by Scott and Gill [17], is illustrated in Fig. 2.11b.

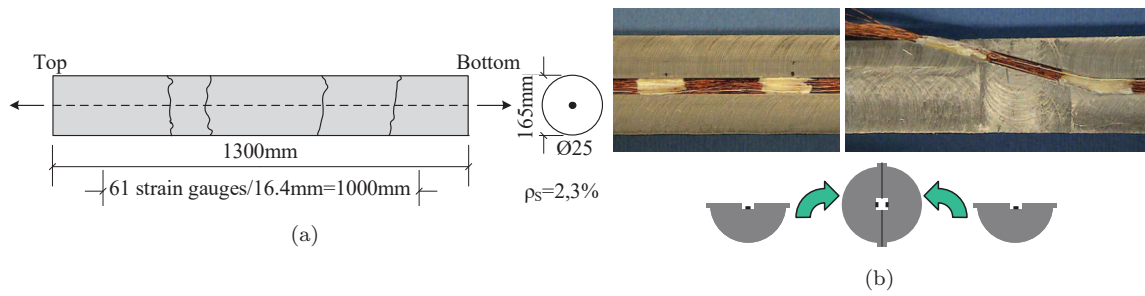


Figure 2.11: (a) Test by Masukawa of reinforced concrete tension bar with strain gauge measurements along the reinforcement, (b) Technique in experimental strain analysis of the use of strain gauges by Scott and Gill [17], reprint from [16]

Fig. 2.12a shows the measured strains along the reinforcement at six different load levels during first time loading of the reinforced concrete cylinder. At the first load level of $25kN$, the concrete is uncracked, which means that nowhere in the concrete have the stresses reached the tensile capacity. At this load level, the strains are largely constant along the reinforcement, except close to the ends.

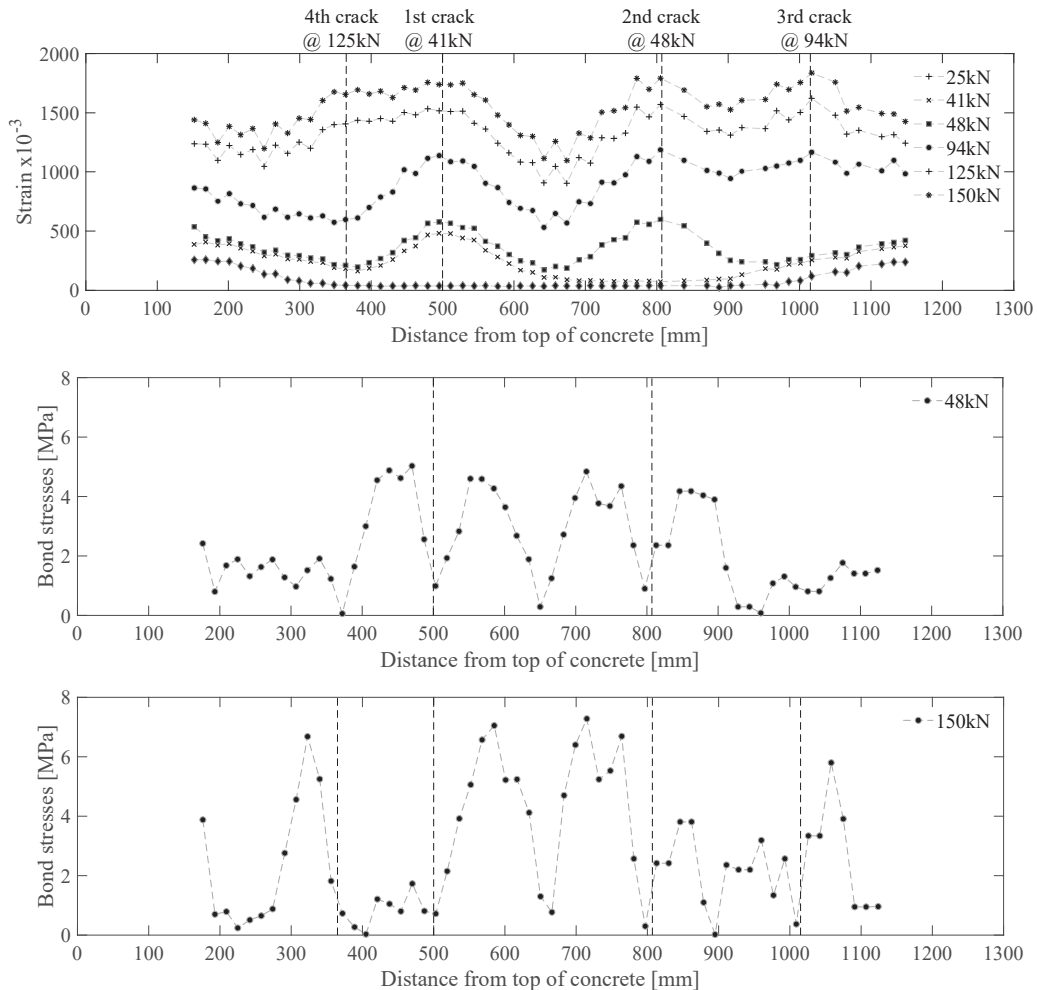


Figure 2.12: Test by Masukawa with deformed reinforcement: (a) Measured strains along reinforcement, (b) Bond stresses at $48kN$ (c) Bond stresses at $150kN$

A crack forms between each of the next four measured load levels: $41kN$, $48kN$, $94kN$ and $125kN$ (corresponding to reinforcement stresses of $84MPa$, $98MPa$, $192MPa$ and $255MPa$). The strain in the

reinforcement is seen to peak at the location of a crack and reached a minimum between the cracks. This result is a sign that the concrete carries a part of the load between cracks while the reinforcement transfers the whole load across a crack.

The force transfer from the reinforcement to the concrete that enables the concrete to carry stresses can be modelled as bond stresses distributed along the interface between reinforcement and concrete. From the strain measurements, the rate of force transfer/the size of the bond stresses can be derived. The change in strains between two adjacent strain gauges is converted into a change of force and then divided by the surface area between two strain gauges which results in the bond stresses. Fig. 2.12b and 2.12c show the derived bond stresses at load level $48kN$ and $150kN$, respectively. The figures show how, the derived bond stress is approximately zero at the cracks, and on each side of a crack it increases because the force is transferred to the concrete from the reinforcement.

Debonding of reinforcement

When taking a closer look at the strain distribution in Masukawa's test, an effect can be seen from the presence of secondary cracks called debonding. In Fig. 2.12a, the strains do not peak at a single point at each crack but are more or less constant within a region on each side of a crack. This result indicates that the bond between reinforcement and concrete is damaged here and the rate of force transfer is, therefore, low. The phenomenon can be interpreted as secondary cracks that have developed into cones separated from the rest of the concrete block between two cracks causing little or no transfer of force to the concrete. The debonded length over which there is an, almost, constant strain level is, from Fig. 2.13, seen to increase as a function of increasing tension. This could indicate that the cones that separate from the concrete block increases in size with the load increase, as illustrated on the 1st crack in Fig. 2.13 and as Goto also observed in his early studies.

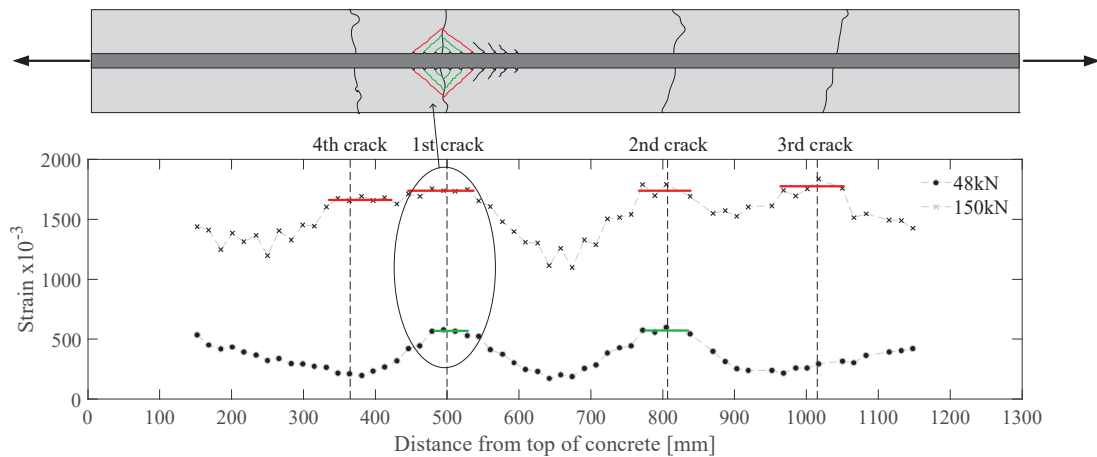


Figure 2.13: Strain distribution from [16] with an indication of debonded zones adjacent to cracks

Influence of reinforcement layout

Fellmann and Menn Cracking in tensile members was studied by Fellmann and Menn[18], where the differences in the crack patterns were investigated with regard to location of the reinforcement and the effect of large unreinforced concrete areas. The crack pattern in a slab with distributed reinforcement subjected to tension was compared to the crack pattern in a slab with reinforcement placed concentrated close to the edges of the slab.

From Fig. 2.14a it can be observed how only some of the cracks penetrated through the whole section of the slab with concentrated reinforcement. On the other hand, in the case of the member with distributed

reinforcement in Fig. 2.14b, more or less all the cracks penetrated through the whole section. In the member with distributed reinforcement, the widths of all the cracks were of similar size, while in the member with concentrated reinforcement, uncontrollably large crack widths occurred in the few cracks penetrating through the whole member due to the absence of reinforcement.

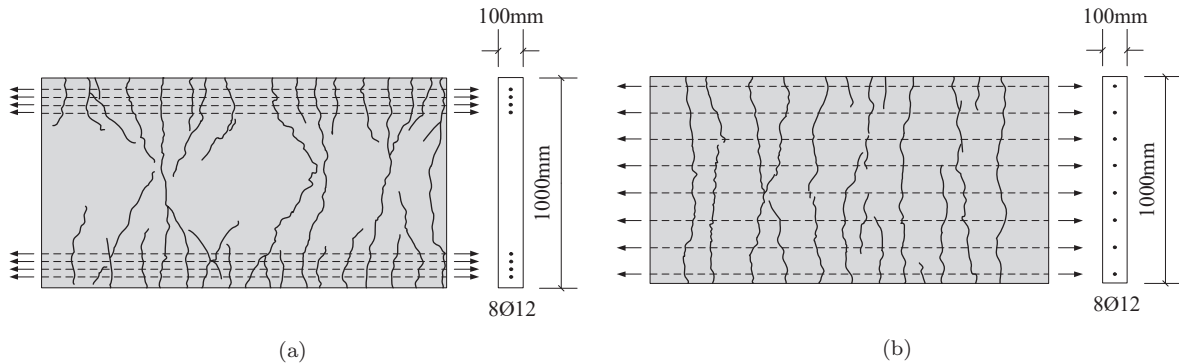


Figure 2.14: Tensile tests by W. Fellmann and C. Menn: (a) concentrated reinforcement, (b) distributed reinforcement, modified illustration from [18]

Summary The experimental study of the influence of reinforcement layout, thus, indicates that:

- Large unreinforced concrete areas can cause large crack widths
- Crack formation is, to a large extent, controlled by reinforcement

Influence of reinforcement profile

Masukawa In the series of tests by Masukawa referred to earlier, the influence of the type of reinforcement profile was investigated. Fig. 2.12a - 2.12c showed strain distributions and bond stress variations for the cylinder with a deformed reinforcement bar. Fig. 2.16a - 2.16c illustrate the same but for a cylinder with an embedded bar that has been grounded to an extent where it is almost smooth as photographed in Fig. 2.15.



Figure 2.15: An almost smooth bar where ribs are grounded of, reprint from [16]

When comparing the reinforcement strain distributions in Fig. 2.12a and 2.16a, larger strain levels are seen between cracks in the plain bar than in the deformed bar at corresponding load levels. The higher strain level must mean that the plain bar does not transfer force to the concrete at the same rate as the deformed bar. The ribs of the deformed bars create an interlock action when the first slip occurs while the only anchorage between the plain bar and the concrete is friction. Notice that there are four formed cracks in the cylinder with the deformed bar and only two cracks form, over that same distance, in the cylinder with the plain bar. Similar results, with respect to a lesser number of cracks in members with plain bars, were found by Scott and Gill[19].

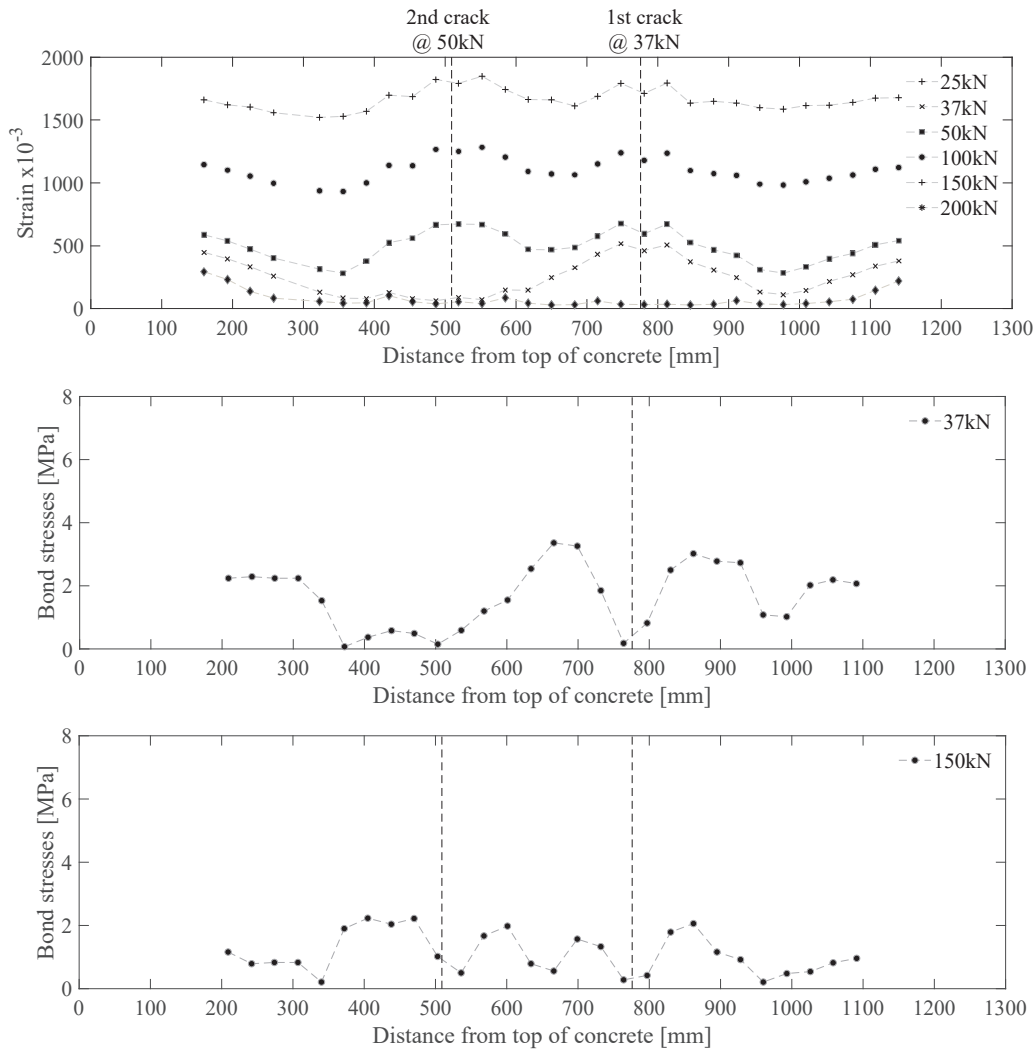


Figure 2.16: Test by Masukawa with almost plain reinforcement: (a) Measured strains along reinforcement, (b) Bond stresses at 40kN along a reinforcement derived from strain gauge measurements, (c) Bond stresses at 150kN

The lower level of force transfer in the cylinder with the plain bar can also be seen directly by comparing bond stresses in Fig. 2.12b to Fig. 2.16b as well as comparing Fig. 2.12c to Fig. 2.16c. In Fig. 2.17, this comparison is also illustrated, where maximum and average bond stresses, over a length of 300mm between two cracks, are plotted as a function of the applied load. First of all, it is confirmed that the size of bond stresses is larger in the cylinder with a deformed bar. Furthermore, the bond stresses along the deformed bar keep increasing with increasing load, also after the first formed crack at 41kN. Meanwhile, the bond stresses along the plain bar decrease slowly as soon as the first crack is formed at 37kN. Similar results were found by Kankam[20] through pull-out tests where strain variations between two simulated cracks for both plain and deformed bars were investigated.

A reason for the continuously increasing mean bond stress in the deformed bar until at least 100kN could be the effect of Poisson's ratio on the steel. If it is assumed that, up until 100kN, the transverse contraction of the steel bar is less than the height of the ribs. The ribs, thus, act as locks until, the strain in the steel results in a contraction that is larger than two rib heights, resulting in a degraded interaction between the two materials. As for the plain bar, only the friction is degraded with the increase in load.

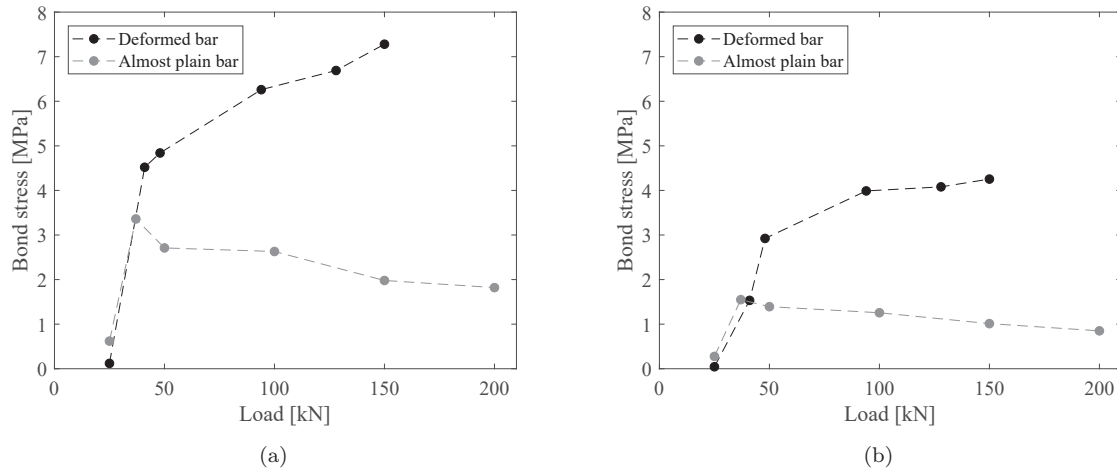


Figure 2.17: Tests by Masukawa with almost smooth and deformed reinforcement: (a) Comparison of maximum bond stresses from 500mm to 800mm, (b) Comparison of average bond stresses from 500mm to 800mm

Summary The experimental study of the influence of reinforcement profile indicates that:

- The ability to transfer force from reinforcement to concrete is better for deformed than for plain bars.
- For deformed bars, the ability to transfer force to the concrete is enhanced with load increase (within the elastic range of the reinforcement).
- For the plain bars, the ability to transfer force is constant or slightly decreasing with load increase (within the elastic range of the reinforcement).

Influence of cover size

Various researchers have, through tests, confirmed that crack widths measured at the concrete surface are dependent on the size of the concrete cover, e.g. Forth and Beeby[21], Tammo and Thelanderson[22], Borosnyói and Snóbli[23] and Yannopoulos[24]. A summary of their results is presented below.

Yannopoulos Yannopoulos[24] tested a series of smaller reinforced concrete tensile members simulating the concrete block between two adjacent primary cracks. The strains on the surface of the concrete were measured and compared to the elongation of the reinforcement. The results showed that the crack width was more than twice as large at the surface of the concrete compared to at the level of the reinforcement, for stress levels larger than approximately 100MPa.

Yannopoulos argued that the internal cracks, that Goto identified as secondary cracks could be the cause for the difference in crack width within one primary crack. If secondary cracks exist at the ribs, then the total elongation of the tensile member, owing mainly to the opening of the cracks, is divided between both secondary and primary cracks, thus a larger number of cracks internally than at the surface. Goto also illustrated this phenomenon in Fig. 2.10. When moving away from the reinforcement, towards the surface of the member, the secondary cracks gradually close and, eventually, there are only a few cracks or they are non-existent. This means that, at the surface, the total elongation of the member happens only in the primary cracks and the width is, therefore, larger here.

Tammo and Thelanderson To investigate the cover's influence on the crack width, Tammo and Thelanderson[22] tested a series of tensile members with three different cover sizes, namely 30mm, 50mm and 70mm. They also tested two different reinforcement diameters of 12mm and 16mm. During the

application of tension to the members, displacements at the ends were measured with LVDT's. These measurements were called the fictitious crack width and should represent the behaviour of one face of a crack. The members were $500 - 1000\text{mm}$ long, which ensured the forming of a primary crack. The surface-width of this crack was also measured and compared to the fictitious crack width to check the validity.

The curves in Fig. 2.18a and 2.18b show the development of the fictitious crack width at two different locations which are 11mm from the reinforcement (w_{11}) and at the concrete surface (w_{SURF}). The curves are regression curves created from several tests to present the average response. The comparison of the two curves shows that the crack width at the concrete surface is significantly larger than at the reinforcement level and that the difference between them increases with an increase in stress level. The width at 11mm from the reinforcement, in Fig. 2.18a, shows only small dependency on the cover as members with three different covers have widths within a small interval. The dependency on the cover is much larger, in Fig. 2.18b, for the width at the concrete surface. Here, the width is close to doubled with a cover increase from 30mm to 70mm .

Additionally, Tammo and Thelandersson performed all tests for two different concrete strengths but found no significant effect on the observed crack widths.

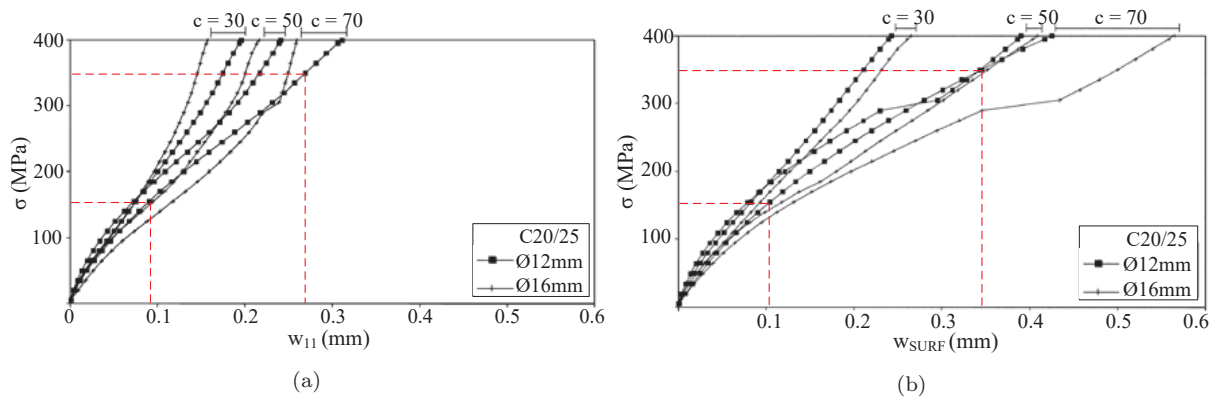


Figure 2.18: Regression curves for fictitious crack widths: (a) measured 11mm from reinforcement, (b) measured at the concrete surface. Reprint from [22]

An analysis of the graphs in Fig. 2.18 also indicate that the shape of the crack changes with the stress level in the members with large covers. In Fig. 2.19a the crack shape at approximately 150MPa is sketched from the readings marked with dashed red lines in Fig. 2.18a and 2.18b. While Fig. 2.19b shows readings of the crack widths at approximately 350MPa . The difference between the crack widths at the surface and the reinforcement is much larger at 350MPa than at 150MPa .

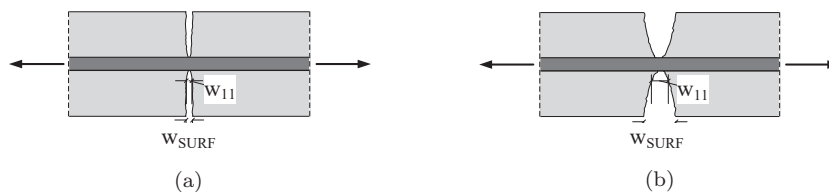


Figure 2.19: Illustration of difference in crack width shape with respect to stress level in reinforcement: (a) At approximately 150MPa , (b) At approximately 350MPa

Borosnyói and Snóbli A smaller study on the variation of crack widths within the concrete cover was carried out by Borosnyói and Snóbli[23]. These tests were part of a larger investigation on how to use

low viscosity PU resin to seal cracks in structures subjected to dynamic loading. The test specimens were 900mm long with a 20mm deformed reinforcement bar embedded in the centre or eccentrically in concrete sections of 120x120mm. Ten specimens were loaded to a stress stage below yielding of the reinforcement where the load was maintained for 12-18 hours while injecting low-viscosity, high-strength epoxy resin into the primary cracks. The surface of the cracks was sealed with a rapid-set epoxy resin. After the epoxy resin set, the specimens were cut open to be able to study the cracks. The crack widths were measured at the surface before unloading and again after unloading to verify that the epoxy resin was strong enough. When the two results were compared, it was concluded that the epoxy was able to withstand the closing of the cracks.

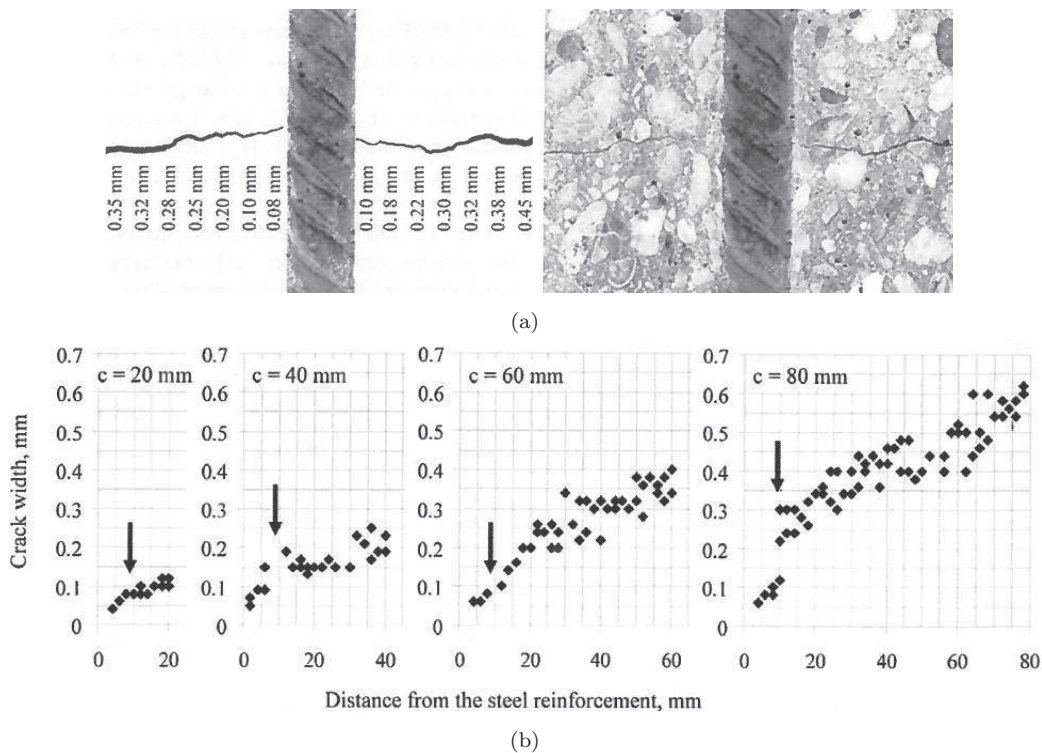


Figure 2.20: (a) Variation of crack width within a tensile member with symmetrically placed reinforcement with 50mm cover, (b) Variation of crack width within tensile members with eccentrically placed reinforcement, reprint from [23]

Fig. 2.20a shows the variation of the crack width in one of the members and confirms the increasing crack width with increasing distance from the reinforcement. Fig. 2.20b shows the crack width variation in the specimens with eccentrically positioned reinforcement for specimens with eccentric reinforcement place in four different positions. By comparison of the four graphs, it is clear how the surface crack widths show dependency on the cover while the crack width at the concrete-reinforcement interface is independent on the size of the cover. Furthermore, the crack widths are not seen to linearly increase with increasing distance from the reinforcement beyond the point indicated by the arrows. The authors, instead, suggest the increase takes the form of a power function and explains it by the existence of secondary cracks in the vicinity of the reinforcement.

Summary The experimental study of the influence of cover size, with a focus on concrete elements with a deformed reinforcement bar, indicates that:

- The crack width of a primary crack varies, being smallest at the reinforcement level and largest at the concrete surface.

- The crack width at the concrete surface increases with the increase of concrete cover size while the width at the level of the reinforcement is less dependent on the cover size.
- The difference between the crack width at the reinforcement and the concrete surface increases with increasing stress in the reinforcement.
- The dependency of the crack width on the cover could potentially be explained by the development of secondary cracks. The secondary cracks mainly develop in tension members with deformed reinforcement and are widest at reinforcement level and gradually closes towards the concrete surface, which, from compatibility considerations, means that the primary crack gradually opens simultaneously.

2.2.2 Modelling of cracking in tensile members

When consulting the existing literature concerning the estimation of crack spacings and crack widths, models rest on fairly different assumptions regarding the governing mechanisms involved. Two well known, and rather conflicting, approaches are 1) the bond-slip approach, first defined by Saliger[25] in 1936 and similarly by Watstein and Parsons[26] in 1943, and 2) the no-slip approach proposed in 1965 by Broms[27]. Both theories are still used today and have been modified and advanced by other researchers. The main principles of the two theories are illustrated in Fig. 2.21a and Fig. 2.21b.

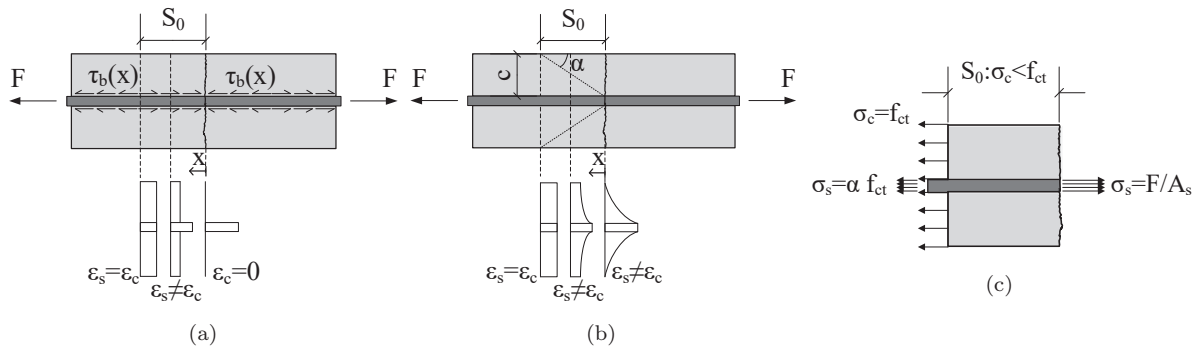


Figure 2.21: Two approaches for estimation of crack spacing: (a) The bond-slip approach, (b) The no-slip approach, (c) Illustration of transfer length, S_0

In general, both approaches rest on the theory that 1) a crack is formed when the stresses in the concrete reach the tensile strength, f_{ct} , and 2) within a distance S_0 from a crack, stresses in the concrete are reduced as illustrated in Fig. 2.21c. A new crack cannot form within this distance from the crack because of the reduced stresses in the concrete. The concrete stresses are rebuilt within the distance S_0 and beyond S_0 the stresses are again uniformly distributed in the concrete section where a new crack can, thus, form.

The main difference between the defined models is the mechanism controlling the distance of reduced concrete stresses, S_0 , and implicitly; what parameters influence the rebuilding of the concrete stresses. Beeby[28] stated in his thesis concerning the subject: "This is where most of the models either rest on the assumption that slip occurs between reinforcement and concrete or the opposite; that strain compatibility between the two materials exist and, therefore, no slip occurs."

In the following section, a selection of models will be introduced where the contradicting assumptions of the two different approaches will be obvious. The bond-slip approach is mainly governed by the ability of the bond to transfer stresses from reinforcement to concrete while the no-slip approach is governed primarily by the size of the cover. Firstly, the two different approaches will be introduced, and secondly, it will be described how they can be used to estimate crack spacing and crack widths in tensile members.

Lastly, a model that combines the two theories will be described, which is the model used in both the Eurocode and the fib Model Code.

The bond-slip approach

The bond-slip approach is accepted and widely used for estimating crack widths. The approach has been refined by various researchers, e.g. Leonhardt[14], Marti et al.[29], Nielsen[7], Holkmann[30], Fernández Ruiz et al.[31] and Shima et al.[32].

The principle drawing in Fig. 2.21a shows how the reinforcement carries the total force at a crack where the strain in the concrete is zero. In between cracks, the bond stresses at the interface between the reinforcement and concrete transfers stresses from the reinforcement to the concrete. The difference between the elongation of the reinforcement and the concrete is defined as the slip. Due to the fact that tensile strains in concrete are very small compared to strains in the reinforcement, they are often neglected[7]. The slip then becomes:

$$\delta(x) = \int_0^x \epsilon_s(x) - \epsilon_c(x) dx \approx \int_0^x \epsilon_s(x) dx \quad (2.7)$$

The largest slip is found at the crack, and then it gradually decreases towards the midpoint between two cracks because of the stress transfer to the concrete. At the distance S_0 from a crack, described earlier, strain compatibility between the concrete and the reinforcement is established, and no slip occurs. This distance is called the transfer length and defines the length required for the stresses in the concrete to reach the tensile strength.

A result of this approach is that the two faces of a crack are parallel through the whole member, hence the crack width is constant and not increasing with distance from reinforcement as seen in the previous test. Fig. 2.22 illustrates the situation around one crack in a tensile member with an idealised non-linear distributed of bond stresses. The bond stresses can be expressed as the variation of the reinforcement stresses along the bar. The relations between the strains in the reinforcement and the bond stresses becomes:

$$\begin{aligned} \tau_b(x) \pi \varnothing_s &= \frac{\pi}{4} \varnothing_s^2 \frac{d\sigma_s(x)}{dx} \rightarrow \\ \tau_b(x) &= \frac{\varnothing_s E_s}{4} \frac{d\epsilon_s(x)}{dx} \end{aligned} \quad (2.8)$$

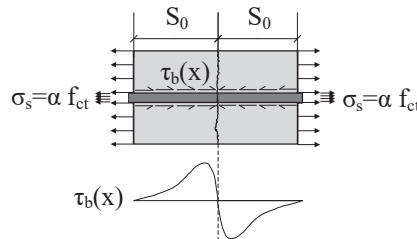


Figure 2.22: The bond-slip approach with non-linear bond stress variation

If Eq. (2.7) and (2.8) are put together, a second order differential equation can express the slip:

$$\frac{\varnothing_s E_s}{4} \frac{d^2 \delta(x)}{dx^2} - \tau_b(\delta(x)) = 0 \quad (2.9)$$

Eq. (2.9) is a general equation expressing the bond stress-slip relations from where a variation of the slip along the reinforcement bar, $\delta(x)$ can be derived for a certain bond stress variation, $\tau_b(\delta)$. [32] The second

order differential equation for the slip becomes more or less complex to solve depending on the expression for the bond stress distribution, $\tau_b(\delta)$. Gambarova et al.[33] describe an approach to solving it analytically while a numerical approach to solve is described by V. Ciampi and R. Eligehausen[34].

No matter how the second order differential equation is solved, the following steps are required to describe the stress, strain, slip, and bond stress variation along a reinforcement bar embedded in concrete:

1. A bond stress-slip relation, $\tau_b(\delta)$, is defined.
2. A relation between the slip and the distance, $\delta(x)$ is deduced from the second order differential equation, in Eq. (2.9).
3. From the slip, $\delta(x)$, the strain variation in the reinforcement can be found:

$$\epsilon_s(x) = \frac{d\delta(x)}{dx} \quad (2.10)$$

4. From the strain, $\epsilon_s(x)$, the bond stress variations along the reinforcement can be found through the constitutive relations:

$$\tau_b(x) = \frac{\phi_s E_s}{4} \frac{d\epsilon(x)}{dx} \quad (2.11)$$

Shima et al. The affinity between reinforcement strain, reinforcement stress, slip and bond stress, just described, were, among others, investigated through tests by Shima et al.[32]. The test program included both pull-out specimens and longer axial tension tests to be able to investigate the influence of the embedment length. At the loaded end, the specimens had an unbounded length of 10 times the reinforcement diameter, which eliminated effect from development of secondary crack cones in the concrete. The result of one of Shima's axial tension tests is shown in Fig. 2.24 where it is compared to two different bond-slip models described below. The specimen has the following properties:

$$\begin{array}{lll} \phi_s = 19.5mm & \phi_c = 500mm & f_y = 820MPa \\ E_s = 190GPa & E_h = 2.06GPa & f_c = 19.6MPa \end{array}$$

The Tension Chord Model The Tension Chord Model (TCM) was established by Marti et al.[29] though the same assumption was used to describe bond-slip by others, for example, Nielsen[7]. The models intended to create a simple yet mechanical model. From studying the tests by Shima, Marti concluded that the intensity of bond stresses could, with good approximation, be assumed constant along the reinforcement. Good results were found when the value of the constant bond stress was assumed equal to twice the tensile strength of the concrete before any yielding was introduced while assumed to decrease to half the size where yielding occurred. Marti calculated f_{ct} from Eq. (2.2) from the Eurocode:

$$\tau_b(x) = \begin{cases} 0.6f_c^{2/3} & \text{if } \sigma_s < f_y \\ 0.3f_c^{2/3} & \text{if } \sigma_s > f_y \end{cases} \quad (2.12)$$

With the use of the relations of Eq. (2.9), (2.10) and (2.11), Marti's assumptions for $\tau_b(x)$ result in a linear variation of concrete- and steel stresses, as illustrated in Fig. 2.23 and in Fig. 2.24a where the model is compared to the test results of Shima's tensile member.

The main difference between Marti's and Nielsen's model is the estimation of the concrete tensile strength, which Nielsen estimates with the earlier described lower bound value in Eq. (2.3) instead of the Eurocode expression.

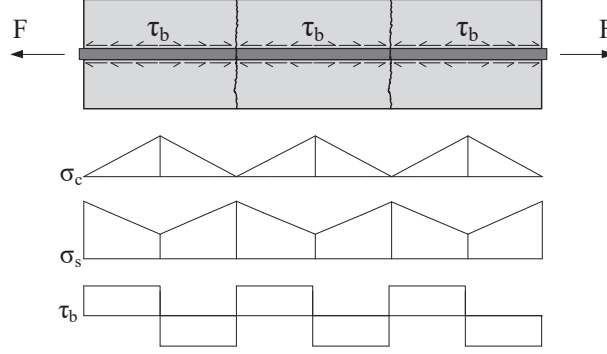


Figure 2.23: Variation of stresses with the use of the Tension Chord Model, for reinforcement in the elastic stage

Fernandez et al. Fernandez et al.[31] also proposed an analytical model for both the pre- and post-yield behaviour of the bond. The model is developed from the assumption that the magnitude of the bond stresses is dependent on the strain in the reinforcement:

$$\tau_b(\epsilon_s) = \tau_{b,max} \sqrt{\frac{\epsilon_s}{\epsilon_y}} \quad (2.13)$$

where $\tau_{b,max}$ is the maximum bond stress from $\tau_{b,max} = f_c^{2/3}$ and ϵ_s and ϵ_y are the actual strain and yield strain, respectively. Firstly, the strain variation is deduced from the affinity between $\tau_b(x)$ and $\sigma_s(x)$ from Eq. (2.11) and (2.13), where $\sigma_s(x) = E_s \epsilon_s(x)$. Secondly the slip is found through Eq. (2.7). Fernandez's Square-Root Model becomes:

$$\epsilon_s(x) = \begin{cases} \left(\sqrt{\epsilon_y} - \frac{2\tau_{b,max}(x-l_p)}{E_s \phi_s \sqrt{\epsilon_y}} \right)^2 & x > l_p \\ \epsilon_{bu} - (\epsilon_{bu} - \epsilon_y) \exp\left[\frac{4\tau_{b,max}(x-l_p)}{E_h \phi_s (\epsilon_{bu} - \epsilon_y)} \right] & x \leq l_p \end{cases} \quad (2.14)$$

$$\delta(x) = \begin{cases} \frac{E_s \phi_s \sqrt{\epsilon_y}}{6\tau_{b,max}} \left(\sqrt{\epsilon_y} - \frac{2\tau_{b,max}(x-l_p)}{E_s \phi_s \sqrt{\epsilon_y}} \right)^3 & x > l_p \\ \frac{f_y \phi_s \epsilon_y}{6\tau_{b,max}} + \epsilon_{bu}(l_p - x) - \frac{\phi_s E_h (\epsilon_{bu} - \epsilon_y)^2}{4\tau_{b,max}} \left(1 - \exp\left[\frac{4\tau_{b,max}(x-l_p)}{E_h \phi_s (\epsilon_{bu} - \epsilon_y)} \right] \right) & x \leq l_p \end{cases} \quad (2.15)$$

where l_p is the extent of the plastic zone and ϵ_{bu} is the bond ultimate strain. The latter is the strain causing a contraction of the reinforcement, perpendicular to the force direction, of two times the rib height. The strain level is derived from the assumption of constant volume under deformation and becomes; $\epsilon_{bu} = \frac{4a}{\phi_s}$ with a being the height of the ribs.

The bond stress distribution is deduced from the constitutive relations in Eq. (2.11) and (2.14):

$$\tau_b(x) = \begin{cases} \tau_{b,max} - \frac{2\tau_{b,max}^2}{\phi_s E_s \epsilon_y} (x - l_p) & x > l_p \\ \tau_{b,max} \exp\left[\frac{4\tau_{b,max}(l_p - x)}{E_h \phi_s (\epsilon_{bu} - \epsilon_y)} \right] & x \leq l_p \end{cases} \quad (2.16)$$

The length of the plastic zone, l_p , can be determined in two different ways. The difference is simply the use of input; one option being the slip at the crack and the other option being the strain at the crack. If the slip at a crack, δ_0 , is used as input, l_p can be derived from the second expression in Eq. (2.15) where $\delta(0) = \delta_0$. This method can be argued to be more theoretical and less applicable because a general way of interpreting and estimating the slip at a crack does not exist. Only if test results exist of the exact case can l_p be determined in this way and for structural design, results of this length does not exist.

The second option is, on the other hand, straight forward as the strain at a crack, $\epsilon_{s,0}$, is a reliable source of input as the reinforcement carries the whole tensile force at a crack. In this case, l_p is derived from the second expression in Eq. (2.14) where $\epsilon_s(0) = \epsilon_{s,0}$:

$$l_p = \ln\left(\frac{\epsilon_{bu} - \epsilon_{s,0}}{\epsilon_{bu} - \epsilon_y}\right) \frac{E_h \bar{\sigma}_s (\epsilon_{bu} - \epsilon_y)}{4\tau_{b,max}} \quad (2.17)$$

In Fig. 2.24b and 2.24c Fernandez's Square Root Model are compared to the test results of Shima's tensile member. The following parameters are used in the model:

$$\tau_{b,max} = 8 \text{ MPa}$$

$$\epsilon_{bu} = 0.07$$

Fig. 2.24b Plastic zone found from slip input δ_0 :

$$l_{p1} = 68 \text{ mm}$$

Fig. 2.24c Plastic zone found from strain input $\epsilon_{s,0}$:

$$l_{p2} = 34 \text{ mm}$$

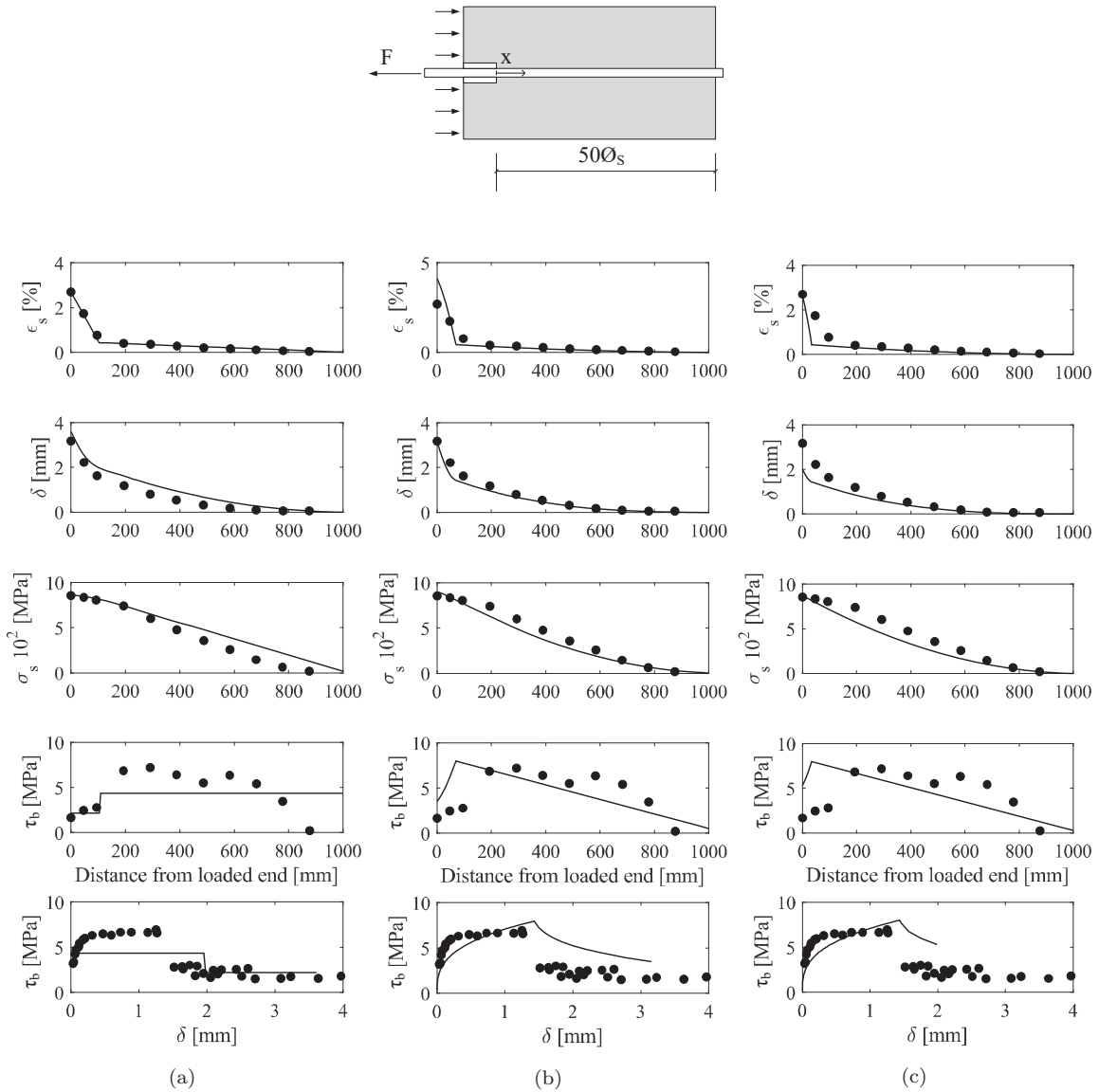


Figure 2.24: Comparison of models and Shima's test: (a) The Tension Chord Model, modified from [29], (b) Fernandez's Model with plastic zone from slip, modified from [31], (c) Fernandez Model with plastic zone from strain, modified from [31]

When comparing the three different modelled stress and strain variations to the test result, none of them stands out by being a significantly better estimate. With respect to the variation of bond stresses $\tau_b(x)$, the more complex model by Fernandez does not seem to estimate the variation better than the TCM. While the TCM estimates the post-yield behaviour best, Fernandez's model estimates the elastic part slightly better. By looking at the graphs, it seems that the TCM estimates the stress and the strain in the reinforcement slightly better, while the slip is best estimated by Fernandez's model when the plastic zone found from the slip is used.

Comparing the two different results found from Fernandez's model (Fig. 2.24b and 2.24c), the estimate using the slip to find the length of the plastic zone yields the overall best result in this particular example. However, as argued earlier, the slip is difficult to estimate without test results, and this model, therefore, relies on the fact that tests have been carried out.

Altogether, the TCM and Fernandez's model both agree well with test, but Fernandez's model is more complex and time-consuming to apply as well because it rests on the undefined slip. It is, therefore, concluded that the TCM and Fernandez's model are of the same quality, but that the TCM is the most applicable because it is more simple and well defined.

Transfer length by the bond-slip approach

For an arbitrary bond stress distribution, the transfer length can be derived from equilibrium considerations, referring to Fig. 2.22:

$$A_s \frac{E_s}{E_c} f_{ct} - A_c f_{ct} = \int_0^{S_0} \tau_b(x) \pi \phi_s dx \quad (2.18)$$

The transfer length, S_0 , is, thus, dependent on the bond stress distribution. The form of $\tau_b(x)$ is proposed both constant, linear and non-linearly by different researchers [35][14][25][26][30][32][31][29]. With a constant bond stress, as in Marti's TCM, $\tau_b(x) = \tau_b$, the expression for the transfer length becomes:

$$S_0 = \frac{f_{ct} \phi_s (1 - \alpha \rho_s)}{4 \tau_b \rho_s} \approx \frac{f_{ct} \phi_s}{4 \tau_b \rho_s} \quad (2.19)$$

In a model resting purely on the bond-slip theory as the TCM the minimum crack spacing is equal to the transfer length as this distance is the smallest from a crack in which the concrete stresses can reach the tensile strength.

Common for the bond-slip models is the fact that they vary with respect to a series of parameters. The following influences the transfer length, and, therefore, also on the crack spacing:

1. The ratio between the bond strength and the tensile strength of the concrete. $\frac{f_{ct}}{\tau_b}$
2. The ratio $\frac{\phi_s}{\rho_s}$, which implicitly means the concrete cover squared.

For quadratic cross-sections:

$$\frac{\phi_s}{\rho_s} \approx \frac{4c^2}{n_s \pi \phi_s} \quad (2.20)$$

No-slip approach

The no-slip models assume as the name indicates that no slip occurs between the concrete and the reinforcement. At the level of the reinforcement, strain compatibility between the reinforcement and the concrete exist and, thus, perfect bond is assumed. Theoretically, a crack is, therefore, of no width at the level of the reinforcement.

From St. Vernants principle [36], concentrated stresses are assumed to spread with a fixed angle to become uniformly distributed at a distance from the applied concentrated stress, as illustrated in Fig. 2.21b. The

transfer length, i.e. the distance from a crack where the concrete stresses are uniformly distributed, thus, becomes proportional to the concrete cover.[37][38][39]

The assumption that the cover is governing for the transfer length, and, therefore, also for the crack spacing, was introduced by Broms, while the approach was later refined by Forth, Base and Beeby extending it to flexural members as well.

Broms Through studies of tests of tensile members, Broms[27] discovered that the spacing of the cracks was approximately equal to the width of the tensile member. He also observed that at stress levels in the reinforcement between $140 - 200MPa$, cracks occurred approximately midway between the first primary cracks.[40] Note that the second observation contradicts what Goto observed concerning the location of the first secondary cracks, which were closest to the primary cracks. The reason is probably that their definition of secondary cracks is different. Broms defines secondary cracks as transverse cracks, like the primary cracks, but which does not penetrate to the surface of the member while Goto defined them as conical cracks.

From his observations, Broms developed a model with the main assumption being that the redistribution of stresses in the concrete at cracking could be based on the theory of elasticity with stress distributions resembling circles. The principle is illustrated in Fig. 2.25. The first primary crack develops at mid-point of the tensile members. Thereafter, circles are drawn with a radius of half the spacing between the primary crack and the end of the member. Within the area of the circle stresses will exceed the tensile strength, and a new crack will form. Whether or not this crack will penetrate through the whole member is determined by whether the circle reaches the surface of the member, if not, it is a secondary crack. The procedure is repeated three times.

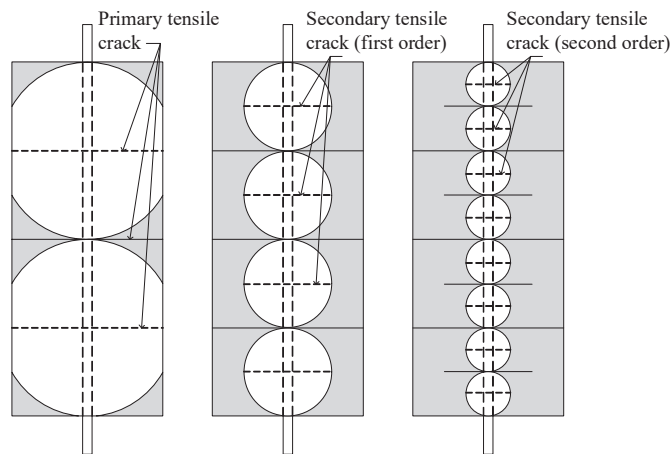


Figure 2.25: Broms assumptions of stress distributions causing the crack pattern in tensile members, reprint from [27]

Beeby In 2004, Beeby[41] investigated the effect of the ratio ϕ_s/ρ_s (the parameter from the bond-slip theory) on the crack width. Through four different test series of tensile members, he concluded that there was no apparent relationship between the crack width and the ϕ_s/ρ_s -ratio. Meanwhile, the investigations showed somewhat linear relations between the crack width and the cover.[42] This conclusion led to Beeby proposing an empirical model for crack width estimates where the spacing of cracks, equal to the transfer length, in this case, is proportional to the cover:

$$S_r = kc \tag{2.21}$$

where c is the cover and $k = 3.05$ is a constant determined from Beeby's tests.

Debonding of reinforcement

Having reviewed the two different approaches to describe the transfer length, S_0 , an additional length, important with respect to cracking, is now discussed called the debonded length. This length is added to the transfer length in some models for estimating crack spacing, which will be treated later in this chapter. The phenomenon of debonding between reinforcement and concrete was illustrated in Section 2.2.1. Here measurements showed a somewhat constant strain level in the reinforcement over a distance on both sides of a primary crack. This result was explained by the conical secondary cracks forming at the ribs of the reinforcement. There are different opinions about why secondary or conical cracks occur and if they occur at all and, therefore, different opinions to how/if they affect the crack spacing. Some models exclude the phenomenon when estimating crack spacing of primary cracks because they believe that they occur after all primary cracks have formed. As an example, Fernandez, in his Square Root Model[31], argues that debonding is a phenomenon that onsets at yielding of the reinforcement. Other tests, by Tammo and Thelandersson[22], showed that conical cracks did not form, but instead the concrete around the bar was merely crushed by the displacement of ribs relative to the concrete. Where the concrete was crushed, the bond was weakened. Thus the same effect of debonding occurred.

The debonded length is the length on each side of the crack where the bond stresses are reduced or non-existing, as illustrated in Fig. 2.26. In this case, the minimum crack spacing becomes a combination of the transfer length and the debonded length:

$$S_{rmin} = S_0 + L_{deb} \quad (2.22)$$

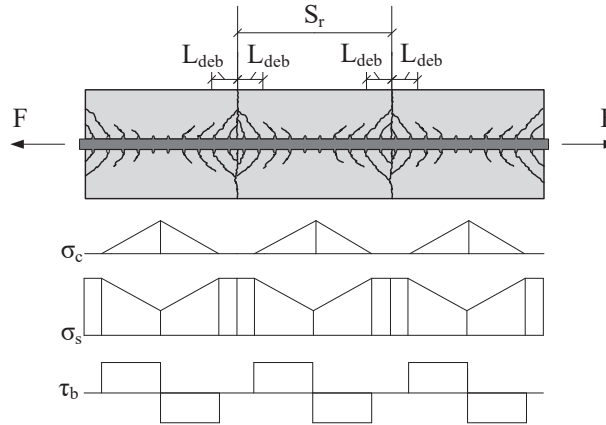


Figure 2.26: Idealised illustration of the debonded length and stress variations between cracks with the assumption of constant bond stresses

Leonhardt Among other researchers, Leonhardt[14] owed the formation of the secondary cracks to the sudden jump in stresses in the reinforcement when a crack is formed, where the tension force is rearranged from the whole reinforced concrete section to the reinforcement alone. Leonhardt's estimate is empirical and dependent on the stress jump at the formation of a crack.

Leonhardt expression for the debonded length:

$$l_{deb,L} = \frac{\Delta\sigma_s}{22.5} \phi_s \quad (2.23)$$

The size of the stress jump is:

$$\Delta\sigma_s = \sigma_{sr} - \frac{E_s}{E_c} f_{ct} \quad (2.24)$$

According to Leonhardt, the secondary cracks causing debonding thus exist on each side of a primary crack at the same load level as the primary crack occurs. The σ_{sr} is the stress in the reinforcement at forming of the primary crack.

This debonding model results in primary cracks that inherits an immediate width at formation. The size of the initial crack width depends on the reinforcement to concrete ratio, being largest for small ratios.

Jokela An empirical expression was introduced for the debonded length by Jokela[43]:

$$L_{deb,J} = \left(1 + \frac{\sigma_{sr}}{200} \right) \phi_s \quad (2.25)$$

In Jokela's expression, the debonded length increases with the increase of the stress level in the reinforcement, σ_{sr} . An increasing number of secondary cracks are assumed to penetrate to the concrete surface with an increase in stress, which will separate an increasingly larger cone from the concrete block between two cracks.

Holkmann An expression for the minimum crack spacing was introduced by Holkmann[30] by combining Jokela's expression for the debonded length with the transfer length derived from the bond-slip approach, similar to that of the Tension Chord Model [29]. When compared to experimental results, Jokela's model seemed to overestimate the crack spacing. As a result, Holkmann proposed an alteration which was consistent with his own analytical model for the debonding, derived from the theory of plasticity:

$$L_{deb,H} = \left(\frac{1}{2} + \frac{\sigma_{sr}}{200} \right) \phi_s \quad (2.26)$$

Nielsen [44] added his considerations to Holkmann's expression for the debonded length by assuming that all cracks develop at the same load level, making the debonded length a constant size, and adding a limit to the value, which is defined by the cover:

$$L_{deb,N} = \min \left(\left(\frac{1}{2} + \frac{f_{ct}}{200\rho_s} \right) \phi_s, 0.67c \right) \quad (2.27)$$

The limit of $0.67c$ is defined from the consideration that if the conical cracks inclined by 1.5:1 relative to the reinforcement, the cracks will become visible on the surface, and thus be regarded as a primary crack when that debonded length is larger than $0.67c$.

Consideration of how the model for the debonded length is verified is crucial. It is difficult to verify the debonded length as the phenomenon occurs internally. The debonded length can be combined with a model for the transfer length and verified through comparison of crack spacings measured in tests. Though, then it is only possible to confirm whether or not the combination of models for the transfer length and the debonded length are in good correlation with experimental results and not whether the estimate of the debonded length resembles the length where stress transfer is reduced.

Relations between extreme and mean crack spacing

Models in the literature, most often, describe the minimum crack spacing and then a factor is required to find the mean or the maximum crack spacing. The spacing of all cracks in a member should lie somewhere in between the minimum spacing, S_{rmin} and twice the minimum spacing. Theoretically, crack spacings will not exceed $2S_{rmin}$ because the stresses in the concrete block between them are able to reach f_{ct} and a third crack will then form.

$$S_{rmin} \leq S_r \leq 2S_{rmin} \quad (2.28)$$

If members were of infinite length, the ratio between the minimum and the mean spacing would be 1.5, but, when taking into account the actual length of members, this relation, by probability, becomes smaller. [45] Beeby [28] derived the ratio for the mean crack spacing by probability considerations of how cracks will distribute within an uncracked length between two formed cracks of four times a minimum crack spacing. The only requirement was that the spacing between two cracks could not be smaller than S_{rmin} and not larger than $2S_{rmin}$. The investigation resulted in an asymmetric probability distribution within the interval in Eq. (2.28) with a mean value of 1.33, resulting in the relations:

$$S_{rm} = 1.33S_{rmin} \quad (2.29)$$

Whether or not a factor like this, determined by Beeby, is used to determine the ratio between minimum, maximum and mean crack spacings with existing models depends on how the model is developed. If the model is empirical, the given spacing is commonly the mean spacing. Meanwhile, a spacing determined as the transfer length with or without some expression for the debonded length is commonly a minimum crack spacing.

Crack width

When it comes to estimating crack widths in structures, the maximum crack width occurring in a member is generally the one of interest. The maximum crack width in a tension member can be derived from the difference between reinforcement and concrete strains between two cracks of maximum spacing. The difference in the existing proposed models, therefore, mainly lies in the way the crack spacing is determined. The general expression for the maximum crack width is:

$$w_{max} = 2 \int_0^{\frac{1}{2}S_{rmax}} \epsilon_s(x) - \epsilon_c(x) dx \approx 2 \int_0^{\frac{1}{2}S_{rmax}} \epsilon_s(x) dx \quad (2.30)$$

where the concrete tensile strains are often neglected, as they are very small compared to strains in the reinforcement, the expression can be simplified even further if applying the mean strain when a linear variation of strains is assumed as in Fig. 2.27.

$$w_{max} = S_{rmax} \epsilon_{sm} \quad (2.31)$$

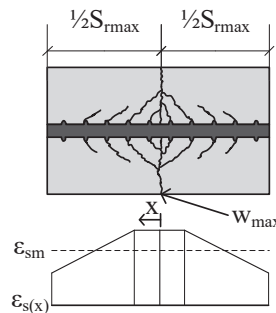


Figure 2.27: Estimation of maximum crack width from a linear variation of strains in the reinforcement

The Eurocode and the fib Model Code 2010

Forth and Beeby [21] argued that the cover is an important parameter with respect to crack width estimates due to shear lag between the reinforcement and the concrete surface and that the effect of the cover is

not nearly significant enough in bond-slip models. They stated, from their investigations, that any model not taking the cover into account, as an independent parameter, cannot be justified when compared to experimental results. This leaves two possibilities for a feasible model, namely where the crack width is; 1) purely dependent on the cover, or 2) a combination of cover and the bond.

In 1965 Ferry-Borges[46] combined the two conflicting approaches; the bond-slip and no-slip theory, into one model, which is the one adopted in the Eurocode[10] and the Model Code 2010[11]. The empirical factors have been adjusted compared to Ferry-Borges' original model and they differ in the Eurocode and the Model Code. The Eurocode design formulas are as follows.

The maximum crack spacing according to the Eurocode 2:

$$S_{rmax} = k_3c + k_1k_2k_4 \frac{\phi_s}{\rho_s} \quad (2.32)$$

where $k_3 = 3.4$, $k_1 = 0.8$ for high bond bars, $k_2 = 1.0$ for pure tension and $k_4 = 0.425$ resulting in:

$$S_{rmax} = 3.4c + 0.34 \frac{\phi_s}{\rho_s} \quad (2.33)$$

The maximum crack width, for tensile members with high bond bars can be estimated with:

$$w_k = S_{rmax} \left(\frac{\sigma_s - k_t \frac{f_{ct,eff}}{\rho_s} (1 + \alpha\rho_s)}{E_s} \right) \quad (2.34)$$

where k_t is dependent on the duration of the load; $k_t = 0.6$ for short-term and $k_t = 0.4$ for long-term loading.

The maximum crack spacing according to the Model Code 2010:

$$S_{rmax} = 2 \left(kc + \frac{1}{4} \frac{f_{ctm}}{\tau_{bms}} \frac{\phi_s}{\rho_s} \right) \quad (2.35)$$

where $k = 1$ and $\frac{f_{ctm}}{\tau_{bms}} = 0.556$ for stabilised cracking, thus resulting in:

$$S_{rmax} = 2c + 0.278 \frac{\phi_s}{\rho_s} \quad (2.36)$$

The crack width is calculated in the same manner as in the Eurocode with one difference, i.e. that the Model Code 2010 adds a contribution from shrinkage.

Instead of considering the Eurocode and the Model Code as models that combine conflicting approaches, of bond-slip and no-slip, they could also be interpreted as bond-slip models that include a debonded length where a cover-term represents the debonded length. The only concern then is the size of coefficient on the cover-term of 3.4 and 2, respectively, resulting in a fairly large debonded length compared to the reviewed models for the debonded length.

2.2.3 Model tendencies

In Fig. 2.28 the reviewed models for the crack spacing and the theory they rest upon are listed. In the following paragraphs, a parameter study of the models is illustrated graphically.

To the right in Fig. 2.29 the variation of the maximum crack spacing is shown with respect to the diameter, ϕ_s , for a tension bar where the cover is kept constant at $c = 50mm$. To the left in the figure, the variation of the other parameters is given, which is a consequence of variation in the diameter. The diameter is increased from $8mm$ to $24mm$ and, as a result, the reinforcement ratio is increased from 0.5% to 4.5% and the ϕ_s/ρ_s -ratio is decreased from $1590mm$ to $530mm$.

Model	Expression	Theory
TCM	$S_{rmin} = \frac{\phi_s}{8\rho_s}$	$2S_{rmin} = S_{rmax}$
	$S_{rm} = \lambda \frac{\phi_s}{8\rho_s}$	$\lambda = 1.33$
Nielsen	$S_{rmin} = \frac{f_{ct} A_c}{\tau_b n\pi\phi_s} + \min\left(\left(\frac{1}{2} + \frac{f_{ct}}{200\rho_s}\right)\phi_s, 0.67c\right)$	$2S_{rmin} = S_{rmax}$
	$S_{rm} = \frac{f_{ct} A_c}{\tau_b n\pi\phi_s} + 2\min\left(\left(\frac{1}{2} + \frac{f_{ct}}{200\rho_s}\right)\phi_s, 0.67c\right)$	
Beeby	$S_{rmin} = 3.05 c$	$2S_{rmin} = S_{rmax}$
	$S_{rm} = \lambda 3.05 c$	$\lambda = 1.33$
EC2	No information is given about relations between mean and extreme	Combined bond-slip and no slip: $S_{rmax} = k_1 c + k_2 S_0$
	$S_{rmax} = 3.4 c + 0.34 \frac{\phi_s}{\rho_s}$	
MC2010	No information is given about relations between mean and extreme	Combined bond-slip and no slip: $S_{rmax} = k_1 c + k_2 S_0$
	$S_{rmax} = 2 c + 0.278 \frac{\phi_s}{\rho_s}$	

Figure 2.28: Reviewed models for spacing of cracks in tensile members

Four out of the five selected models, namely the TCM, Nielsen, EC2 and MC2010, behave in the same manner with respect to variation in the diameter. The tendency for these models is that the crack spacing decreases non-linearly with the increase in diameter. When the diameter is increased the reinforcement ratio increases correspondingly, which means a decrease in the ϕ_s/ρ_s -ratio. Hence, the crack spacing increases with the increase in the ϕ_s/ρ_s -ratio. What the four models have in common is that they all consist of a ϕ_s/ρ_s -term, although only some have included the cover or the debonded length.

Even though the models behave similarly, the value of the crack spacing is very different. Nielsen's model gives higher results than the TCM because the debonded length is included. The MC2010 and the EC2 yield higher crack spacings due to the inclusion of the cover term. The only difference between the two latter models is the different empirical coefficients. Lastly, Beeby's model shows a radically different behaviour where the crack spacing is constant with constant cover, regardless of what reinforcement diameter is used.

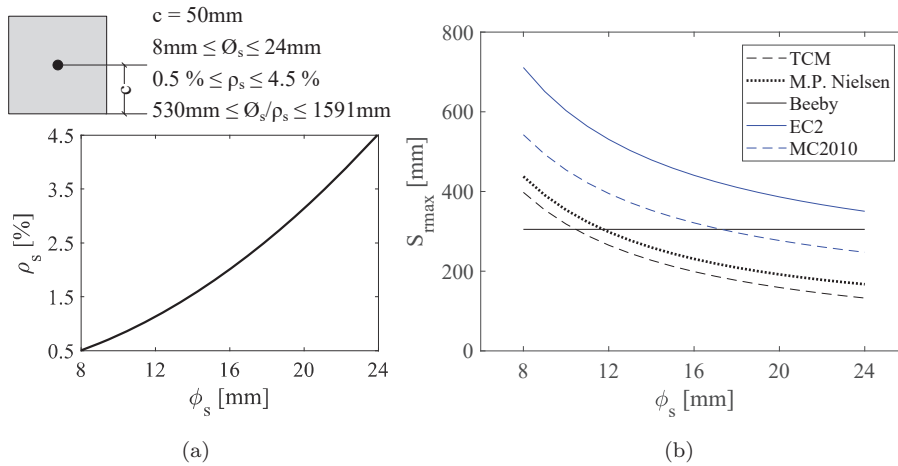


Figure 2.29: Model tendency for a constant cover

In Fig. 2.30 the variation of the crack spacing is shown for a tension bar where the reinforcement ratio is kept constant at $\rho_s = 1.5\%$. Meanwhile, the reinforcement diameter is increased from 8mm to 24mm . To maintain the same reinforcement ratio, the cover is increased from 25mm to 75mm and the ϕ_s/ρ_s -ratio is increased from 400mm to 1200mm .

In this case, all five models show similar behaviour. When the cover and the diameter is increased proportionally, to keep the reinforcement ratio constant, the crack spacing increases for all models, but with different rates. Due to the fact that the cover and the ϕ_s/ρ_s -ratio is increased proportionally the bond-slip and the no-slip models also increase proportionally because their variables increase proportionally.

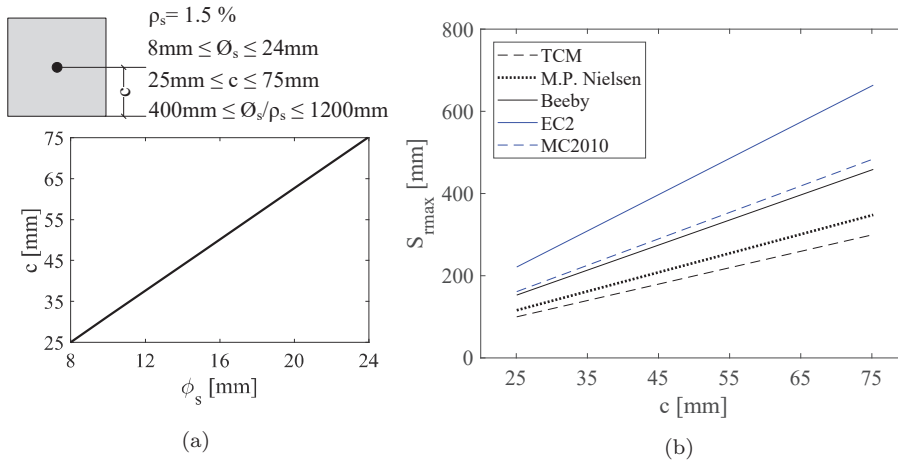


Figure 2.30: Model tendency for a constant reinforcement ratio

In Fig. 2.31 the variation of the crack spacing is shown for the case where the diameter is kept constant at $\phi_s = 16\text{mm}$ while the cover is increased from 35mm to 75mm , resulting in a decrease in reinforcement ratio from 4.1% to 0.9% and an increase in the ϕ_s/ρ_s -ratio from 390mm to 1790mm .

The result of increasing the cover while keeping the same diameter is an increase in crack spacing for all models. When the reinforcement ratio is decreased by enlargement of the cover, the crack spacing increases. Beeby's model behaves slightly different than the other four models, being less sensitive to an increase in cover than the other models. This is due to the fact that the four other models include the squared value of the cover while the cover is only varied linearly in Beeby's model.

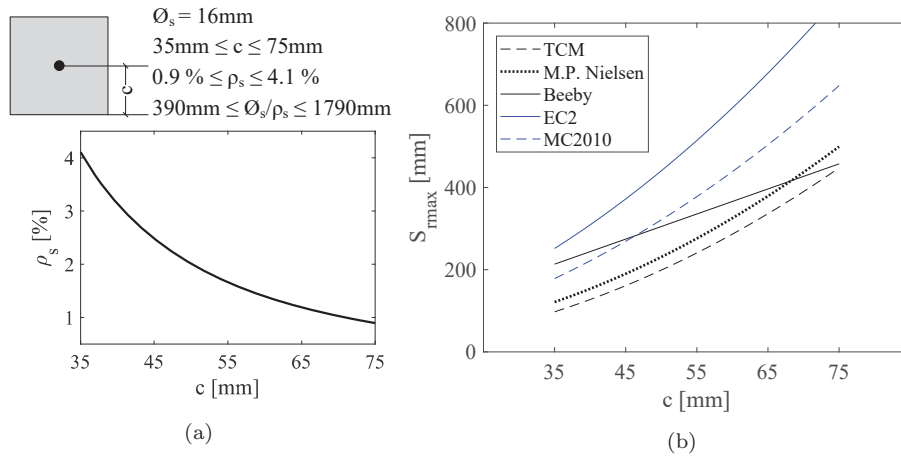


Figure 2.31: Model tendency for a constant reinforcement diameter

The variation of terms in the combined models

The combined models in the Eurocode and the Model Code, consisting of two terms, one dependent on the ϕ_s/ρ_s -ratio and another term dependent on the cover, are investigated further in the following section. Due to the fact that the ϕ_s/ρ_s -term is also dependent on the cover, the relative size of the two terms with respect to different cover sizes is not clear simply from looking at the formulas. Therefore this will now be briefly explored. In Fig. 2.32 the variation of the two different terms in the models is plotted for increasing cover. The parameters used are the same as provided in the left side of Fig. 2.31a.

Fig. 2.32 shows that there is no real difference in how the two models vary, only the size of the terms is different. The plot also shows how the ϕ_s/ρ_s -term's influence increases as the cover increases. This is due to the fact that, as mentioned earlier, the cover-term is proportional to the cover while the ϕ_s/ρ_s -term increases by c^2 .

It is important to notice how the ϕ_s/ρ_s -term almost resembles a straight line even through it is dependent on c^2 . The variation in the cover seems to be too small to cause a parabolic shape. The two different terms dependent on c and c^2 , respectively, are thus approximately two straight lines increasing with the increase in cover, just with different slopes. The parameter study therefore indicates that the cover and the ϕ_s/ρ_s -ratio can be regarded as approximately proportional/correlated within a realistic interval of the cover. However, it should be mentioned that that this proportionality becomes more vague when the cover and diameter are of extreme values, i.e. very small or very large.

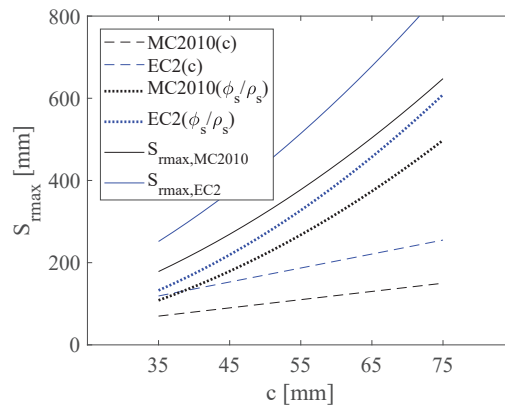


Figure 2.32: Variation of terms in the Eurocode Model and the Model Code

2.3 Cracking in flexural members

This section, concerning cracking in flexural members, is structured in the same manner as Section 2.2 about tensile members. Firstly, a study of different tests is used to describe the cracking behaviour and how it is affected by different parameters. Secondly, selected models describing the crack types, their crack spacings and crack widths are reviewed. Lastly, a short parameter study is carried out for the selected models.

2.3.1 Studies of tests

In 1982 Base[47] stated, in the context of his experimental studies of cracking in flexural members, that the most misleading generalisation in existing models was to assume that the description of flexural cracking could be derived from mechanisms and behaviour observed in tests of uni-axial tensile members. Due to this, Base claimed that a satisfying explanation of the control mechanisms of flexural cracking was absent. This can still be said to be the case, at least in relations to what can be considered a thorough and acknowledged description of the different types of cracks originating from flexure and their cause. Nevertheless, although ambiguous, experimental research of cracking in flexural members exists, which will be describe in the following sections. Base's statement is one of the reasons that the study of cracking in tensile members and flexural members are entirely separated in this current literature review.

Studies of the existing test include the investigation of the influence of the following parameters:

- Depth of the beam
- Reinforcement profile
- Bottom and side cover
- Reinforcement ratio and diameter
- Transverse reinforcement
- Distributed reinforcement
- Concrete compressive strength
- Stress level in the longitudinal reinforcement

The studied parameters are believed to be those that could have influence on the cracking in flexural members. The depth, reinforcement ratio, reinforcement diameter, concrete cover and concrete strength are selected from a review of existing models and represent parameters that could change the spacing of cracks. The stress level in the reinforcement, the type of reinforcement profile, the presence of distributed reinforcement, the depth of the member and the presence of transverse reinforcement are selected because they are believed to change the overall flexural crack pattern and not just the spacing of the cracks.

Types of cracks in flexural members and influence of beam depth

The crack pattern is studied in beams with various depths as the occurrence of the different type of cracks is found to be dependent on the depth.

Sherwood The considerations in the following section are originally from a paper written by the author of this thesis[48] and therefore contain phrases that are directly reused from the paper.

Sherwood[49] studied the size effect related to beams in shear, through an extensive experimental investigation, by varying two parameters; the effective depth of the member and the aggregate size. As part of the analysis, Sherwood observed the development of cracks in the beams in a detailed manner.

The test series consisted of beams with two different effective depths; a small d of 280mm and a five times larger d of 1400mm . The reinforcement arrangement of both the longitudinal and transverse reinforcement was also varied in order to study differences in behaviour with and without transverse reinforcement and distributed longitudinal reinforcement. Here, the beams without transverse and distributed reinforcement are studied.

In Fig. 2.33a and 2.33b the crack pattern at failure is shown for a small and a large beam with the same reinforcement ratio. The shear span was scaled according to the depth to maintain a constant slenderness while concrete cover and beam width were randomly increased in the large beam. When studying the pattern in the large beam, two different systems of cracks are observed; one type penetrating to at least mid-height of the beam and one type concentrating around the longitudinal reinforcement. In contrast, in the small beam, more or less all cracks extend to mid-height.

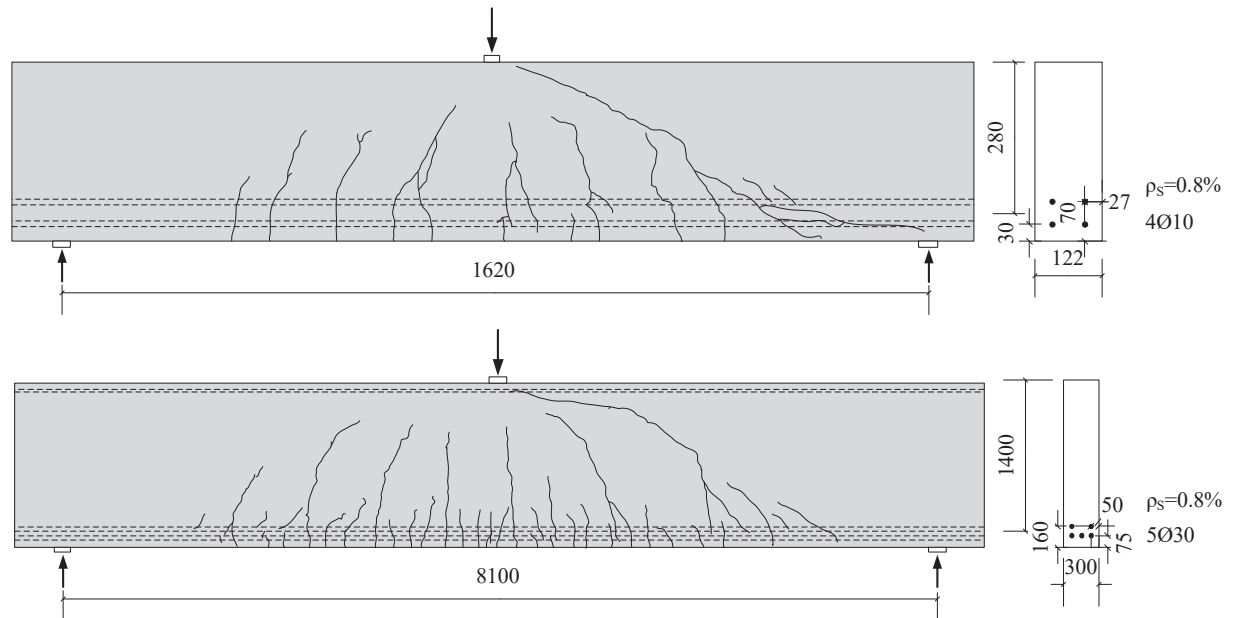


Figure 2.33: Failure crack patterns in beams tested by Sherwood: (a) Small beam (S20-N1), (b) Large beam, scaled 1:5 (L20-N1). Modified illustrations from [49]

In Fig. 2.34a the average spacing of cracks, S_{rm} , relatively to the effective depth d , is plotted as a function of the applied load in the case of the small beam of $d = 280\text{mm}$. The crack spacing is measured at two different levels of the beam; at the level of the concentrated tensile reinforcement and at mid-height of the member. The applied load is represented by the average shear stress across a section in the shear span.

In Fig. 2.34a, attention is given to the observation that the mean crack spacing is of the same order at the two different levels, and roughly equals one half of the effective depth. This observation holds at least for as long as the member is subjected to what must be regarded as service load intensity; an average shear stress less than approximately 0.8MPa . The spacing at mid-height is seen to be slightly smaller than at the level of the reinforcement. This is primarily due to the somewhat curved shape of the cracks in the shear span. When the applied load is increased beyond 0.8MPa , the crack spacing at reinforcement level is seen to decrease. This is due to a gradual development of more cracks, locally around the reinforcement

likely to be associated with initiating failure.

In Fig. 2.34b similar measurements are shown for the large beam. With regard to the relative crack spacing at mid-height, it is seen that the ratio S_{rm}/d remains approximately the same for the two beams, despite the great difference in effective depth.

Even though the large beam failed at a considerably lower shear stress the spacings in the two specimens are comparable at a stress level of around 0.5MPa where the crack spacing at mid-height compared to the location of the reinforcement is increased by 4.4 times in the large specimen and only by 1.4 in the small specimen. In the case of the large beam, it thus makes sense to distinguish between at least two different type of cracks.

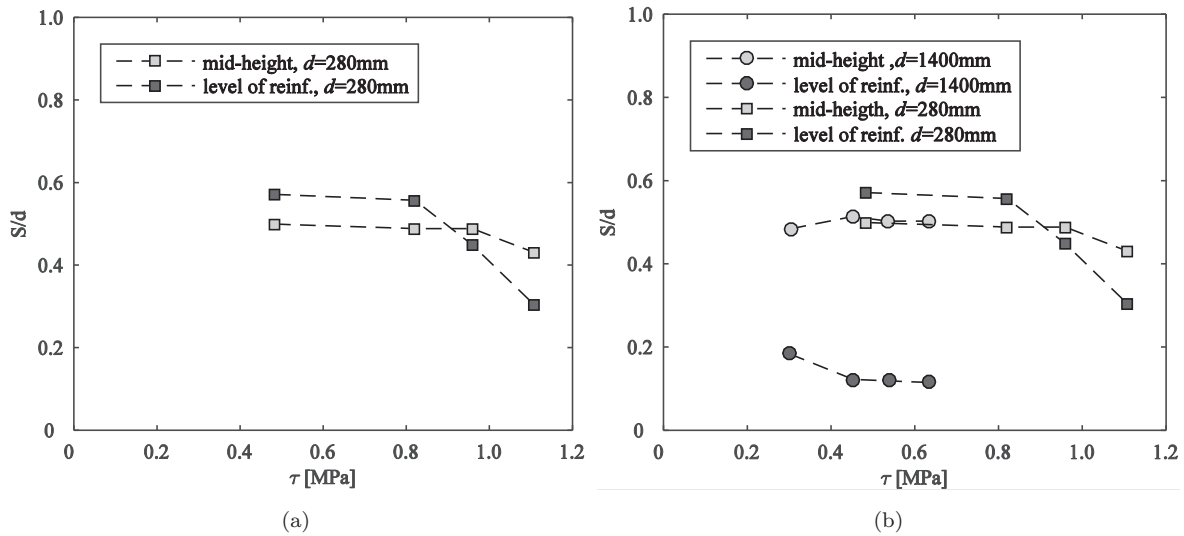


Figure 2.34: Tests by Sherwood: (a) relative crack spacing for small beam, (b) for large and small beam, reprint from [48]

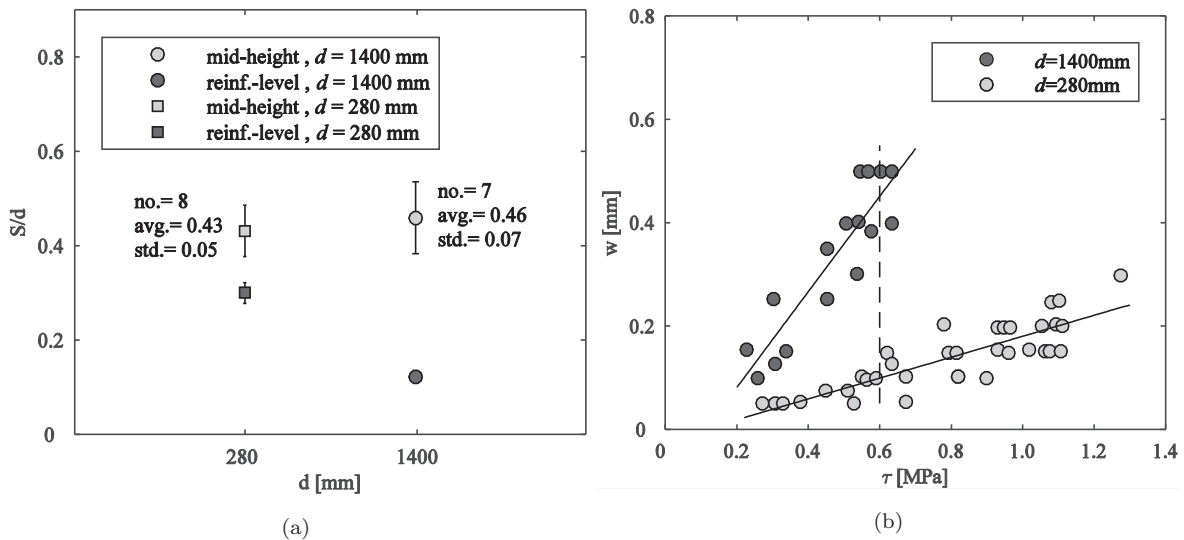


Figure 2.35: Test by Sherwood: (a) mean crack spacing for complete test series, (b) measured crack widths in small and large beams, reprint from [48]

In Fig. 2.35a the mean relative crack spacing at failure is shown for the complete test series, involving a total of eight small beams and seven large beams, and with the depth being the only intended variation.

The crack measurements all refer to a load stage just prior to failure, and basically confirm the tendency just described with respect to the spacing of the cracks at mid-height of the member; an apparent linear relation between the depth of the member and the spacing of cracks. The direct consequence of this linear relation is illustrated in Fig. 2.35b. The plot shows the measured maximum crack width along the shear span for a small and a large beam, respectively, and includes a linear fit for each of the two sets of measurements. For the same relative load level, the expected maximum crack width in the large beam is seen to be approximately five times greater than for the case of the small beam. In other words, the size effect is seen in both the crack width and the crack spacing at mid-height which is scaled by five times, just as the effective depth was scaled by five.

Kim and Park In an experimental investigation of the shear capacity of beams without transverse reinforcement Kim and Park[50] also observed the general behaviour with respect to cracking and presented two types of cracks in the beams.

Eight of the tested beams were subjected to four-point-bending and reserved for the investigation of the effect of size on the shear capacity. The beams had identical slenderness ($a/d = 3.0$) and reinforcement ratio ($\rho_s = 1.9\%$) while they were of four different effective depths ($d = 142, 270, 550, 915\text{mm}$). Unfortunately the author did not provide any information about the concrete cover and as none of the other parameters are scaled accordingly, the cover is not assumed to be either.

Fig. 2.36 illustrates the crack patterns of the four different beams, in which it was observed that the spacing of the cracks at mid-height increased approximately proportionally to the effective depth. Hence, more or less the same number of cracks formed at mid-height in all the beams regardless of the effective depth. The crack patterns also indicate an increasing number of formed cracks at the level of the reinforcement with the increase of effective depth.

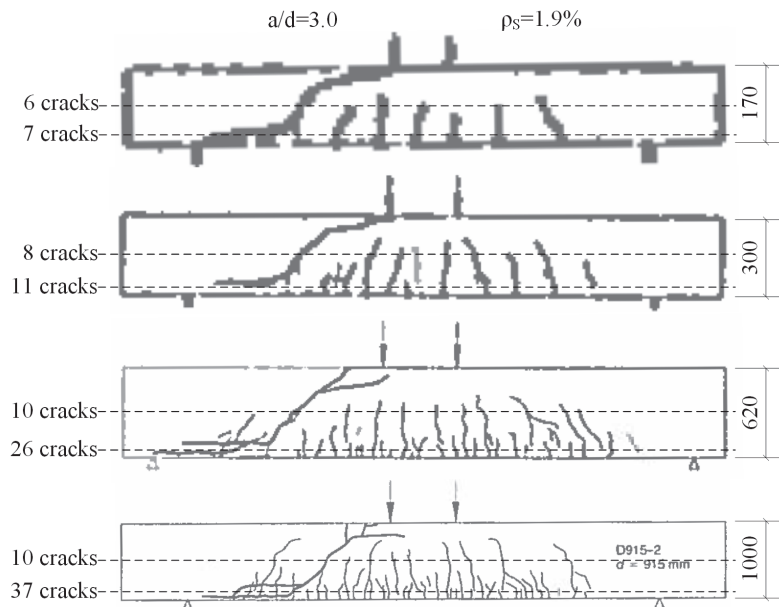


Figure 2.36: Crack pattern at failure in beams by Kim and Park: (a) $h=170\text{mm}$, scaled 5.9:1, (b) $h=300\text{mm}$, scaled 3.3:1, (c) $h=620\text{mm}$, scaled 1.6:1, (d) $h=1000\text{mm}$, reprint from [50].

Kani The proportionality between the crack spacing at mid-height and the depth and the fact that only one type of cracks occurs in low beams of less than $d \sim 300\text{mm}$ was also clearly illustrated by Kani's test [51] in Fig. 2.37. In his four beams, which were part of a larger test series, the cover and width were not

scaled according to the beam depth. However, the reinforcement ratio and the slenderness ratio was kept constant, at 2.8% and 4.0, respectively.

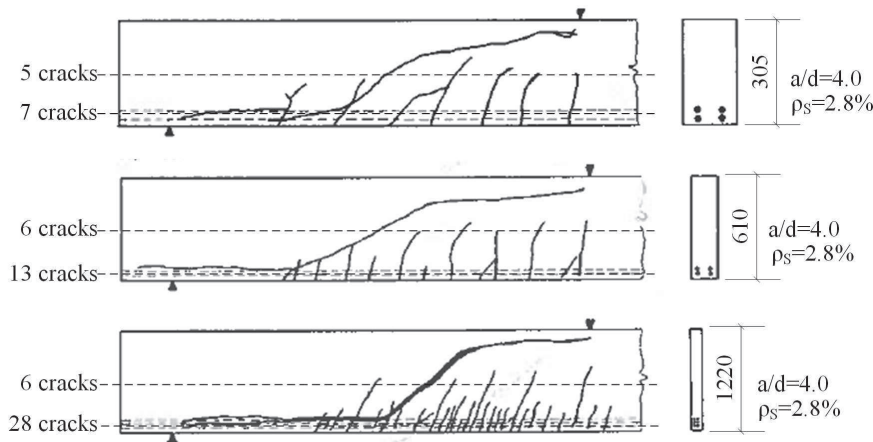


Figure 2.37: Failure crack patterns of test beams by Kani: (a) $h=305\text{mm}$, scaled 4:1, (b) $h=610\text{mm}$, scaled 2:1, (c) $h=1220\text{mm}$ modified from [52]

Summary The two different overall crack systems, observed by the above-mentioned researchers, owing to flexure have also been observed by a number of other researches. Aside from the above, the following can be mentioned: Braam[53], Broms[27], Cavnagnis et al.[54], Feddersen and Nielsen[55], and Leonhardt[14], all of whom differentiate between the following two types of cracks:

Primary flexural cracks: A system of cracks that penetrates approximately to the position of the neutral axis.

Local secondary cracks: A system of minor cracks found in between the primary cracks that are located in the vicinity of the longitudinal reinforcement.

The experimental study of the influence of beam depth indicates that:

- Two different crack types owing to flexure develop in beams which are described above. The secondary cracks are not always present and appear to form when beams reach a height of around $250 - 350\text{mm}$. At this stage it is uncertain whether parameters other than the depth (such as cover) could also have an influence on the development of secondary cracks.
- The spacing between the primary cracks is proportional to the beam depth. As a consequence the maximum crack width also increases proportionally to the depth of the beam.

Influence of reinforcement profile

Base et al. One of the main reasons that Base[47] believed that cracking in flexural members could not be solely explained from mechanisms of uni-axial tension was owed to his observations regarding the influence of bond on cracking in flexural members. He studied this through an extensive experimental investigation presented in a two-part research report from 1966[39]. From the findings in these tests, Base states the following:

“With the benefit of hind-sight it is obvious that, in a reinforced concrete beam subjected to significant bending moment, a pattern of closely spaced flexural cracks is a prerequisite to its adoption of a (smooth)

deflection profile - and that this prerequisite exists even if there is no 'local bond' between the concrete and the reinforcing bars.”[47]

His test results thus convinced him that multiple cracking would occur in flexural members, irrespective of the type of reinforcement used, because it was necessary if deformation primarily takes place in the cracks and if the beam should deform with a smooth deflection curve. The main conclusion from his extensive research was that the principal influencing parameter on crack spacing and width was the distance from the reinforcement to the considered location and the distance from the neutral axis.

A total of 133 beams were tested in four-point-bending to investigate factors influencing both width and spacing of cracks in the constant moment span without transverse reinforcement. Sixty of these beams were reserved for the investigation of the influence of the type of reinforcement. These 60 beams were divided into two major groups; the A-series of 36 beams all with a reinforcement ratio of $\sim 2.3\%$ and the M-series of 24 beams, with a reinforcement ratio of 0.93% . In the A-series, five different reinforcement profiles were tested; mild plain round steel and four different deformed bars (square twisted, deformed - cold worked, lightly deformed - hot rolled, heavily deformed - hot rolled). In the M-series only plain and heavily deformed steel bars were included. All types of reinforcement were described as being in the state “as milled” and any possible rusting was removed by wire brushing. Fig. 2.38 provides a picture from the report of the different reinforcement bars.

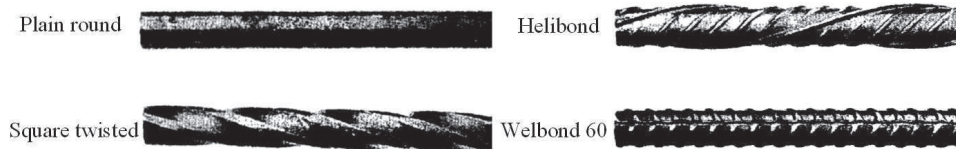


Figure 2.38: Different reinforcement types used in the test series by Base et al., reprint from [39]

The effective depth, width, bottom and side cover and total reinforcement area were all kept constant within each of the two series. The only variables were the reinforcement diameter, number of bars and type of reinforcement, as shown on Fig. 2.39. In the A-series, six beams were cast with plain bars and 30 with deformed bars, while in the M-series, 12 beams were cast with each of the two reinforcement types.

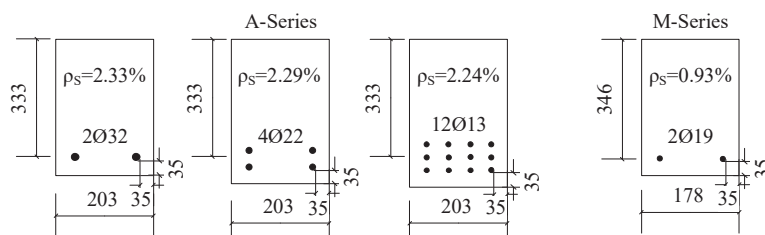


Figure 2.39: Cross-sectional properties of tests series by Base et al.

From looking at the crack patterns in the tested beams, the beams equipped with the plain bars could not be distinguished from the others. An example of this is shown for two beams from the M-series in Fig. 2.40. When studying the measurements of the crack widths and the number of cracks a small difference was found. On average, about 10% fewer cracks had developed in the beams with plain bars, resulting in 20% and 13% larger mean crack widths, measured at the same steel stress, for the A- and M-series, respectively.

Base et al. stated that a reason for the unexpectedly small difference could be that the adhesion between that reinforcement and concrete was not lost at the stress levels the reinforcement reached ($300 - 450\text{MPa}$). Base et al. also emphasised that within the results for the deformed bars alone the variations were just as

large as they were between the beams with plain and deformed bars.

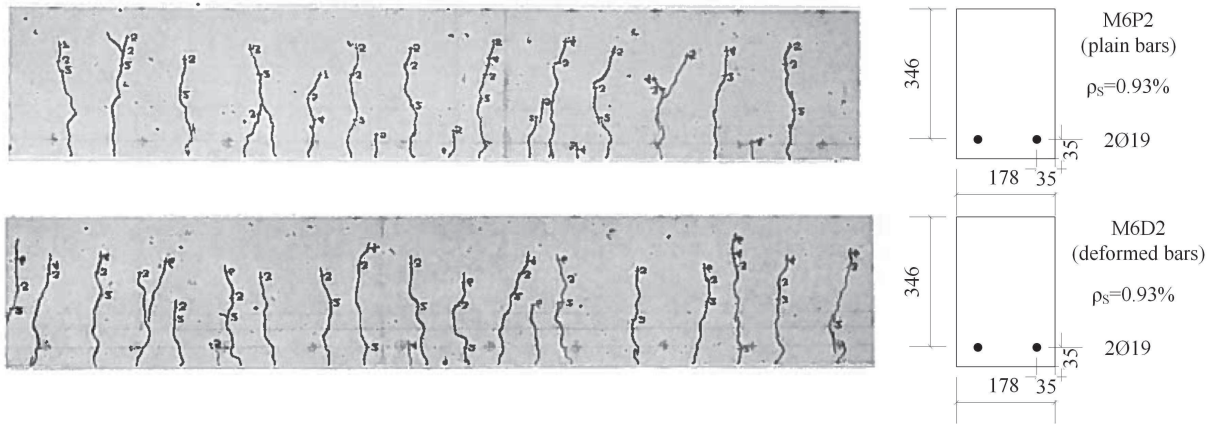


Figure 2.40: Comparison of crack patterns in constant moment span of beams with plain and deformed bars from M-series

The following are subjective notes on the results of Base et al.'s tests. Some uncertainty is related to the results due to the quality of measurements. The crack widths are measured with a microscope (25 magnification) and compared across all beams at the same level of concrete surface tensile strains. These surface stains are measured with demec gauges placed in the same level as the cracks are being measured. Because the crack widths and the tensile strains are two independent manual measurements, it is slightly uncertain whether crack widths in the different beams are, in fact, compared at similar stress levels.

From the information and the pictures in the reports, it is not possible to observed actually how smooth the plain bars are and whether they have a rough surface from the wire brushing. A roughness from the wire brushing could be a reason for the similar results for the beams plain and deformed bars.

Leonhardt and Walter The objective of the Stuttgart Shear Tests by Leonhardt and Walter[56] was to investigate the influence of effective depth, reinforcement ratio, bond quality and type of loading on the shear capacity of beams without transverse reinforcement. As part of their study they reported and analysed the crack patterns for all the beams. There were eight beams in the series dedicated to investigating the influence of bond quality on the shear strength of rectangular beams. For all eight beams the width, effective depth, reinforcement ratio and bottom cover were kept constant. The variables were the reinforcement diameter, the number of bars, the type of reinforcement and the type of loading. A photo from the experimental report of the two types of reinforcement is provided in Fig. 2.41.

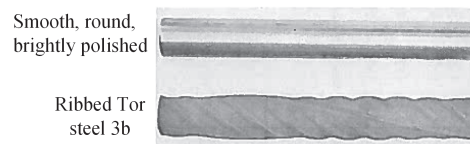


Figure 2.41: The two reinforcement types used in the test series by Leonhardt and Walter, reprint from [56]

In Fig. 2.42 crack patterns are compared for two of the eight beams with a similar reinforcement layout and both subjected to four-point-bending. As the figure shows, there are considerably fewer cracks, approximately half the number, in the beam with plain reinforcement compared to the beam with deformed bars. Measurements of the crack widths also showed wider cracks in the beams with plain bars.

The crack pattern in the beams with plain bars resulted a completely different load transfer than for the beams with deformed bars. Three out of four beams with plain bars failed in bending whereas the four with deformed bars failed in shear. The authors describe this as being due to the lack of stress transfer

between reinforcement and concrete. Instead of a classic beam action, the load was carried by compression trusses from the point load to the bearing with a constant stress in the reinforcement “tie”.

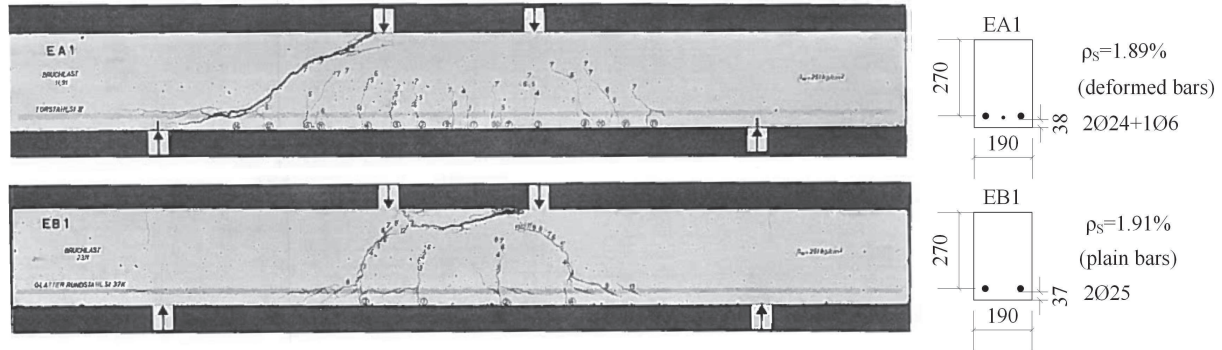


Figure 2.42: Comparison of crack patterns beams with plain and deformed bars from test by Leonhardt and Walter

The following are comments on the results from the author of this thesis. No information exists regarding the size of the side cover, which could have an influence on the number of cracks visible on the side face of the beams. However, it can be assumed that the side cover is approximately the same as the bottom cover in these tests.

Attisha To investigate the effect of type of reinforcement, among other things, in both serviceability and in ultimate limit state, Attisha [57] conducted a series of tests. The main variables in series A and B, listed in Fig. 2.43b, were the type of reinforcement, reinforcement diameter and reinforcement ratio. The cross-sectional dimensions, number of bars and cover were kept constant, which meant a slight variation in effective depth with variation in the reinforcement diameter. A total of eight beams were comparable with respect to reinforcement type, where two beams were cast with plain bars degreased with acetone before casting and the remaining with the four different deformed bars shown in Fig. 2.43a.

The results of the measured crack spacings, listed in Fig. 2.43b, show a slightly larger mean crack spacing in the beams with plain bars, which is comparable to the results by Base et al. Attisha refers to Base’s tests and states that the results of crack width measurements were found to agree well with his own. The beams failed at very different loads due to different yield stresses of the reinforcement ranging from 276MPa for the plain bars to 414 – 897MPa for the deformed bars. Attisha accounts for the fact that the crack patterns in all the beams stabilised at steel stress ranging from 200 – 250MPa which allows for the values in Fig. 2.43b to be compared. Attisha’s investigation of the influence of stress level on the crack pattern will be reviewed in a later section of this chapter.

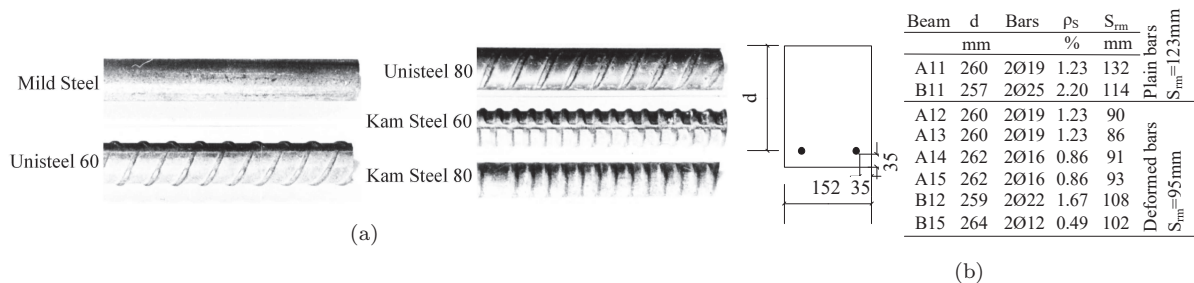


Figure 2.43: (a) Five reinforcement types used in the test by Attisha, (b) Cross-sectional properties and measured mean crack spacings at failure

Summary The experimental study of the influence of the type of reinforcement profile gives somewhat conflicting results. Two of the three authors (Base et al. and Attisha) agree on the fact that plain bars do not have at large influence on the crack spacing and crack width compared to beams with deformed bars. In their tests the difference between the crack widths in beams with deformed and plain bars was only 13 – 20%, which was within the variation of the results of identical beams. There are a number of possible reasons why Leonhardt and Walter’s results contradict this:

- The most obvious is that there was a large difference in how smooth the plain bars in the different test series were. Leonhardt and Walter describe their bars as bright while Base et al. state that rust was removed with a wire brush. This could indicate that the surface of Base et al.’s plain bars were more rough and therefore able to transfer larger stresses to the concrete between cracks.
- The second large difference in Leonhardt and Walter’s beams is that the constant moment span is approximately three times smaller than in Base et al.’s and Attisha’s beams. As Leonhardt and Walter’s main focus was the shear span, the constant moment span was only $500mm$, while it was $1500mm$ in the two other test series. This could potentially also have an influence on the crack pattern.
- Lastly, the lack of information about the side cover in the test by Leonhardt and Walter should be mentioned because the side cover could have an influence on how many cracks are visible on the surface of the beam.

A couple of other conclusions from the investigations are:

- No significant secondary cracking was seen to develop in any of the beams. This may be because they did not occur, due to the small effective depth of all beams ($247mm - 346mm$) or possibly that focus on registering them was not there.
- More than one crack developed in all the beams with plain bars from three independent test series. In all cases, it can therefore be concluded that multiple flexural cracks can be developed regardless of the bond quality.

Influence of bottom and side cover

Through a study of existing tests as well as his own tests, Taylor[52] investigated how the shear capacity of beams was affected by the structural scale. Previous tests had shown that the relative strength decreased significantly with the increase of beam depth. This was sought to be validated or invalidated. Taylor addressed the incorrect scaling of the geometrical properties as one of the main issues of many existing test series which showed great importance, not only for the shear capacity, but also with regard to cracking. He claimed that only when concrete cover, both bottom and side cover, reinforcement layout, bar dimensions and aggregate size were scaled properly according to the beam depth was it possible to compare crack patterns and most clearly identify controlling mechanisms. From renderings of crack patterns in beams from three different test series, Taylor showed that the scaling, in particular, of the cover had an influence on the crack pattern. The three test series were conducted by Leonhardt and Walter[56], Taylor[52] and Kani[51]. The authors’ findings and Taylor’s comments are elaborated in the following.

Leonhardt and Walter Two sub-series within Leonhardt and Walter’s[56], aforementioned test programmes were reserved to investigate influence of scale. In the D-series, shown in Fig. 2.44a, four different beam depths ($d = 70mm - 280mm$) were tested, with a scaling of 1:2:3:4. The slenderness and reinforcement ratio were kept constant, at 3.0 and $\sim 1.6\%$, respectively, while the cover, shear span, and reinforcement diameter were scaled. The same concrete mixture, including aggregate size, was used in all

members. As Fig. 2.44a shows, the four different beams had similar crack patterns at failure without any real increase in the number of cracks with the increase of beam depth. Furthermore, all cracks were more or less primary, penetrating towards the neutral axis, while no secondary cracking was detected. The four beams thus confirm the primary crack spacing's proportionality to the member depth.

In Fig. 2.44b the C-series, from the same programme, is shown. The depths of these four beams were again scaled by 1:2:3:4 with depths of $d = 150\text{mm} - 600\text{mm}$. However, cover, diameter and layers of reinforcement were not scaled properly with respect to the depth as they were in the D-series. The reinforcement ratio was kept at 1.3% which was achieved with different numbers of 16mm rebars. The bottom cover was kept constant at 30mm and the side cover was arbitrary chosen to 50mm, 30mm, 35mm, 40mm, respectively.

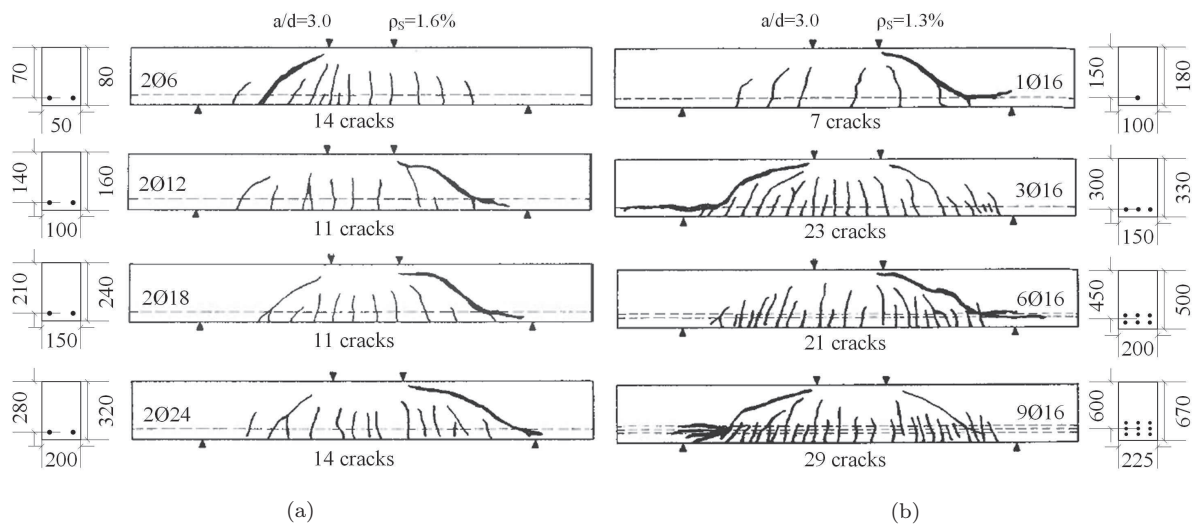


Figure 2.44: Test by Leonhardt and Walter[56], modified from [52]: (a) D-series, beams with scaled parameters, (b) C-series, beams without properly scaled parameters

When comparing the crack patterns illustrated in Fig. 2.44b, a large difference can be observed, especially between the beam with $d = 150\text{mm}$ and the other three of $d = 300, 450, 600\text{mm}$. An increasing number of cracks at the tensile reinforcement is seen with the increase of member depth. In Taylor's analysis of the results he attributed this to the fact that the tensile reinforcement was better distributed in the large beams. The amount of reinforcement compared to the area of concrete symmetrically around the reinforcement was larger in the highest beams.

The following are subjective comments to the results of the tests. Out of the eight beams in total, three of the beams develop significantly more cracks than the others. These beams were the three largest of the eight beams, which could indicate that it is due to the formation of secondary cracks that did not develop in the beams below 330mm. It could also be due to the decreased cover compared to the size of d . The smallest beam ($d = 180\text{mm}$) had the largest cover and the smallest amount of cracks while the three other beams in the C-series had a similar number of cracks.

Taylor With regards to Taylor's own tests, the four beams were scaled on all parameters with the factors 1 : 1.66 : 3.32 : 6.64 with effective depths between $d = 140\text{mm} - 930\text{mm}$. The crack patterns in Fig. 2.45 show similar tendencies as the results reported in Leonhardt and Walter's D-series, where the same procedure was used with respect to scaling of all geometrical sizes.

From his investigations regarding the crack patterns, Taylor concluded that the geometry of the beam (the concrete area) in relation to the reinforcement design had a large influence on the crack pattern. In other words, he regarded the concrete cover to be a governing parameter.

What Taylor did not comment on, with regard to the secondary cracks, is that because the beams all failed in shear, the stresses in the reinforcement, causing the crack pattern, are different and not necessarily yielding. In Sherwood's[49] tests, discussed earlier, new secondary cracks kept occurring until failure and therefore the reinforcement stress level at failure could be influential with respect to the number of developed secondary cracks. Another concern is how the crack patterns were registered, since no secondary cracks were observed in Taylor's beams even though they are above the aforementioned limit of around $d = 300 - 500mm$, above which secondary cracks are seen to form. It is unknown whether it was because they did not occur or that they were not observed due to either quality of equipment or simply because attention was mainly directed towards the primary cracks.

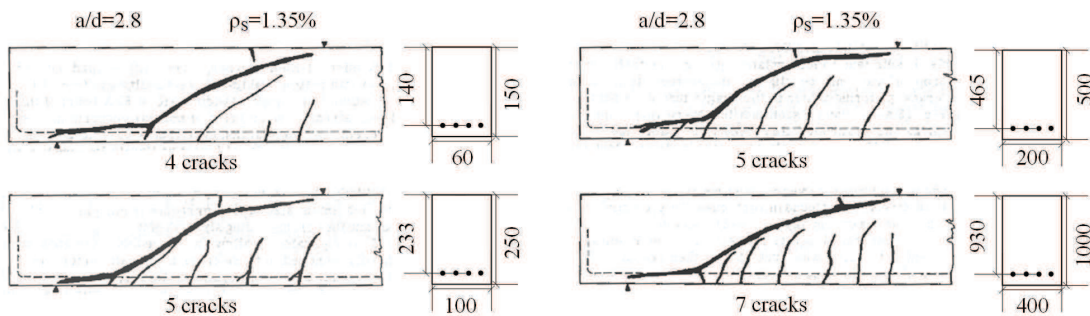


Figure 2.45: Test by Taylor, modified from [52].

Kani The last test series that Taylor commented upon with respect to importance of the scaling of depth to the cover was the tests by Kani[51], also referred to earlier. In these tests, the cover was not scaled according to the beam depth, thus the same prerequisites as the C-series by Leonhardt and Walter. If Fig. 2.37 and Fig. 2.44b are compared it is also clear how the tendency is the same with respect to an increasing number of cracks appearing as the depth to cover ratio becomes larger.

Caldentey et al. A paper by Caldentey et al.[58] presents an experimental study of the effect of cover, $\phi_s/\rho_{s,eff}$ -ratio and transverse reinforcement on crack spacing and crack widths in beams subjected to four-point-bending. The current study consists of 12 beams with the following parameters kept constant; cross-sectional area, span of constant moment ($3520mm$) and concrete strength. The main measurements during testing were crack spacings and surface strains. The crack widths were determined from measurements of the strains using extensometers on the surface of the beam along the tensile reinforcement. The mean crack width was determined from the strain divided by the number of cracks within the measuring length. Crack spacings were determined by direct measurements on the surface of the beam. The specimens were named after the structure; xx-yy-zz, where xx denotes the bar diameter, yy is the cover in mm and zz is the stirrup spacing in cm where 00 means no stirrups.

In Fig. 2.46 crack patterns are shown for the beams without stirrups. Within the four beams, two different cover sizes ($20mm$ and $70mm$) and two reinforcement diameters ($12mm$ and $25mm$) are used. By comparison, it is clear how the increase in cover from $20mm$ to $70mm$ decreases the number of cracks. This is further elaborated in Fig. 2.47, which plots the maximum crack width on the side of the beams with respect to the theoretical reinforcement stress. The trendlines for the beams with the large cover clearly have a larger inclination than the results for the beams with the small cover. The increase in crack spacing due to increase in cover thus also result in an increase in crack width.

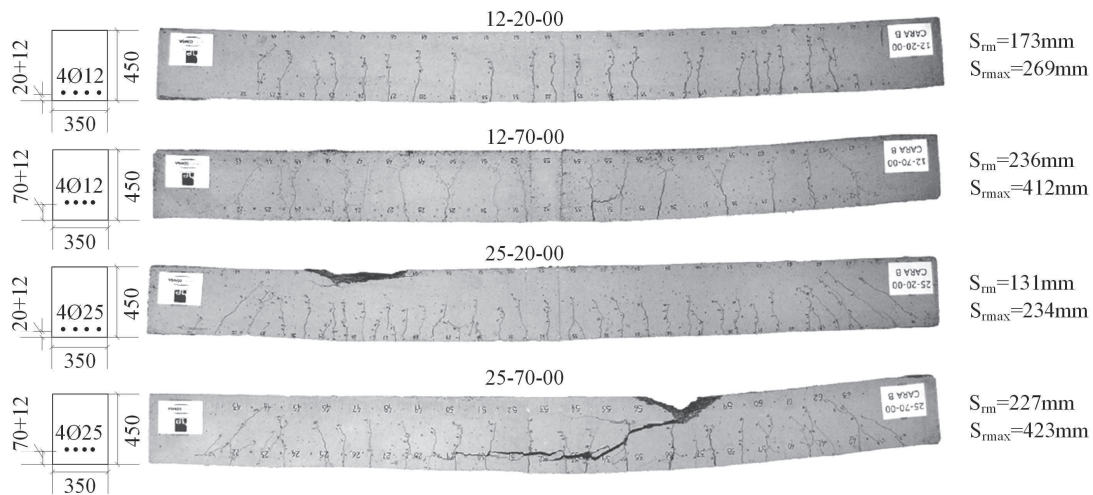


Figure 2.46: Crack patterns at failure for beams with variable cover and reinforcement diameter by Caldentey et al., modified from [58]

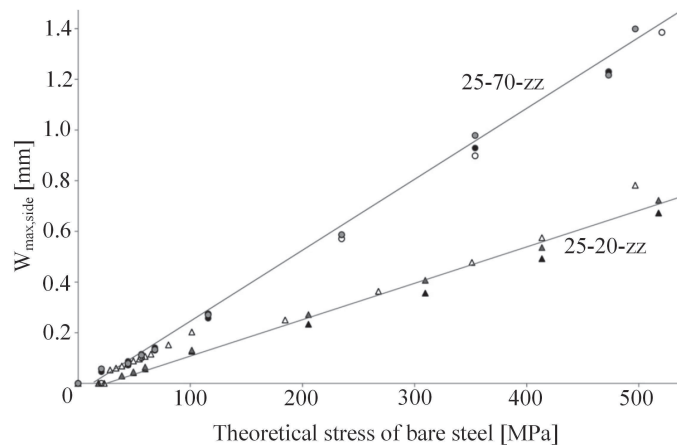


Figure 2.47: Results by Caldentey et al. of maximum crack widths with respect to theoretical stress level in reinforcement in beams bar diameter of 25mm, 20mm and 70mm cover and different stirrup spacings, reprint from [58].

Caldentey et al. claims that there is a connection between the amount of secondary cracks and the cover size. The explanation why is illustrated in Fig. 2.48, where it is assumed that the same amount of secondary cracks exists internally, near the reinforcement, in beams with both 20mm and 70mm cover but some of them have not penetrated to the surface in the beams with the large cover. This could also explain why cracks vary in width within each crack as discussed in the review of tensile members in Section 2.2. At the reinforcement level there are more cracks than at the surface and therefore smaller crack widths than at the surface where there are fewer cracks to distribute the deformation across.

The theory explained above and by Fig. 2.48 is not confirmed by the tests in this study but if it holds, the crack widths at the concrete-reinforcement interface would be the same regardless of the cover. With respect to corrosion of the reinforcement in the large beam, with the largest crack widths at the surface, it could be argued that it would be just as protected as the reinforcement in the beam with a small cover because the crack width is not larger at the level of the reinforcement, only at the surface.

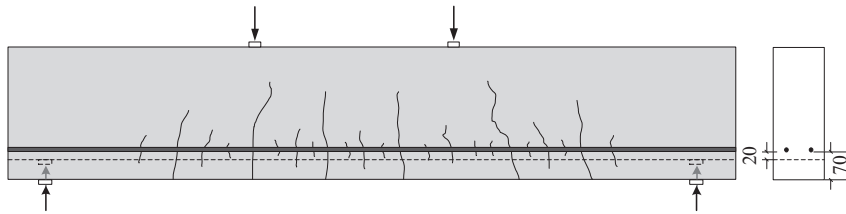


Figure 2.48: Illustration of amount of visible cracks depending on cover size

Base et al. In the experimental study by Base et al.[39], presented earlier, the influence of both bottom and side cover were investigated in 30 beams across three series; C, D and E. In the E-series, both the side and bottom cover were varied by changing the layout of the reinforcement while keeping the outer dimensions constant.

The graphs at the top of Fig. 2.49 show the variation of crack width for three different E-beams where the only variable is the bottom and side cover. The crack widths were measured in the five different levels in the tensile zone shown on the cross-section; b, a-c, d-g, e-h and f-j. The measured crack widths are plotted against the average concrete surface strain at the corresponding level, where the latter is found from Demec gauges and the sum of all crack widths. The straight lines in the three plots illustrate the apparent linear relations between the mean concrete strain and the mean crack width.

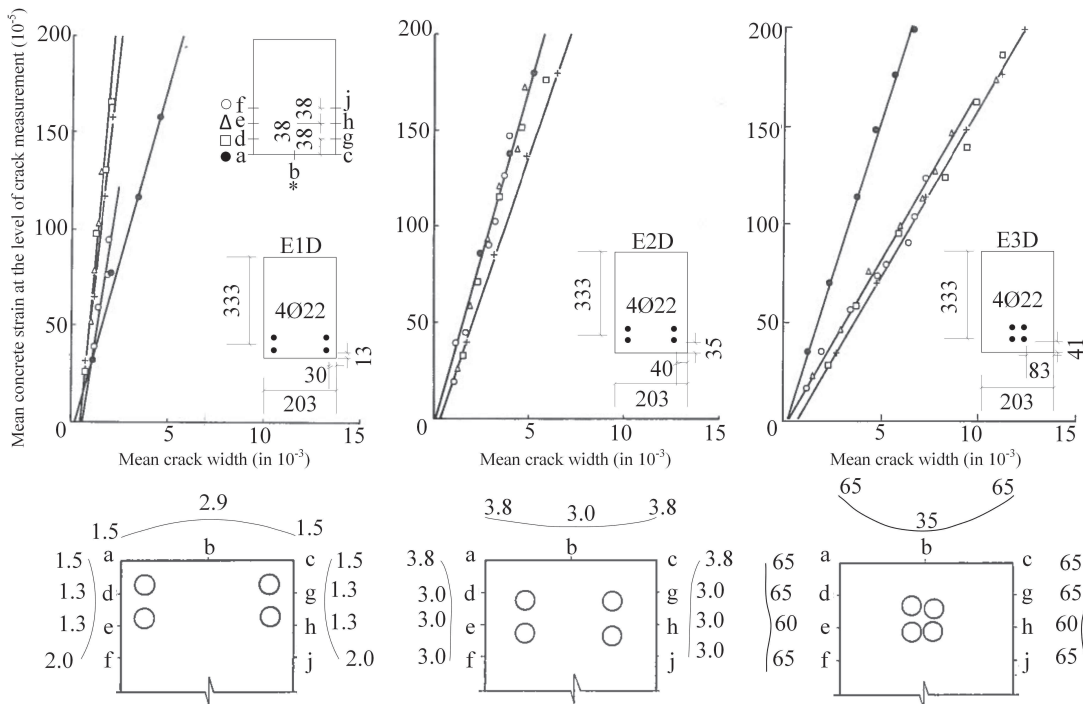


Figure 2.49: Test by Base et al. (top) Mean crack width in relations to mean concrete surface strain (bottom) Variation of crack widths ($in 10^{-3}$) at surface strain of 0.001, for beams with three different side and bottom covers, modified from [39]

Below the graphs in Fig. 2.49, the crack width variations in the cross-sections are shown at mean concrete strains of 0.001. The variations are notably different for the three different reinforcement layouts and it is clear how a larger cover results in a larger crack width at the surface. From this, Base et al. concluded that the crack widths were highly dependent on the distance to the nearest reinforcement bar. It should be noted that the smooth lines between points where the crack widths were measured in the cross-sections

at the bottom of the figure must be an interpretation by the author. The variation could just as well be linear as polynomial.

Beeby A test series by Beeby[59] was conducted as a continuation of the aforementioned tests by Base et al.[39]. From the 133 beams Base et al. analysed, one of the main conclusions was that crack spacing and width showed little or no dependency on bar diameter and reinforcement ratio while a clear linear relation to the distance to the nearest tensile reinforcement was found. The subsequent test by Beeby aimed to investigate whether the same conclusion would hold when the reinforcement had large spacings (more than four times the cover) as can be the case in slabs.

The slabs were tested vertically in order to be able to study the bottom tensile face. A constant moment and a normal force were applied by subjecting the slab to eccentric axial compression. The results of the slab tests led to a number of additional conclusions, the main being that the crack spacing was not only dependent on the distance to nearest bar (the cover) but also on the initial crack height (the depth of the member). Fig. 2.50 illustrates the crack patterns for the R-series, where the total height and effective depth were the only variables whereas the cover was kept constant at 19mm. The patterns show how the crack spacing over bars remains somewhat constant while between bars it increases with increasing depth of the slab. This was also observed by Kaklauskas[60], who stated that the more the height and reinforcement ratio increased, the more clear it became that the crack spacing was not only dependent on the reinforcement ratio both also on the effective depth of the member.

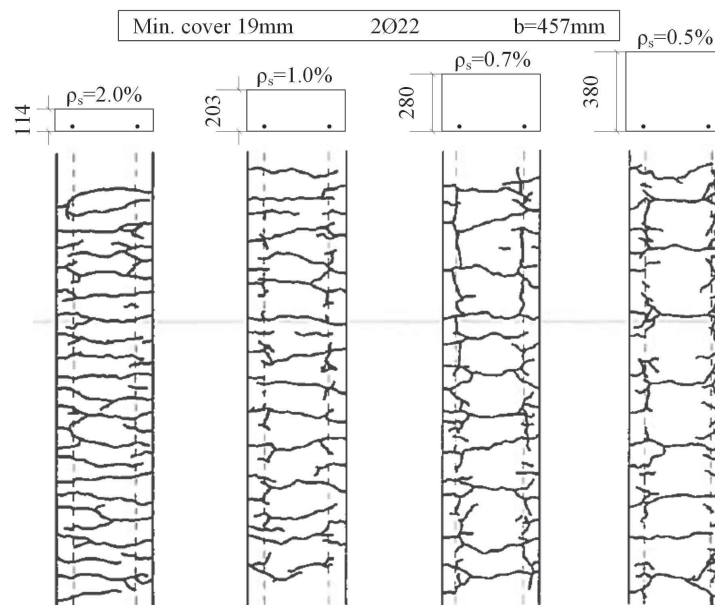


Figure 2.50: Crack pattern on bottom face at failure for R-series by Beeby with variable total height and constant cover, reprint from [59]

Fig. 2.51 shows the crack pattern of the S-series where, in contrast to the R-series, the cover was varied and the effective depth kept constant, thus resulting in a slight increase in total height. Consequently, the crack spacing both over bars and between bars increases with the increase in cover.

Beeby observed that when the distance to the nearest reinforcement became larger than approximately twice the minimum cover, the crack spacing approached a constant value. Hence, the width and spacing of these cracks would be overestimated if they were calculated from the assumption that proportionality exists between the distance from the nearest bar and the crack spacing. In theory, Beeby's crack patterns can be compared to cracking at the side face of beams. Beeby differentiated between two fundamentally

different crack types: 1) being the cracks where the spacing is proportional to the minimum cover/minimum distance to a rebar (secondary cracks), and 2) being the cracks that extend further from the bar than twice the cover, where the spacing is proportional to the initial crack height (primary cracks).

In Beeby's experimental report and analysis there are no comments on how the axial compression force applied to the slabs could potentially effect the cracking. It should also be noted that Beeby actually relates the primary cracking to the initial crack height and not the effective depth as many of the aforementioned researchers.

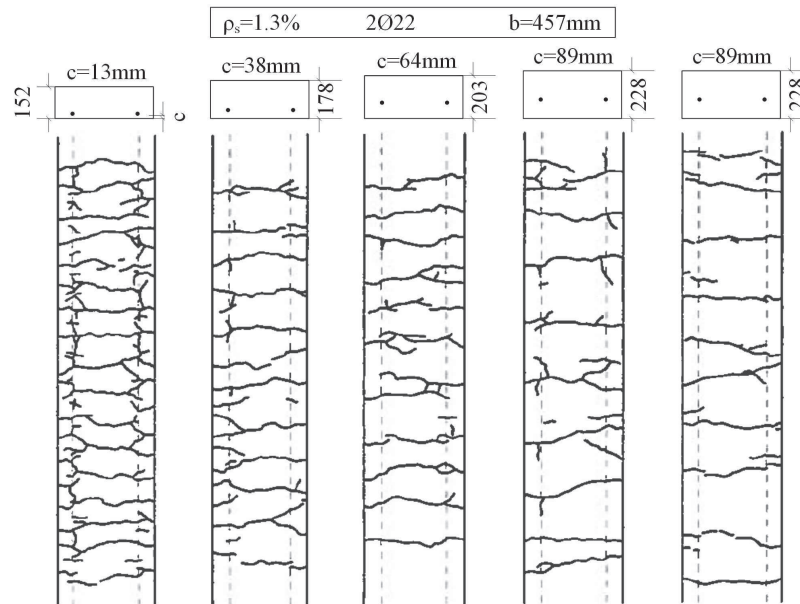


Figure 2.51: Crack pattern on bottom face at failure for S-series by Beeby with variable cover, variable total height and constant effective depth, reprint from [59]

Summary The experimental study of the influence of cover indicates that:

- The number of secondary cracks is dependent on the size of the cover (Taylor, Caldentey et al. and Leonhardt and Walter). The number of cracks visible on the surface decreases significantly with the increase of cover but the same number of cracks exists internally, irrespective of the cover size (Caldentey et al.).
- If the following parameters are scaled corresponding to the depth, the number of cracks is similar regardless of beam depth; bottom and side cover, reinforcement dimensions, and aggregate size. The scaling results in a constant reinforcement ratio. This was concluded from Leonhardt and Walter's beams with $d = 70 - 300\text{mm}$ and Taylor's beams with $d = 140 - 930\text{mm}$. It is uncertain whether no attention was given to the secondary cracks or if they did not occur.
- A linear relation between the surface concrete tensile strains and the crack width was observed (Base et al.). The mean concrete strains means the strains on the surface measured from Demec gauges and the sum of crack widths.
- The crack width on the surface increases with the increase in the cover size/distance to nearest bar (Base et al., Beeby, and Caldentey et al.).
- Crack width and crack spacing is linearly proportional to the distance to nearest reinforcement (minimum cover) when observed at a distances smaller than twice the cover size, which is the cracks that were earlier referred to as the secondary cracks (Base et al. and Beeby).

- Cracks observed at a larger distance than twice the cover, earlier described as primary cracks, have a constant spacing which is linearly proportional to the initial crack height (\approx beam depth) (Beeby).

Influence of reinforcement diameter and ratio

The next section involves investigations of the influence of both diameter and reinforcement ratio. These two parameters are discussed together because, firstly, they are related and, secondly, a great deal of researchers have already investigated the influence of the $\phi_s/\rho_{s,eff}$ -ratio on cracking. The reason is that this ratio is a dominating parameter in a number of acknowledged models resting on the bond-slip approach mentioned in relation to tensile members in Section 2.2.2. The investigations concerning the influence of $\phi_s/\rho_{s,eff}$ thus become investigations into whether these bond-slip models can describe the behaviour of flexural members with respect to crack spacings and crack widths.

Before the results of selected tests are presented, a few comments on the $\phi_s/\rho_{s,eff}$ -ratio will be made. The ratio contains the reinforcement diameter ϕ_s and the effective reinforcement ratio, $\rho_{s,eff}$. The latter is a measure of the amount of reinforcement within an effective concrete tensile zone. This effective concrete area is variously defined from being a concrete area symmetrically around the longitudinal tensile reinforcement to a larger area limited by the location of the neutral axis. The $\phi_s/\rho_{s,eff}$ -ratio can be rewritten to depend on the circumference of the reinforcement:

$$\frac{\phi_s}{\rho_{s,eff}} = \frac{\frac{\phi_s}{n_s \frac{\pi}{4} \phi_s}}{A_{c,eff}} = \frac{4A_{c,eff}}{n_s \pi \phi_s} = \frac{4A_{c,eff}}{C_{rein}} \quad (2.37)$$

where n_s is the number of bars, $A_{c,eff}$ is the effective concrete tensile area and C_{rein} is the total circumference of the reinforcement bars.

Base et al. In the previously presented study by Base et al.[39] of 133 tests, the influence of reinforcement diameter and ratio were investigated separately. In the A-series, presented in Fig. 2.39, a constant reinforcement ratio of $\sim 2.3\%$ was obtained by using different numbers of bars with three different diameters; 2Ø32.8, 4Ø22.2 and 12Ø12.7. In the analysis of the results, Base saw no consistent variation with respect to crack width and number of cracks. For the beams with deformed bars, those with the smallest reinforcement surface area (A1: 2Ø32.8) formed 37 cracks while the A2 beams with 4Ø22.2 formed 38 cracks on average. The A3 beams, with the largest surface area, formed 44 cracks on average though these beams were unintentionally cast with a 20% smaller cover, which Base blamed for the larger number of cracks.

In the G-series, the reinforcement ratio was varied by: 1) using three different diameters with the same numbers of bars, and 2) using the same diameter and three different numbers of bars. The reinforcement ratio varied from 1.12% to 2.29%. Cover and effective depth of the beams were kept constant. No graphs or numbers represent the results, but Base et al. state that from a straight line regression analysis, no correlation between the reinforcement ratio and cracking was found.

Beeby In 2004 Beeby[42] published a paper using, among others, Base et al.'s test results to investigate the influence of $\phi_s/\rho_{s,eff}$ on the crack width. Fig. 2.52a provides the results of the G-series, referred to above, where the cover was kept constant and $\phi_s/\rho_{s,eff}$ was varied by either changing the number of bars or bar diameter. From this plot, as well as plots of results from two other researchers, Beeby concludes that there was no significant influence from $\phi_s/\rho_{s,eff}$ on the crack width variation. On the other hand, if the beams from Base et al.'s investigation, with constant $\phi_s/\rho_{s,eff}$ and variable cover, were plotted against the crack width, as in Fig. 2.52b, a linear proportionality was found.

With regards to a possible subjectivity of Beeby's and Base et al.'s tests, the conclusions are drawn upon results of beams with a limited height and a limited interval of the $\phi_s/\rho_{s,eff}$ -ratio. No beams in the

investigation were larger than 400mm . Furthermore, only a very small number of secondary cracks was observed in the beams by Base et al. Hence, the secondary cracks in larger beams could be affected by the reinforcement diameter and ratio.

At no point has Beeby stated how the effective concrete area was calculated when the relations between $\phi_s/\rho_{s,eff}$ and the crack width were investigated in Fig. 2.52a. Beeby referred to the Eurocode[10] where two different expressions are stated depending on the reinforcement layout. It is uncertain whether both of these were used which makes the investigation slightly in-transparent. In addition, the investigation does not say much about the physical relations between the crack width and the parameters involved in $\phi_s/\rho_{s,eff}$ ($A_s, \phi_s, c, d, h, x_{cr}$) and does not rule out an influence of all of them. Nevertheless, Beeby presents a significantly large study which shows that $\phi_s/\rho_{s,eff}$ seemingly does not have any unique influence on the crack width.

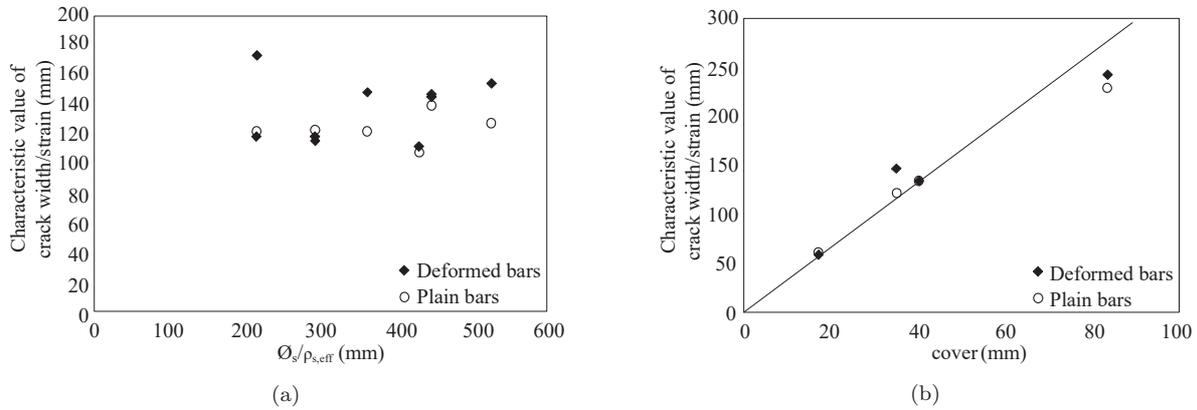


Figure 2.52: Tests by Base et al., reprint from [42]: (a) Relations between crack width relative to concrete strain and $\phi_s/\rho_{s,eff}$ for beams with constant cover, (b) Relations between crack width relative to concrete strain and cover for beams with constant $\phi_s/\rho_{s,eff}$

Fig. 2.53a shows the relations between cover and crack width for all the 133 beams by Base et al. where it is clear that a linear relations exist, but also that some of the other parameters mentioned could have influence, for example, because of the large deviation in results for the many beams with a cover of 35mm . Moreover, it is not stated whether the bottom or side cover have been used in the investigation in Fig. 2.52b and 2.53a or whether the two covers are equal. Hence, the possibility that there is a difference in the influence of the bottom and side cover is not addressed.

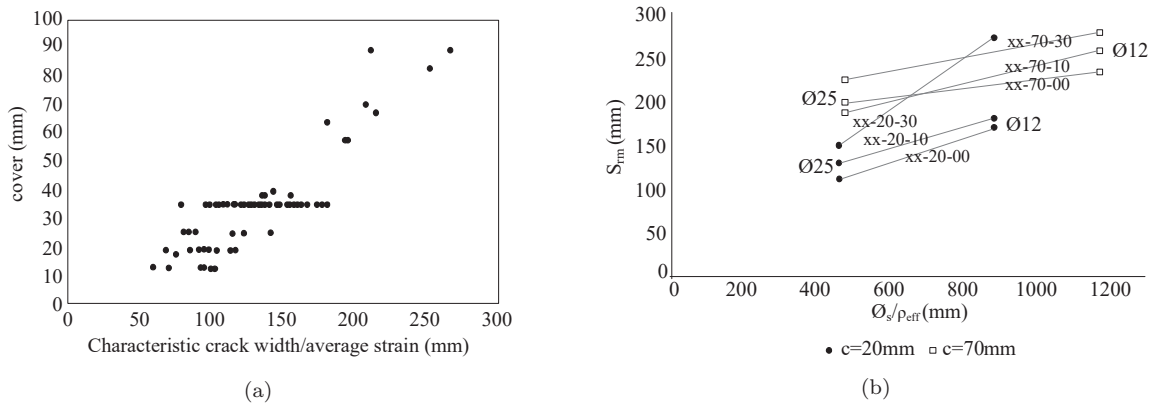


Figure 2.53: (a) Relations between cover and crack width relative to concrete strain for all beams by Base et al. [39], reprint form [42], (b) Relations between measured mean crack spacing and $\phi_s/\rho_{s,eff}$ by Caldentey et al., reprint from [58]

Caldentey et al. In the experimental study by Caldentey et al.[58], also previously discussed, the influence of the $\phi_s/\rho_{s,eff}$ -ratio, estimated by the Eurocode, was investigated. Fig. 2.53b plots the results of the investigation for the beams with two different covers ($20mm$ and $70mm$), two different bar diameters ($12mm$ and $25mm$) and three different arrangements of transverse reinforcement (no reinforcement, $s = 100mm$, $s = 300mm$). Caldentey et al. concluded that a clear tendency towards an effect of $\phi_s/\rho_{s,eff}$ was seen owing to the increase in crack spacing with the increase of $\phi_s/\rho_{s,eff}$ in the figure.

The comments given to the investigations by Beeby and Base et al. also apply to the results by Caldentey et al. even though the conclusion contradicts those of the two other researcher. The effective reinforcement ratio is calculated from two different expressions from the Eurocode. The $\rho_{s,eff}$ for the beams named 25-70-zz are calculated differently than all the other beams. Investigation of the influence of the individual parameters included in $\phi_s/\rho_{s,eff}$ might offer further insight into their connection to the crack spacing. Additionally, due to a possible influence of the stirrups, it could be argued that the results can only be compared two-by-two for beams with the same stirrup spacing.

Kim and Park In Kim and Park's[50] experimental investigation, referred to earlier, the influence of the reinforcement ratio was investigated for beams with a constant height of $300mm$ and ratios of 1% , 1.9% , 3.3% , and 4.6% . The crack patterns of the four beams looked very similar and Kim and Park concluded that the reinforcement ratio showed only little or no significant influence on the crack spacing.

Summary The experimental study of the influence of reinforcement diameter and ratio indicates that:

- For beams up to $h = 400mm$ no consistent variation in crack spacing and crack width was found with respect to either ϕ_s or ρ_s separately (Kim and Park) or the ratio $\phi_s/\rho_{s,eff}$ (Base et al.).
- Beeby found no influence of the ratio $\phi_s/\rho_{s,eff}$ ($h \leq 400mm$) while Caldentey et al. conclude that an increase in crack spacing is seen with the increase of $\phi_s/\rho_{s,eff}$ ($h = 450mm$). Both investigations are slightly vague with respect to how $\rho_{s,eff}$ is calculated.
- From the investigations within this section it cannot be ruled out that one or more of the following parameters has an influence on cracking: $A_s, \phi_s, c, d, h, x_{cr}$, due to the fact that they are not investigated separately and for a representing interval of d bearing in mind that secondary cracks occur for $d \geq 300 - 400mm$.
- With respect to the influence of the cover, nowhere in the literature was it discussed whether it is necessary to distinguish between the influence of the bottom cover and influence of the side cover. Nevertheless, large numbers of the tested beams were cast with different bottom and side covers.

Influence of transverse reinforcement

Caldentey et al. In the previously discussed experimental investigations by Caldentey et al.[58], the influence of stirrups and their individual spacing are investigated. The crack patterns in Fig. 2.54 and 2.55 show the overall effect of stirrups. For each cover size and reinforcement diameter one beam without transverse reinforcement is tested which are compared to beams with the same diameter and cover with transverse reinforcement at spacings of $100mm$ and $300mm$, respectively.

In the beams with a cover of $20mm$, the crack spacing coincided more with the stirrup spacing than the beams with $70mm$ cover. Some tendencies will therefore first be discussed for the beams with the $20mm$ cover. If it is assumed that the beams without transverse reinforcement represent the "natural" crack pattern, it can be seen that the mean crack spacing in the beams with stirrups coincided with the stirrup spacing but with a dependency on the "natural" mean crack spacing. For the beam with $12mm$ bars and cover of $20mm$, in the top of Fig. 2.54, the "natural" mean crack spacing was $173mm$. The mean crack

spacing in the beam with 100mm stirrup spacing was 183mm, which means that one crack forms almost every second stirrup. Meanwhile, for the beam with 300mm stirrup spacing, the mean crack spacing was increased to 281mm, forming a crack for almost every stirrup.

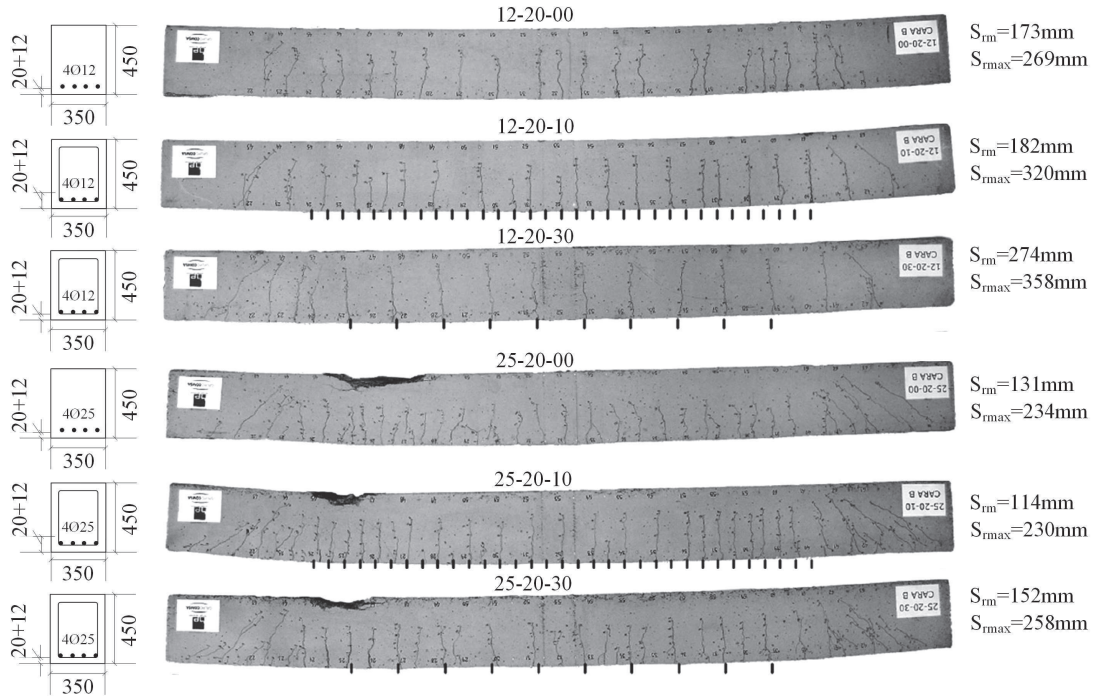


Figure 2.54: Crack pattern at failure in beams with 20mm cover by Caldentey et al. The locations of stirrups are indicated with black marks, reprint from [58]

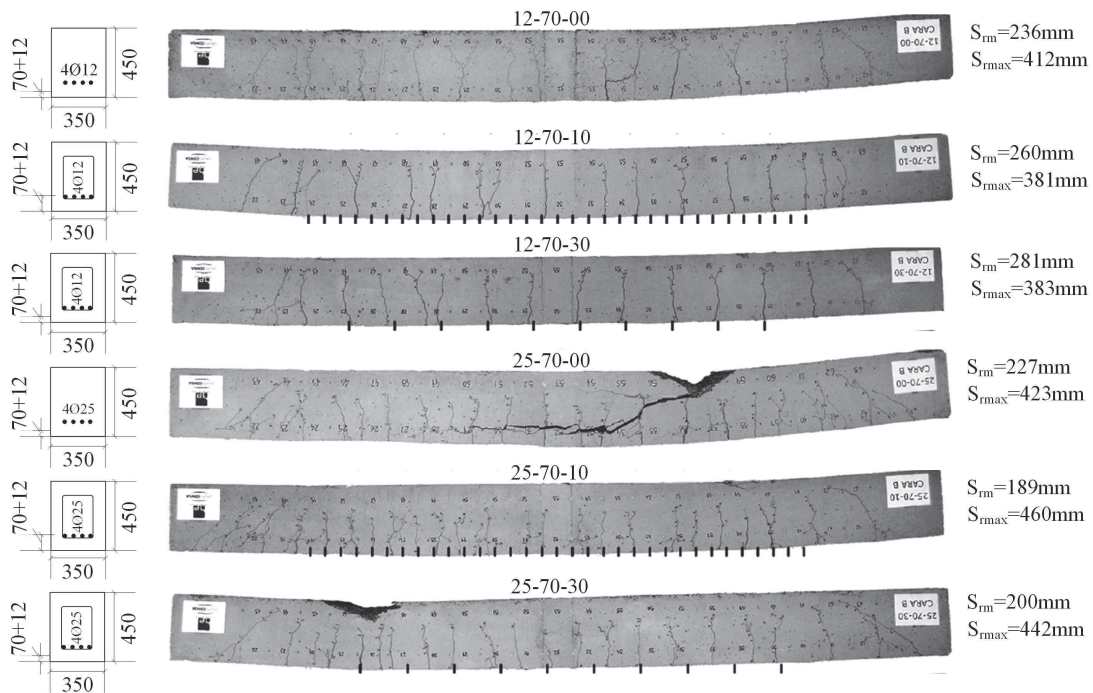


Figure 2.55: Crack pattern at failure in beams with 70mm cover by Caldentey et al., reprint from [58]

The tendency found for beams with $\phi_s = 12mm$ and $c = 20mm$ also applies for the three beams with $\phi_s = 25mm$ and $c = 20mm$ at the bottom of Fig. 2.54. The “natural” mean spacing in the beam without stirrups was $131mm$. While the mean crack spacing was reduced to $114mm$ in the beam with $100mm$ stirrup spacing, forming a crack for approximately every stirrup. In the beam with $300mm$ stirrup spacing, the mean crack spacing was $150mm$, with a crack at every stirrup and also one in-between.

It can be concluded from the above findings that the stirrups have a tendency to act as crack inducers, at least for the beams with with the small cover. For the beams with the large cover, of $70mm$, in Fig. 2.55, the tendency is not as pronounced as for the small cover. Whether this is due to the large cover or to the rather small pool of tests results is uncertain.

Caldentey et al. offered an important observation about the maximum crack spacing in this study. Within the three beams with the same bar diameter and cover but different stirrup spacing, the maximum crack spacing did not change significantly even though stirrups were added. Only the mean spacing, as discussed above, changed. This was most clear in the beams with a cover of $70mm$ but also applied for the beams with the small cover.

A larger amount of tests to support the findings by Caldentey et al. could be beneficial in order to draw any final conclusions to what effect transverse reinforcement has on cracking. The 12 beams in the investigation indicate that the relations between the crack spacing without stirrups (“natural” crack spacing) and the stirrup spacing has an influence on the final mean spacing of cracks in beams with stirrups. However, the maximum crack spacing is not notably influenced by the presence of stirrups.

Base et al. A smaller number of tests within Base et al.’s[39] experimental study were reserved for the investigation of the influence of transverse reinforcement. Eight beams were cast with stirrups of plain bars with a spacing of $3/2$ of the crack spacing observed in similar beams without transverse reinforcement. Two different cover sizes were tested, namely $20mm$ and $35mm$ of both side and bottom cover. Base et al.’s comments on the test results were that an insufficient number of tests were conducted in order to draw any final conclusions, but, in general, the stirrups appeared to act as crack inducers. This trend was most significant on the beams with the smallest cover, while, in the beams with the largest cover, there were more stirrup locations where cracks had not formed.

Summary The experimental study of the influence of transverse reinforcement indicates that:

- Transverse reinforcement seems to act as a crack inducer, however, this tendency is most clear for beams with a $20mm$ concrete cover (Caldentey et al. and Base et al.). For larger covers the tendency is more vague (Base et al. for $35mm$ cover and Caldentey et al. for $70mm$ cover).
- The mean crack spacing does not necessarily equal the spacing of the transverse reinforcement. There is an indication that the mean crack spacing in beams without stirrups still has an influence on the mean crack spacing in beams with stirrups (Base et al. and Caldentey et al.).
- The transverse reinforcement seems to have the largest effect on the mean crack spacing while the maximum crack spacing is not changed significantly compared to beams with no transverse reinforcement (Caldentey et al.).

Influence of distributed reinforcement

Braam To investigate the influence of distributed reinforcement in the web of deep beams Braam[53] conducted a test series of 15 beams in four-point-bending. The beams were T-shaped or rectangular and equipped with different variations of distributed reinforcement. Beams 1-6 of the series all had the same

concentrated tensile reinforcement ($4\text{Ø}20$) and a cover of 20mm to the stirrups of $\phi_s = 10\text{mm}$. Only two stirrups were placed within the constant moment span of 1200mm length.

Fig. 2.56 shows the results from crack width measurements in nine levels of the web in the constant moment span using a microscope with a magnification of 100. The two figures clearly illustrate Braam’s conclusion that the crack width decreased as the amount of distributed reinforcement increased and how crack widths can be controlled in this manner. In Fig. 2.56a the spacing of the distributed reinforcement was varied from 100mm in Beam 4 to 200mm in Beam 6. Here, it is seen how the location of where the crack was widest moved away from the location of the distributed reinforcement. In Fig. 2.56b the diameter of the reinforcement in the web was varied from $2\text{Ø}10$ in Beam 6 to $2\text{Ø}12$ in Beam 3. The result was that the maximum width in the crack was reduced with the increase in the diameter. Furthermore, in Beam 1, with no distributed reinforcement, the cracks were observed to be widest halfway between the concentrated reinforcement and the neutral axis.

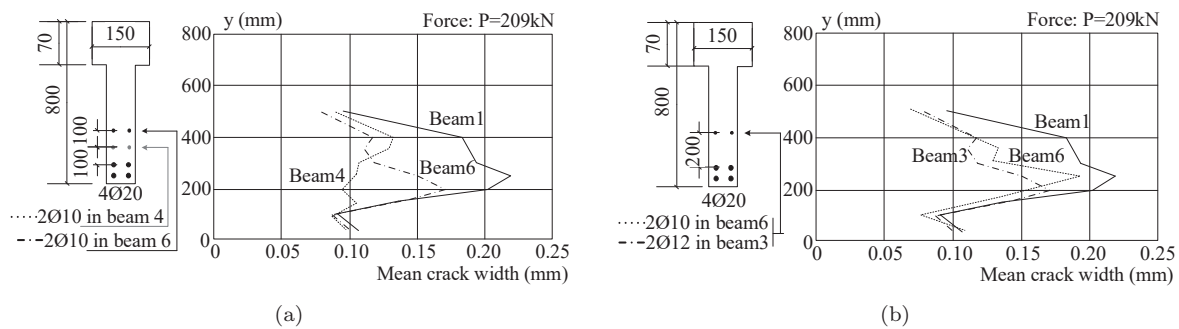


Figure 2.56: Mean of crack width measurements over the height of beams by Braam, reprint from [53]: (a) Influence of spacing of the distributed reinforcement, (b) Influence of diameter of the distributed reinforcement

Fig. 2.57 represents crack patterns for four other test beams in Braam’s test series, which illustrate how the distributed reinforcement induced cracks to penetrate further into the web. Beam 8, with the largest amount of distributed reinforcement and placed furthest away from the concentrated reinforcement, had the largest amount of cracks penetrating to the neutral axis, resulting in the smallest mean crack widths. It can also be observed how the amount of secondary cracks decreased while the amount of primary cracks increased from the beam with no web reinforcement (Beam 7) to the beams with increasing web reinforcement (Beam 10, Beam 9, Beam 8).

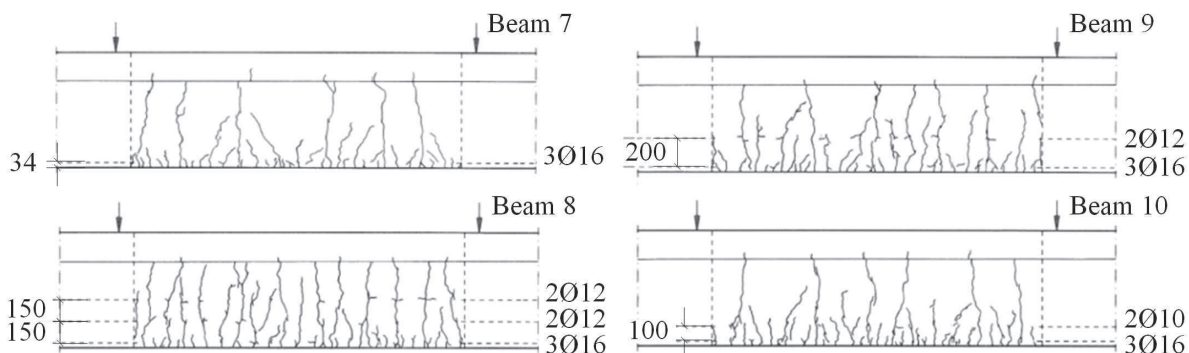


Figure 2.57: Crack patterns at maximum load for beams with different arrangements of distributed reinforcement by Braam, reprint from [53]

Frantz and Breen From tests of large beams, Frantz and Breen[61] also concluded that the crack pattern changed when distributed reinforcement was added because a larger amount of cracks extending

further towards the neutral axis instead of curving towards the primary cracks formed a curtain-like pattern as seen in Beam 7 in Fig. 2.57.

Beeby Beeby[62] conducted a smaller series of tests, primarily to investigate whether conclusions found for beams and slabs, in his earlier tests[39][59], also would hold for deeper beams. The series consisted of five 750mm deep T-shaped beams, two without and three with different layouts of distributed reinforcement. From his study, Beeby concluded that the distributed reinforcement did not have any significant effect on the crack pattern within the range of bar sizes and bar spacings he used. The crack patterns of four of the beams are shown in Fig. 2.58.

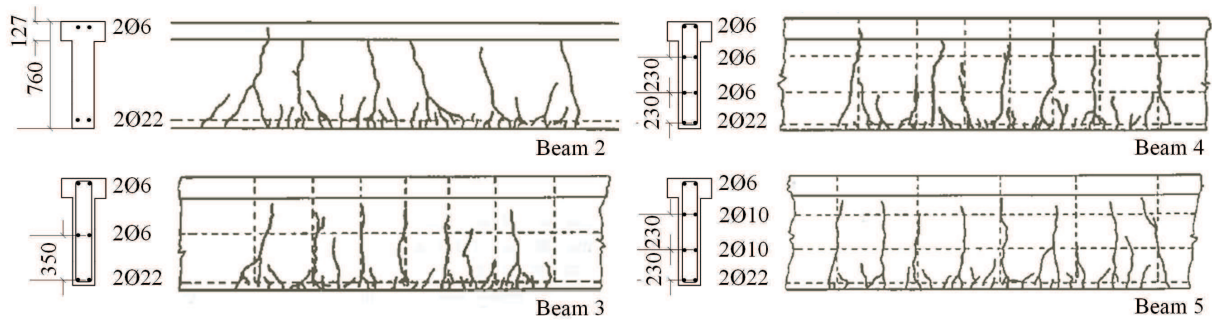


Figure 2.58: Crack patterns at maximum load for beams with different arrangement of distributed reinforcement by Beeby, reprint from [62]

The following are subjective comments on Beeby’s results. The contradicting results from Beeby’s investigation compared to those of the other researchers (Braam and Frantz & Breen) could indicate that the spacing between bars of the distributed reinforcement is of influence. In Beeby’s tests the spacings were 230mm and 350mm whereas in Braam’s tests the bar spacing was smaller and ranged from 100mm to 200mm.

The ratio of concrete to distributed reinforcement could also have an influence on the effect of the distributed reinforcement. A reinforcement ratio of the distributed reinforcement is calculated from the concrete area symmetrically placed around the distributed reinforcement, as illustrated in Fig. 2.1. The ratios are listed in Table 2.59 for three of Braam’s and three of Beeby’s beams. The ratios in Beeby’s tests are very low in two of the beams compared to Braam’s tests and also compared to the knowledge of minimum reinforcement[10]. The ratio of Beeby’s Beam 5 is somewhat close to Braam’s Beam 6, which is also the beam within Braam’s investigation where the distributed reinforcement had the least effect. It thus seems as though a certain amount of distributed reinforcement is needed for it to act as a crack controller.

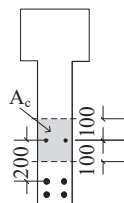


Figure 2.59: Concrete area for distributed reinforcement ratio

	Braam’s tests			Beeby’s tests		
Beam no.	3	4	6	3	4	5
ρ [%]	1.13	1.57	0.785	0.13	0.19	0.54

Table 2.1: Coefficients and statistics of linear regression for large beams $300 \leq d \leq 2100$

No literature was found concerning the investigation of the most beneficial spacing of the distributed reinforcement. Nor was there found any experimental investigations on the minimum height of a beam in which the widest crack appears in the web instead of at the outermost tensile fibres.

Summary The experimental study of the influence of distributed reinforcement indicates that:

- Distributed reinforcement can be used as crack control due to that fact that, when it is used, more cracks penetrate further towards the neutral axis. This results in decreased crack widths in the web (for distributed reinforcement with max. spacing of 200mm; Braam and Frantz and Breen).
- No influence of distributed reinforcement was found for spacings of 230mm – 350mm (Beeby). This indicates a upper limit for spacing of the distributed reinforcement and/or a lower limit of the distributed reinforcement ratio.

Influence of concrete strength

Base et al. In the experimental work by Base et al.[39], referred to several times earlier, six beams were cast to investigate the influence of concrete strength on crack spacing. Within the six beams of cube strength ranging from 19 to 34MPa no correlation was found between the concrete strength and the crack width or crack spacing.

Pedersen and Eriksen A series of tests by Pedersen and Eriksen[63] had the main purpose of investigating the influence of the concrete strength on the shear capacity of beams without transverse reinforcement. The beams were subjected to three-point-bending. As part of the analysis, crack spacings and number of cracks were measured at failure. The mean crack spacings of the 12 beams with concrete strength ranging from 18 to 59MPa are shown in Fig. 2.60. These results were not discussed by the authors. The results seemingly agree well with Base’s statement, only with a minor increase in spacing with the increase in concrete strength which could just as well be due to normal variation in results.

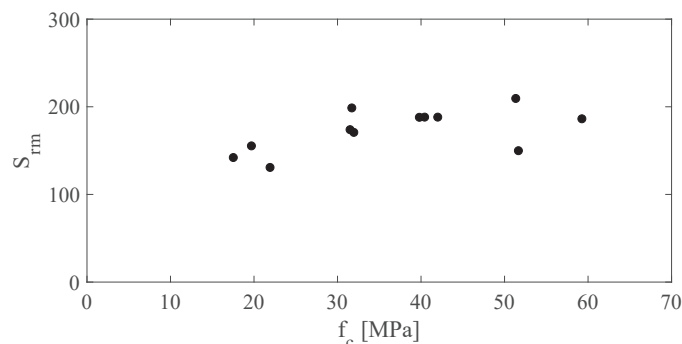


Figure 2.60: Mean crack spacing in relations to compressive strength of concrete, constructed with data from [63]

Summary The experimental study of the influence of concrete strength thus indicates that:

- There is no significant influence of the concrete strength on crack spacing for normal strength concrete (Beeby and Pedersen and Eriksen, $f_c = 18 - 59MPa$).

Influence of stress level in longitudinal reinforcement

Several researchers have concluded, through tests, that crack widths at the concrete surface are proportional to the tensile stress level in the reinforcement (Base et al.[39], Broms[27], Caldentey et al.[58] and Sherwood[49]. Sherwood’s documentation of this is provided in Fig. 2.35b. However, the linear relations between the stress level and crack width are shown to be most clear within the stage of a stabilised crack system and for stresses below the yield stress. The stress level to which a stabilised crack system is reached is investigated in the following.

Stabilised crack systems with respect to stress level

The following section summarises the results of a selection of the researchers' investigations of whether a stabilised cracking stage can be determined from experimental observations. A stabilised crack stage is defined by a stress level in the reinforcement at which further increase in stress does not result in the formation of any new cracks and hence the crack spacing is constant with increase of stress. Exceptionally, it is accepted that a few new cracks form after this stress level if the crack spacing is not notably altered. The stabilised crack stage is analysed separately for the two different crack types; primary and secondary cracks.

Primary flexural cracks From observation of Sherwood's[49] crack spacing measurements at different levels of shear stress in Fig. 2.34b, the crack spacing at mid-height of the member seems almost constant within the entire service load range. Hence, they all form at a load level close to the cracking load. Broms[27] stated a similar observation about the development of the primary crack pattern, namely that it was more or less fully developed at early load levels of the elastic stage, thereafter secondary cracks continued to form.

Local secondary cracks The results from the literature with regard to a stable secondary crack system are contradicting. There is no general consensus present of what stress level the crack system is stabilised. Broms[27] reports that no more cracks formed after stresses in the reinforcement had reached $140\text{--}210\text{MPa}$ for concrete covers ranging between 32mm and 76mm and at around 345MPa for a cover of 152mm . The reinforcement ratio varied from $1.3\% - 1.8\%$ and the effective depth was $d \sim 400\text{mm}$.

Attisha[57] tested beams all had a cover of 35mm , reinforcement ratios between $0.6 - 2.0\%$, and an effective depth of $d \sim 260$. The measured average crack spacing at the level of the reinforcement approached a constant value for steel stresses around $200 - 300\text{MPa}$. Attisha's results are shown in Fig. 2.61.

Sherwood's crack spacing measurements have previously been presented in Fig. 2.34b. Here, the secondary crack spacing for the small beam of $d = 280\text{mm}$, decreases significantly after reaching a shear stress of 0.8MPa which is close to yielding of the reinforcement. This could indicate that new secondary cracks will develop when failure of the beams are initiating. The secondary crack spacing in his large beams of $d = 1400\text{mm}$ did not change significantly after forming at low stress levels.

The various different observations indicate that a stabilised crack stage for the secondary cracks could not only be dependent upon the stress in the reinforcement, but also on a number of other parameters, such as stress in the reinforcement at first cracking, the reinforcement ratio, the ratio σ_s/ρ_s and/or the cover. Nevertheless, none of these parameters' influence on the stabilised cracking have been investigated in the literature. It is, however, obvious, at least for beams with a reinforcement ratio close to the minimum required to ensure yielding, that cracks will easily form at stress level higher than $200 - 300\text{MPa}$.

Summary The experimental study of the influence of stress level in the longitudinal reinforcement and identification of a stabilised crack pattern indicates that:

- Primary cracks are fully developed and stabilised early in the elastic stage, meaning almost immediately after the cracking load is reached (Sherwood and Broms).
- Ambiguous stress level is found with respect to a stabilised secondary crack system. Comparison of the test results indicates that the stress level could be dependent on a number of parameters, such as the reinforcement ratio ρ_s , the ratio σ_s/ρ_s and/or the cover.

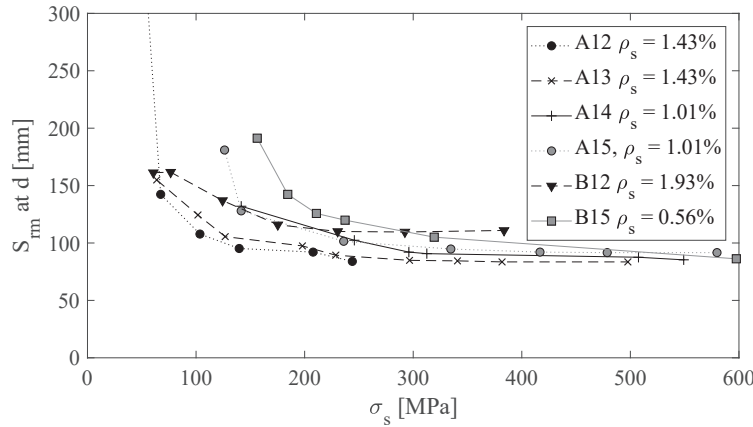


Figure 2.61: Measured crack spacings in relations to reinforcement stress from test by Attisha, modified illustration from [57]

2.3.2 Modelling of cracking in flexural members

The amount of models proposed for estimating crack spacings and crack widths in flexural members is just as many, if not more, than the models for tensile members. Borosnyói and Balázs[64] reviewed 23 models for the estimation of crack spacings and 33 different formulations for the estimate of crack widths. In the following section, a selection of these will be presented, reflecting the overall three different assumptions the models rest upon. Most models for beams rest on either the bond-slip, the no-slip theory or a combination of the two, just as the models for tensile members did. However, the bond-slip models are only used for estimating the crack spacings of the secondary cracks while the no-slip theory is more straightforward to use for estimating crack spacings in various different levels of the beam.

Only a few researchers treat both the secondary and primary crack types, whereas the majority propose an estimate for the spacing of secondary cracks. The reason for this could be that the focus has been to protect the reinforcement and thus limit the crack widths at that level.

Relations between extreme and mean crack spacing

With respect to the relations between extreme and mean crack spacing, Beeby[28] transferred his probabilistic theory about crack forming in the tensile members to flexural members.

The solid lined skew probability distribution in Fig. 2.62 represents the distribution of the secondary crack spacing proposed by Beeby[28]. The dashed line corresponds to the probabilistic distribution of spacings from the general assumption described in Section 2.2 concerning tensile members where all spacings are within the interval $[S_{rmin}; 2S_{rmin}]$ and the mean value is $1.33S_{rmin}$. However, Beeby claimed that two different mechanisms related to the bond could cause both smaller and larger crack spacings.

Premature failure, which was guilty of larger crack spacings than $2S_{rmin}$, was owed to failure of the bond, causing a reduction in stress transfer between concrete and reinforcement and resulting in cracks forming further away from the first formed crack. Beeby also claimed that some crack spacings would be reduced due to the formation of conical cracks, i.e. the cracks that Goto called secondary cracks. If these cracks penetrated to the surface of the member they would reduce the crack spacing.

The spacings outside the dashed lines thus represent the cracks that formed due to bond mechanisms. Therefore, Beeby argued that the dashed distribution was the distribution of the spacing of primary cracks as the formation of these was not seen to be interfered by the bond of the reinforcement, while the solid line represented the distribution of the secondary cracks.

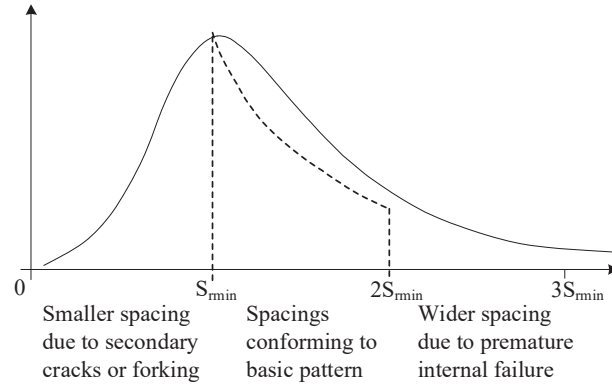


Figure 2.62: Probability distribution of crack spacings in flexural members by Beeby, reprint from [28]

Crack spacing

The study of the tests in the previous sections showed that the crack spacing on the side face of beams varies with respect to the distance to the reinforcement. When reviewing existing models, in the following a distinction will be made between models that estimate the spacing at the level of the reinforcement and models intended to predict the crack spacing in the web of deep beams without distributed reinforcement. The crack spacings are referred to as secondary and primary crack spacings and are denoted $S_{r,sec}$ and $S_{r,fl}$, respectively.

The bond-slip approach

Even though most bond-slip models are derived from physical assumptions associated with tension members, the theory has also been widely used on flexural members. Here, a fictitious tension bar is assumed to be located in the tensile zone in which uniformly distributed stresses occur. The fictitious tension bar carrying tensile stresses between cracks is called the effective concrete area, $A_{c,eff}$. Several models for flexural members rely on this approach with variations in the assumptions for the parameters, namely size of the effective concrete area and bond stress intensity.

To a large extent, the bond-slip theory seems appealing as it rests on assumptions that can be accounted for through physical mechanisms. In contrast, no-slip models most often include empirical coefficients relating the cover and distance to the neutral axis to the crack spacing.

Marti et al. - Crack spacing at reinforcement level The Tension Chord model by Marti et al.[29] presented in 2.2.2 is one of the models developed from consideration of tensile members but also used on flexural members. As for tensile members, the bond stresses are assumed to be constant, only changing size when yielding occurs.

The mean crack spacing is expressed by the transfer length, S_0 :

$$S_{rm,sec} = \lambda S_0 \quad 1 \leq \lambda \leq 2 \quad (2.38)$$

$$S_0 = \frac{f_{ct} \emptyset}{4\tau_b \rho_{s,eff}} \quad (2.39)$$

The effective concrete area can either be calculated as the symmetric area around the reinforcement $A_{c,eff} = 2bc$ or derived from equilibrium:

$$A_{c,eff} = \alpha A_s \left(\frac{I_{uncr}}{I_{cr}} \frac{d - x_{cr}}{h - x_{uncr}} - 1 \right) \quad (2.40)$$

The deduction of the expression above is elaborated by Burns[65] and Bigaj[45]. The considered equilibrium is based on the stage immediately after a crack has formed, at the load level where the stresses in the concrete are equal to the tensile strength of the concrete. The reinforcement stress in a elastic cracked section, $\sigma_{s,cr}$, is equated to the reinforcement stress in the fictitious tension bar in a cracked section, $\sigma_{s,cr,TC}$.

$$\sigma_{s,cr} = \frac{\alpha M_{cr}(d - x_{cr})}{I_{cr}} \quad (2.41)$$

$$\sigma_{s,cr,TC} = \frac{A_{c,eff}f_{ct} + \alpha A_s f_{ct}}{A_s} \quad (2.42)$$

The cracking moment, M_{cr} , is found from an uncracked section with a concrete stress at the tensile edge equal to the uni-axial tensile strength: $M_{cr} = f_{ct}W_{uncr}$.

Leonhardt - Crack spacing at reinforcement level Leonhardt[14] also proposed a way to estimate the secondary crack spacing from the transfer length, although he also included a debonded length:

$$S_{rm,sec} = 2l_{deb,L} + S_0 \quad (2.43)$$

where $l_{deb,L}$ is Leonhardt's expression for the debonded length on both sides of a crack presented in Section 2.2.2. Leonhardt's transfer length consists of two parts; one similar to Marti et al.'s expression, and an additional one taking the cover into account:

$$S_0 = k_1(c_{ver}, a_v) + k_2 k_3 \frac{\phi_s}{\rho_{s,eff}} \quad (2.44)$$

where the constant $k_3 = 0.125$ is empirically determined for members subjected to pure bending. The also empirically determined k_2 is the relations between the concrete tensile strength and the average bond stress; $k_2 = 0.4$ for ribbed bars and $k_2 = 0.74$ for plain bars. The function $k_1(c_{ver}, a_v)$ describes the length by which the concrete stresses are distributed across the whole section, similar to St. Vernant's Principle:

$$k_1 = \begin{cases} 1.2c_{ver} & a_v \leq 2c_{ver} \\ 1.2(c_{ver} + \frac{a_v - 2c_{ver}}{4}) & a \geq 2c_{ver} \text{ and } a_v \leq 14\phi_s \end{cases} \quad (2.45)$$

where a_v is the vertical distance between the layers of reinforcement for beams with multiple layers in the tensile zone.

Leonhardt specified the effective concrete area as illustrated in Fig. 2.63a for both beams and slabs:

$$A_{c,eff} = \begin{cases} b(c_{ver} + a_v + 7\phi_s) & \text{for beams} \\ b(c_{ver} + 5\phi_s) & \text{for slabs where } \frac{1}{2}(h - x_{cr}) \leq 5\phi_s + c \end{cases} \quad (2.46)$$

The no-slip approach

With regard to the no-slip models, the foundation is more or less the same for all of them, namely that the distance from a crack, where stresses are uniformly distributed, is defined from St. Vernant's Principle. The main difference in the models is the angle under which stresses spread in the concrete cross-section, which is most often expressed by an empirical factor resulting in proportionality between the cover/distance to the reinforcement and the crack spacing.

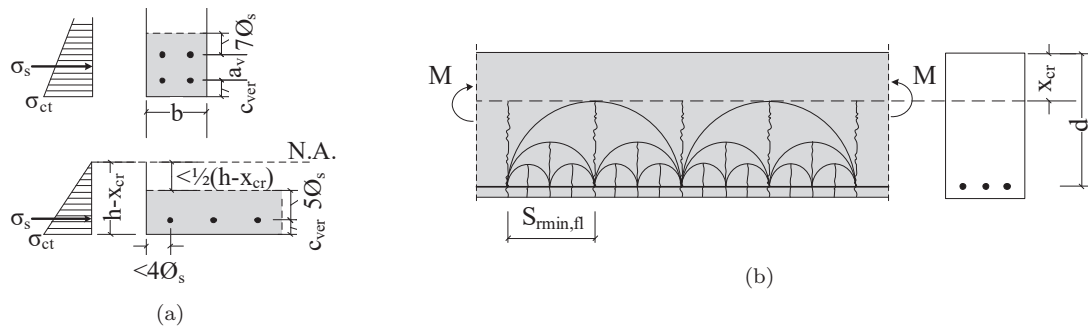


Figure 2.63: (a) Effective concrete area for beams and slabs by Leonhardt, reprint from [14], (b) Circular stress distributions in beams by Broms, reprint from [66]

Broms - Crack spacing at neutral axis Similar to Broms'[27] theory for tensile members in Section 2.2.2, he proposed that, in beams, the concrete stresses would distribute in circles with diameters equal to the size of the minimum distance to the reinforcement. The concept is illustrated in Fig. 2.63b. For the crack spacing at the neutral axis this meant:

$$S_{rmin,fl} = d - x_{cr} \quad (2.47)$$

Reineck - Crack spacing at $d/2$ Reineck[66] also believed that the crack spacing in the web was proportional to the height of the primary cracks ($d - x_{cr}$) also in accordance with St. Vernant's Principle. Therefore he compared Broms' model (Eq. 2.47) to average crack spacings in 23 beams from six different test series. Reineck's comparison is shown in Fig. 2.64a and indicates that the crack spacing was shorter in the tests than estimated by Broms' model. Reineck therefore proposed adding an empirical constant of 0.7:

$$S_{rm,fl} = 0.7(d - x_{cr}) \quad (2.48)$$

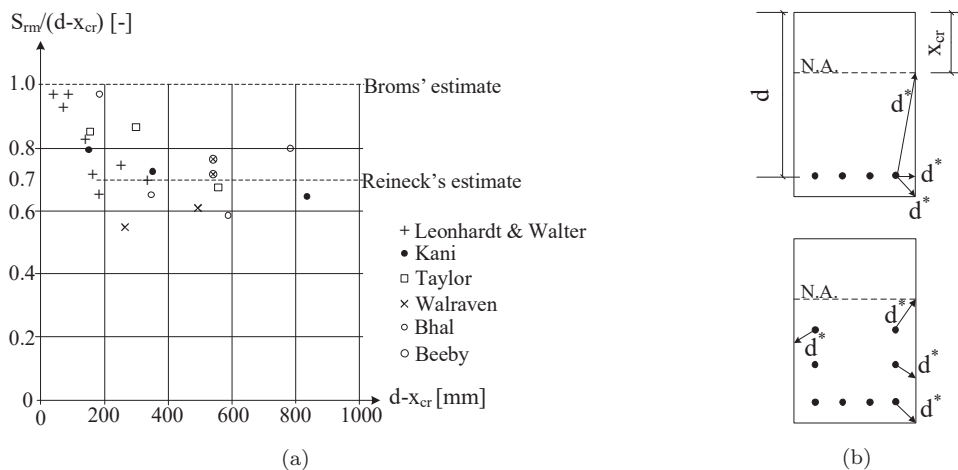


Figure 2.64: (a) Relations between crack height and ratio between crack spacing and crack height, modified from [66], (b) Frosch's controlling distance for estimation of crack spacing for members with and without distributed reinforcement, modified illustration from [67]

Reineck's comparison with tests also indicated that the empirical relations did not apply to beams with a primary crack height smaller than approximately 200mm . In Fig. 2.64a these beams are seen to have a larger crack spacing. Reineck suggested that the variation of crack spacing for these small beams followed a bond-slip approach and therefore depended on the ϕ_s/ρ_s -ratio instead of the cracks height.

Hamadi - crack spacing at $d/2$ Reineck's estimate is similar to an even simpler relation proposed by Hamadi[68] for the primary crack spacing. The expression, however, carries no apparent explanation to its origin.

$$S_{rm,fl} = 0.5d \quad (2.49)$$

Frosch - Crack spacing at reinforcement level and in the web Frosch[67] proposed a model for estimation of the crack spacing at the reinforcement level directly from Broms' ideas presented earlier. He relates the crack spacing to the minimum distance to the reinforcement as illustrated in Fig. 2.64b where d^* is called the controlling cover distance:

$$S_{rm,sec} = \lambda d^* \quad (2.50)$$

The crack spacing can thus be estimated at a arbitrary level in the tensile zone where d^* is always the smallest distance to a rebar. As the figure shows, the model also applies for beams with distributed reinforcement in the web. The mean crack spacing is found for $\lambda = 1.5$, while the minimum and maximum spacings are characterised by the commonly used interval $1 \geq \lambda \geq 2$.

Crack width

The general way of estimating the maximum crack width is the same as for tensile members. The strain in the reinforcement over the length between two cracks is assumed to be the crack width as the strains in the concrete are neglected. However, in beams, the strain in the reinforcement varies both due to variation in moment and due to the transfer of stresses to the concrete:

$$w_{max} = \int_{-\frac{1}{2}S_{rmax}}^{\frac{1}{2}S_{rmax}} \epsilon_s(x) dx \quad (2.51)$$

The Eurocode 2 and the fib Model Code 2010

The design models in the Eurocode 2[10] and the Model Code 2010[11] for beams are similar to the models for tensile members with one important adjustment, namely the reinforcement ratio. For tensile members the whole cross-section was included while, for flexural members, an effective area is defined.

There is also a rather large difference between the Eurocode and the Model Code because the Eurocode takes into account the gradient of the strain variation in a beam cross-section compared to the uniform distribution of strains in a tensile member. The effect is taken into account by adding a coefficient of $k_2 = 0.5$ on the $\phi_s/\rho_{s,eff}$ -term in the model for beams. Hence, the effect of the $\phi_s/\rho_{s,eff}$ -ratio is reduced to half in the Eurocode compared to that of tensile members, while the cover has the same effect on both tensile members and flexural members.

Maximum crack spacing according to the Eurocode:

$$S_{rmax,sec} = k_3c + k_1k_2k_4 \frac{\phi_s}{\rho_{s,eff}} \quad (2.52)$$

where $k_3 = 3.4$, $k_1 = 0.8$ for high bond bars, $k_2 = 0.5$ for bending and $k_4 = 0.425$:

$$S_{rmax,sec} = 3.4c + 0.17 \frac{\phi_s}{\rho_{s,eff}} \quad (2.53)$$

Maximum crack spacing according to the Model Code 2010:

$$S_{rmax,sec} = 2c + 0.278 \frac{\phi_s}{\rho_{s,eff}} \quad (2.54)$$

The crack width is calculated in the same manner in the Eurocode and in the Model Code 2010, but the Model Code adds a contribution from shrinkage.

Maximum crack width, for high bond bars, without shrinkage:

$$w_k = S_{rmax,sec} \left(\frac{\sigma_s - k_t \frac{f_{ct,eff}}{\rho_{s,eff}} (1 + \alpha \rho_{s,eff})}{E_s} \right) \quad (2.55)$$

where k_t is dependent on the duration of the load; $k_t = 0.6$ for short-term and $k_t = 0.4$ for long-term loading. The effective concrete area, $A_{c,eff} = bh_{c,ef}$ is the minimum of three expressions:

$$h_{c,ef} = \min \begin{cases} 2.5(h - d) \\ \frac{1}{3}(h - x_{cr}) \\ \frac{h}{2} \end{cases} \quad (2.56)$$

As mentioned in Section 2.2.2, Ferry-Borges[46] combined the bond-slip and no-slip theory, into one model which is the one adopted, with adjustments, in the Eurocode and the Model Code.

To calculate the crack spacing and the crack width in the web of a beam, Eurocode specifies that the crack spacing in the tension zones where there is no reinforcement or the spacing of it exceeds $5(c + \phi_s/2)$, the maximum crack spacing may be taken as:

$$S_{rmax,fl} = 1.3(h - x_{cr}) \quad (2.57)$$

2.3.3 Model tendencies

In Fig. 2.65 the different formulations for the effective concrete area are listed. Furthermore, the reviewed models for the secondary crack spacing, and the theories they rest upon, are listed in Fig. 2.66. All the models, whether being from the bond-slip or no-slip theory, rest on the overall same assumptions as those for tensile members in Section 2.2.3, the only difference being some of the empirical factors.

Model	Expression
TCM - symmetric	$A_{c,eff} = 2b(h - d)$
TCM - Bigaj	$A_{c,eff} = \alpha A_s \left(\frac{l_{uncr}}{l_{cr}} \frac{d - x_{cr}}{h - x_{uncr}} - 1 \right)$
Leonhardt	$A_{c,eff,beam} = b(c_{ver} + a + 7\phi_s)$ $A_{c,eff,slap} = b(c_{ver} + 5\phi_s)$
EC2	$A_{c,eff} = bh_{c,ef} \quad h_{c,ef} = \min \begin{cases} 2.5(h - d) \\ \frac{1}{3}(h - x_{cr}) \\ \frac{h}{2} \end{cases}$

Figure 2.65: Reviewed models for the effective area around the tensile reinforcement

Model	Expression	Theory
TCM	$S_{rmin} = \frac{\emptyset_s}{8\rho_{s,eff}}$ $2S_{rmin} = S_{rmax}$	Bond-slip: $S_{rmin} = S_0$
	$S_{rm} = \lambda \frac{\emptyset_s}{8\rho_{s,eff}}$ $\lambda = 1.33$	
Frosch	$S_{rmin} = c_{hor}$ $2S_{rmin} = S_{rmax}$	No slip: $S_{rmin} = k c$
	$S_{rm} = \lambda c_{hor}$ $\lambda = 1.5$	
Leonhardt	$S_{rmin} = \frac{\Delta\sigma_s}{22.5} \emptyset_s + 1.2c + 0.05 \frac{\emptyset_s}{\rho_{s,eff}}$	Combined bond-slip and no slip with debonding: $S_{rmin} = k c + S_0 + L_{deb}$
	$S_{rmax} = \frac{\Delta\sigma_s}{45} \emptyset_s + 1.2c + 0.05 \frac{\emptyset_s}{\rho_{s,eff}}$	
EC2	No information is given about relations between mean and extreme	Combined bond-slip and no slip: $S_{rmin} = k c + S_0$
	$S_{rmax} = 3.4 c + 0.17 \frac{\emptyset_s}{\rho_{s,eff}}$	
MC2010	No information is given about relations between mean and extreme	Combined bond-slip and no slip: $S_{rmin} = k c + S_0$
	$S_{rmax} = 2 c + 0.278 \frac{\emptyset_s}{\rho_{s,eff}}$	

Figure 2.66: Reviewed models for spacing of cracks in flexural members at the level of the reinforcement

The models for estimating the flexural crack spacing are listed in Fig. 2.67. In all these models, the crack spacing is proportional to a geometrical parameter associated with the height of the member.

Model	Expression	Theory
Hamadi	No information is given about relations between mean and extreme	Empirical
	$S_{rm} = 0.5d$	
Reineck	No information is given about relations between mean and extreme	No-slip/Empirical
	$S_{rm} = 0.7(d - x_{cr})$	
Frosch	$S_{rmin} = d^*$ $2S_{rmin} = S_{rmax}$	No-slip/Empirical
	$S_{rm} = \lambda d^*$ $\lambda = 1.5$	
EC2	No information is given about relations between mean and extreme	The origin is unknown
	$S_{rmax} = 1.3(h - x_{cr})$	

Figure 2.67: Reviewed models for spacing of web cracks in flexural members

The variation of terms in the combined models for secondary crack spacing

The differences in behaviour of a bond-slip and a no-slip model, for the secondary crack spacing, have already been discussed through a parameter study in the section relating to tensile members. However, the changes in the Eurocode model from tension to bending will now be investigated through a parameter study.

As described earlier, the models in the Eurocode and the Model Code consist of two terms; a bond-slip-term (ϕ_s/ρ_s) and no-slip-term dependent on the cover. For tensile members, it was discovered how the ϕ_s/ρ_s -term had an increasing influence on the spacing of cracks with the increase of cover. The reason being that the ϕ_s/ρ_s -ratio involves c^2 and the cover-term only involves c .

For beams, the influence of the two terms is again sought to be investigated graphically because the expression for the ϕ_s/ρ_s -ratio has changed, replacing the reinforcement ratio with the effective ratio, $\rho_{s,eff}$. The investigation focuses on the Eurocode Model, however, the same trends apply for the Model Code expression.

In Fig. 2.68b the variation of the two different terms in the Eurocode model is plotted with respect to the cover for a beam with six reinforcement bars of three different diameters, as shown in Fig. 2.68a. The distance between the bars in the cross-section is kept constant (30mm) while the cover is increased from 15mm to 75mm. As a consequence, the width of the beam is increased from 230mm to 450mm.

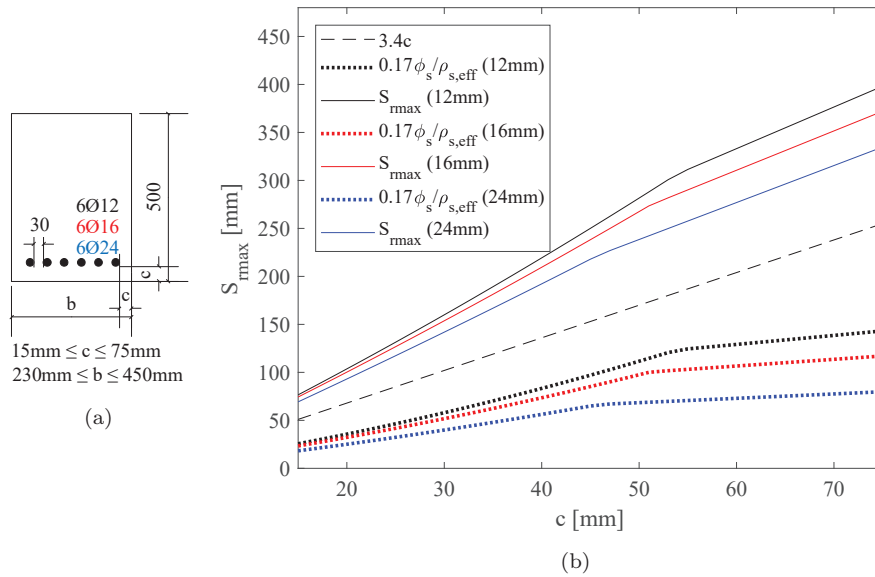


Figure 2.68: Variation of terms in the Eurocode 2 Model

The plot shows how the cover-term, $3.4c$, varies in the same way, regardless of variation in bar diameter, whereas the $\phi_s/\rho_{s,eff}$ -term is obviously dependent on the diameter. The variation of the $\phi_s/\rho_{s,eff}$ -term and the total crack spacing, S_{rmax} , for the beam with 12mm bars is illustrated with the two black lines while the beams with 16mm and 24mm bars are plotted with red and blue lines, respectively.

In contrast to what was discovered regarding the Eurocode model for tensile members, the $\phi_s/\rho_{s,eff}$ -term does not become the most influential with an increase in cover. Irrespective of the size of the cover, the cover-term is of most influence. This is because the increase of $\phi_s/\rho_{s,eff}$ is restricted by the different formulations of the height of effective concrete. For small covers, the effective concrete area is calculated from: $A_{c,eff} = 2.5(h - d)b$ while for large covers the area becomes: $A_{c,eff} = 1/3(h - x_{cr})b$. The first part of the red, blue and black dotted lines, representing the use of $A_{c,eff} = 2.5(h - d)b$, are actually parabolas

if the width is a function of the cover. Nevertheless, they approach what looks like a straight line because the interval of the cover is not sufficiently large to create an effect from c^2 . This is the same conclusion as that found for the variation of the Eurocode model for tensile members.

Variation in models for the two crack types

The difference in variation of the secondary crack spacing and the primary crack spacing is studied through two models, both representing one of the crack types, namely the Tension Chord Model for secondary cracks and the estimate by Reineck for primary cracks. The following study originates from earlier publications by the author of this thesis[48][69].

Fig. 2.69 illustrates the relative crack spacing, S/d , estimated by Reineck, S_{fl} , and by the Tension Chord Model, S_{sec} , with respect to effective depth for three different reinforcement ratios; 0.35%, 0.7% and 1.05%. The plot reveals that for beams smaller than roughly $250\text{mm} - 300\text{mm}$, the secondary crack spacing is larger than the primary crack spacing. This could indicate that only one crack type will develop from estimates of these two models. For beams with a greater effective depth, the secondary crack spacing is smaller than the primary. In this case the secondary cracks will develop in-between the primary cracks. It is also seen how the primary crack spacing is linearly proportional to the effective depth of the member when adopting the expression proposed by Reineck. This is in accordance with the findings in the investigation by Sherwood in Fig. 2.33-2.35a.

If the spacing of the secondary cracks is approximated by the Tension Chord Model, the ratio S/d exhibits a hyperbolic shape; hence this crack spacing is not influenced by the variation in effective depth. This is because the effective concrete area is not dependent on the effective depth.

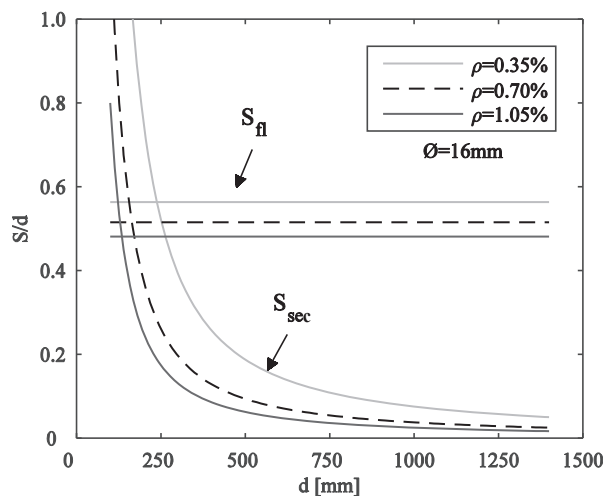


Figure 2.69: Relations between relative crack spacing and effective depth, for reinforcement ratios; $\rho_s = 0.35\%$, $\rho_s = 0.7\%$ and $\rho_s = 1.05\%$, reprint from [48]

From the parameter study in the paper[69] it was also observed that the estimate by Reineck shows only a minor dependency on the reinforcement ratio, while, at least for shallow beams, the Tension Chord Model shows a greater dependency on the ratio. Furthermore, the estimate by Reineck is independent of the diameter of the reinforcement, whereas the Tension Chord Model shows a dependency on the diameter due to the fact that the bond stress transfer is dependent on the surface area of the reinforcement.

2.4 Stiffness and deformation of flexural members

Fig. 2.70a illustrates a stress-strain response of a reinforced concrete tensile member compared to the response of a bare reinforcement bar. It can be seen how, for the same stress level, the strain in the reinforced concrete member is lower than in the bare reinforcement. The stiffness of the reinforced concrete members is thus larger than the bare reinforcement bar. The tension-stiffening is the effect that increases the stiffness, EA , compared to the bare reinforcement due to the fact that the intact concrete between cracks exhibits the ability to carry tensile stresses.

The same principle applies for reinforced concrete members in bending, as illustrated by Gilbert[70] in Fig. 2.70b. The solid line in the plot illustrates an idealised load-deflection response of a simply supported, one-way spanning, reinforced concrete slab. The first part of the solid line, until P_{cr} is reached, is the uncracked response of a beam with a stiffness estimated from the whole concrete section ($E_c I_{uncr} = E_c \frac{1}{12} bh^3$). The straight dashed line to the far right, with the largest deflection at all load levels, represents a beam that is fully cracked in its whole length where only the reinforcement can carry tension. This corresponds to the response of the bare reinforcement bar in Fig 2.70a for the tensile member. The non-linear dashed line to the left of the fully cracked response represents the response from the assumption that concrete can carry tension in the regions of the beam where the moment has not reached the cracking moment, M_{cr} . This response gradually approaches the response of the fully cracked beam as a larger and larger part of the beam cracks with the increase in load. The tension-stiffening effect lies in the difference between the latter mentioned response and the solid line, as illustrated in the figure. The physical difference is that the concrete can carry tension in-between cracks in the response of the solid line. The tension-stiffening thus increases the flexural stiffness, EI , compared to the stiffness of a beam where the concrete can carry no tension at all and assumed to be fully cracked in the whole length.

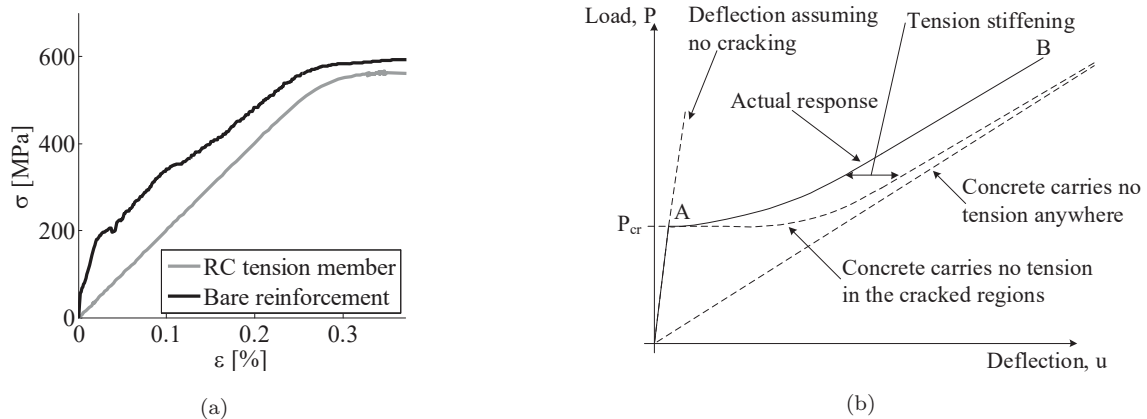


Figure 2.70: (a) Test response of reinforced concrete tensile member versus a bare reinforcement bar, reprint from [71], (b) Idealised load-deflection relations for a beam, modified from [70]

2.4.1 Modelling the deflection including tension-stiffening

A commonly used method to estimate the response of flexural members from A to B in Fig. 2.70b including the effect of tension-stiffening is to use a deformation parameter, which is a weighted value between the uncracked and fully cracked cross-sectional properties. The size of the deformation parameter, in the interval between the uncracked and the fully cracked parameter, is dependent on the size of the bending moment relative to the cracking moment. This method is used in both the Model Code 2010 and the Eurocode 2 and was proposed by Bischoff[72]. The deformation parameter, α , can both be considered as the rotation, the strain or the curvature:

$$\alpha = \zeta \alpha_{II} + (1 - \zeta) \alpha_I \quad (2.58)$$

where α_I and α_{II} is the deformation parameter for the uncracked and fully cracked state, respectively, while ζ is the distribution coefficient taking tension-stiffening into account:

$$\zeta = 1 - \beta \left(\frac{M_{cr}}{M} \right)^2 \quad (2.59)$$

here β is a coefficient taking the influence of the duration of the load into account, where $\beta = 1$ for short-term load and $\beta = 0.5$ for sustained load. If the deformation parameter, α , is chosen to express a variable curvature with respect to the location in the beam, the moment of inertia can be deduced from Eq. (2.58) and (2.59) and considerations of virtual work to estimate the deformation:

$$EI_{EC2} = \frac{EI_{cr}}{1 - \left(1 - \frac{EI_{cr}}{EI_{uncr}} \beta \left(\frac{M_{cr}}{M_{max}} \right)^2 \right)} \quad (2.60)$$

This model has been shown to provide good estimates of the deflection of lightly reinforced concrete structures such as slabs where tension-stiffening has the largest influence [73],[74].

The model does not take into account the stiffness dependency on the type of loading or the support conditions.

Another method was proposed by Christiansen[75] and is based on the assumption that tension-stiffening can be related to the average crack width and thus takes into account the degree of cracking with respect to load level.

Energy concepts

When dealing with statically indeterminate structures in the ultimate limit state it is possible to take advantage of the material's plastic properties by choosing the distribution of force. In contrast, in order to be able to investigate the behaviour of statically indeterminate concrete structures in the serviceability limit state, knowledge of the actual force distribution is necessary. An approach to achieving the moment distribution in the elastic stage is by using energy concepts, where the state of equilibrium is found by minimising the potential energy. When dealing with a material with a linear elastic behaviour, this can be reduced to minimisation of the strain energy, due to the fact that the stress distribution is going through states of equilibrium.[76] The total elastic energy of a system can be expressed by:

$$U = \int_V \sigma \epsilon dV \quad (2.61)$$

For a statically indeterminate system with n unknowns, the total elastic energy becomes a function of n variables, where the unknowns X_i in the system, related to the true state of stress, can be found through minimisation:

$$\frac{\delta U}{\delta X_1} = 0, \frac{\delta U}{\delta X_2} = 0, \dots, \frac{\delta U}{\delta X_{n-1}} = 0, \frac{\delta U}{\delta X_n} = 0 \quad (2.62)$$

3 EXPERIMENTAL INVESTIGATION OF FLEXURAL CRACKING WITH RESPECT TO MEMBER DEPTH

Subsequent to the literature review regarding cracking in flexural members in Section 2.3, a test series was conducted at Aarhus University, as part of current research project, to clarify some unresolved questions regarding the behaviour of flexural members as well as to support some already stated conclusions in the literature review. The test results are reproduced from a conference paper by the author of this thesis[77], which describes the test set-up and all the test results.

The test series' primary objective was to investigate the development of cracks from first cracking to yielding of the reinforcement. As it was discovered from the literature review that the crack system appears different for small and large beams, it was found relevant to investigate this further and study the difference, not only with respect to the visible crack pattern, but also with respect to the crack widths. The test series therefore consisted of beams with two different member depths; one depth to represent the small beams, where only one crack system should form and one depth to represent the large beams, where two different crack types were predicted to develop.

The tests are firstly introduced and hereafter four main results are summarised from the paper. Three of the results concern the difference in behaviour with respect to the beam depth while one presents a similarity in behaviour of the beams with different depths. The results concern the following:

- The difference in system of cracks
- The difference in development of crack height
- The difference in crack width shape
- The similarity with respect to sum of crack widths

3.1 Introduction to the test

A test series of eight simply supported beams, subjected to two symmetrically placed forces, was conducted. The tests consisted of four beams with an effective depth of $270mm$ and four beams with an effective depth of $d = 570mm$. The geometry and reinforcement layout are sketched in Fig. 3.1 and the properties are listed in Table 3.1. Each of the four beams in the table was duplicated once.

	h	d	a	a/d	ρ_s
Specimen	[mm]	[mm]	[mm]	[-]	[%]
BE01A	300	273	1000	3.49	0.50
BE02A	300	271	1000	3.66	0.89
BE01B	600	573	2000	3.49	0.47
BE02B	600	571	2000	3.66	0.85

Table 3.1: Dimensions of test beams from [77]

CHAPTER 3. EXPERIMENTAL INVESTIGATION OF FLEXURAL CRACKING WITH RESPECT TO MEMBER DEPTH

The concrete compressive strength was measured from cylinder tests which were between 40 – 50MPa for all members. The beams were subjected to four-point-bending with a constant moment span of 1000mm for the small beams and 2000mm for the large beams.

Surface displacements were continuously measured in the constant moment span with the use of the ARAMIS measuring system, based on digital image correlation. Both crack spacings and crack widths in the constant moment span were obtained from the analysis of the surface displacements.

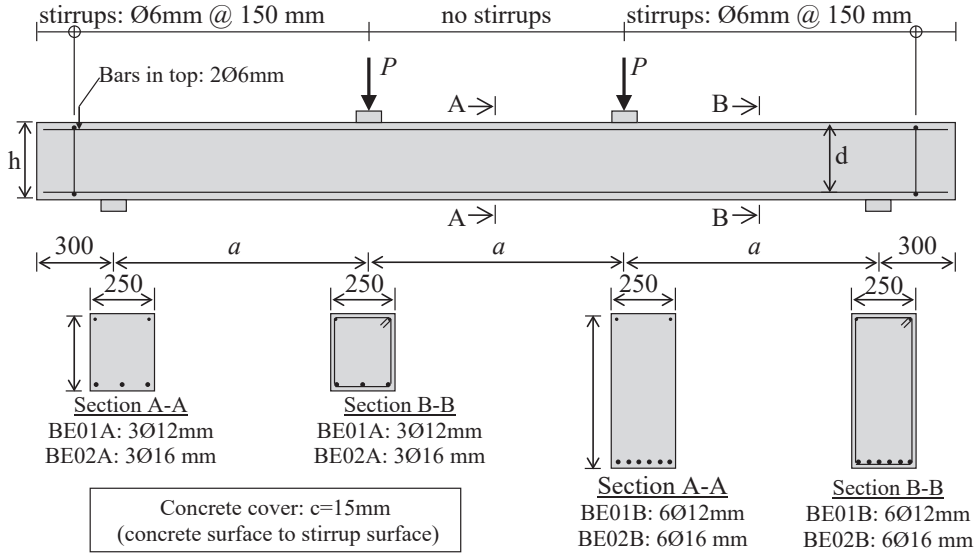


Figure 3.1: Geometry of tested beams, reprint from [77]

3.2 Results

3.2.1 System of cracks

Fig. 3.2 shows the development of cracks within the constant moment span of one of the small beams and one of large beams with respect to four load intervals. For the small beam in Fig. 3.2a, nine of the total 12 cracks started forming at a load lower than 50% of P_y and continued to propagate towards the neutral axis as the load increased. The remaining three cracks formed between 50 – 60% of P_y and propagated to a smaller height than the earlier formed cracks. No new cracks formed after 60% of P_y .

While most of the 21 cracks in the large beam, as shown in Fig. 3.2b, also formed at load levels lower than 50% of P_y , only six of them propagated further than mid-height of the beam. The remaining 15 cracks stayed concentrated around the tensile reinforcement, curving towards the six higher cracks and formed a forking pattern, also observed by Leonhardt[14], which was not seen in the small beam.

The crack patterns in the two beams thus have very obvious differences. In the large beams two different crack systems were observed where a significantly smaller spacing between cracks was seen at the level of the tensile reinforcement compared to that at mid-height of the member. The two different systems were identified as the primary flexural cracks and the local secondary cracks. In the small beams, primarily one system of cracks developed, thus secondary cracking did not occur.[77]

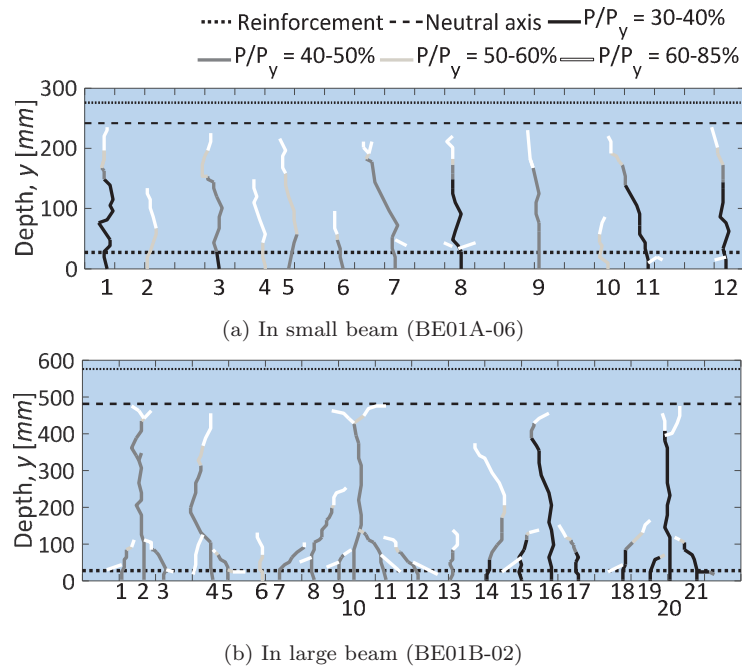


Figure 3.2: System of cracks in constant moment span, reprint from [77]

3.2.2 Development of crack height

In Fig. 3.3 the measured crack height relative to the beam height is plotted with respect to the increase of load for the first five flexural cracks in two small beams and two large beams. When comparing the two plots, a difference can be observed in the way the cracks propagated and the load interval in which the cracks grew. For the small beams, the cracks in both beams all grew slowly towards a constant value over a load span of 10 – 30% of P_y . Meanwhile, the cracks in the large beams developed significantly faster, immediately reaching a height close to the final height.[77]

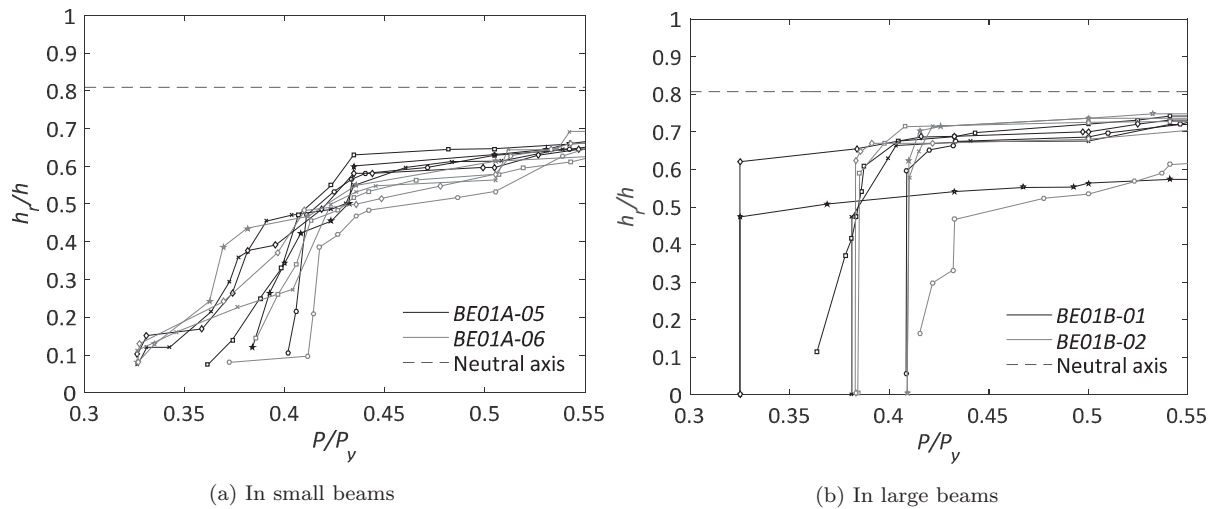


Figure 3.3: Development of crack height relative to height of beam, reprint from [77]

This difference in the development of the crack height in the small and large beams could possibly be explained through the phenomenon of tensile softening, which was reviewed in Section 2.1. If it is assumed

that the concrete can still transfer tension across a crack until the crack has reached a certain width, w_0 , it would mean that equilibrium can be established at a lower reinforcement stress than if the concrete was stress-free. Due to the difference in the steepness of the stress variations in the cross-sections of a small and a large beam, equilibrium would be established at a lower crack height in a small beam than in a larger beam.

3.2.3 Variation of crack width

In Fig. 3.4 the crack width, measured in various levels, is shown for all cracks at 60% of P_y for a small and a large beam. The two figures make it possible to study the variation of the crack width along the height of the cracks and compare the crack-width-shape for the small and the large beam.

When drawing attention to the primary cracks, a clear difference is seen in the crack-width-shape between the small and large beam. For the small beam in Fig. 3.4a, more or less all the cracks were widest at the tension face and decreased uniformly towards the crack tip. The maximum width in the primary cracks in the large beam was, on the other hand, found in the web, while the width at the tension face and at the reinforcement was significantly smaller. The primary cracks of the large beam exhibited a shape comparable to a fish, as also observed by previous researchers for members without sufficient distributed reinforcement in the web, e.g. Nielsen [7].

The maximum crack width measured in the small beam at 60% of P_y was 0.26mm at the tension face and was found in crack no. 12. For the large beam, the largest widths of the primary cracks were located in the web, approximately $150 - 180\text{mm}$ from the tension face. The maximum width was measured to 0.39mm in crack no. 10. The same crack had a width of 0.075mm at the tension face.[77]

The difference in crack-width-shape in the small and large beams can be owed to the existence of the secondary cracks in the large beams only. At reinforcement level of the large beams the number of cracks is significantly greater than at mid-height. From a requirement of compatibility this must result in smaller crack widths at the reinforcement level because the total deformation is distributed across a larger number of cracks. When moving away from the reinforcement towards mid-height, the secondary crack gradually closes and the remaining cracks thus have a large width.

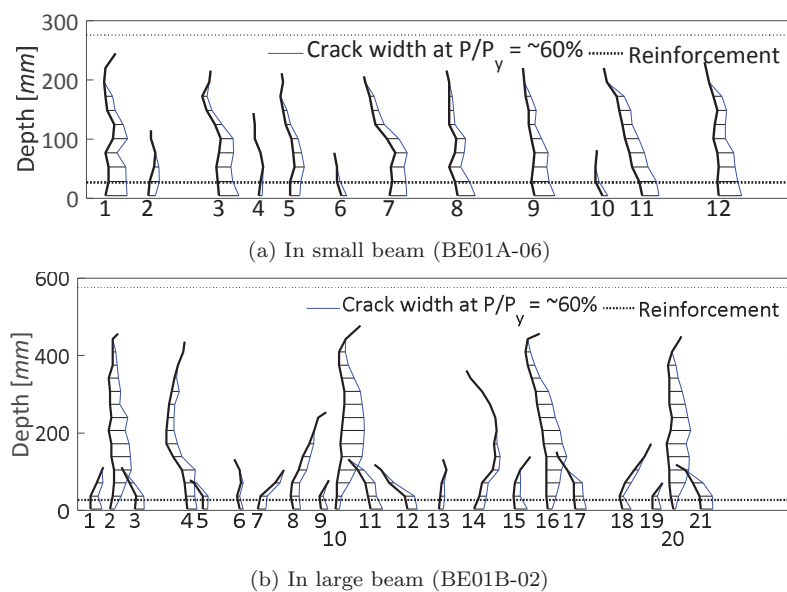


Figure 3.4: Crack width variation at 60% of yield load, reprint from [77]

3.2.4 Sum of crack widths

When a beam is subjected to a given curvature it will result in an elongation of the part of the beam that is subjected to tension. When assuming that plane sections remain plane, the largest elongation will occur at the tension face and decrease towards the neutral axis. Due to the fact that the concrete's ability to elongate is very limited, it must be reasonable to assume that crack widths are associated with this elongation resulting in the deflection of the beam.

To support the above-stated, the sum of all crack widths within the constant moment span was investigated. In Fig. 3.5 the summations of all cracks are plotted for five different load levels for a small and a large beam, respectively. As can be seen, the crack width variation for the small beam in Fig. 3.5a resembled the shape of the individual cracks seen in Fig. 3.4a in the small beams.

The result of the summation of crack widths in the large beam, in Fig. 3.5b, was also linear although the individual primary cracks were fish-shaped. This could imply that, in the large beams, the primary cracks were restrained from opening due to the reinforcement and therefore additional (secondary) cracks formed together with a primary crack.

The shape of the total deformation in cracks is thus the same for the small and the large beams.

The sum of crack widths at the tensile face in the large beam is approximately double the size of the sum of widths in the small beam. This indicates a linear proportionality between with the depth of the member when the reinforcement is scaled accordingly.[77]

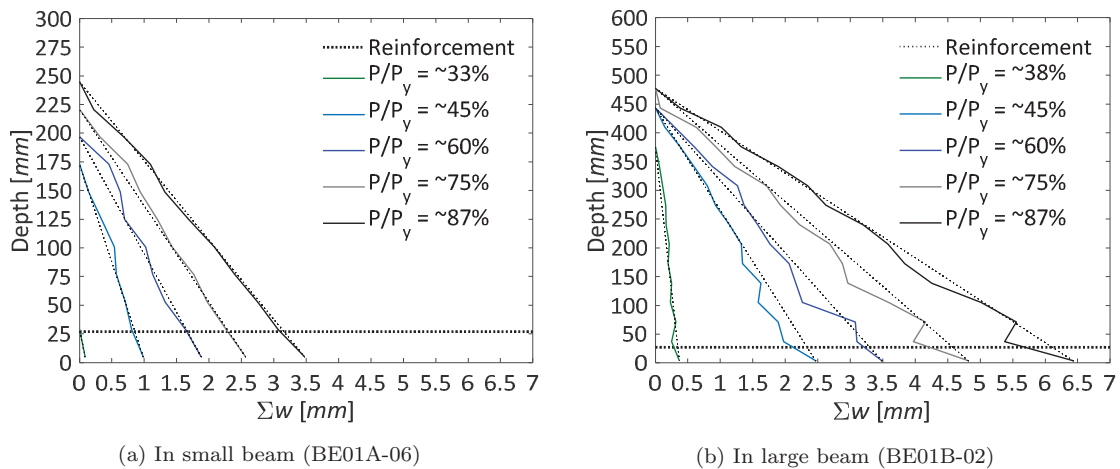


Figure 3.5: Sum of crack widths of all cracks in one member at five different load levels, reprint from [77]

CHAPTER 3. EXPERIMENTAL INVESTIGATION OF
FLEXURAL CRACKING WITH RESPECT
TO MEMBER DEPTH

4 EMPIRICAL STUDY OF CRACK SPACINGS

4.1 Introduction

From the literature review in Chapter 2 it is clear that cracking in both tensile and flexural members is a complex phenomenon. In terms of the physical interpretation of it, the models referred to for the estimation of crack spacing also rest on fairly different assumptions as to which parameters are of influence. These models are all, to some extent, validated against experimental results but most often only compared to one or a few experimental series with limited parameter variation. Furthermore, cracking in concrete is, to a certain level, a random process primarily due to the material's heterogeneity, and it is therefore associated with large uncertainties. In the light of the aforementioned circumstances, it is deemed relevant to investigate the variation of crack spacing in a statistical manner, on a basis of a large dataset.

This chapter concerns the analysis of crack spacings measured from test of, firstly, tensile members and, secondly, flexural members. For this purpose two databases are established, one with a total of 142 reinforced concrete tensile members and another with 462 members subjected to bending. The tensile members originate from 15 different experimental programmes while the beams originate from 75 different programmes found in the existing research. This includes eight flexural tests and four tensile tests conducted at the University of Aarhus as part of this current research project.

The following chapter consists of four parts. After a few important introductory remarks, the statistical methods used to analyse the databases are briefly described. Then the tensile members are treated followed by the flexural members, which are treated in approximately the same manner. Lastly, the crack spacing in tensile members and the cracks spacing at the level of the reinforcement in flexural members are compared due to the fact that reviewed existing models are more or less the same for the estimation of these two different crack spacings.

4.1.1 Categorisation of beams with respect to dimensions

The beams in the database are divided into groups with respect to their depth under the assumption that there is a lower limit of $d = 300mm$ for beams used for structures:

- $d < 300mm$ Beams for laboratory testing
- $300mm \leq d \leq 1000mm$ Structural beams for buildings
- $d > 1000mm$ Structural beams for buildings and bridges (usually prestressed)

Within the three different categories; laboratory, structural beams for buildings and structural beams for bridges it obviously seems most relevant to investigate the structural beams because these are the most practically applicable beams. However, the laboratory beams are also investigated in the current study for academic reasons and because many existing tests stem from this group, which means that many existing models are established from observations of these. If the laboratory-sized beams behave differently to the structural beams this is thus important information with regard to the validation of results. Furthermore, if it is the case, it can be part of the reason why some conclusions in the reviewed literature are conflicting.

4.1.2 Aim of study

The empirical study has primarily been carried out in order to gain more knowledge of crack spacings in flexural members. However, it is relevant to first study crack spacings in tensile members as this is

the simple case of tensile cracking and most theory on crack spacing in flexural members (at the level of reinforcement) is based on observations of test of uni-axial tensile members.

The aim of the study is to gain greater knowledge of the following subjects of cracking and crack spacings:

- Which parameters control crack spacings in tensile and flexural members, respectively?
- What are the relations between extreme and mean crack spacings in tensile and flexural members, respectively?
- Which existing models are able to estimate crack spacings across the two databases with the best precision?
- Is cracking in tensile members and flexural members directly associated and dependent on the same controlling parameters?

Only investigated for flexural members:

- Can a stabilised crack system in the flexural members be identified? Specifically, a stress level to which the crack spacing is constant above this.
- Do the beams, characterised as laboratory beams and structural beams in the introduction above, behave in the same manner or do different behaviour patterns apply?

4.1.3 Consistent method of collecting crack spacing data

Flexural members

The test beams included in the database all have one thing in common, which is that photos exist of their crack pattern induced by loading. This important prerequisite was established in order to be able to measure all crack spacings in the same consistent manner from the photos. It is thus an attempt to avoid subjectivity and to create comparable data resting on the same basis. This means that no crack spacing data is copied directly from the literature. Instead, all crack spacings are measured from the crack pattern of the test specimens. The details of the process of measuring the crack spacings will be described in a later section.

This consistent way of collecting the crack spacing data means that the database not only hold mean crack spacings but also hold every single crack spacing within a test member. Furthermore, several uncertainties are excluded by measuring the spacings in this manner. One of the most common uncertainties that could arise, is not knowing where crack spacings given in an experimental report have been measured; whether it is at the side face of a beam, at the bottom of a beam, at mid-height or at reinforcement level. As the literature review revealed, the crack spacing varies with respect to the location considered. It is therefore important to have information about this in order to be able to accurately analyse the results. Another uncertainty is not knowing whether any cracks have been excluded from the measurements and why. With the method used in this thesis, it is always possible to go back and study the crack pattern and analyse its reliability.

An uncertainty arising from the method used in the current study is that cracks of very small crack widths are difficult to observe with the naked eye and will therefore only be detected if images of the test members have been treated with digital image correlation. It is thus accepted that cracks smaller than approximately 0.05mm in width have not been detected and are thus not included in the database.

Tensile members

With respect to the database of the tensile members, 85 members out of the total 142 members, include photos of the crack pattern. In these 85 members, the crack spacings are thus measured from photos while the data of the tensile members without photos are evaluated and concluded to be reliable with respect to the reported crack spacings. The expansion of the database to tests without photos was performed to broaden the statistical basis.

One of the largest uncertainties with respect to crack spacing measurements in tensile members is whether the distance from the end of the member to the nearest crack is regraded as a crack spacing. The reason why this could interfere with results is elaborated in the section concerning the tensile members. The crack spacings in the current database do not include the distance to the end of the specimens.

Another uncertainty connected to the tensile members which cannot be avoided in this current study, is the influence of the limited length of the test members. If, for example, a member with a length of 1000mm has five formed cracks but in a member with a length of 1010mm, but otherwise the same properties, six cracks would form, then the mean crack spacing in the first member is larger than in the latter even though they should be the same in theory. This uncertainty is accepted as it is believed that, for a large database, the issue will resolve itself and more or less even out because both too small and too large crack spacings are produced from it. The issue is also sought to be eliminated in some of the following analysis by excluding members which are regarded to have a small length and a small number of cracks.

4.2 Statistical toolbox

The statistical theories used in the analysis of the crack spacings in tensile and flexural members are briefly described in this section and involves the topics; test of normality, correlation, linear regression and assessment of model error.

4.2.1 Test of normality

To investigate whether the crack spacing data can be assumed to originate from a normal population, two different methods are used. Firstly, it is investigated graphically through a q-q plot and secondly, a statistical test of normality is applied.

A q-q plot is a plot of the quantiles of a standard normal distribution against the quantiles of the sample data. The latter should resemble an approximate straight line if the data sample is from a normal population. The q-q plot is often used instead of plotting the data in a histogram for the reason that the q-q plot is more sensitive to deviation from the normal distribution.[78]

The statistical test of normality is a significance test with a null-hypothesis being that a certain data sample is from a population which is normally distributed. According to D'Agostino et al.[79] the Shapiro-Wilk Test and D'Agostino & Pearson Test are both test well-suited for moderate sample sizes as well as being powerful and informative because they test for non-normality associated with both skewness and kurtosis. In the current study, the D'Agostino & Pearson Test is used as the primary test while the Shapiro-Wilk Test is used as a subsequent check. The D'Agostino & Pearson Test is briefly described below, where some of the quantities involved are given, while the whole method is found in [79].

The test statistics, which combines skewness and kurtosis are:

$$K^2 = Z^2(\sqrt{b_1}) + Z^2(b_2) \quad (4.1)$$

where $Z(\sqrt{b_1})$ and $Z(b_2)$ are the normal approximation of $\sqrt{b_1}$ and b_2 which are the descriptive statistics of the skewness and the kurtosis, respectively:

$$\sqrt{b_1} = m_3/m_2^{3/2} \quad (4.2)$$

$$b_2 = m_4/m_2^2 \quad (4.3)$$

$$m_k = \frac{\sum_{i=1}^n (x_i - \bar{x})^k}{n} \quad (4.4)$$

where \bar{x} is the mean value of the sample and n is the sample size.

If $\sqrt{b_1}$ and b_2 are close to 0 and 3, respectively, there are indications of the sample being from a normal distribution. How significantly these deviate from 0 and 3 provide information about the form of non-parametric distribution.

P-values can be found for $\sqrt{b_1}$ and b_2 separately, where, for a null hypothesis of population normality, $Z(\sqrt{b_1})$ and $Z(b_2)$ are both approximately normally distributed. For calculation of these see [79]. The K^2 statistics, on the other hand, is approximately a chi-squared distribution when the population is normally distributed, which should therefore be used to find the p-value for this combined statistics.

4.2.2 Correlation

The coefficient of correlation between two parameters can be used, as part of the regression analysis, to investigate whether any of the included variables are dependent on each other. This is important because if two variables are dependent/correlated in a data sample, they will not necessarily both show as significant in a linear regression model even though they could both have influence on the variable that is sought to be described, which is called the dependent variable.

The correlation coefficient, r , between two variables, is calculated with Pearson's linear correlation coefficient:

$$r = \text{corr}(x, y) = \frac{\sum_{i=1}^n (x_i - \bar{x}) \sum_{i=1}^n (y_i - \bar{y})}{\sqrt{\sum_{i=1}^n (x_i - \bar{x})^2 \sum_{i=1}^n (y_i - \bar{y})^2}} \quad (4.5)$$

where x_i and y_i are the two variables with i number of data in the sample and \bar{x} and \bar{y} are the mean values.

The r-coefficients can take a value between -1 and 1 and describes the linear association between two variables. If $r = 0$ there is no apparent linear relation between the two variables. A value above 0 indicates that the variables are associated positively, so that if one variable increases, so does the other. The size of r indicates how close the association/correlation is between the variables where a value of $r = 1$ means total correlation where the plotted data (x,y) will form a straight line with a positive slope. The smaller r is, the more the data deviate from the straight line.

For negative r-coefficients, the same applies, but for a linear association with a negative slope. [80]

4.2.3 Multi-variable linear regression

In the analysis of the databases, regression is used to investigate which parameters are of influence to the variation of the crack spacing. The regression model used for the purpose is a multi-variable linear model with a constant term:

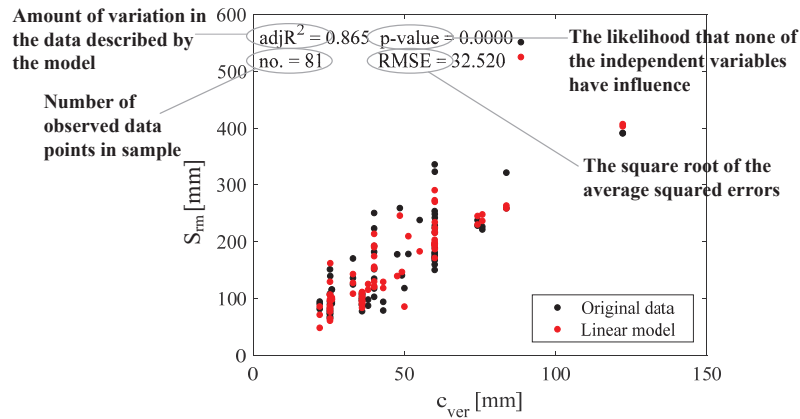
$$S_{rm} = k_0 + k_1d + k_2x_2 + k_3x_3 + \dots + k_nx_n \quad (4.6)$$

where the mean crack spacing, S_{rm} , is the dependent variable while x_n are the independent variables with an associated coefficient, k_n , and a constant term, k_0 . The coefficients k_n are estimated from the least square method where the sum of the squared errors is minimised. The errors, also called the

residuals, are the differences between the values estimated by the regression model and the observed values. This approach requires that the following conditions are met: 1) the relations between the independent variables and the dependent variable are linear, 2) the residuals of the regression model should be normally distributed, 3) the data cannot be heteroscedastic, and 4) the independent variables should not be too closely correlated ($r < |0.8|$) [80]. It is assumed that the databases of crack spacings in tensile members and flexural members meet the above conditions.

The result of a regression model is, in the following analysis of this chapter, presented in a plot and/or a table like the example shown in Fig. 4.1 and Table 4.1. The table lists statistics of the model and the coefficients for each independent variable in the model. In the example, the model consists of two independent variables, x_1 and x_2 , which are multiplied by the coefficients k_1 and k_2 , respectively. A p-value is given for each of the terms in the model, which describes the probability of whether the coefficients are random or due to variation in the data.

The p-value is determined through hypothesis testing and describes the statistical significance of a parameter. The null hypothesis states that the coefficient is zero (the variable in question has no influence). If the p-value is less than or equal to 0.05 there is no evidence that the variable does not have an influence. On the other hand, if the p-value is larger than 0.05 it is likely that the coefficient is random and not due to any real variation in the data. Accepting a value of 0.05 means that, when a null-hypothesis is rejected, there is “only” 5% probability that a different sample of data, describing the same, would show a larger probability (larger p-value) of the null-hypothesis being true.



Regression model		
$adjR^2 = 0.865$		
$RMSE = 32.5$		
	k_n	p-value
k_0	10.340	0.301
k_1	0.920	8.4 e-13
k_2	-1.102	3.86 e-4

Table 4.1: Explanatory table of coefficients and statistics of linear regression

Figure 4.1: Explanatory plot of linear regression model

At the top of the Fig. 4.1, there are four different values. The bottom left value is the number of data in the sample used to create the regression model. The three other values describe the regression model’s performance. The top right value is the p-value for the whole model, describing the probability that all the coefficients, $k_0 - k_n$, are insignificant. The top left is the adjusted R^2 also listed in the table, which describes how much of the variation in the data is described by the model. “Adjusted” means that the influence of the number of independent variables is taken into account. The general R^2 will increase when adding independent variables to a model, not necessarily because the model is better but because more degrees of freedom are added. The general R^2 is estimated by [80]:

$$R^2 = 1 - \frac{SSE}{TSS} \quad (4.7)$$

where SSE is the sum of squared errors: $SSE = \sum_{i=1}^n (y_i - \hat{y}_i)^2$. Here y_i is the observed data and \hat{y}_i is the modelled data. TSS is the total sum of squares: $TSS = \sum_{i=1}^n (y_i - \bar{y}_i)^2$, where \bar{y}_i is the mean value of the observed data. In other words, the R^2 is the ratio of the total sum of squares, which is described by the model.

Lastly, the bottom right value in the figure is the root mean square error, denoted RMSE, which is a measure for the model's average deviation from the observed data. The RMSE is the square root of the squared average distance between the observed data and the modelled data [80]:

$$RMSE = \sqrt{\frac{SEE}{n}} = \sqrt{\frac{\sum_{i=1}^n (y_i - \hat{y}_i)^2}{n}} \quad (4.8)$$

4.3 Tensile members

In the following section the crack spacing in tensile members is analysed empirically by use of the database of tests. Firstly, the content of the database and the method of measuring the crack spacing are described. Secondly, the results of the analysis are presented and discussed. Thirdly, the measured crack spacings are compared to estimates of crack spacings with the use of the reviewed existing models from Chapter 2.

The analysis of the crack spacing in tensile members is divided into three parts:

1. Through multi-variable linear regression it is investigated which parameters have a significant influence on the variation of the crack spacing. The combinations of parameters used in reviewed existing models are also investigated.
2. The relations between minimum, maximum and mean crack spacings are investigated through distribution plots.
3. The reviewed existing models are compared with the test data.

4.3.1 Introduction to the database

The tensile members in the database originate from 15 different experimental programmes collected from existing literature and include four specimens conducted at Aarhus University as part of the present research project[81]. Table 4.2 lists all the test series in the database and states their original focus. In an attempt to create a database of comparable members all the tensile members satisfy the following:

- All specimens are quadratic
- All specimens are subjected to pure tension
- The specimens are reinforced with normal deformed steel reinforcement bars and the concrete is of normal strength or high-strength regular concrete mix. Thus fibre-reinforced members, glass fibre bars etc. are not considered in this study
- The specimens have been subjected to normal temperatures and curing conditions
- A stabilised crack pattern is developed in the specimens

Reference	Country	No. of specimens	Experimental focus	Category
Thangaratnam & Østrup (2018) [81]	Denmark	4	Influence of bar diameter on cracking	I
Rimkus & Gribniak (2017) [82]	Lithuania	19	Influence of multiple bars on cracking	I
Baah (2014) [83]	Ohio U.S.	4	Cracking in bridge structures	II
Kharal (2014) [84]	Canada	6	Cracking in fibre reinforced concrete	II
Wenkenbach (2011) [85]	UK	4	Tension-stiffening with large ϕ_s	I
Wu & Gilbert (2008) [86]	Australia	6	Tension stiffening under sustained loads	I

Bischoff (2003) [87]	Canada	2	Cracking in fibre reinforced concrete	III
Arduini & Russo, S. (2001) [88]	Italy	10	Cracking in NS and HS concrete	III
Bigaj & Uijl (2001) [89]	Germany	7	Influence of f_c and ρ_s on cracking	III
Eligiehausen et al. (2001) [90]	Germany	8	Influence of f_c and ρ_s on cracking	III
Hikosaka et al. (2001) [91]	Japan	3	Influence of ρ_s on cracking	I
Al-Fayadh (1997) [92]	Sweden	9	Cracking in NS and HS concrete	II
Lorrain et al. (1997) [93]	France	25	Cracking in HS concrete	III
Farra & Jaccoud (1993) [94]	Switzerland	33	Cracking and deformation	II
Van der Veen (1990) [95]	Netherlands	2	Influence of temperature variations on cracking	III

Table 4.2: Experimental programmes in database of tensile members

Measuring technique

Initially, when tests were collected for the database, the intention was to restrict the database to members where photos of the final crack pattern existed in order to be able to measure spacings directly on the photos. However, a majority of the tests in the existing literature do not contain photos of the cracked members making the database and thus the statistical basis for the results is too small. Therefore, carefully selected members without photos have been added to the database. With respect to these tests, the mean crack spacing, and if available, the minimum and maximum spacing, are copied from the text or tables in the experimental reports. This resulted in a database of 37 tests without photos of the crack pattern and 85 with photos and a total of 458 single measurements of crack spacings.

The members are grouped into three categories concerning the quality of the results. The individual categories are characterised by:

Category I: Photos are of good quality with clearly visible cracks. The information regarding the experimental set-up, materials, techniques of measurements and other parameters in relation to the specimens are clear and unambiguous.

Category II: Photos of the crack pattern are of good or medium quality. A few of the specimens are without photos, but in this case there are tables of results and very clear descriptions of how the measurements are carried out and they are in line with the criteria for the measuring described below. The circumstances of the experimental set-up are described well but in some cases with a few uncertainties.

Category III: There are no photos available of the crack pattern and the technique used to measure the spacing of cracks is not described in detail. Information about the experimental circumstances is inadequate in some cases.

All 85 crack patterns are measured in the same manner and are achieved by, firstly, copying the photo into a CAD software program where it is scaled according to the geometry of the specimen. Secondly, a measuring string is placed in the centre of the tensile member on the photographed surface, as shown in Fig. 4.2a. Lastly, measuring points are placed each time a crack meets the string.

The distance from the end of the member to the nearest crack is not regarded as a crack spacing. The reason for this is that the boundary effects are unknown. The end of the specimen cannot be assumed to be the same as an internal crack face because the concrete surface at the end is stress-free and the bond between concrete and reinforcement adjacent to the end surface has not been subjected to the same effects as the bond adjacent to a formed crack.

Fig. 4.2b shows how the measured crack spacings in each member deviate from the mean crack spacing for each member. On average, the crack spacing of a member deviates 25% from the mean spacing.

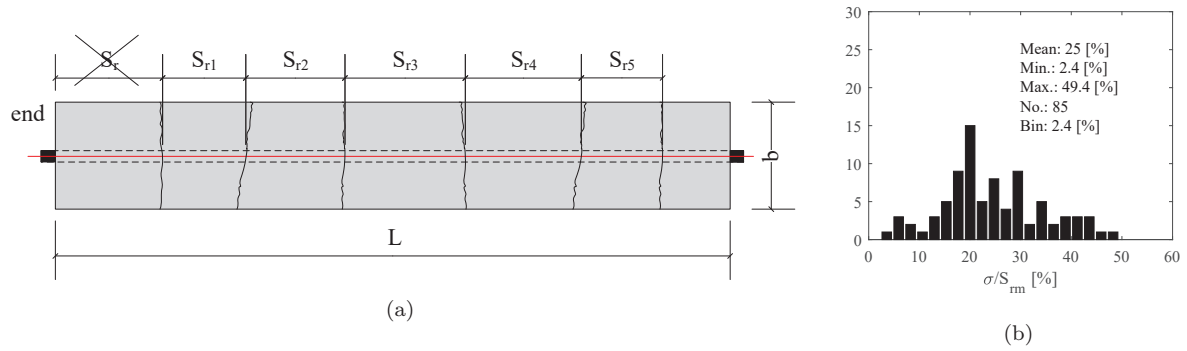
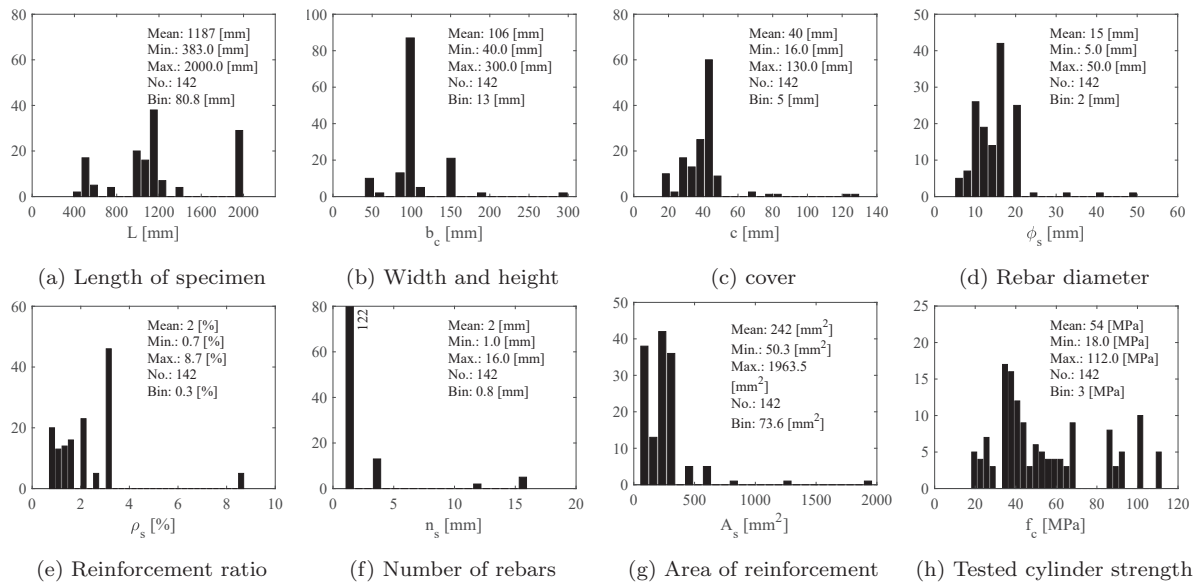


Figure 4.2: (a) Crack spacing measurements in tensile members, (b) Distribution of the standard deviation of crack spacings relative to the mean crack spacing

Distribution of parameters

All geometric and material parameters associated with each test member, collected from the experimental reports, are summarised in the histograms in Fig. 4.3. Most of the parameters are represented in a large interval which should make it possible to analyse the influence of the different parameters on the crack spacing over large parameter spans.



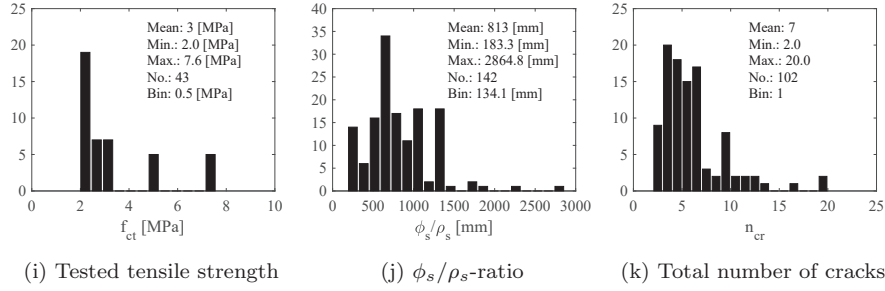


Figure 4.3: Distribution of parameters in the tensile test members

Correlation between parameters

The included parameters in the regression analysis are listed in Table 4.3. They are selected on the basis of the literature review to either verify or reject that they have an influence on the crack spacing.

Parameter	Description
h	Height and width
c	Cover
ϕ_s	Diameter of reinforcement
n_s	Number of rebars
A_s	Area of reinforcement
ρ_s	Reinforcement ratio
ϕ_s/ρ_s	ϕ_s/ρ_s -ratio
f_c	Compressive strength

Table 4.3: Parameters included in the regression analysis

For the coming regression analysis the correlation between the listed parameters and the most important two parameters, c and ϕ_s/ρ_s , are listed in Table 4.4. The correlation coefficients, $r = corr(x, y)$, between two variables, x and y are listed for two different data samples, described below, where coefficients above 0.65 are highlighted as this is assumed to be a high level of correlation. Correlation is investigated in order to be able to determine whether later results are affected by the distribution of the available data.

The regression analysis is carried out for a selection of tests in the database with the best reliability. This data sample holds 50 test members and includes the tensile members:

- from category I and II
- with one reinforcement bar ($n_s = 1$)
- with 5 or more cracks ($n_{cr} \geq 5$)
- longer than or equal to $L = 960mm$

In order to be able to investigate the crack spacing with a larger statistical basis than the 50 selected members, an analysis is also carried out for the whole database of 142 members.

The table shows how the cover and the ϕ_s/ρ_s -ratio is positively correlated with coefficients of $r = 0.88$ and $r = 0.87$ for all members and selected members, respectively. Only 20 members out of all the members have

more than one rebar, which is why the cover and the height of the members are highly correlated because the height and two times the cover is approximately the same measure. For the selected 50 members, the reinforcement ratio, ρ_s , and the ϕ_s/ρ_s -ratio as well as ρ_s and the cover, c , are positively correlated with a relatively high r-coefficient.

x,y	All test		Selected tests		x,y	All tests		Selected tests	
	no.	r	no.	r		no.	r	no.	r
$\phi_s/\rho_s, L$	142	0.40	50	0.38	c, L	142	0.43	50	0.63
$\phi_s/\rho_s, h$	142	0.55	50	<u>0.79</u>	c, h	142	<u>0.73</u>	50	<u>0.99</u>
$\phi_s/\rho_s, c$	142	<u>0.88</u>	50	<u>0.87</u>					
$\phi_s/\rho_s, \phi_s$	142	0.31	50	-0.09	c, ϕ_s	142	0.62	50	0.37
$\phi_s/\rho_s, n_s$	142	-0.31	50	-	c, n_s	142	-0.19	50	-
$\phi_s/\rho_s, A_s$	142	0.21	50	0.03	c, A_s	142	0.55	50	0.46
$\phi_s/\rho_s, \rho_s$	142	-0.62	50	<u>-0.77</u>	c, ρ_s	142	-0.45	50	<u>-0.66</u>
$\phi_s/\rho_s, f_c$	142	-0.10	50	-0.12	c, f_c	142	-0.16	50	-0.21

Table 4.4: Correlation between various parameters

4.3.2 Analysis of crack spacing

As explained above, the regression analysis is carried out for both a sample of the most reliable 50 members and the whole database. In the following section, detailed results are shown for the sample of the 50 members, while the results of the whole database are only explained briefly as, in most of the investigations, the results hold the same conclusions and thereby only serve to emphasise that they also hold for a larger number of tests.

Study of parameters of influence

The influence of various parameters is studied through the multi-variable linear regression model described earlier. In most of the investigations that follow, the mean crack spacing is analysed, not the maximum or minimum. Here one data point represents each test member as the average of all measurements in that member.

An iterative process is used to determine the regression model that only holds the parameters of statistically significant influence to the variation of crack spacing. The first of several regression models, holds all the nine parameters in Table 4.3. The parameter with the largest p-value for k_n in this model is removed and a new regression model is estimated. This procedure is repeated until the regression model only holds the parameters with p-values of less than 0.05. Only one parameter is removed for each iteration to account for correlation between some of the parameters.

The models shown in the following paragraphs are the result of this iterative process and therefore they only hold the significant parameters and a constant term. The regression models shown should describe the variation of the crack spacing with approximately the same precision as that of a regression model holding all the nine parameters. Thus the excluded parameters, statistically, do not describe any of the variation in the crack spacing.

Selected members

The result of the process described above is a regression model with only two significant parameters, namely the ϕ_s/ρ_s -ratio as the primary parameter with the lowest p-value and the diameter, ϕ_s , as the secondary parameter with a higher p-value and therefore less influence. This model, called Linear Model 1, shown in Table 4.5 and Fig. 4.4, explains 70% of the variation in the crack spacing and the constant term has a p-value well above 0.05, which means that it is insignificant and can with reason be excluded from the model.

Linear Model 1		
$adjR^2 = 0.701$		
RMSE = 31.1		
x_n	k_n	p-value
Const. term	-20.933	0.340
ϕ_s	2.995	0.007
ϕ_s/ρ_s	0.145	3.9 e-14

Table 4.5: Coefficients and statistics of linear regression form 50 selected tensile test

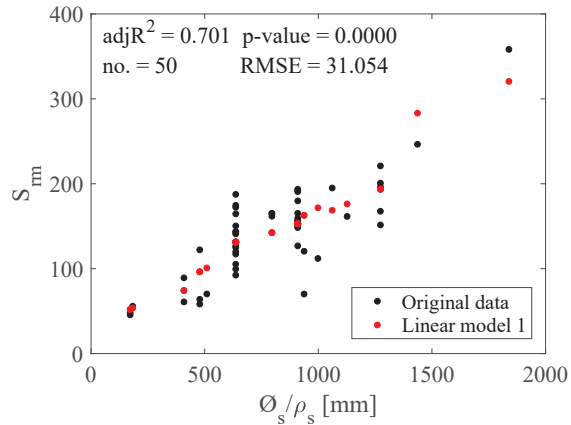


Figure 4.4: Linear regression from 50 selected tensile tests with ϕ_s/ρ_s and ϕ_s as predictors

Due to the fact that the ϕ_s/ρ_s -ratio and the cover were found to be highly correlated with an $r = 0.87$, it is investigated whether the cover is wrongly removed from the regression model and also if the cover can be used as a good predicting parameter. In Fig. 4.5 the distribution of the cover and the ϕ_s/ρ_s -ratio are illustrated for the data sample used in the regression analysis. A large number of the tensile members have a cover between 40 – 50mm while the ϕ_s/ρ_s -ratio is evenly distributed over a large interval.

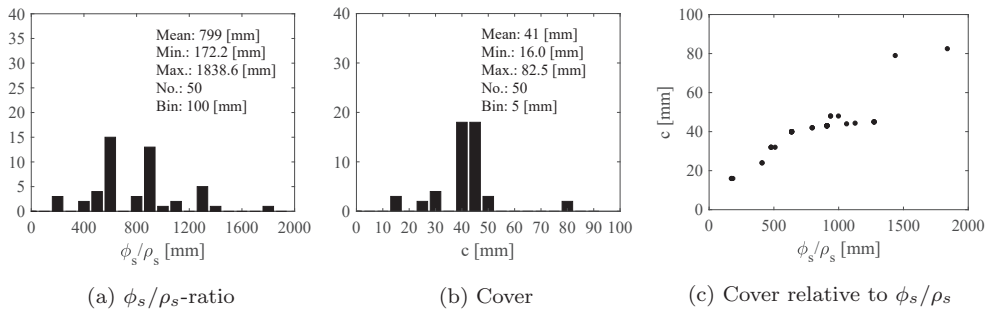


Figure 4.5: Distribution of correlated parameters in the selected data

Table 4.6 lists four regression models with four different combinations of the three parameters; c , ϕ_s/ρ_s and ϕ_s that show good performance with respect to the statistics $adjR^2$ and $RMSE$. The Linear Models 2, 3 and 4, which include the cover, are seen to perform well, with almost identical statistics as the Linear Model 1 without the cover.

Linear Models 4 and 5, holding only c and ϕ_s/ρ_s , respectively, both describe approx. 65% of the variation while Linear Model 2, which includes all three parameters describes 70% of the variation. With only an increase of 5%, this means that the two parameters; c and ϕ_s/ρ_s , describe almost the same variation in the crack spacing. The last parameter, ϕ_s , thus only contributes by describing 5%.

The p-values of the coefficients are overall larger in Linear Model 2 and 3 compared to Linear Model 4 and 5 due to the large correlation between the two parameters.

Through these regression models it seems that the following three combinations of parameters describe the same amount of variation in the crack spacing:

$$S_{rm} = k_0 + k_1\phi_s + k_2\phi_s/\rho_s \quad (4.9)$$

$$S_{rm} = k_0 + k_1c + k_2\phi_s/\rho_s \quad (4.10)$$

$$S_{rm} = k_0 + k_1\phi_s + k_2c + k_3\phi_s/\rho_s \quad (4.11)$$

where it would be possible to remove the constant term in all three models, because it has a p-value well above 0.05. This especially holds true for the model in Eq. (4.10) where the p-value is 0.88 and the constant term is very close to zero.

	Linear model 2		Linear model 3		Linear model 4		Linear model 5	
	$adjR^2 = 0.696$		$adjR^2 = 0.690$		$adjR^2 = 0.643$		$adjR^2 = 0.658$	
	RMSE = 31.3		RMSE = 31.6		RMSE = 33.9		RMSE = 33.2	
	k_n	p-value	k_n	p-value	k_n	p-value	k_n	p-value
Const. term	-25.400	0.230	-2.790	0.879	-21.850	0.235	30.833	0.017
c	-0.992	0.667	2.000	0.018	4.055	1.6 e-12	-	-
ϕ_s	4.218	0.169	-	-	-	-	-	-
ϕ_s/ρ_s	0.176	0.021	0.081	0.006	-	-	0.141	5.7 e-13

Table 4.6: Coefficients and statistics of linear regression for selected tensile members in the database

In Fig. 4.6a and 4.6b Linear Model 1 and 3, respectively, are used to describe the variation of crack spacing for a constant cover of 40mm and diameter varied from 8mm to 24mm. In the plots, the variations of the two terms in the models are shown separately and together. When comparing the plots, it can be observed that the final variation is very similar for the two different models.

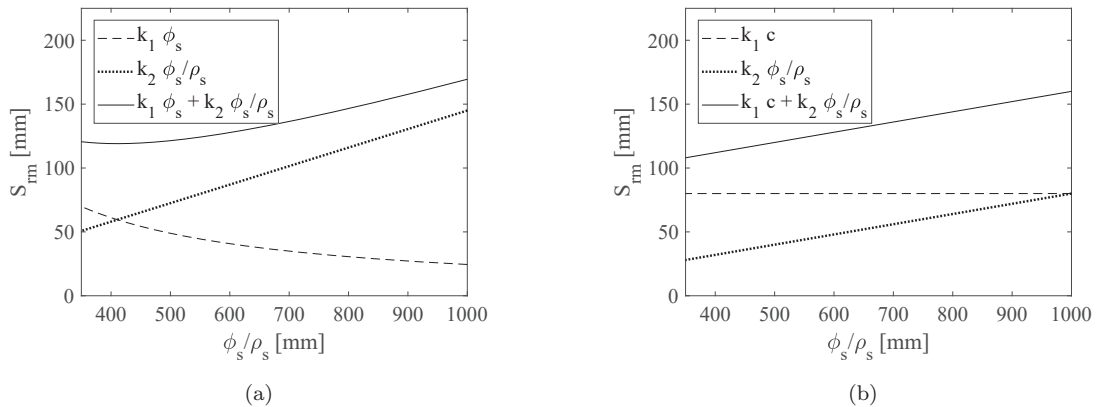


Figure 4.6: Variation of crack spacing with respect to ϕ_s/ρ_s -ratio (a) Linear model 1 with ϕ_s and ϕ_s/ρ_s as parameters (b) Linear Model 3 with c and ϕ_s/ρ_s as parameters

Model parameters

In the forthcoming regression analysis five different combinations of parameters, which are used in reviewed existing models from the literature review, are tested. The tested models are described in Section 2.2 and are: the Eurocode 2/the Model Code 2010 (EC2/MC2010), the Danish National Annex of the Eurocode 2 (EC2-NA(DK)), Nielsen’s model (MPN), the Tension Chord Model (TCM) and Beeby’s model (Beeby). Only the models’ parameter combinations are tested here, not the coefficient of each parameter from the models. The constant term of the linear regression model is excluded in this investigation because it does not exist in any of the reviewed models. As a consequence, both the $adjR^2$ and RMSE should be compared between the models. The highest $adjR^2$ means that the overall variation in the crack spacing is described well. Though, if the RMSE is high as well, there is a significant deviation between the estimated value and the observed data. This could mean that a constant term or a parameter is missing to describe the variation well.

The results of the regression analysis, using parameters from the reviewed models, are provided in Table 4.7. When comparing both the $adjR^2$ and the RMSE for the five different regressions models, they all perform fairly well, with only smaller differences in the $adjR^2$ and the RMSE.

Model param.	EC2/MC2010		EC2-NA(DK)		MPN		TCM		Beeby	
	$adjR^2 = 0.691$		$adjR^2 = 0.655$		$adjR^2 = 0.676$		$adjR^2 = 0.729$		$adjR^2 = 0.582$	
	RMSE = 31.3		RMSE = 32.7		RMSE = 31.0		RMSE = 34.9		RMSE = 34.1	
	k_n	p-value	k_n	p-value	k_n	p-value	k_n	p-value	k_n	p-value
c	1.906	7.6 e-4	-	-	-	-	-	-	3.557	5.2 e-34
ϕ_s	-	-	-	-	2.134	4.8 e-4	-	-	-	-
ϕ_s/ρ_s	0.083	0.003	0.127	3.8 e-09	0.137	1.6 e-16	0.175	1.7 e-33	-	-
$c^{1/3}$	-	-	12.406	0.008	-	-	-	-	-	-

Table 4.7: Coefficients and statistics of linear regression with various model parameters for 50 selected tensile tests in the database

The model parameters that perform best are the Eurocode/Model Code and the M.P. Nielsen because the $adjR^2$ is high combined with a low RMSE. Both models describe nearly 70% of the variation in the crack spacing. The expressions found from the regression are as follows.

Regression model with Nielsen’s parameters:

$$S_{rm} = 2.14\phi_s + 0.13\phi_s/\rho_s \tag{4.12}$$

Regression model with the Eurocode / Model Code parameters:

$$S_{rm} = 1.91c + 0.083\phi_s/\rho_s \tag{4.13}$$

Assuming that the relations between the mean and the maximum crack spacing are $S_{rm} = 0.665S_{rmax}$, the Eurocode Model formula with the original coefficients is: $S_{rmax} = 2.26c + 0.23\phi_s/\rho_s$ and the Model Code is: $S_{rmax} = 1.33c + 0.18\phi_s/\rho_s$. Their coefficients of the ϕ_s/ρ_s -term are seen to be larger than in the regression models in Eq. (4.12) and (4.13), which means that both the Eurocode and the Model Code suggests the ϕ_s/ρ_s -ratio to be more influential than the tests in the database indicates.

Beeby’s model, with only the cover as a parameter, both have the lowest $adjR^2$ and one of the highest RMSE, and is therefore the worst fit of the five regression models. The TCM, with only ϕ_s/ρ_s as a

parameter, has a good $adjR^2$, which means that the variation is described well but, with a high RMSE, the model deviates considerably from the observed data in some intervals. The Eurocode using the Danish National Annex with $c^{1/3}$ instead of just c does not give better results than the general Eurocode parameters.

The conclusion to the study of the 50 selected members is that a model with the parameters ϕ_s/ρ_s and c or ϕ_s/ρ_s and ϕ_s approximate the mean crack spacing with the best precision. However, it is important to add that other combinations of the three parameters c , ϕ_s/ρ_s and ϕ_s or even just c or ϕ_s/ρ_s alone make almost as accurate estimates of the crack spacing.

Non-linear regression analysis

Non-linear combinations of the three parameters appointed above as significant, namely c , ϕ_s/ρ_s and ϕ_s , have also been investigated. In the investigation the three parameters were allowed an exponent of the power n . The results were non-linear models that showed no notable improvement with respect to either the $adjR^2$ or the RMSE compared to the presented linear models. Therefore, the results are not shown here and the idea of a non-linear relations between the parameter was not pursued further.

All members

A regression model is also estimated for all the tensile members in the database (no.=142). This data sample contains 20 members with multiple reinforcement bars whereas the rest of the members only have one reinforcement bar in the centre of the rectangular cross-section. The coefficients of the estimated regression model are listed in Table 4.8 and illustrated with statistical values in Fig. 4.7. Here, 77% of the variation in the crack spacing is described with the same two independent variables as for the 50 selected tests, namely the diameter ϕ_s and the ϕ_s/ρ_s -ratio.

Linear Model 1		
$adjR^2 = 0.774$		
RMSE = 32.3		
Parameter	k_n	p-value
Const. term	-10.038	0.227
ϕ_s	3.194	3.1 e-9
ϕ_s/ρ_s	0.127	2.6 e-38

Table 4.8: Coefficients and statistics of linear regression for all tensile members

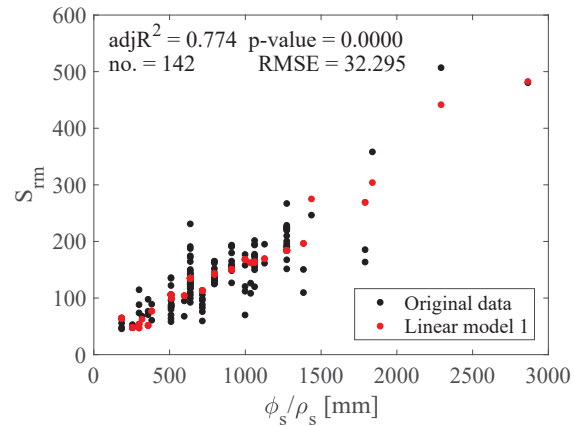


Figure 4.7: Linear regression for all tensile members, no. = 142, with ϕ_s/ρ_s and ϕ_s as predictors

Table 4.9 lists the other models with good results. The coefficients here are in the same size range as the models for the 50 selected members. Here, the Linear Model 2, with all three parameters, actually shows slightly better results than Model 1 in Fig. 4.8. The same three parameter combinations as for the 50 selected members (Model 1, 2 and 3) make the best models.

	Linear model 2		Linear model 3		Linear model 4		Linear model 5	
	$adjR^2 = 0.776$		$adjR^2 = 0.762$		$adjR^2 = 0.720$		$adjR^2 = 0.711$	
	RMSE = 32.2		RMSE = 33.2		RMSE = 36.0		RMSE = 36.5	
Parameter	k_n	p-value	k_n	p-value	k_n	p-value	k_n	p-value
Const. term	-12.867	0.133	-6.598	0.440	-18.571	0.038	25.487	3.0 e-4
c	0.831	0.177	2.192	1.398 e-7	3.940	8.5 e-41	-	-
ϕ_s	2.392	0.002	-	-	-	-	-	-
ϕ_s/ρ_s	0.105	1.7 e-8	0.072	1.6 e-6	-	-	0.141	7.8 e-40

Table 4.9: Coefficients and statistics of linear regression for all tensile members in the database

Model parameters

The regression models with the use of the parameters from reviewed models give more or less the same results as for the selected 50 tests, listed in Table 4.7. There are only small changes in the size of the coefficients k_n . The model parameters with the best fit are again the Eurocode/the Model Code and Nielsen’s model while the model parameter resulting in the least accurate fit is Beeby’s. The regression models from Nielsen’s parameters and Beeby’s parameters, which are the best and least accurate fit, respectively, are illustrated by the plots in Fig. 4.8. At the top of plots the coefficients of the two models are shown. The Table listing the coefficients for all five models, as for the selected models in Table 4.7 is not shown due to the very similar results.

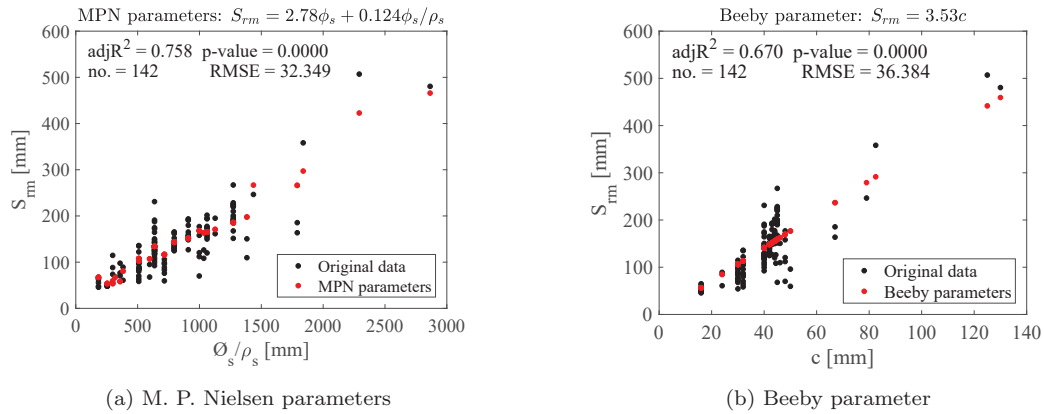


Figure 4.8: Regression with models for all tensile members in the database

Relations between extreme and mean crack spacings

All members

From Fig. 4.9–4.11 the relations between the extreme and the mean crack spacings are investigated where the relations S_{rmax}/S_{rmin} , S_{rm}/S_{rmin} and S_{rm}/S_{rmax} are plotted, respectively. The three relations are plotted against the ϕ_s/ρ_s -ratio because the former regression analysis showed that this was the most influential parameter on the crack spacing. The plots hold all the tensile tests in the database where the max., min. and mean spacing are known values. The dashed lines in the three graphs indicate the ratio found by most researchers to be the ratio between the extreme and mean spacing, discussed in the

literature review in Chapter 2.

The investigation has also been carried out for the 50 selected tests treated individually earlier, but the results are not shown here as they are similar to the following ones. The only difference was a small increase in the standard deviation and mean value of the relations S_{rmax}/S_{rmin} , S_{rm}/S_{rmin} and S_{rm}/S_{rmax} , most likely owing to the smaller amount of data.

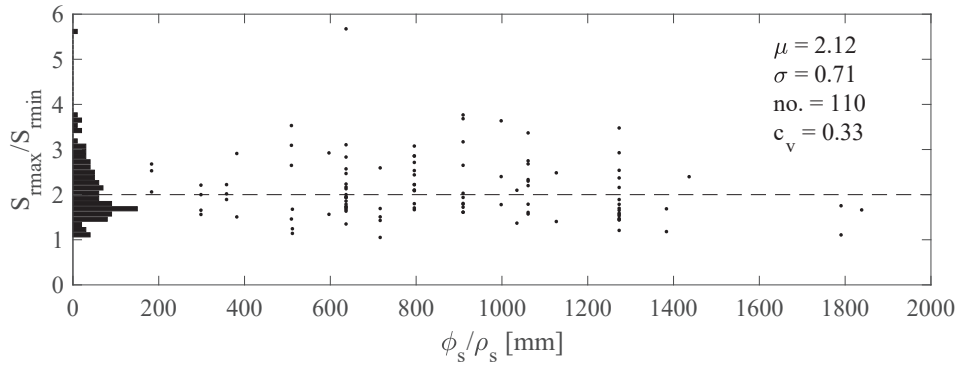


Figure 4.9: Relations between the maximum and minimum crack spacing as a function of the ϕ_s/ρ_s -ratio

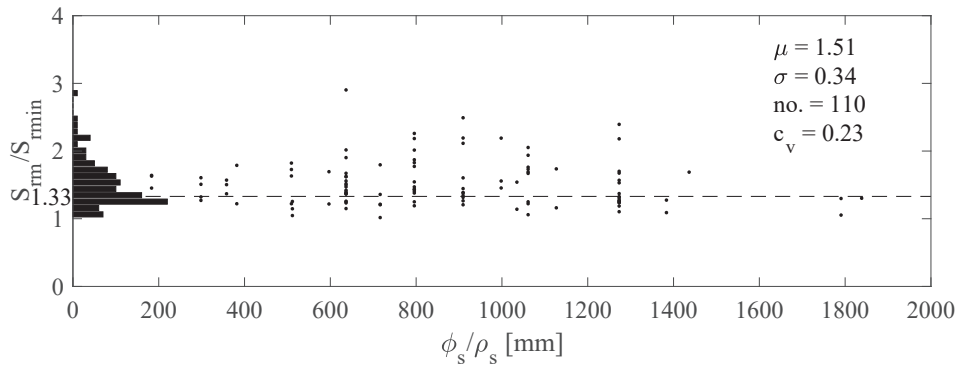


Figure 4.10: Relations between the mean and minimum crack spacing as a function of the ϕ_s/ρ_s -ratio

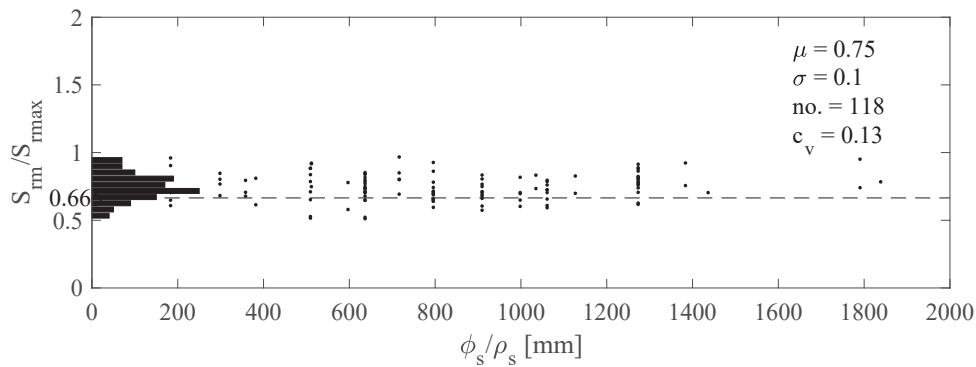


Figure 4.11: Relations between the maximum and mean crack spacing as a function of the ϕ_s/ρ_s -ratio

The mean values of the three ratios S_{rmax}/S_{rmin} , S_{rm}/S_{rmin} and S_{rm}/S_{rmax} , given as μ in the figures, are in fairly good agreement with the findings in the existing literature, despite the fact that the mean

values found from the database are slightly higher. The distribution of S_{rmax}/S_{rmin} is skew, exactly as Beeby[28] proposed it to be.

No notable difference is observed in the relations with respect to the parameter ϕ_s/ρ_s .

When comparing the coefficient of variation, denoted c_v on the plots, a larger deviation from the mean is seen for the minimum crack spacing than for the maximum crack spacing. The ratio between the mean and the minimum crack spacing varies 23% from the mean spacing whereas the ratio between mean and maximum spacing varies by only 13%. It can thus be concluded that, within the available data, there are larger uncertainties connected to the minimum crack spacing than to the maximum crack spacing and therefore the maximum crack spacing is a better basis for estimation.

4.3.3 Comparison of existing models and tests

The reviewed models, treated earlier with respect to their combination of parameters, are now compared to the tests using the models' original coefficients to estimate the crack spacing. For this comparison all tests are included. The same comparison was made for the 50 selected tests where the same tendency was found. The performances of the different models are compared with respect to the mean value, μ , of $S_{rm,test}/S_{rm,model}$ and the coefficient of variance, c_v , also called the relative deviation in the following. The value makes it possible to compare the deviation from the mean value even though the mean values are different for each model.

All members

The five different models are compared for the estimation of the mean crack spacing. Due to the fact that the Eurocode, the Model Code and Nielsen's model are formulated to estimate maximum crack spacings, these three models are also compared separately for estimation of the maximum crack spacing.

Two regression models found from the earlier investigations are also compared to the tests. The two chosen models are those that had the largest $adjR^2$ and lowest $RMSE$ without a constant term.

Mean crack spacing

The model comparisons are shown in Fig. 4.12 and 4.13. Notice the different scaling on the y-axis which was necessary to be able to observe the variation in the results. None of the models provide significantly better results than the others with respect to the relative deviation, c_v , which in all cases is between 24 – 29%. This is the consequence of the large correlation between the cover and the ϕ_s/ρ_s -ratio because all the models include at least one of the two parameters and are therefore fairly accurate.

The only conservative model, for all tests, is the Eurocode, where none of the estimated crack spacings are smaller than the observed crack spacings. On average, the crack spacings estimated by the Eurocode are twice the size of the ones observed, which is a notably large difference.

Overall, the comparison shows that the coefficients for the parameters in the different models are very important with respect to which model estimates the crack spacing most accurately. Beeby's model is the one that performs best with respect to a low relative deviation of $c_v = 0.25$ together with a mean value of $S_{rm,test}/S_{rm,model}$ of $\mu = 0.85$ which is the closest to 1 of the five models. This contradicts the result from the regression analysis of which model parameters that described the variation of the crack spacing with best precision, where the cover-parameter alone performed worst.

The EC2, MC2010, MPN and TCM all show weakness with respect to variation of the parameter ϕ_s/ρ_s . For the interval of ϕ_s/ρ_s below approx. 700mm, the models result in larger $S_{cm,test}/S_{cm,model}$ -ratios compared to ϕ_s/ρ_s -ratios above 700mm. This confirms that the models overestimate the influence of the ϕ_s/ρ_s -ratio as indicated earlier in the regression analysis, where coefficients for the ϕ_s/ρ_s -ratio were found to be considerably smaller than in the models.

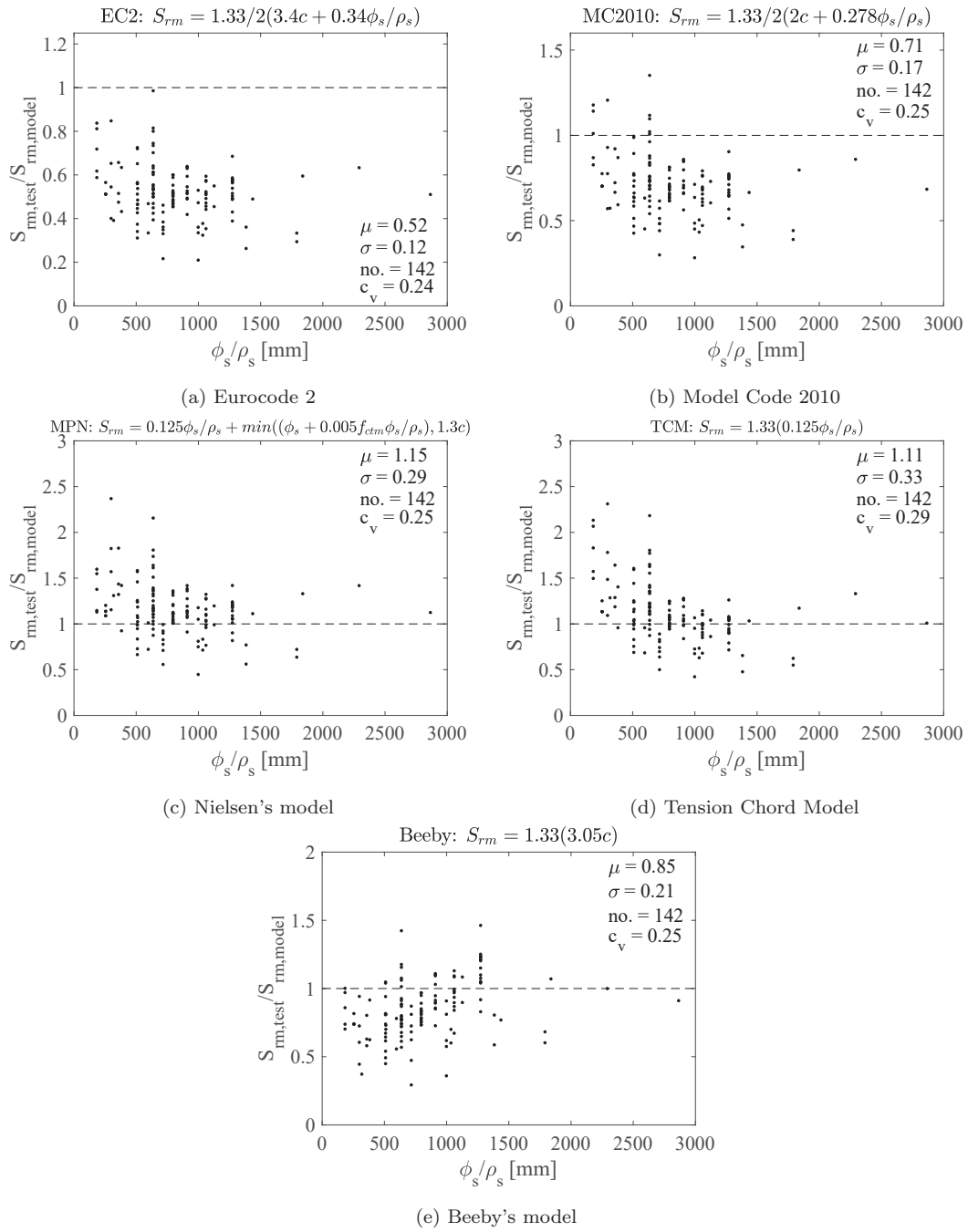


Figure 4.12: Comparison of model and test results for estimation of mean crack spacings

When the regression models, with a smaller influence of the ϕ_s/ρ_s -ratio is compared to the tests, as shown in Fig. 4.13, they estimate the crack spacing well for both small and large ϕ_s/ρ_s -ratios. The regression model which includes the cover as a parameter shows the best result with a mean value of $\mu = 1$ and a variation from the mean of 22%. The other regression model in Fig. 4.13b with ϕ_s as the second parameter has a slightly larger deviation from the mean of 24%. A large part of the variation in these two models must be owed to the random variation of the crack spacing.

The accuracy of the different models with respect to variation of a certain parameter has also been investigated for the following: the concrete compressive strength, the diameter, the reinforcement ratio and the cover. None of the models showed weakness for a certain interval for any of these parameters as they did with respect to ϕ_s/ρ_s .

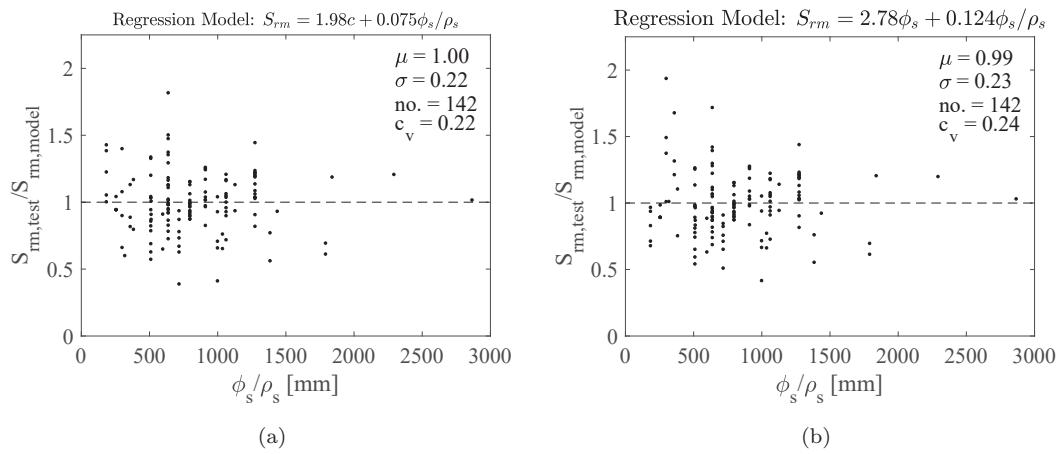


Figure 4.13: Comparison of regression model and test results (a) Best regression model with c and ϕ_s/ρ_s as parameters (b) Best regression model with ϕ_s and ϕ_s/ρ_s as parameters

Maximum crack spacing

In Fig. 4.14 the comparison for the models estimating the maximum crack spacing is provided, namely the Eurocode, the Model Code and Nielsen's model. All three models again show the same weakness when estimating the crack spacing for small ϕ_s/ρ_s -ratios.

When comparing the Model Code and the Eurocode, there are only small differences. It could be argued that the Model Code, with a mean value of $\mu = 0.64$, is a slightly better fit because it does not overestimate the crack spacings as much as the Eurocode which has a very small mean value of $\mu = 0.47$. The average deviation from the tests is the same for both models (24 – 25%).

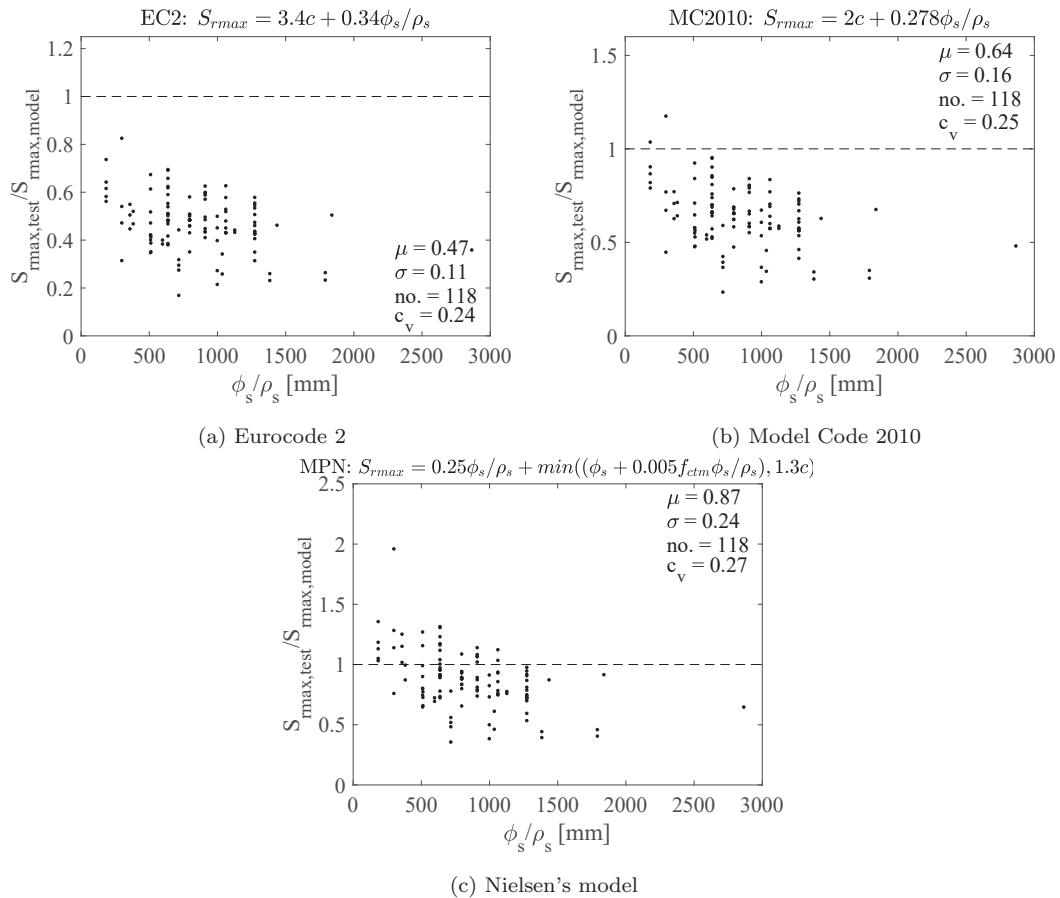


Figure 4.14: Comparison of model and test results for estimation of maximum crack spacing

4.4 Flexural members

This section concerns crack spacings in flexural members which are treated in more or less the same manner as the tensile members in the previous section. Some details with regard to the method of analysis will therefore not be explained repeated.

The investigation of crack spacings in flexural members is divided into four parts. Firstly, the crack spacings are analysed in two levels; the level of the reinforcement (secondary cracks) and in the web of the beams (primary cracks). Secondly, the beams are split into two groups with respect to application due to size, as discussed in the introduction to this chapter, namely laboratory beams with $d < 300mm$ and structural beams with $d \geq 300mm$.

4.4.1 Introduction to the database

Crack development in flexural members is important with respect to many aspects other than in relations to estimation of crack widths and deformation. Therefore, existing research within other topics related to flexural members holds wealth of useful experimental information about cracking, which can be used in this current research project, even though this was not the original focus of the tests. Table 4.10 holds all the experimental programmes in the database and states their original focus. The focus in many of the tests was shear capacity or rotational capacity.

In the attempt to create a database where the crack patterns are comparable across all members, the tests are selected because they satisfy the following criteria:

- Photos exist of the crack pattern making it possible to measure all crack spacings in the same manner. For further elaboration of this choice, see the introduction to this chapter.
- All members are rectangular
- All members are subjected to bending
- No members have transverse reinforcement in the inspected area
- No members have distributed reinforcement in the web in the inspected area
- The beams are statically determined and subjected to three- or four-point-bending from a concentrated load or from an evenly distributed load

The above geometrical and statical restraints are set up to avoid different crack formations resulting from different static, reinforcement or cross-sectional designs.

Each test series is categorised from I to III, like the tensile members were. Here, the category is specified on the basis of the quality of the photo of the crack pattern. The tests in category I have photos of very good quality where the crack formation is clear. In category II, the pattern is of good quality, but can be pixelated or unclear in parts of the photo. The crack patterns in category III are of poor quality and uncertainty can therefore occur when identifying cracks during the measurement of the spacings.

Reference	Country	No. of specimens	Experimental focus	Category
Belbachir et al. (2016) [96]	France	3	Shear	I
Gribniak et al. (2016) [97]	Lithuania	5	SLS, stiffness, influence if reinforcement layout	II

Høegh & Jørgensen (2016) [98]	Denmark	8	SLS, influence of d and ρ_s on cracking	I
Cavagnis et al. (2015) [54]	Switzerland	1	Failure, cracking	I
Daluga (2015) [99]	USA	12	Shear, influence of aggregate size	I
Mohammadyan-Yasouj et al. (2015) [100]	Malaysia	5	Wide beams	I
Baah (2014) [83]	USA	1	Cracking, Influence of epoxy coating	I
Campana et al. (2014) [101]	Switzerland	2	Shear, Arches	I
Pedersen & Eriksen (2014) [63]	Denmark	12	Shear, influence of concrete strength	I
Korol & Tejchman (2013) [102]	Poland	3	Shear, investigation of size effect	I
Mihaylov et al. (2013) [103]	Canada	3	Anchorage	I
Møller & Rasmussen (2013) [104]	Denmark	5	Shear	I
Perera & Mutsuyoshi (2013) [105]	Japan	3	Shear, influence of HPC	III
Yu et al. (2013) [106]	China	6	Shear, influence of d and ρ_s	I
McCain (2012) [107]	USA	10	Shear, investigation of size effect	I
Slowik & Nowicki (2012) [108]	Poland	4	Shear, influence of a/d	I
Slowik & Smarzewski (2012) [109]	Poland	5	Cracking during failure process	I
Birgisson (2011) [110]	Iceland	12	Shear	III
Gedik (2011) [111]	Japan	3	Shear in deep beams	II
Nghiep (2011) [112]	Germany	4	Shear, study of the compression chord	I
Sagaseta & Vollum (2011) [113]	UK	2	Shear, influence of aggregate size and loading	I
Thamrin et al. (2011) [114]	Malaysia	10	Shear, influence or GFRP bars	II
Mihaylov et al. (2010) [115]	Canada	2	Shear, influence of cyclic loading	I
Murray (2010) [116]	USA	8	Shear, scaling	I
Anastasi (2009) [117]	Switzerland	2	Shear, with and without stirrups	I
Hassan et al. (2008) [118]	Canada	10	Shear, influence of SC concrete	I
Hassan et al. (2008) [119]	USA	4	Shear, influence of HS steel in large beams	II
Sherwood (2008) [49]	Canada	23	Shear, large beams	I
Sneed (2007) [120]	USA	10	Shear, influence of d	I

Zhang & Tan (2007) [121]	Singapore	11	Shear, investigation of size effect	I
Gaudagnini et al. (2006) [122]	UK	3	Shear, FRP	II
Lubell (2006) [123]	Canada	17	Shear, wide members	II
Bentz & Buckley (2005) [124]	Canada	9	Shear, investigation of size effect	III
Tan et al. (2005) [125]	Singapore	7	Shear, investigation of size effect and a/d	I
Minelli (2005)[126]	Italy	4	Shear, crack formation	I
Gilbert & Nejadi (2004) [2]	Australia	12	SLS, cracking and crack control	I
Vecchio & Shim (2004) [127]	Canada	3	Shear, influence of stirrups, ρ_s and a/d	II
Yang et al. (2003) [128]	South Korea	9	Shear, influence of a/d , d	II
Hibino et al. (2002) [129]	Japan	3	Shear, FEM-modelling	I
Kwak et al. (2002) [130]	USA	1	Ductility	I
Tompos & Frosch (2002) [131]	USA	1	Shear, size effect and influence of stirrups	II
Cao (2001) [132]	Canada	2	Shear, investigation of size effect	I
Kenel & Marti (2001) [1]	Switzerland	4	Fiber optic strain measurement	I
Oh & Shin (2001) [133]	South Korea	1	Shear in deep beams and influence of HPC	II
Tureyen (2001) [134]	USA	3	Shear, influence of FRP reinforcement	II
Yoshida (2000) [135]	Canada	1	Shear in deep beams	I
Angelakos (1999) [136]	Canada	7	Shear, investigation of size effect	II
Bigaj (1999) [45]	Netherlands	5	Investigation of rotation capacity	II
Tan & Lu (1999) [137]	Singapore	3	Shear, investigation of size effect	II
Kulkarni & Shah (1998) [138]	USA	7	High strain rates	III
Podgorniak-Stanik (1998) [139]	Canada	8	Shear, investigation size effect	I
Yoon et al. (1996) [140]	USA	3	Shear, influence of HPC	I
Abrishami et al. (1995) [141]	Canada	1	Flexure, influence of epoxy coating and HPC	III
Khorasgany (1994) [142]	USA	15	Shear, influence of size effect and HPC	II
Kim & Park (1994) [50]	South Korea	10	Shear, influence of a/d and d	I

Walraven & Lehwalter (1994) [143]	Germany	3	Shear, investigation of size effect	II
Johnson & Ramirez (1989) [144]	USA	1	Shear, influence of HPC	II
Kim (1987) [145]	USA	6	Shear, investigation of failure mechanisms	II
Niwa et al. (1987) [146]	Japan	3	Shear in large beams	II
Iguro et al. (1985) [147]	Japan	7	Shear in large beams	I
Mphonde (1984) [148]	USA	18	Shear, influence of HPC	II
Smith & Vantsiotis (1982) [149]	Canada	5	Shear in deep beams	III
Cederwall et al. (1974) [150]	Sweden	1	Shear in pre-stressed beams	II
Attisha (1972) [57]	UK	4	Behaviour of RC beams	III
Manuel et al. (1971) [151]	Canada	2	Shear in deep beams	II
Bahl (1968) [152]	Germany	8	Shear, investigation of size effect	I
Taylor (1968) [153]	UK	12	Shear, dowel effect	I
Kani (1967) [51]	Canada	7	Shear, influence of d	I
Kani (1966) [154]	Canada	4	Shear, influence of a/d	III
Base et al. (1966) [39]	United Kingdom	16	Cracking with plain vs. deformed steel	I
Kani (1964) [155]	Canada	6	Shear	II
Bresler & Scordelis (1963) [156]	USA	1	ULS, cracking	II
Taylor & Brewer (1963) [157]	UK	1	Shear, influence of aggregates	I
Leonhardt & Walther (1962) [158]	Germany	30	Shear, influence of ρ_s	II
Taylor (1960) [159]	UK	2	Shear, influence of type of reinforcement	II

Table 4.10: Experimental programmes in database of flexural members

Within the database there are four overall variations related to the crack spacing measurements. These are shown in Fig. 4.15 and are: 1) the type of failure, 2) the type of loading, 3) whether the measurements are available for more than one load level, and 4) the stress level in the reinforcement at time of measuring. The number of tests (no.) stated in each sub-figure refers to the number of tests out of the total of 462 where the information was available in the experimental report. In the remaining tests, no information was given about this certain parameter/circumstance.

The majority of the crack spacing measurements are from beams that failed in shear either in three- or four-point-bending. Most of the measurements are carried out on crack patterns from a load level close to or at failure. In 80 of the test members the crack spacings were measured in more than one load stage (including the failure load step).

Fig. 4.15d shows the large variation in the reinforcement stress level, σ_{sPic} , causing the measured crack spacings. This stress level is theoretically estimated from the parameters given in the experimental reports.

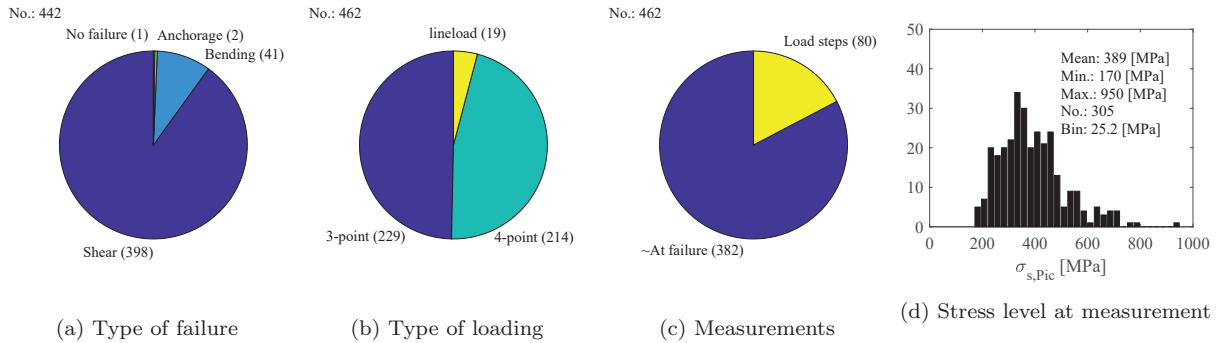


Figure 4.15: Overall variations within tests

Measuring technique

All crack patterns are measured in the same manner with inspiration from the experimental work by Sherwood[49]. A horizontal line in three different levels indicates a measuring string, as shown in Fig. 4.16. The three levels are defined as distances from the compression edge; d , $3d/4$ and $d/2$ which represent the reinforcement level, the lower web and mid-height, respectively.

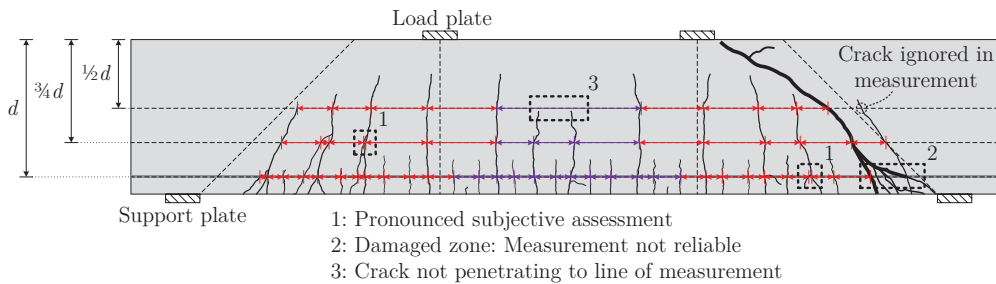


Figure 4.16: Crack measurements at three different levels of a beam, reprint from [160]

The crack pattern is, firstly, copied from the experimental report into a CAD software program where it is scaled according to the size given in the experimental report. Secondly, lines are drawn to mark the three measuring levels. Lines are also drawn to mark the support zones to exclude local failure from the measurements. These zones are defined with two lines of 45 degrees from the edge of the support plates inclined towards the loaded area. Lastly, the crack spacings can be measured by placing measuring points each time a crack crosses the level-lines. Spacings in the constant moment span are separated from spacings in the shear span by colour coding.

To create consistent measurements, three overall rules are followed. These are numbered 1, 2 and 3 in Fig. 4.16. These are: 1) If two cracks meet just below the level-line, they are identified as one crack, 2) cracks in the zone of a local shear failure can be disregarded due to that fact that closely spaced cracks could have formed, making it hard to distinguish between a new crack and a crack initiated by the actual failure, 3) cracks must cross the level-line, hence if they stopped just below they are not included.

Overview of measurements

The two tables below summarise the number of measurements carried out and how they are distributed between shear and constant moment spans. Table 4.11 lists the measurements of the crack patterns close to or at failure where around 20% of the measurements are from the constant moment span. The number of measurements at the reinforcement level is larger than in the web due to the fact that only some cracks extend to the web and in some beams no cracks extend all the way to $d/2$.

	Constant moment, n_{CM}	Shear span, n_V	Total, n_t	n_{CM}/n_t [%]	n_{CV}/n_t [%]
Measurements at $d/2$	633	2336	2969	21	79
Measurements at $3d/4$	1060	3746	4806	22	78
Measurements at d	1464	5636	7100	21	79

Table 4.11: Number of crack spacing measurements at failure

Table 4.12 lists the number of measurements in the beams where crack spacings were measured at load steps other than at failure. As all these beams were subjected to three-point-bending, no measurements exist from constant moment spans. These measurements are only used to analyse and possibly identify a stabilised crack pattern. In all other investigations the measurements from the highest stress level are used.

	Total no. of measurements
Measurements at $d/2$	1420
Measurements at $3d/4$	2634
Measurements at d	4308

Table 4.12: Number of crack spacing measurements in load steps other than at failure

Fig. 4.17 shows how much the measured crack spacings in each member deviate from the mean crack spacing for each member. The figure includes both measurements at shear spans and constant moment spans. The smallest or largest crack spacing measured in a member deviates, on average, approximately 40% from the mean crack spacing. Furthermore, the crack spacings at $d/2$ have a larger deviation from the mean than the crack spacings measured at the level of the reinforcement. Both distributions have a small positive skewness, which means that in a small number of beams there is a very large difference between the mean and the maximum or minimum crack spacing.

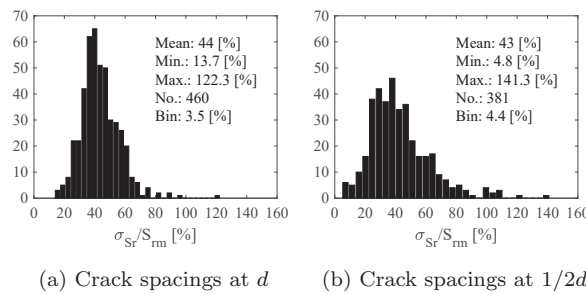


Figure 4.17: Distribution of the standard deviation of crack spacings relative to the mean crack spacing.

Distribution of parameters

All geometric and material parameters associated with each test member are collected from the experimental reports and summarised in the histograms in Fig. 4.18. Most of the parameters are represented in a large interval and with a mean value around the most commonly used values. This should make it possible to analyse the influence of the different parameters on the crack spacing over large parameter spans.

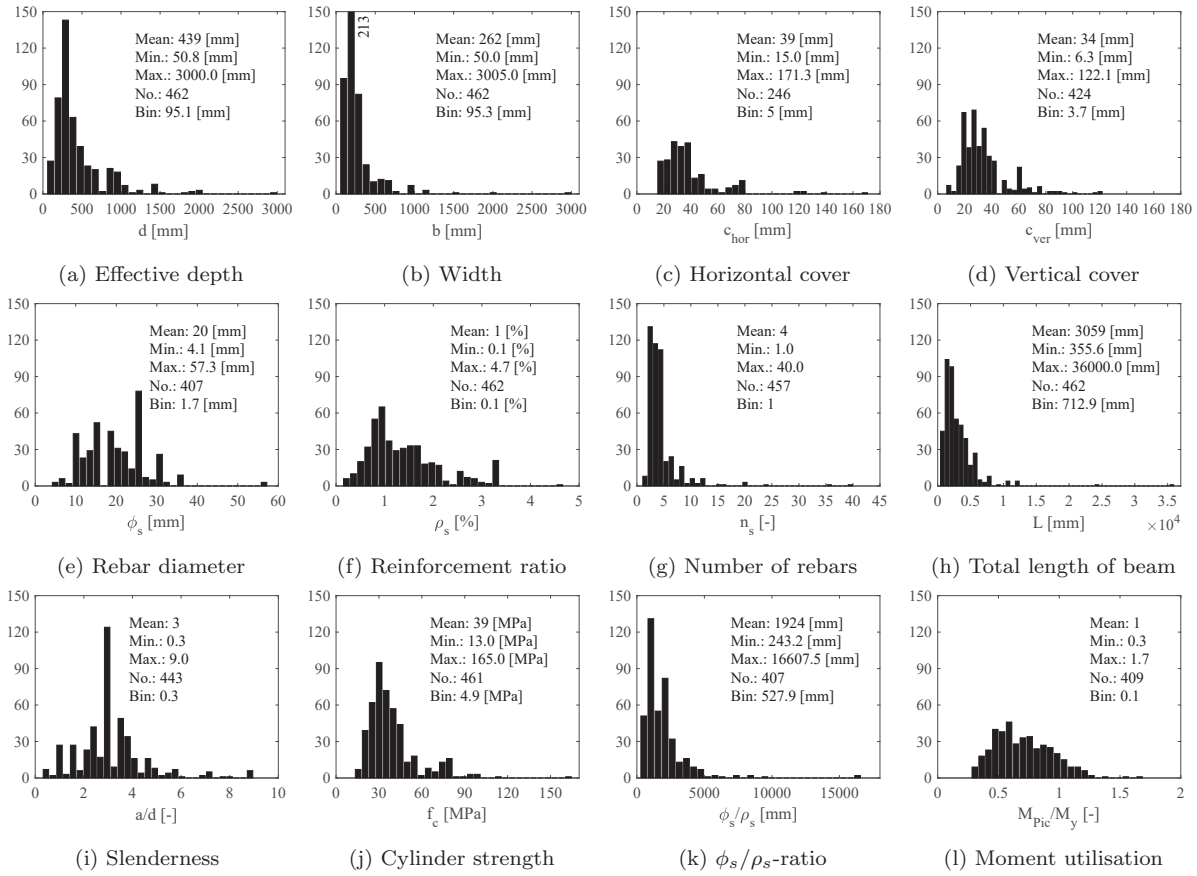


Figure 4.18: Distribution of parameters of the test members

4.4.2 Analysis of primary flexural crack spacing

In the following section, the crack spacings in the zone between the compression zone and the reinforcement are treated. In other words, these are the cracks that extend further than the nearest vicinity of the longitudinal reinforcement, earlier named the primary flexural cracks, or just primary cracks. For the analysis of the spacing of the primary cracks, the measurements at both the level-line $d/2$ and $3d/4$ are used, although primarily the measurements at $d/2$, which are referred to as mid-height.

The investigation of the spacing of the primary cracks is divided into four parts:

1. The distribution of the crack spacing. It is investigated whether the crack spacing relative to the effective depth, S_{rm}/d is from a normally distributed or a non-parametric population. The reasons for the results are discussed.
2. Through multi-variable linear regression it is investigated whether any parameters, other than the effective depth, have a significant influence on the variation of the crack spacing. The combinations of parameters used in the reviewed existing models from Chapter 2 are also investigated.
3. The relations between minimum, maximum and mean crack spacings are investigated through distribution plots.
4. A stabilised crack system with respect to a stress level is investigated through results from a single test series conducted at Aarhus University as part of this current research project.
5. The reviewed existing models are compared to the test data.

Number 1. is not carried out for the crack spacing at the level of the reinforcement, otherwise the same procedure applies. These cracks are treated subsequent to the primary cracks.

Correlation between parameters

For the coming regression analysis, correlation between the effective depth and the remaining parameters is investigated. This also provides an indication as to whether the overall trend is that the beams are scaled according to the effective depth or if the different geometrical parameters are varied more randomly. Figs. 4.19 and 4.20 show a selection of parameters plotted against the effective depth while the remaining parameters' correlation with d are listed in Table 4.13, where the correlation coefficient between two random parameters x and y is $r = corr(x, y)$. The sizes of the datasets in the table and figures are considerably smaller than the total number of laboratory and structural beams. This is due to the fact that, in the regression analysis, the data used are only from those beams where all of the parameters in Table 4.13 are given, hence no information about the analysed beams is missing.

It appears that, in a large proportion of the tests, the shear span length, a , is scaled according to the effective depth, with a factor of 3, which is therefore also the most commonly used slenderness ratio a/d , as seen in Fig. 4.18i. This is most pronounced for the structural beams with an effective depth above 300mm. With respect to the cover, it is notable that the vertical cover, c_{ver} , in Fig. 4.19c, is fairly well correlated with d for the structural beams ($r = 0.58$) while the correlation coefficient is smaller for the horizontal cover ($r = 0.40$). This means that, in many of the tests, the horizontal and vertical cover differ from each other. The ϕ_s/ρ_s -ratio also has a fairly high correlation with d for the structural beams.

For laboratory beams, the reinforcement diameter, ϕ_s , moment utilisation and the slenderness, a/d , shows correlation, to some extent, with d .

Nevertheless, besides the shear span length, a , none of the parameters are correlated with the effective depth to an extent that will interfere with the regression analysis for either the structural or the laboratory beams.

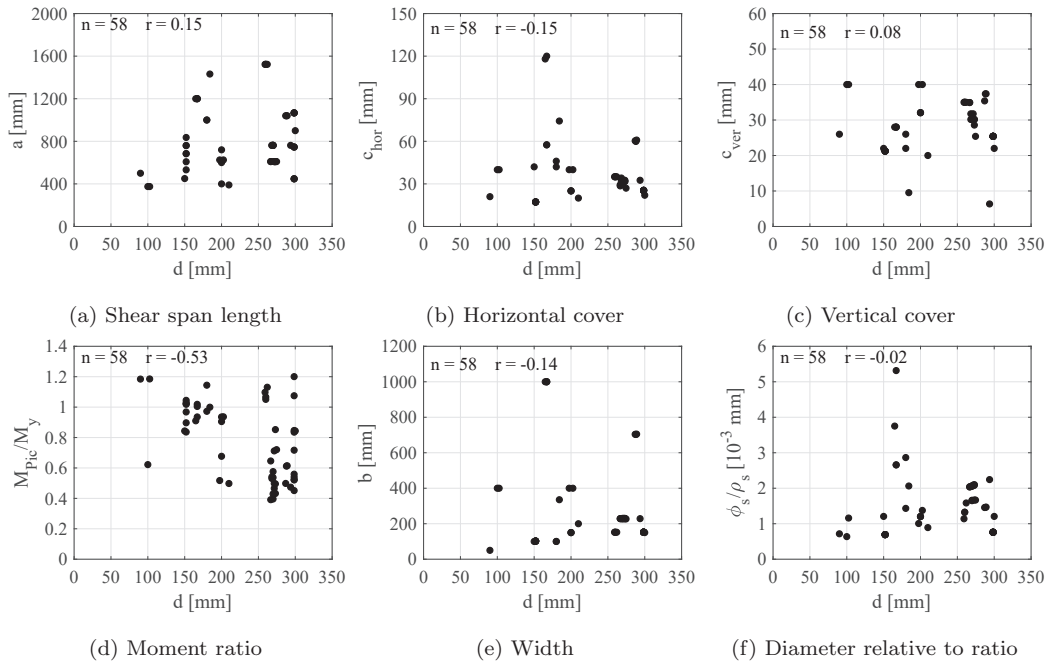
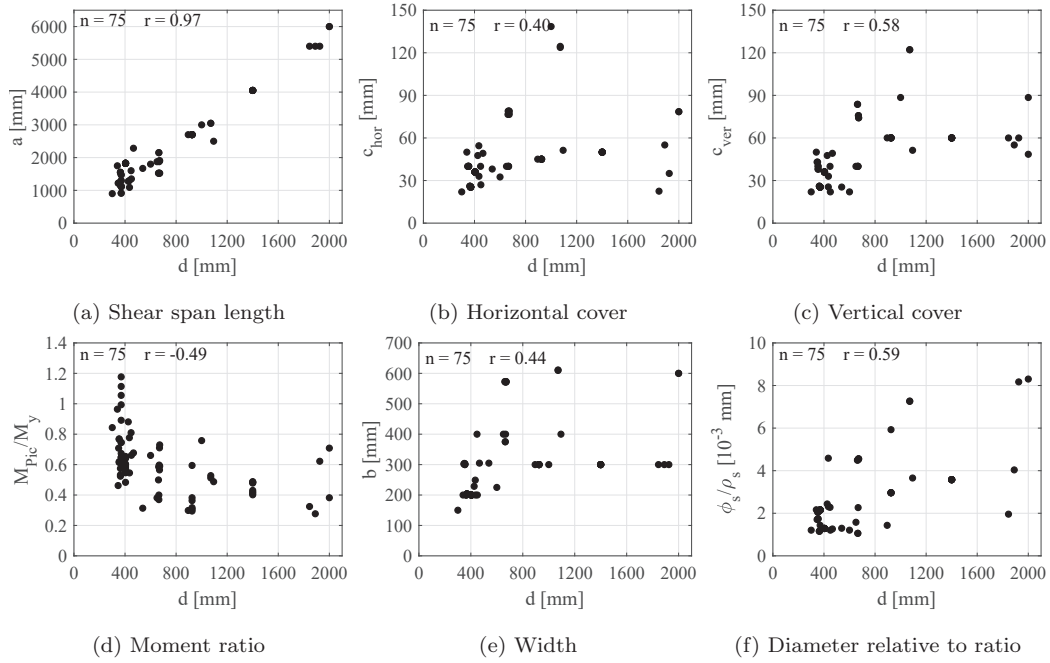


Figure 4.19: Correlation between effective depth and various other parameters, for $50 \leq d < 300$


 Figure 4.20: Correlation between effective depth and various other parameters, for $300 \leq d \leq 2000$

	$50 \leq d < 300$		$300 \leq d \leq 2000$			$50 \leq d < 300$		$300 \leq d \leq 2000$	
x, y	no.	r	no.	r	x, y	no.	r	no.	r
d, b	58	-0.14	75	0.44	d, σ_{sPic}	58	-0.41	75	-0.26
d, ϕ_s	58	0.58	75	0.42	$d, M_{Pic}/M_y$	58	-0.53	75	-0.49
d, n_s	58	0.06	75	0.42	d, a	58	0.15	75	<u>0.97</u>
d, c_{ver}	58	0.08	75	0.58	$d, a/d$	58	-0.54	75	-0.45
d, c_{hor}	58	-0.15	75	0.40	$d, \phi_s/\rho_{s,effEC2}$	58	-0.15	75	0.35
d, ρ_s	58	0.31	75	-0.45	$d, \phi_s/\rho_{s,effSYM}$	58	-0.35	75	0.30
$d, \phi_s/\rho_s$	58	-0.02	75	0.59	$d, \phi_s/\rho_{s,effLeo}$	58	-0.29	75	0.15
$d, f_{c,cyl}$	58	0.21	75	-0.12	$d, \phi_s/\rho_{s,effBigaj}$	58	-0.20	75	0.51

Table 4.13: Correlation between effective depth and various parameters

Distribution of data

From former research, discussed in Chapter 2, it is known that the spacings of the primary flexural cracks show a correlation with the effective depth (e.g. [49]). Therefore, it is investigated whether the distribution of the relative crack spacing, S_r/d , is Gaussian.

In Fig. 4.21a the relative crack spacing for every single crack spacing measurement is plotted against the effective depth. Fig. 4.21b shows the same but for the mean crack spacing of each test member. Both plots show a clear difference in the data for $d < 300$ and $d \geq 300$ mm. For the structural beams, the S_r/d seems reasonably independent of d while the results for the laboratory beams are more scattered. In other words, the crack spacings' proportionality to d is clear for structural beams but not for laboratory beams. In the

following paragraphs, possible reasons for the scatter in results of the laboratory beams are investigated.

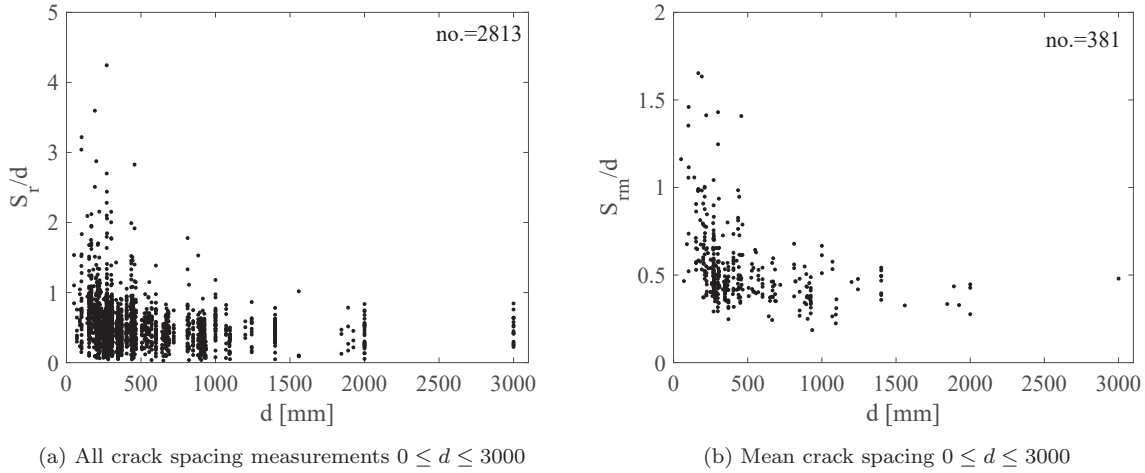


Figure 4.21: Relative crack spacing as a function of the effective depth

There may be several reasons for the laboratory beams not showing the same behaviour with respect to d as the structural beams. Two overall different reasons may be: 1) the crack spacings in the laboratory beams are influenced by other parameters than the effective depth, or 2) the development of cracks extending to mid-height of the laboratory beams is disrupted causing a larger crack spacing in a laboratory beam. Reasons for this could be:

- The utilisation of the beams with respect to bending is small. When the beams fail in shear, the flexural crack pattern might not be fully developed, hence the cracks do not reach the level of mid-height. (The slow development of the flexural crack pattern was seen to be more significant for laboratory beams, as illustrated by the conducted tests presented in Chapter 2).

In the meantime, this is rejected by Fig. 4.22a. Here, the relative crack spacing is plotted for beams smaller than 500mm where the low utilised beams are marked by green and red dots. The green dots represent the beams utilised less than 50% of M_y and the red dots are the beams utilised between 50% and 60%. Because these dots are placed randomly in the whole spectre of results, it does not seem plausible to assume that the low utilised beams are guilty of the scatter or the higher values of S_r/d for laboratory beams compared to structural beams.

- Assuming that the extension of the flexural cracks is dependent on the level of the neutral axis, the cracks may not extend all the way to the level of $d/2$ if the reinforcement ratio is very large causing a large compression zone.

Fig. 4.22b illustrates that this hypothesis can not be confirmed either. The beams with the reinforcement ratios above 2.5% (red dots), does not have a large relative crack spacing. Neither are the beams with low reinforcement ratio marked as green dots (below 0.6%) reason for the scatter.

- The photos used for crack measurements are not detailed enough. It might be that the exact extension of the flexural cracks are not investigated with a microscope and therefore not highlighted in their full height. This would result in a smaller number of cracks registered at the level of $d/2$.
- The boundary conditions might have a larger effect on the crack pattern of laboratory beams than on structural beams. For example, the local effects from large compression stresses close to the load plates could affect a relatively larger area of a laboratory beam and therefore disturb the "normal" formation of cracks.

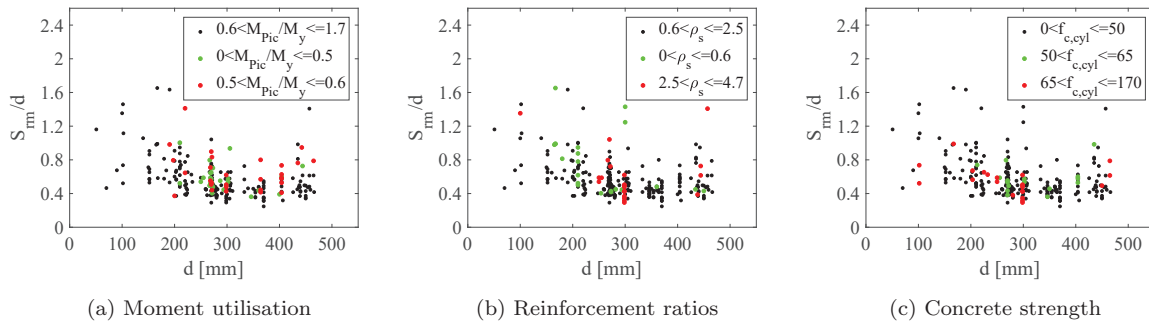


Figure 4.22: Investigation of possible outliers in the data of the laboratory beams

The final two bullet points in the list will now be considered. Fig. 4.23 shows three typical test beams from the database with an effective depth of more than 300mm. A clear difference between primary and secondary cracks can be seen and the majority of the primary cracks extend well above mid-height ($d/2$). This is the overall tendency of all the structural beams in the database.

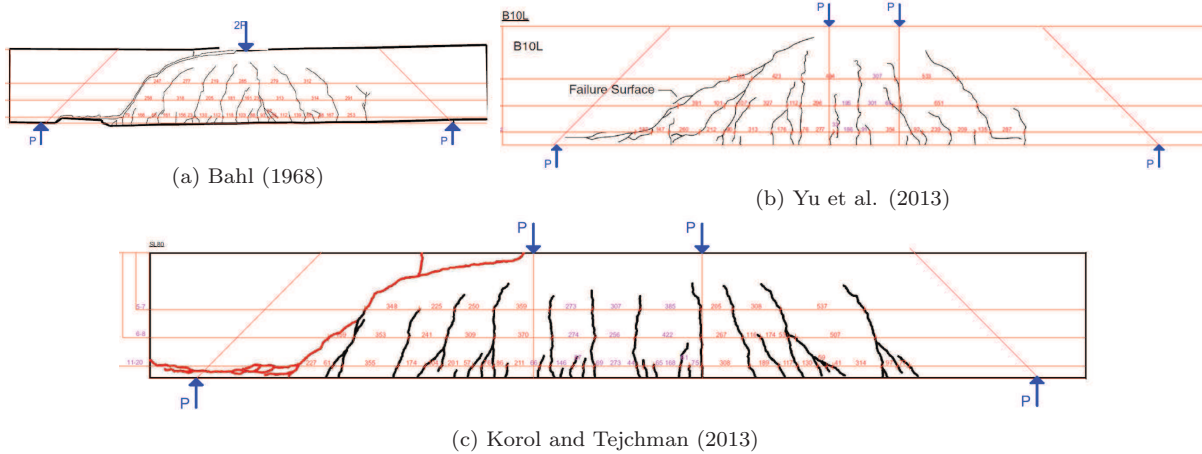


Figure 4.23: Crack patterns of from the database beams where $d \geq 300mm$

In Figs. 4.24 and 4.25 two different scenarios for the crack patterns in the laboratory beams are illustrated. In the three beams in Fig. 4.24 the primary cracks extend above $d/2$, just as in the structural beams. In contrast, in Fig. 4.25, it becomes harder to distinguish between the primary cracks and the cracks concentrated around the tensile reinforcement. Only a few cracks extend to above the level of $d/2$, which results in a large crack spacing at mid-height compared to the previous beams in Fig. 4.24. When comparing the six beams and their parameters, no apparent reason for the difference in crack pattern is found.

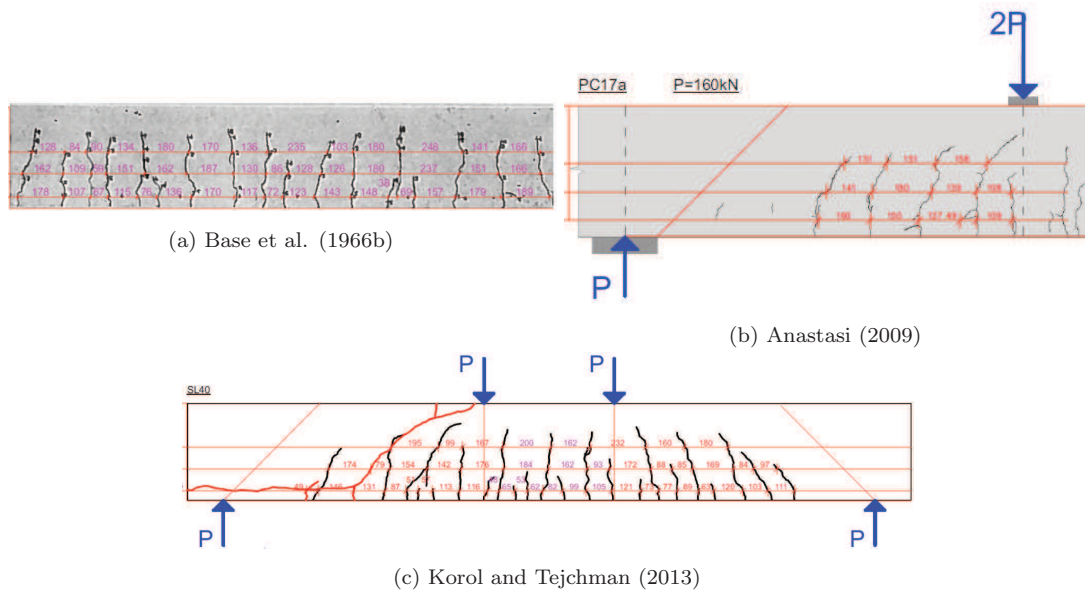


Figure 4.24: Crack patterns of beams from the database where $d < 300\text{mm}$ with fully developed primary flexural cracks

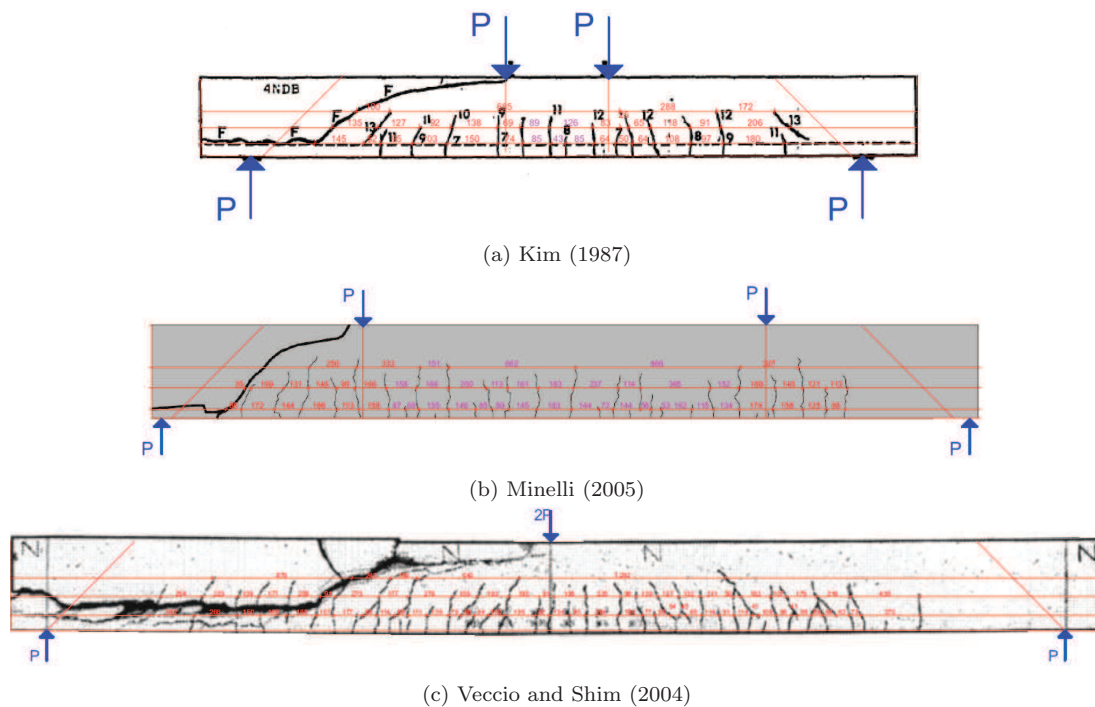


Figure 4.25: Crack patterns of beams from the database where $d < 300\text{mm}$ with little or no fully developed flexural cracks

The above difference in crack patterns could indicate that the measuring line at $d/2$ is placed too high to measure the primary crack spacing in the laboratory beams. Therefore, the level of $3d/4$ is investigated in Fig. 4.26, which shows that the same scatter in results is found at this level because of the high values of S_{rm}/d for the beams smaller than 300mm .

The conclusion to the investigation of why the primary crack spacing in the laboratory beams acts differently with respect to the effective depth is that the difference cannot only be attributed to the fact that the primary cracks do not extend to mid-height but that larger uncertainties and different behaviour apply for

the laboratory beams. This justifies the grouping of the beams into laboratory and structural beams at the limit of $d = 300mm$.

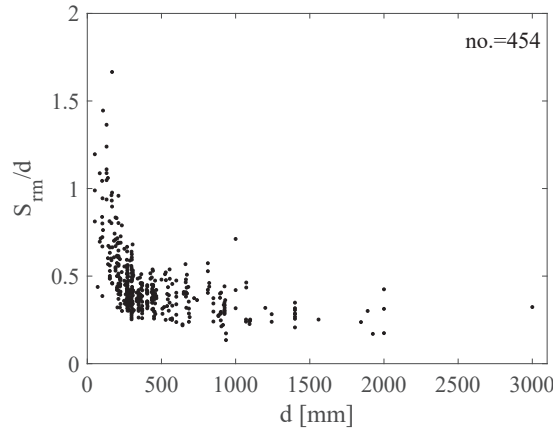


Figure 4.26: Relative mean crack spacings as a function of the effective depth at the level of $3d/4$

Outliers of the structural beams

With regard to the measured crack spacings at the level of $d/2$, some data points are regarded as outliers. Firstly, the beams with a slenderness ratio below 2 ($a/d \leq 2$) are disregarded. In these beams the primary cracks closest to the supports are shear cracks with a large inclination towards the applied load, which results in a very small crack spacing at mid-height. The reason for this is that the shear is mostly carried by a compression strut directly from the applied load to the support. This carrying mechanism is fundamentally different than that seen in slender beams. Secondly, slab-like beams with $b/d \leq 1$ are disregarded because it is believed that slabs could show a fundamentally different behaviour than in beams where the depth is larger than the width of the member.

In Fig. 4.27a the disregarded beams, with respect to slenderness and width to depth ratio, are illustrated with red and green dots, respectively. In particular, the beams with low slenderness have an overall smaller relative crack spacing whereas the slab-like beams show more scattered results with some very large crack spacings among them.

Thirdly, outliers are also regarded as the beams of $d = [300mm; 500mm]$ where the primary cracks do not extend to the level of $d/2$ as illustrated in Fig. 4.25. These beams are marked with red in Fig. 4.27b.

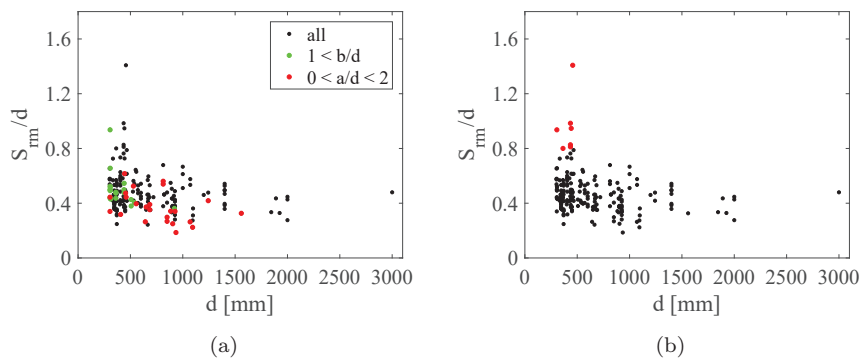


Figure 4.27: Removed outliers in the dataset for the structural beams: (a) beams with low slenderness and slab-like beams, (b) beams where the cracks does not extend to mid-height

Test of normality

In Figs. 4.28 and 4.29 the variable S_r/d is tested for normality, for laboratory beams and structural beams, respectively, with the use of density and q-q plots. Figs. 4.28a and 4.28b show how S_r/d in the beams smaller than $d = 300\text{mm}$ is not normally distributed but show closer resemblance to a Burr-distribution, which is characterised by being non-negative and skewed. Both the Shapiro-Wilk Test and the D'Agostino & Pearson Test reject the null-hypothesis of the data being from a normal distribution.

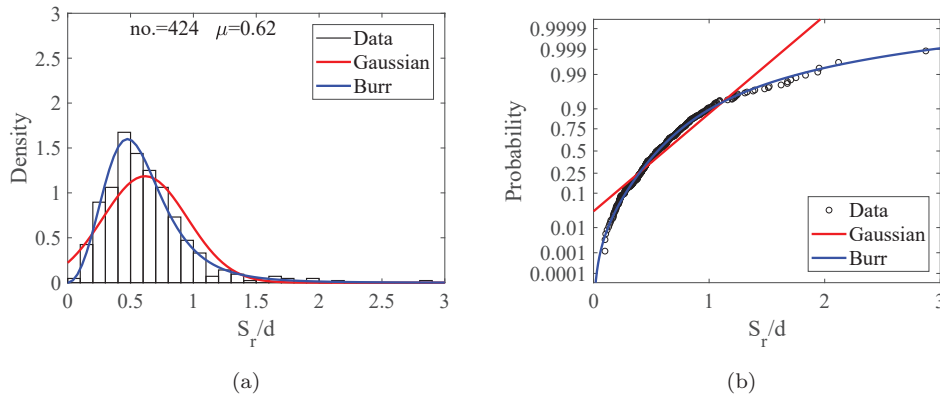


Figure 4.28: Test of Normality for all crack measurements for $50 \leq d < 300$

For the structural beams, in Figs. 4.29a and 4.29b, the density and q-q plot more closely resemble that of a normal distribution function. However, when testing for normality, the two different tests still reject the null-hypothesis.

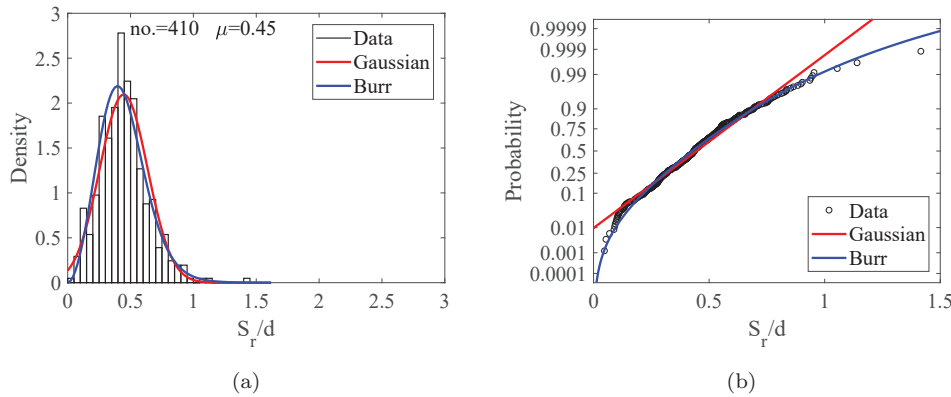


Figure 4.29: Test of Normality for all crack measurements for $300 \leq d \leq 2000$

The same test of normality is carried out for the mean crack spacing in the figures below, where the distribution for the laboratory beams is still non-parametric. On the other hand, for the mean crack spacings of the structural beams, the distribution more closely approaches a normal distribution. Besides, the hypothesis tests did not reject that the data sample is from a normally distributed population.

The investigation of normality thus also confirms that there are two groups of beams which exhibits different behaviour with respect to the primary crack spacing; the laboratory $50 \leq d < 300$ and the structural beams $300 \leq d \leq 2000$, where only the primary crack spacing in the structural beams has a strong dependency on the effective depth.

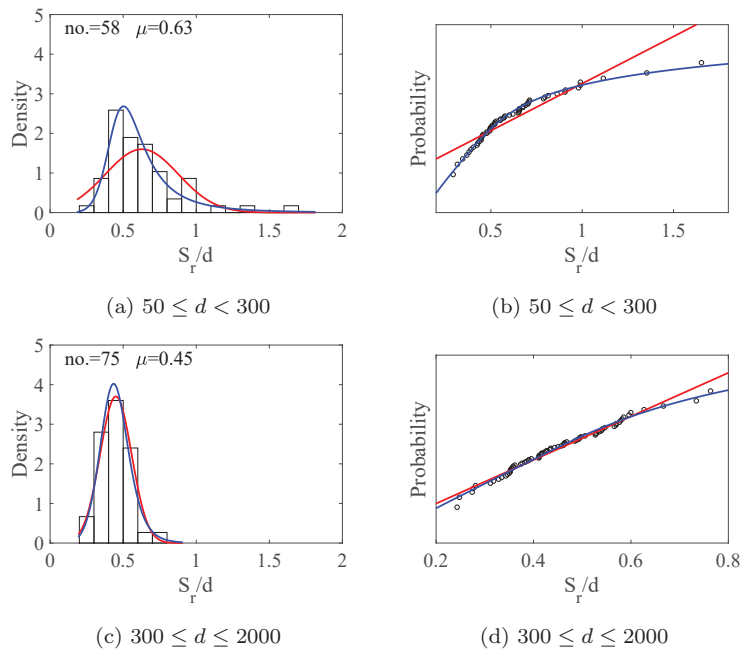


Figure 4.30: Test of Normality for mean crack spacings

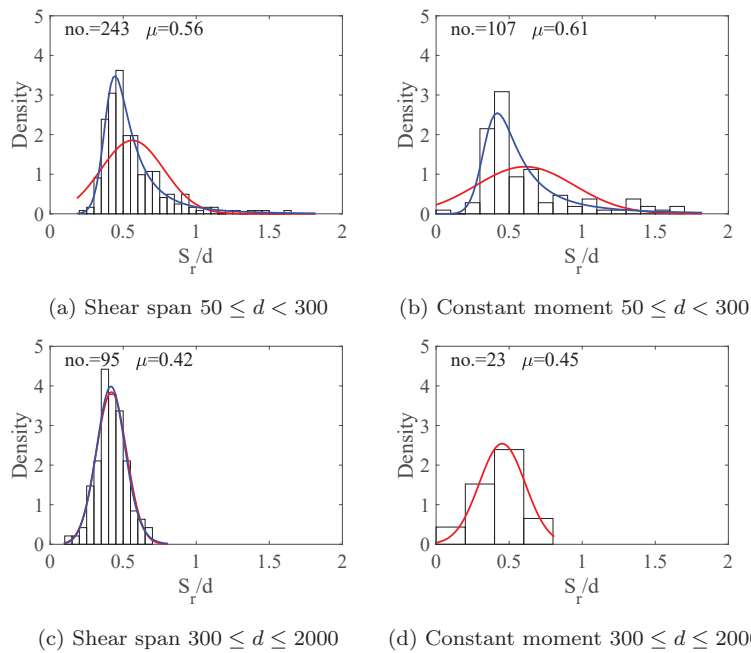


Figure 4.31: Test of Normality for shear span and constant moment span, respectively

In Fig. 4.31 it is investigated whether there is an overall difference in the relative crack spacings when beams are subjected to a constant bending moment or to combined bending and shear. Here, all beams in the database are included. The distribution of the data is still normal for the structural beams and skewed for laboratory beams, although, from comparison of the mean values, a somewhat larger relative crack spacing is found in the constant moment span than in shear span. The mean value of S_r/d for structural beams is 0.42 and 0.45 for shear span and constant moment span, respectively. While the

mean values are 0.56 and 0.61 for the laboratory beams in the shear span and constant moment span, respectively. However, the statistical basis for the constant moment span in the structural beams is too small to conclude anything.

Study of parameters of influence

The influence of the parameters listed in Table 4.14 is studied through a multi-variable linear regression model. The independent variables are selected on the basis of the literature review to either verify or reject that they have an influence.

The analysis is carried out separately for the laboratory and the structural beams. This decision is made on the basis of the investigations in the previous sections as well as the fact that the existing literature and the conducted test presented in Chapter 3 point to this.

Parameter	Description
d	Effective depth
b	Width
ϕ_s	Diameter of reinforcement
n_s	Number of rebars
c_{ver}	Vertical cover
c_{hor}	Horizontal cover
ρ_s	Reinforcement ratio
ϕ_s/ρ_s	ϕ_s/ρ_s -ratio
$f_{c,cyl}$	Measured compressive strength
σ_{sPic}	Steel stress in picture
M_{Pic}/M_y	Moment utilisation
a	Length of shear span
a/d	Slenderness ratio

Table 4.14: Parameters included in the regression analysis for the primary crack spacing

Non-linear regression analysis

As for the tensile members, it has also been investigated whether any of the significant parameters found by the coming linear regression analysis should instead be non-linearly connected to the crack spacing by introducing an exponent of the power n . The investigation showed no reason to pursue this further because the non-linear models did not give significantly better results with respect to the $adjR^2$ and the RMSE values compared to the linear models represented in the following paragraphs.

Laboratory beams $50 \leq d < 300$

The regression model for the laboratory beams, holding only the significant parameters, is shown in Table 4.15 and Fig. 4.32. The 58 beams in the data sample are the beams where all parameters were available in the experimental reports.

The model, which consists of a constant term, the ϕ_s/ρ_s -ratio, σ_{sPic} and c_{ver} describes 62% of the variation in crack spacing. Out of the three parameters, the ϕ_s/ρ_s -ratio has the largest influence together with the constant term while the vertical cover has the smallest influence. Some possible reasons to why the regression model is able to describe “only” 62% of the variation and that a large part of it is described by a constant term could be: 1) that there is a large number of outliers within the laboratory beams, as indicated in the earlier normality tests, 2) that other parameters have larger influence than those chosen, or 3) that there are many beams with a small reinforcement stress and thus not a fully developed crack pattern.

The crack spacing predicted by the regression model will decrease as the stress in the reinforcement increases, which confirms previous observations of tests in the literature review. A regression analysis was also carried out where beams with $\sigma_{sPic} \leq 250MPa$ were excluded, leaving 52 beams in the dataset. The result was a model with less dependency on σ_{sPic} , but still with a constant term of great significance.

Linear Model 1		
$adjR^2 = 0.623$		
RMSE = 21.9		
	k_n	p-value
Const. term	117.25	2.0 e-9
c_{ver}	0.933	0.036
ϕ_s/ρ_s	0.031	5.8 e-12
σ_{sPic}	-0.129	1.5 e-6

Table 4.15: Coefficients and statistics of linear regression for laboratory beams $50 \leq d < 300$

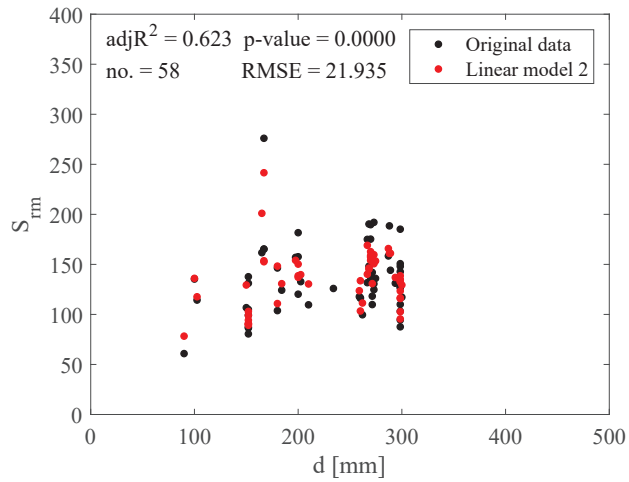


Figure 4.32: Linear regression for $50 \leq d < 300$, no. = 58 beams, with ϕ_s/ρ_s , c_{ver} and σ_{sPic} as predictors

A regression analysis of the crack spacing at the lower web, $3d/4$, was also carried out. The result is not illustrated here because the same parameters were of significant influence, namely the ϕ_s/ρ_s and σ_{sPic} . The effective depth shows no influence on the crack spacing of the laboratory beams. The parameters d and ϕ_s/ρ_s are not correlated, which means that correlation in the data is not the reason for d not being of influence. Taking into consideration that the beams’ effective depths are smaller than $300mm$, it makes sense that most of the cracks at reinforcement level also extend to mid-height. The small beam depth means that the concentrated tensile reinforcement also acts as distributed reinforcement. Hence, the laboratory beams do not lack distributed reinforcement/are not affected by lack of distributed reinforcement and the one type of crack existing in these beams is therefore not controlled by the depth of the member but principally by the bond mechanism.

From the perspective that crack spacings are primarily used to calculate crack widths, there is good reason for only estimating the crack spacing at the reinforcement level in the laboratory beams. Furthermore, the conducted test presented in Chapter 3 showed that the crack width was largest at the outermost tensile fibre in these beams.

Model parameters

A linear regression model is also used to test the significance of the parameters used in the reviewed existing models in Chapter 2 for estimating crack spacing at mid-height. Only the significance of the parameters in

the models is tested, not the size of the coefficients originally used in the models. The precision of each model with its original coefficients will be compared to the tests later.

The three tested models are Reineck's, Hamadi's and Frosch's, reviewed in Section 2.3.3. The Eurocode parameters are also tested, indirectly, as they coincide with Reineck's parameters.

Table 4.16 lists the parameters, their coefficients and associated p-values for each model and Fig. 4.33 illustrates the regression models' variation with respect to the effective depth. The three models only describe around 40% of the variation and have RMSEs of approximately 38 – 46, which means that none of the model parameters describe the crack spacing variation to a satisfying degree. It should be noted that Reineck also stated that his model only applies for beams in shear with a depth greater than 200mm.

Reineck parameters			Hamadi parameters			Frosch parameters		
$adjR^2 = 0.415$			$adjR^2 = 0.372$			$adjR^2 = 0.406$		
RMSE = 41.1			RMSE = 45.5			RMSE = 37.5		
x_n	k_n	p-value	x_n	k_n	p-value	x_n	k_n	p-value
d	0.920	8.4 e -13	d	0.550	3.78 e-30	d^*	1.042	4.75 e-35
x_{cr}	-1.102	3.86 e-4	-			-		

Table 4.16: Coefficients and statistics of linear regression with model parameters

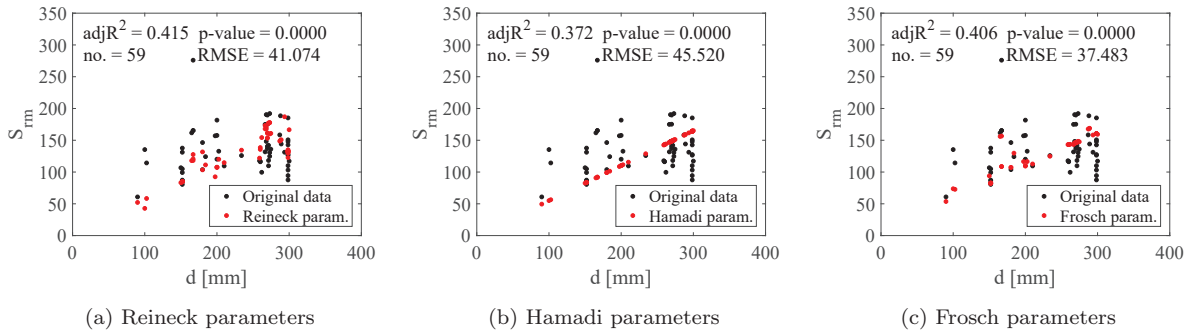


Figure 4.33: Linear regression with model parameters for laboratory beams $50 \leq d < 300$ no. = 59 beams

Structural beams $300 \leq d \leq 2000$

The linear regression model for structural beams is estimated from a sample of 75 beams. In Fig. 4.34 the sample is plotted together with the results predicted by Linear Model 1, listed in Table 4.17. The adjusted R^2 value of 0.88 indicates that a very high percentage of the variation in the data is described by the model. The model holds three independent variables; d , c_{hor} , b and a constant term, listed in the order of highest significance to the variation of S_{rm} .

The constant term has a p-value of 0.22, indicating that it does not have a significant influence and that the variation in the crack spacing is described well by the effective depth as the dominating parameter. The width and the horizontal cover are secondary parameters and it can be questioned whether they have a physical influence. The width and the horizontal cover have a correlation coefficient of $r = 0.78$, which means that correlation of the parameters could influence the p-values. No clear physical explanation has been found as to why the width of the beams should influence the crack spacing. On the other hand, it seems plausible that an increase in horizontal cover could increase the crack spacing.

Note that the parameter σ_{sPic} does not have any influence even though there are 21 beams in the sample where $\sigma_{sPic} \leq 250MPa$. Hence, the stress level in the reinforcement does not have an influence on the primary crack spacing in the structural beams as it did in the laboratory beams.

Linear Model 1		
$adjR^2 = 0.881$		
RMSE = 68.5		
x_n	k_n	p-value
Const. term	26.657	0.215
d	0.372	2.5 e-30
b	-0.416	1.0 e-4
c_{hor}	3.232	1.1 e-7

Table 4.17: Coefficients and statistics of linear regression for $300 \leq d \leq 2000$

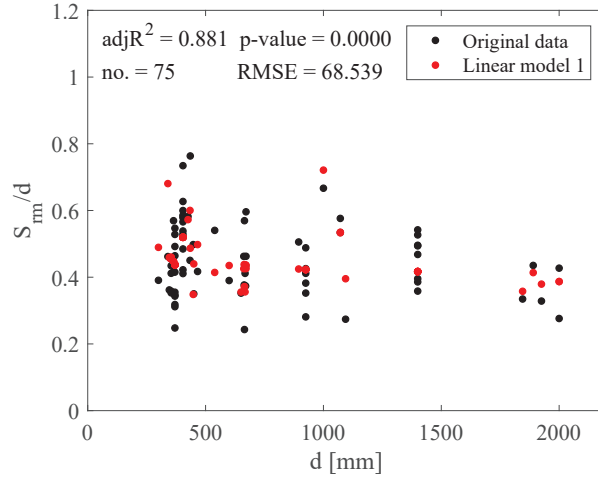


Figure 4.34: Linear regression for $300 \leq d \leq 2000$ with d , b , and c_{hor} as predictors

Model parameters

Table 4.18 and Fig. 4.35 show the results of the regression models using the parameters of the three reviewed existing models. Frosch’s parameter d^* shows the best results, which is the parameter dependent on both the horizontal cover and the effective depth, i.e. the same parameters as in Linear Model 1. However, all three model parameters are more or less of the same quality. The fact that Frosch’s parameter d^* and d yield almost the same result is because the two parameters are almost perfectly correlated for structural beams. This is due to the fact that the effective depth becomes relatively larger than the horizontal cover used to calculate d^* . The height of the compression zone, x_{cr} , does not have a significant influence in Reineck’s expression because of a high p-value of 0.27.

Reineck parameters			Hamadi parameters			Frosch parameters		
$adjR^2 = 0.840$			$adjR^2 = 0.846$			$adjR^2 = 0.851$		
RMSE = 84.5			RMSE = 84.7			RMSE = 81.5		
x_n	k_n	p-value	x_n	k_n	p-value	x_n	k_n	p-value
d	0.375	2.2 e -12	d	0.423	1.1 e-49	d^*	0.864	2.5 e-50
x_{cr}	0.178	0.273	-			-		

Table 4.18: Coefficients and statistics of linear regression with model parameters

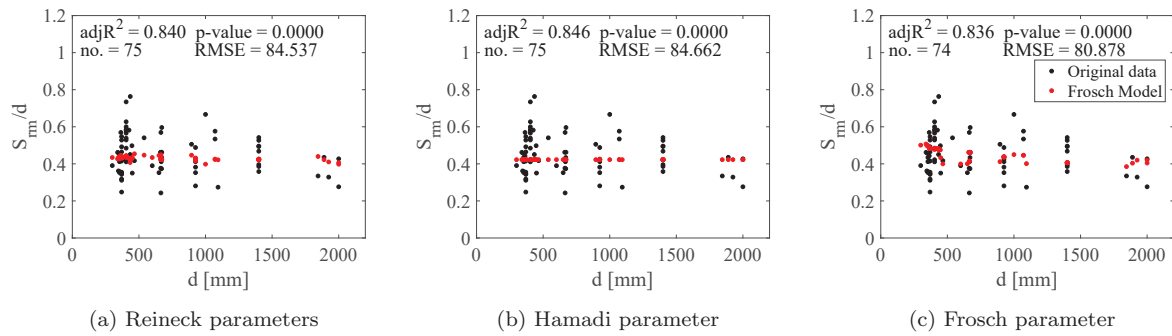


Figure 4.35: Linear regression with model parameters for $300 \leq d \leq 2000$, no. = 75 beams

All beams $50 \leq d \leq 2000$

From the above regression analysis of the structural beams, it can be concluded that the effective depth is the parameter that shows the largest influence on the crack spacing at mid-height. Therefore, a regression model is estimated with only this parameter. The result is the same as for Hamadi’s parameter above but is reproduced in Table 4.19 and Fig. 4.36.

	Only structural beams		All beams	
	$adjR^2 = 0.846$		$adjR^2 = 0.812$	
	RMSE=84.7		RMSE=71.7	
	k_n	p-value	k_n	p-value
Const. term	-	-	51.445	8.0 e-8
d	0.423	1.1e-49	0.368	2.8 e-58

Table 4.19: Coefficients and statistics of linear regression with only d as a predictor

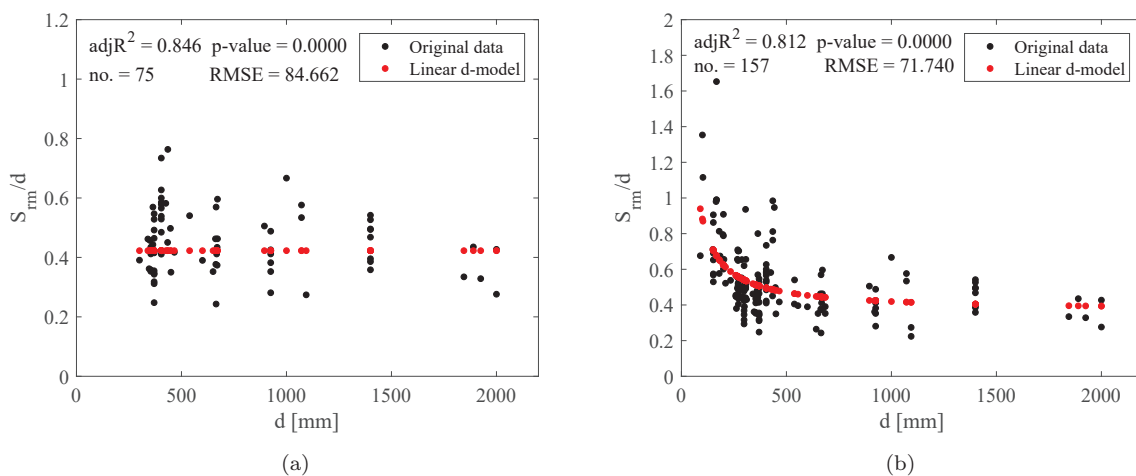


Figure 4.36: Linear regression: (a) for $300 \leq d \leq 2000$, no. = 75, with only d as predictor, (b) for $50 \leq d \leq 2000$, no. = 157, with only d and a constant term as predictors

The model estimates 85% of the variation in crack spacing for the structural beams with effective depth

greater than $300mm$. Thus, the mean primary crack spacing can be approximated by:

$$S_{rm} \approx 0.42d \tag{4.14}$$

A regression model is also estimated using the entire dataset of both laboratory and structural beams. Here a constant term is necessary, resulting in a linear relations of $S_{rm} \approx 51 + 0.37d$ describing 81% of the variation in the crack spacing af beams from $50mm$ to $2000mm$ in effective depth.

Relations between extreme and mean crack spacings

In Figs. 4.37–4.39 the relations between the extreme and mean crack spacings are investigated for all available data in the database of both laboratory and structural beams. Fig. 4.37 shows the relations between the maximum and minimum measured spacing in each beam as a function of the stress level in the reinforcement at the time the spacings were measured.

There is a large variation in the results and, by observation, it does not seem to get smaller with the increase of stress level. The mean value of S_{rmax}/S_{rmin} , in Fig. 4.37, is 4.5, which is significantly higher than the ratio of 2, which is the ratio most researchers have reported. An important observation, however, is that the largest amount of data lies close to the bin of $S_{rmax}/S_{rmin} = 2$. The same tendency applies for the relations S_{rm}/S_{rmin} in Fig. 4.38. The variation and mean value are large, but the largest bin is found around the ratio $S_{rm}/S_{rmin} = 1.33$, which is the mean value from the literature review.

It was investigated whether excluding the results from the beams with slenderness ratios below 2, the slab-like beams or the laboratory beams, resulted in less deviation, which was not the case.

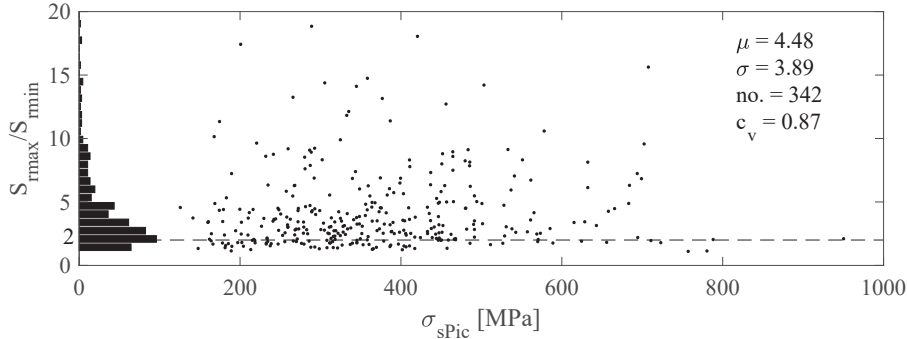


Figure 4.37: Relations between the maximum and minimum crack spacing against the stress level in the reinforcement

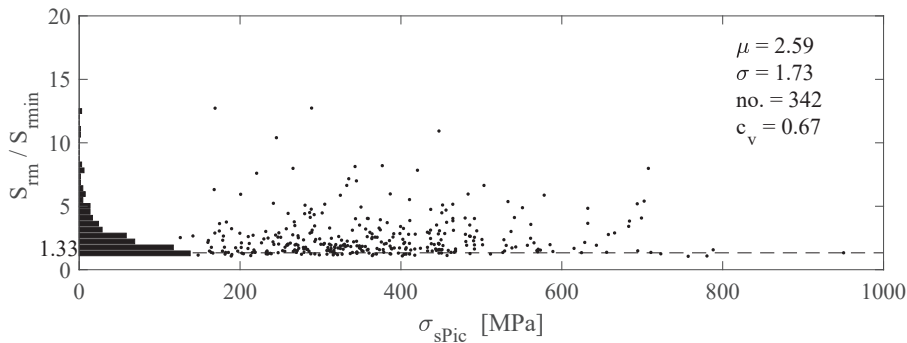


Figure 4.38: Relations between the mean and minimum crack spacing against the stress level in the reinforcement

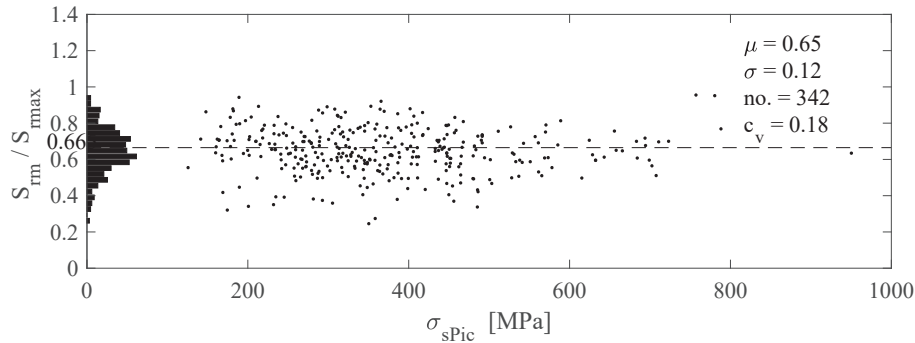


Figure 4.39: Relations between the mean and maximum crack spacing against the stress level in the reinforcement

In Fig. 4.39, which shows the distribution of S_{rm}/S_{rmax} , the relative deviation from the mean of 18% is smaller than for previous ratios S_{rmax}/S_{rmin} (87%) and S_{rm}/S_{rmin} (67%). Furthermore, the distribution also more closely resembles a normal distribution than the other two. Hence, the maximum spacing varies less from the mean than the minimum spacing. This must mean that it is more common for the minimum crack spacing to be smaller than $S_{rm}/1.33$ while the maximum is normally distributed around the value $1.5S_{rm}$. This seems quite convenient as crack widths are always estimated from maximum crack spacing in order to be able to find the maximum crack width.

4.4.3 Comparison of existing models and tests for the primary crack spacing

The existing models, treated earlier in this chapter, are now compared to the tests in the database with the use of the models' original coefficients. The comparisons are made for the 75 structural beams and the 58 laboratory beams previously used to estimate the regression models.

An investigation of a stabilised crack system, which will be explained later, in Section 4.5, shows that the primary cracks in structural beams all develop at an early stress level, and, after that, the spacing therefore does not change notably with an increase in stress level. Due to this finding, the comparisons between models and tests are plotted as a function of the effective depth, instead of the stress level, to investigate whether the models perform better for some interval of the effective depth.

In Fig. 4.40 the model-test comparison is shown for the four selected models for laboratory and structural beams together. All four models include the effective depth or the total height of the member as a variable. When comparing the relative standard deviation, c_v , the model by Frosch performs notably better than the other three, with a relative standard deviation of 0.28 compared to 0.38 in the other models. Frosch's model takes the horizontal cover into account whereas the other models only include vertical dimensions. With respect to the mean value of $S_{rm,test}/S_{rm,model}$, the very simple model by Hamadi has a value closest to 1, whereas the model by Frosch has too small a coefficient on d^* , resulting in a larger crack spacing than the test result. This is the overall trend for all the four models with respect to estimation crack spacings of the beams larger than 300mm. The models are thus all conservative with respect to the estimation of crack widths in structural beams.

In Tables 4.20 and 4.21 the performances of the models are tested separately, for laboratory and structural beams. Here, a difference is found in which model is the most accurate. In Table 4.20 the laboratory beams with stress levels in the reinforcement larger than 250MPa are compared to the four models. By comparing the relative standard deviation, Frosch's model is much better than the other three models, which have very large deviations from the mean. However, both Frosch's model and the Eurocode expression overestimate the crack spacing, with mean values significantly below 1 while the opposite applies for Reineck's and Hamadi's estimates.

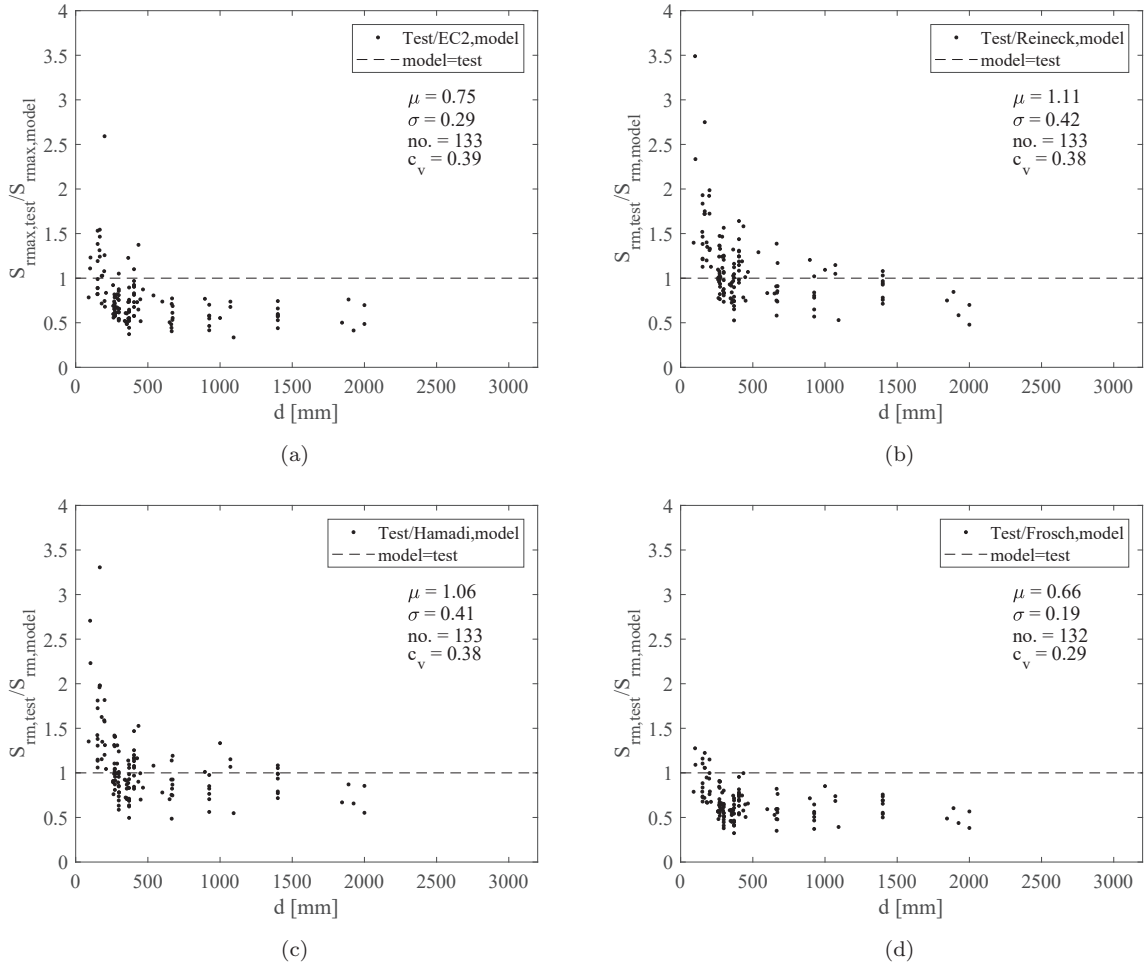


Figure 4.40: Comparison of tests and models for primary crack spacing: (a) The Eurocode 2, for maximum crack spacings, (b) Reineck’s estimate, (c) Hamadi’s estimate, (d) Frosch’s estimate

Model	no.	σ	μ	c_v
EC2	52	0.37	0.88	0.42
Reineck	52	0.51	1.29	0.39
Hamadi	52	0.52	1.27	0.41
Frosch	52	0.22	0.75	0.29

Table 4.20: Comparison of model and tests for beams where $d < 300mm$ and $\sigma_{sPic} \geq 250MPa$

Model	no.	σ	μ	c_v
EC2	75	0.19	0.65	0.29
Reineck	75	0.25	0.94	0.26
Hamadi	75	0.21	0.90	0.24
Frosch	75	0.14	0.60	0.23

Table 4.21: Comparison of model and tests for beams where $d \geq 300mm$

In the structural beams, it is not necessary to remove the beams with small stress levels. The four models perform just as well for stress levels below $250MPa$. Table 4.21 shows the model comparison of the structural beams, where all four models perform well with relative deviations in the range of $c_v = 23 - 29\%$. Frosch’s model still has the smallest relative deviation but overestimates the crack spacing by 40%. For the structural beams, Hamadi’s estimate of the mean crack spacing is almost of the same quality as Frosch’s model. This verifies that, in structural beams, the only dominating parameter for the primary

flexural cracks, which penetrate to the level of $d/2$, is the effective depth, d . This conclusion is found from (and therefore applies for) rectangular beams with an effective depth between 300mm and 2000mm with no distributed reinforcement in the web and no transverse reinforcement.

The Eurocode is the model with the largest relative deviation from the mean for both laboratory and structural beams, and, as for the tensile members, the model estimates the crack spacings to be significantly larger than the observed crack spacings. No apparent reason is found for why the empirical factor in the Eurocode is chosen to give such conservative estimates other than that the mean value for the laboratory beams is higher than for the structural beams, which could indicate that the empirical factor is determined from tests of small effective depths only.

4.4.4 Analysis of secondary crack spacing

In the following section, the crack spacing at the level of the reinforcement is studied. The main difference in the analysis compared to the analysis of the primary flexural cracks, is that normality of the relative crack spacing is not investigated due to the fact that there is no single parameter that shows strong linearity with the spacing of the secondary cracks as d does for the primary cracks.

The analysis of the parameter's influence on the crack spacing is carried out in two separate groups, as it was for the primary cracks, namely for the laboratory beams that are smaller than $d = 300\text{mm}$, and structural beams larger than $d = 300\text{mm}$. On the basis of the literature review, this division was not intended initially, as existing tests showed the same behaviour with respect to secondary cracking, irrespective of the depth of the beams, or at least no attention has, in the past, been paid to difference in behaviour. Nevertheless, the following analysis shows a difference which could be due to larger uncertainties or size effects related to the laboratory beams.

The beams included in the following regression analysis are those where all parameters are given in the experimental reports.

Correlation between parameters

Initially, the correlation between various parameters has been studied and the knowledge is used in the subsequent regression analysis. Tables 4.22 and 4.23 list all the correlation coefficients, r , between ϕ_s/ρ_s , c_{ver} , c_{hor} or c_{max} and the remaining parameters. These four parameters are chosen because they showed influence on the secondary crack spacing in the literature review. The maximum of the vertical and the horizontal cover is denoted c_{max} . This parameter is included in the following analysis since some existing models do not specify which cover is to be used while in tests there can be a large difference between the size of the cover in the two directions.

In the tables, the correlation coefficients larger than 0.65 are highlighted as these are assumed to be significant correlations. The correlation coefficients for the laboratory beams in Table 4.22 reveal that, in a majority of the beams, the maximum cover is the horizontal cover, because the correlation between these two is $r = 0.99$. The correlation coefficients in the two columns, c_{hor} and c_{max} , are therefore almost equal. Furthermore, the horizontal cover is highly correlated with the ϕ_s/ρ_s -ratio, including the effective ratios where different effective concrete areas are used. On the other hand, the vertical cover does not correlate with any of the parameters.

For the structural beams in Table 4.23, the difference, compared to the laboratory beams, is that a larger part of the beams have equal cover sizes in the vertical and horizontal directions. This can be seen from the fact that the maximum cover correlates well with both the horizontal and vertical cover as well as c_{ver} and c_{hor} have a large correlation of $r = 0.88$. The ϕ_s/ρ_s -ratio and the $\phi_s/\rho_{s,eff}$ -ratios also correlate highly with the covers.

In relation to both the laboratory and the structural beams the different $\phi_s/\rho_{s,eff}$ -ratios, correlate with the plain reinforcement ratio ϕ_s/ρ_s . The ratio estimated by the Eurocode, $\phi_s/\rho_{s,effEC2}$, and the expression

found from equilibrium, by Bigaj, $\phi_s/\rho_{s,effBigaj}$, correlate almost perfectly with the plain ratio, with r-coefficients between 0.93 – 0.99. It could therefore be argued that, when using linear regression modelling, the use of these effective ratios compared to the plain ratio, will not give a notably different result because they are so highly correlated. The main difference in using the effective ratio compared to the plain ratio would be the size of the coefficients, k_n for the parameter. On the basis of this, it was decided to use the plain reinforcement ratio instead of the effective ratio in the regression analysis that follows. However, the effective ratios will be tested, subsequently, in the regression models testing the reviewed existing model's parameters.

r-coefficients for $d < 300$, no. = 64				
Parameters	ϕ_s/ρ_s	c_{ver}	c_{hor}	c_{max}
d	0.17	0.27	-0.04	-0.06
b	0.59	0.27	<u>0.81</u>	<u>0.81</u>
ϕ_s	-0.23	0.27	0.09	0.05
n_s	-0.05	0.14	0.32	0.29
$n_s\phi_s$	-0.08	0.30	0.32	0.29
c_{ver}	0.20	-	0.20	0.22
c_{hor}	<u>0.76</u>	0.20	-	<u>0.99</u>
c_{max}	<u>0.77</u>	0.22	<u>0.99</u>	-
ρ_s	-0.65	-0.06	-0.30	-0.32
ϕ_s/ρ_s	-	0.20	<u>0.76</u>	<u>0.77</u>
$f_{c,cyl}$	-0.23	-0.12	-0.01	-0.04
σ_{sPic}	0.25	0.05	0.14	0.15
M_{Pic}/M_y	-0.13	-0.04	0.15	0.16
a	0.43	0.18	0.51	0.50
a/d	0.35	-0.06	0.55	0.55
$\phi_s/\rho_{s,effEC2}$	<u>0.97</u>	0.27	<u>0.78</u>	<u>0.79</u>
$\phi_s/\rho_{s,effSYM}$	<u>0.86</u>	0.38	<u>0.81</u>	<u>0.83</u>
$\phi_s/\rho_{s,effLeo}$	<u>0.86</u>	0.29	<u>0.91</u>	<u>0.92</u>
$\phi_s/\rho_{s,effBigaj}$	<u>0.97</u>	0.22	<u>0.81</u>	<u>0.82</u>

Table 4.22: Correlation coefficients between the parameters of laboratory beams

r-coefficients for $d \geq 300$, no. = 81				
Parameters	ϕ_s/ρ_s	c_{ver}	c_{hor}	c_{max}
d	0.53	0.56	0.39	0.56
b	0.49	<u>0.77</u>	<u>0.76</u>	<u>0.75</u>
ϕ_s	0.42	<u>0.85</u>	<u>0.69</u>	<u>0.74</u>
n_s	-0.22	-0.01	-0.12	-0.02
$n_s\phi_s$	-0.07	0.27	0.10	0.22
c_{ver}	<u>0.67</u>	-	<u>0.88</u>	<u>0.95</u>
c_{hor}	<u>0.80</u>	<u>0.88</u>	-	<u>0.96</u>
c_{max}	<u>0.83</u>	<u>0.95</u>	<u>0.96</u>	-
ρ_s	<u>-0.66</u>	-0.40	-0.42	-0.46
ϕ_s/ρ_s	-	<u>0.67</u>	<u>0.80</u>	<u>0.83</u>
$f_{c,cyl}$	-0.23	-0.18	-0.20	-0.19
σ_{sPic}	-0.29	-0.18	0.14	0.00
M_{Pic}/M_y	-0.02	-0.34	-0.17	-0.29
a	0.47	0.50	0.33	0.50
a/d	-0.41	-0.38	-0.32	-0.39
$\phi_s/\rho_{s,effEC2}$	<u>0.93</u>	<u>0.72</u>	<u>0.88</u>	<u>0.86</u>
$\phi_s/\rho_{s,effSYM}$	<u>0.88</u>	<u>0.78</u>	<u>0.93</u>	<u>0.88</u>
$\phi_s/\rho_{s,effLeo}$	<u>0.80</u>	<u>0.74</u>	<u>0.87</u>	<u>0.81</u>
$\phi_s/\rho_{s,effBigaj}$	<u>0.99</u>	<u>0.65</u>	<u>0.81</u>	<u>0.81</u>

Table 4.23: Correlation coefficients between the parameters of structural beams

Study of parameters of influence

The following regression models are estimated from the same list of possible parameters as for cracks at mid-height, listed in Table 4.14, except for the added parameter $\sum u/\pi = n_s\phi_s$. This parameter represents the total length of the circumference of the reinforcement bars in a beam.

Laboratory beams $50 \leq d < 300$

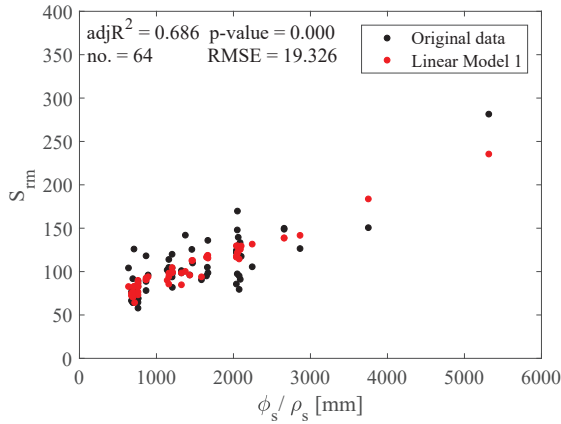
Beams with small stress levels in the reinforcement ($\sigma_{sPic} \leq 250MPa$) are excluded from the regression analysis of the laboratory beams due to the fact that when they are included, the stress level shows as a significant parameter. The intention of the regression analysis is to estimate which parameters describe the crack spacing in a stabilised crack pattern, not in the developing crack phase.

Linear Model 1		
$adjR^2 = 0.686$		
RMSE = 19.3		
	k_n	p-value
Const. term	77.541	6.2 e-11
ϕ_s/ρ_s	0.035	2.1 e-12
σ_{sPic}	-0.058	0.011

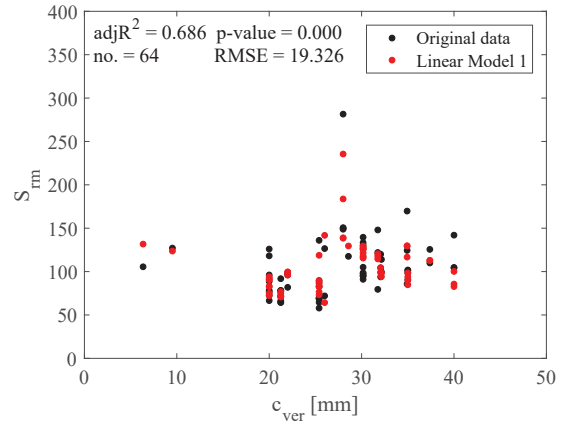
Table 4.24: Coefficients and statistics of linear regression for $50 \leq d < 300$ with two independent variables

Linear Model 2		
$adjR^2 = 0.656$		
RMSE = 20.2		
	k_n	p-value
Const. term	55.182	7.2 e-16
ϕ_s/ρ_s	0.034	3.2 e-16
σ_{sPic}	-	-

Table 4.25: Coefficients and statistics of linear regression for $50 \leq d < 300$ with one independent variable



(a) With respect to ϕ_s/ρ_s



(b) With respect to c_{ver}

Figure 4.41: Linear regression model and observed data for $50 \leq d < 300$ with ϕ_s/ρ_s and σ_{sPic} as predictors

The results of the regression analysis for secondary crack spacing in laboratory beams are shown in Tables 4.24 and 4.25 and Fig. 4.41. The Linear Model 1 describes 69% of the variation in the crack spacing with ϕ_s/ρ_s -ratio as the primary significant parameter, with a low p-value:

$$S_{rm} = 77.5 + 0.035\phi_s/\rho_s - 0.058\sigma_{sPic} \quad (4.15)$$

Even though beams with low stress levels have been excluded the stress level in the reinforcement, σ_{sPic} , still shows a small influence on the variation, with a p-value close to 0.05. The p-value for the constant term is very low, indicating that there is a large scatter in the results or that the available parameters cannot describe the whole variation in crack spacing. This was also the case for the regression model for the flexural crack spacing in the laboratory beams.

The significant parameters for the secondary crack spacing are also the same as the significant parameters for primary crack spacing in the laboratory beams, namely the ϕ_s/ρ_s -ratio and the stress level in the reinforcement, σ_{sPic} . This confirms the aforementioned conclusion that only one type of crack exists in the laboratory beams, which are mainly controlled by the bond-parameter. The stress level is of minor influence because, apparently, not all of the beams with a developing crack pattern are excluded. Linear Model 2, in Table 4.25, is a regression model with only the ϕ_s/ρ_s -ratio as an independent variable:

$$S_{rm} = 55.2 + 0.034\phi_s/\rho_s \tag{4.16}$$

The variable σ_{sPic} is thus removed even though it shows significance. When comparing $adjR^2$ and RMSE values for Linear Model 1 and 2 it is confirmed that σ_{sPic} only is of minor influence. Linear model 2, excluding σ_{sPic} , describes 66% of the variation while Linear Model 1, including σ_{sPic} , only describes 3% more.

The secondary crack spacings in the laboratory beams do not show sensitivity to variation in either the vertical or horizontal cover of the beams. In Fig. 4.41 the data sample and the Linear Model 1 are plotted in relation to both the ϕ_s/ρ_s -ratio and the vertical cover, respectively, to illustrate the clear linear relations in the data of the mean crack spacing and the ϕ_s/ρ_s -ratio. However, in contrast, no apparent linear relations between the mean crack spacing and the vertical cover can be observed, at least not for this sample of 64 test beams.

A regression model including the 14 beams with $\sigma_{sPic} \leq 250MPa$ has the same significant parameters and coefficients, the only difference is that σ_{sPic} is of higher influence and the regression model explained only 52% of the variation instead of 69%.

Model parameters

The regression models made with parameter combinations of the reviewed existing models are estimated from the same data sample as the previous regression models. The results are shown in Fig. 4.42 and listed in Table 4.26 for the Eurocode Model and Table 4.27 for the remaining four models; the Tension Chord Model, with two different effective concrete areas, Leonhardt’s model and Frosch’s model. There is some uncertainty regarding whether the cover used in the Eurocode model should be the horizontal or the vertical cover when estimating the crack spacing at the side face of beams. It seems logical that the horizontal cover would be applied because this is the distance from the reinforcement to the surface in question. However, in the following section, the performance of both the horizontal, vertical and maximum cover are investigated.

EC2 parameters			EC2 parameters			EC2 parameters		
$adjR^2 = 0.688$			$adjR^2 = 0.695$			$adjR^2 = 0.698$		
RMSE = 24.2			RMSE = 36.6			RMSE = 35.1		
x_n	k_n	p-value	x_n	k_n	p-value	x_n	k_n	p-value
$\phi_s/\rho_{s,effEC2}$	0.100	2.6 e-13	$\phi_s/\rho_{s,effEC2}$	0.103	1.2 e-4	$\phi_s/\rho_{s,effEC2}$	0.086	9.4 e-4
c_{ver}	2.137	5.0 e-16	c_{hor}	1.328	1.4 e-4	c_{max}	1.530	8.5 e-6

Table 4.26: Coefficients and statistics of linear regression with EC2 parameters

The different parameter combinations are able to describe 62 – 72% of the variation in the secondary crack spacing which is the same amount of variation the Linear Model 1 describes, which only holds the ϕ_s/ρ_s -ratio as a variable and a constant term.

There is no clear picture regarding which of the parameter combinations would be best because the models with the largest $adjR^2$ also have a large RMSE. The Eurocode Model with the use of the vertical cover is a little better than the other in terms of comparing both the RMSE and $adjR^2$ values.

With respect to the Eurocode model and the use of three different covers, on the one hand, the $adjR^2$ is approximately the same for all three models. However, on the other hand, the RMSE increases from approx. 25 to 35 when the horizontal cover and the maximum cover are used instead of the vertical cover. The p-values for both $\phi_s/\rho_{s,effEC2}$ -ratio and the cover also decrease when the horizontal or maximum cover is used. The decreasing influence of the parameters must be due to the fact that the horizontal and the maximum cover are correlated with the $\phi_s/\rho_{s,effEC2}$ -ratio. Generally, the high correlation makes it hard to conclude whether both the cover and $\phi_s/\rho_{s,eff}$ have an influence on the crack spacing.

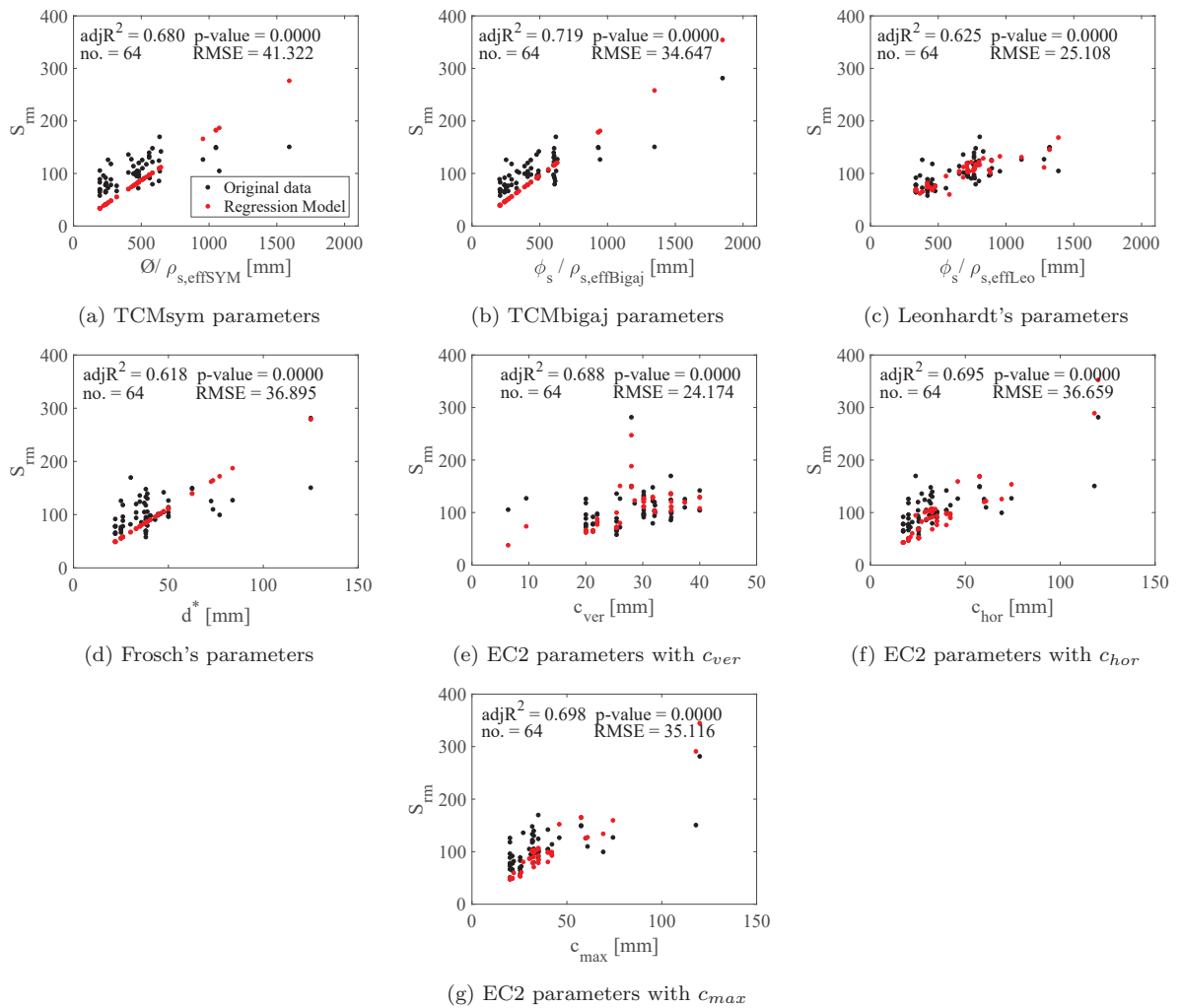


Figure 4.42: Linear regression with model parameters for $50 \leq d < 300$

From the regression analysis of the secondary crack spacing in the laboratory beams it can be concluded that there is no clear picture of which parameters describe the variation best, whether it is the cover, the ϕ_s/ρ_s , $\phi_s/\rho_{s,eff}$ or a combination of the cover and the ϕ_s/ρ_s -ratio. In any case, when a constant term is added, the RMSE is significantly smaller, which indicates a large random scatter in the data. With respect to the Eurocode model, the vertical cover shows slightly better results than the horizontal and maximum cover but again the results are quite unclear due to the fact that none of the models give good results.

TCMsym parameters			TCMbigaj parameters			Leonhardt parameters			Frosch parameters		
$adjR^2 = 0.680$			$adjR^2 = 0.719$			$adjR^2 = 0.625$			$adjR^2 = 0.618$		
RMSE = 41.3			RMSE = 34.6			RMSE = 25.1			RMSE = 36.9		
x_n	k_n	p-value	x_n	k_n	p-value	x_n	k_n	p-value	x_n	k_n	p-value
$\frac{\phi_s}{\rho_{s,effSYM}}$	0.174	1.4 e-28	$\frac{\phi_s}{\rho_{s,effBigaj}}$	0.192	2.0 e-33	$\frac{\phi_s}{\rho_{s,effLeo}}$	0.066	4.1e-11	d^*	2.235	1.1 e-31
-			-			σ_{sPic}	0.028	0.209	-		
-			-			c_{ver}	1.546	5.8 e-5	-		

Table 4.27: Coefficients and statistics of linear regression with various model parameters

Structural beams $300 \leq d \leq 2000$

The regression analysis for the secondary crack spacing in structural beams, shown in Table 4.28 and Fig. 4.43, is carried out on a sample of the 81 beams with all parameters given in the experimental reports and for beams where $a/d \geq 2$ and $b/d \leq 1$. The formulation for the Linear Model 1 is:

$$S_{rm} = -14.6 + 0.36n_s\phi_s + 1.76c_{ver} + 0.02\phi_s/\rho_s \quad (4.17)$$

with the significant parameters; ϕ_s/ρ_s -ratio, c_{ver} and $n_s\phi_s$ listed in the order of greatest significance. With these three parameters, 83% of the variation in the secondary crack spacing can be described. With a constant term being insignificant with a p-value of 0.18, the three parameters can be said to describe the variation well. The parameter $n_s\phi_s$ has only a minor influence since a regression model with only ϕ_s/ρ_s and c_{ver} as independent variables describes 77%. Furthermore, a model only holding ϕ_s/ρ_s or c_{ver} describes 60% and 69%, respectively, making the vertical cover the most influential parameter. Due to the fact that these two parameters are correlated with a $r = 0.67$ they describe some of the same variation in the crack spacing.

When comparing the distribution of data with respect to variation in the two variables c_{ver} and ϕ_s/ρ_s , shown in Figs. 4.43a and 4.43b, the crack spacing plotted as a function of c_{ver} more closely resembles a straight line than when it is plotted against ϕ_s/ρ_s . This confirms that the c_{ver} has the strongest influence on S_{rm} . Another argument for this is that the constant term becomes highly significant for a regression model only holding the ϕ_s/ρ_s -ratio as the independent variable.

Linear Model 1		
$adjR^2 = 0.830$		
RMSE = 36.5		
	k_n	p-value
Const. term	-14.558	0.181
$n_s\phi_s$	0.356	2.0e-6
c_{ver}	1.763	5.1e-8
ϕ_s/ρ_s	0.020	2.2e-11

Table 4.28: Coefficients and statistics of linear regression for $300 \leq d \leq 2100$

The current model is significantly better than the regression model estimated for the laboratory beams, earlier, which could only describe 69% of the variation with a highly significant constant term, confirming that the random scatter is large for the laboratory beams.

Recalling the results of the regression analysis of the tensile members, the exact same three parameters were of significance to the crack spacing. The main difference is that for the tensile members, the cover and the ϕ_s/ρ_s -ratio was even more correlated to such an extent that the two terms described almost the same variation and therefore one of the terms became insignificant. As previously listed in the tables, the ϕ_s/ρ_s -ratio had a correlation of $r = 0.88$ with the cover in the tensile members and $r = 0.67$ with the vertical cover in the structural beams.

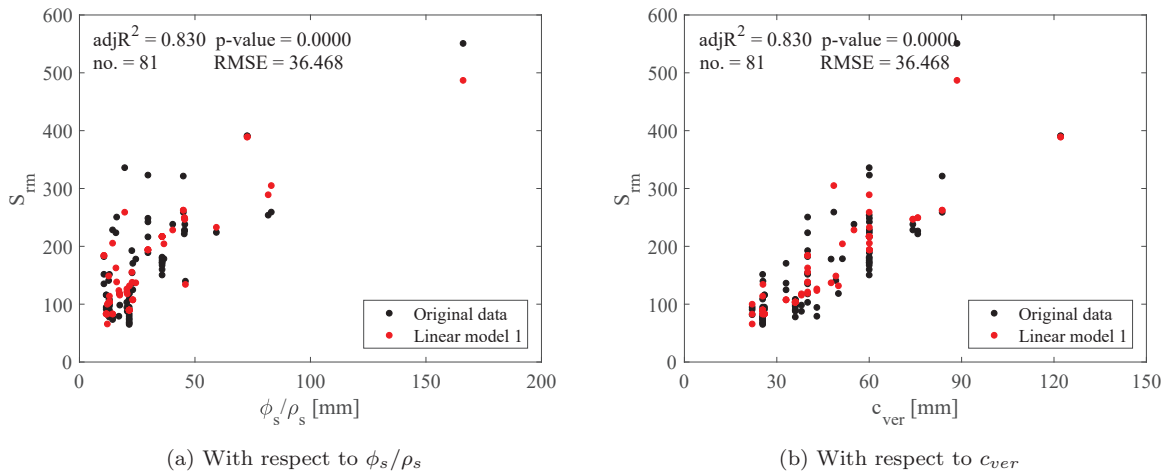


Figure 4.43: Linear regression for $300 \leq d \leq 2100$ with 3 parameters of influence

Model parameters

The analysis of the parameter combinations of the reviewed existing models is carried out on the same data sample as the previous regression analysis. The results are listed in Table 4.29 for the Eurocode model and in Table 4.30 for the remaining three models. In Fig. 4.44 the observed data are plotted together with the estimated data of each regression model.

EC2 parameters			EC2 parameters			EC2 parameters		
$adjR^2 = 0.766$			$adjR^2 = 0.702$			$adjR^2 = 0.790$		
RMSE = 44.3			RMSE = 52.8			RMSE = 40.4		
x_n	k_n	p-value	x_n	k_n	p-value	x_n	k_n	p-value
$\phi_s/\rho_{s,effEC2}$	0.057	3.1e-5	$\phi_s/\rho_{s,effEC2}$	0.025	0.235	$\phi_s/\rho_{s,effEC2}$	0.009	0.52
c_{ver}	2.650	8.1e-20	c_{hor}	3.141	1.0e-13	c_{max}	3.234	6.0e-23

Table 4.29: Coefficients and statistics of linear regression with EC2 model parameters

From comparison of the size of the RMSE and the $adjR^2$, the EC2 parameters with the use of the maximum cover describe the variation with the most precision. It should here be noted, that when the maximum cover is used, the $\phi_s/\rho_{s,effEC2}$ -ratio becomes insignificant. In conclusion, the parameter c_{max} alone, describes 79% of the variation in the secondary crack spacing of the structural beams. The reason for

this result could be because c_{max} and ϕ_s/ρ_{effEC} have a high correlation coefficient of $r = 0.83$ and thus describe the same variation in the crack spacing. This latter statement is investigated further by a new regression analysis with a sample of beams where $c_{ver} = c_{hor}$. This is elaborated in the following section.

TCMsym parameters			TCMbigaj parameters			Leonhardt parameters			Frosch parameters		
$adjR^2 = 0.693$			$adjR^2 = 0.669$			$adjR^2 = 0.705$			$adjR^2 = 0.654$		
RMSE = 73.6			RMSE = 73.0			RMSE = 48.6			RMSE = 50.5		
x_n	k_n	p-value	x_n	k_n	p-value	x_n	k_n	p-value	x_n	k_n	p-value
$\frac{\phi_s}{\rho_{s,effSYM}}$	0.224	1.6e-33	$\frac{\phi_s}{\rho_{s,effbigaj}}$	0.223	8.5e-34	$\frac{\phi_s}{\rho_{s,effLeo}}$	0.027	0.067	d^*	2.810	1.3e-46
-			-			σ_{SPic}	-0.007	0.830	-		
-			-			c_{ver}	3.030	1.9e-16	-		

Table 4.30: Coefficients and statistics of linear regression with various model parameters

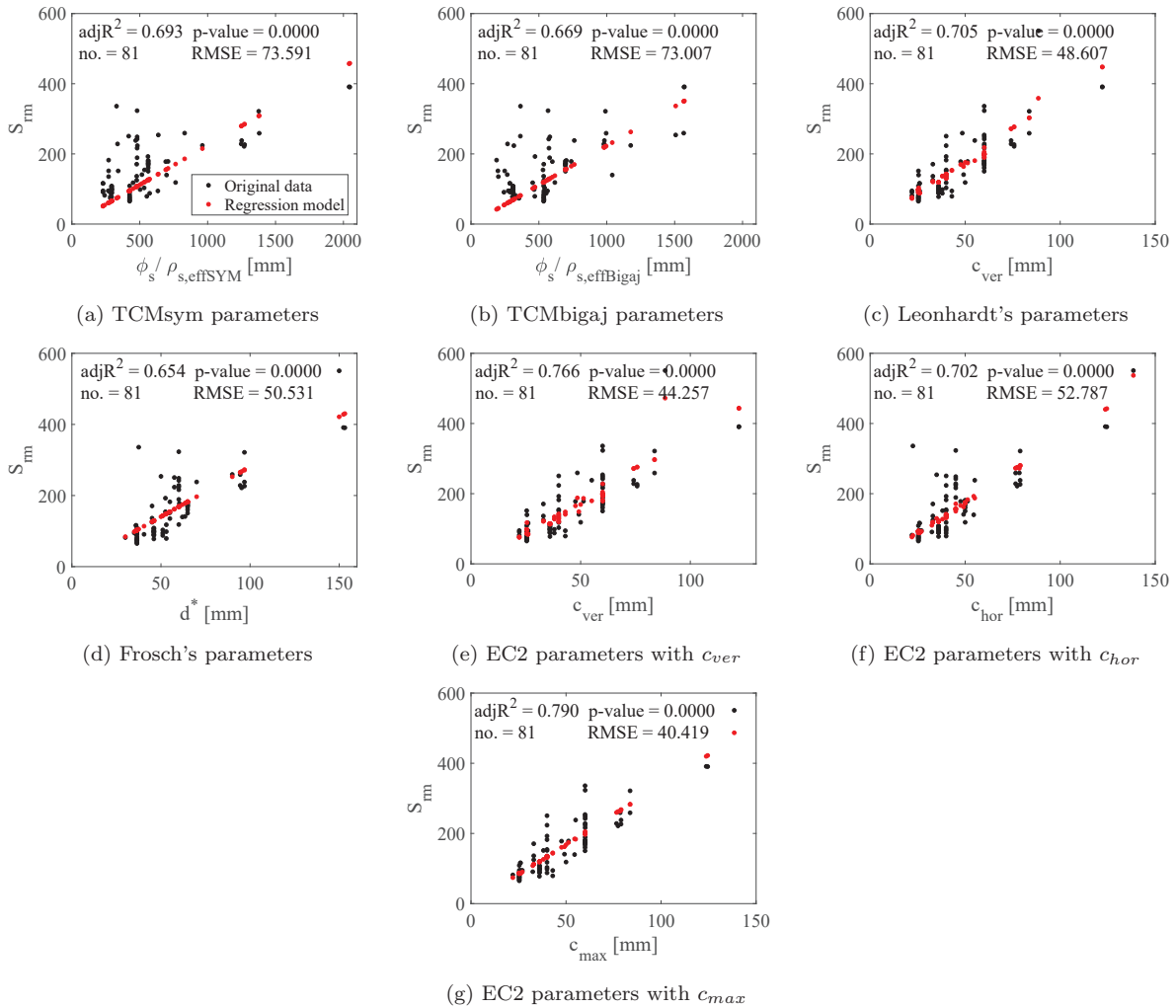


Figure 4.44: Linear regression with model parameters for $300 \leq d \leq 2000$

With respect to the other models, aside from the EC2, the same conclusions apply as for the laboratory beams. The models describe more or less the same amount of variation, 65 – 71%. The two models that only consist of the bond-parameter, $\phi_s/\rho_{s,eff}$, which are the TCMsym model and the TCMbigaj model, both have a large RMSE compared to the other models, which makes them the least accurate estimates. Both Leonhardt’s and Frosch’s model parameters perform quite well. The only parameter in Frosch’s model is the horizontal distance to the reinforcement while in Leonhardt’s model both the bond-parameter, the cover and the stress level are included.

All beams $50 \leq d \leq 2000$ with $c_{ver} \approx c_{hor}$

The previous regression analysis indicated that if the maximum cover is used to estimate the secondary crack spacing in the structural beams, the ϕ_s/ρ_s -ratio becomes insignificant. Due to this finding, a final regression model is estimated from a sample of beams where the criterion: $|c_{ver} - c_{hor}| \leq 5mm$ is met. Hence, the vertical and the horizontal cover are more or less the same and the maximum cover is of course then equal to both of them. Firstly, the structural beams are used to create a regression model and secondly a regression model is made for all beam sizes. The relations between c_{ver} and ϕ_s/ρ_s are shown in Fig. 4.45 for the structural beams and for all the beams, respectively. Under both circumstances, the two parameters are highly correlated.

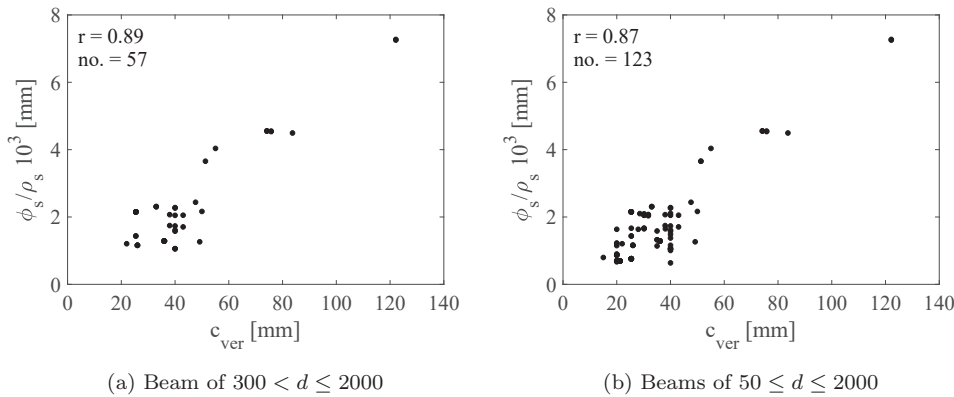


Figure 4.45: Distribution of the data and correlation with the ϕ_s/ρ_s -ratio for beams where $|c_{ver} - c_{hor}| \leq 5mm$

In Table 4.31 and Fig. 4.46 the regression models with only the cover, c , as the independent variable, are shown. For the structural beams and for all the beams, respectively, 79% and 71% of the variation in crack spacing is described by the parameter c alone. If the ϕ_s/ρ_s -ratio is included, it would be insignificant due to a high p-value. As the table shows, the constant term is insignificant for the model for the structural beams. The $\phi_s/\rho_{s,eff}$ -ratio, calculated from the Eurocode formulation of the effective concrete area, has also been tested and has also shown to be insignificant, with a very high p-value.

A regression model was also estimated for a sample of 91 beams where $c_{ver} = c_{hor}$ was met. By random chance the cover and the ϕ_s/ρ_s were not correlated in that case. Still, the ϕ_s/ρ_s -ratio turned out to be insignificant.

The high $adjR^2$ values are largely due to the fact that two beams are included with a cover of $130mm$. The second largest cover represented is $85mm$ which means that a fairly significant interval between a cover of $85mm$ and $130mm$ is not represented. The use of the two data points with $c_{ver} = 130mm$ is justified by the fact that there are two of them. If only one beam represented this large cover, it would have been excluded. The $adjR^2$ is approx. 0.65 if the two beams are excluded, which is concluded to still be a good model.

	$300 \leq d \leq 2000$		All beams	
	$adjR^2 = 0.793$		$adjR^2 = 0.712$	
	RMSE = 34.3		RMSE = 31.8	
	k_n	p-value	k_n	p-value
Const. term	4.157	0.682	16.296	0.013
c	3.195	1.1e-20	2.988	1.022e-34

Table 4.31: Coefficients and statistics of linear regression for beams where $c_{ver} \approx c_{hor}$

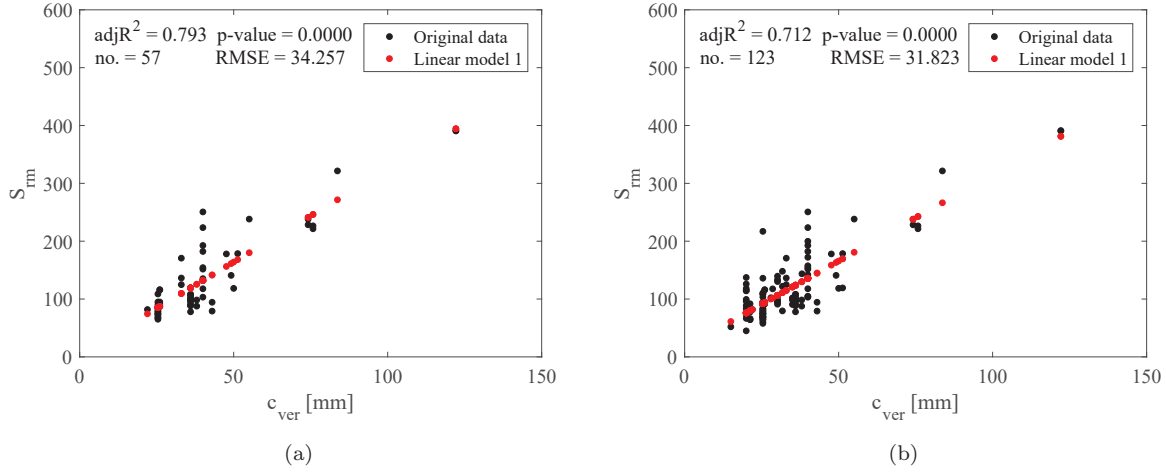


Figure 4.46: Linear regression for beams where $c_{ver} \approx c_{hor}$: (a) for $300 \leq d \leq 2000$, (b) for all beams

Relations between extreme and mean crack spacings

The results of the investigation of the relations between the extreme and mean spacing of the secondary cracks are rather different than for the primary cracks if all beams in the database are taken into consideration. In this case, the relations between the maximum and minimum spacing, S_{rmax}/S_{rmin} , have a mean value of 6 and the largest bin is between 4 and 5, which is considerably larger than the expected value from the literature review of approximately 2. The same applies for the relations between the mean crack spacing and the maximum and minimum spacing, respectively. It was investigated whether excluding the results from the beams with slenderness ratios below 2 and the slab-like beams resulted in smaller variation, which is not the case.

In Figs. 4.47 - 4.49 the ratios S_{rmax}/S_{rmin} , S_{rm}/S_{rmin} and S_{rm}/S_{rmax} , of crack spacings within the constant moment span of the 150 beams subjected to four-point-bending are plotted. The figures show how the spacings of the secondary cracks in the constant moment span are distributed more or less in the same way as the spacings of the primary cracks. When excluding the crack spacings measured in the shear span it eliminates the problem of the ongoing formation of new cracks, closer and closer to the supports, with an increase in load.

Generally, the mean values of the ratios S_{rmax}/S_{rmin} , S_{rm}/S_{rmin} and S_{rm}/S_{rmax} are higher than those found by previous researchers but the largest bins are placed at the values previously found to be the mean, which, in the graphs below, are indicated by the dotted lines. Moreover, the ratio S_{rm}/S_{rmax} has the smallest deviation from the mean value, which was also the case for the primary cracks. In this case,

the mean value of 0.70 is also quite close to the ratio found in existing literature of 0.665.

The distribution of the minimum spacings relative to the maximum, S_{rmax}/S_{rmin} , also resembles the distribution of crack spacings that Beeby[28] proposed for the secondary crack spacings in beams, discussed in Chapter 2.

From observation of the data plotted in Figs. 4.47 - 4.49 the deviation from the mean value does not decrease with an increase in reinforcement stress level.

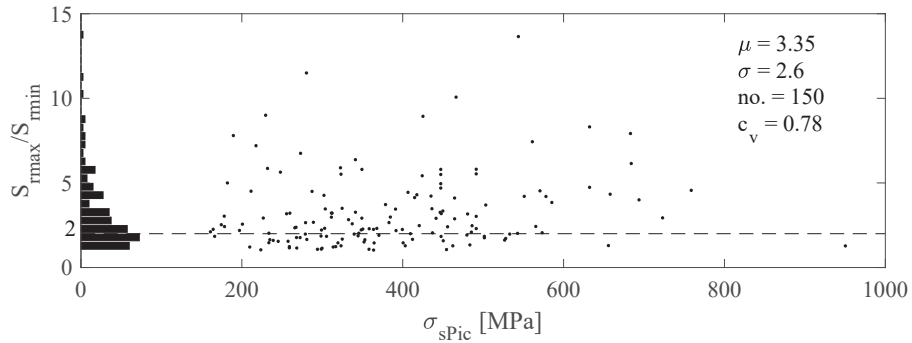


Figure 4.47: Relations between maximum and minimum secondary crack spacing in constant moment spans in relations to stress

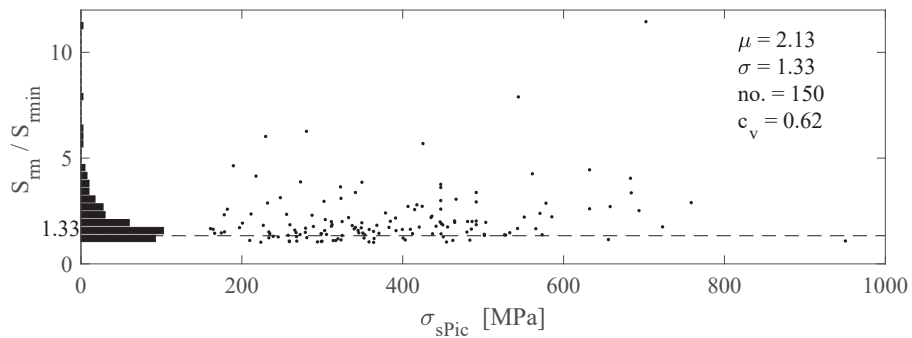


Figure 4.48: Relations between mean and minimum secondary crack spacing in constant moment spans in relations to stress

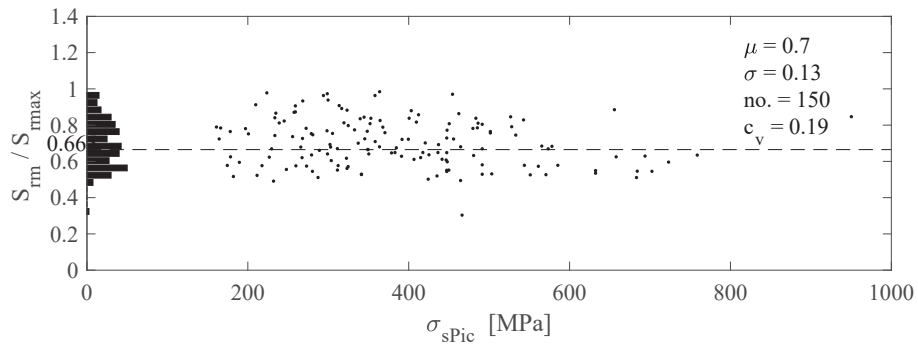


Figure 4.49: Relations between maximum and mean secondary crack spacing in constant moment spans in relations to stress

4.4.5 Comparison of existing models and tests for the secondary crack spacing

In the comparison between the models and the observed spacing of the secondary cracks, the results are treated in two parts. Firstly, the result of the comparison with the Eurocode model is presented. This is found to be the model that best agrees with the tests with respect to the lowest relative deviation, c_v . Subsequently, the results of the comparison with the other models, which yields higher relative deviation, are briefly described. The beams included in the comparison are the 64 laboratory beams and the 81 structural beams also used for the regression analysis in the previous sections.

The Eurocode 2 Model

The comparison is carried out for four different scenarios, all shown in Fig. 4.50: 1) estimation of S_{rmax} with the use of c_{ver} , 2) estimation of S_{rmax} with the use of c_{hor} , 3) estimation of S_{rmax} with the use of c_{max} , and 4) estimation of S_{rmi} with the use of c_{ver} and $\lambda = 1.33$. λ is the most commonly used relations between the minimum and mean spacing also statistically supported by Beeby[28] as well as agreeing well with the results of crack spacings in the constant span in the previous section. This relation is used in connection with the Eurocode model even though the Eurocode does not specify any relations between extreme and mean values of the spacing between cracks.

The four comparisons of $S_{r,test}/S_{r,model}$ are plotted with respect to the stress level in the reinforcement, σ_{sPic} , which shows that there is a larger scatter for small stress levels, indicating that the Eurocode is less accurate for beams with stress levels smaller than approx. $250MPa$. This is investigated further later in this section.

From comparing the mean value and relative deviation given in the plots, the Eurocode estimates the crack spacing with almost the same precision regardless of whether the vertical cover or the maximum cover are used. This must be due to the fact that these two parameters have a high correlation. When using the horizontal cover, the deviation from the test value becomes greater, thus from the comparison with these 145 tests, the use of the horizontal cover with the Eurocode model provides inaccurate results. This is quite surprising, since it could be argued that the horizontal cover should be used when seeking to determine the crack spacing at the side face of a beam.

The mean value is closest to 1 when using the maximum cover, making this the best fit for estimation of maximum secondary crack spacing. However, all three mean values, when estimating the maximum crack spacing, are larger than 1, which means that the Eurocode, on average, for all beam depths, estimates the crack spacing too small compared to the test results. Therefore, the model is not conservative when the crack spacing is used for predicting maximum crack widths.

With respect to the estimation of the mean crack spacing in Fig. 4.50d, the Eurocode becomes more accurate, compared to the estimation of maximum spacings, with a smaller relative deviation of 31% and a mean value just below 1. Moreover, from comparing the plots in Fig. 4.50a and 4.50d, where the same cover is used, the maximum spacing seems to be more noticeably affected by the stress level than the mean spacings are.

It should be mentioned that the Model Code 2010 was also compared to the test in the same manner as above but this gave very similar results, though the mean values and the standard deviation were a little higher, making the Eurocode slightly more accurate.

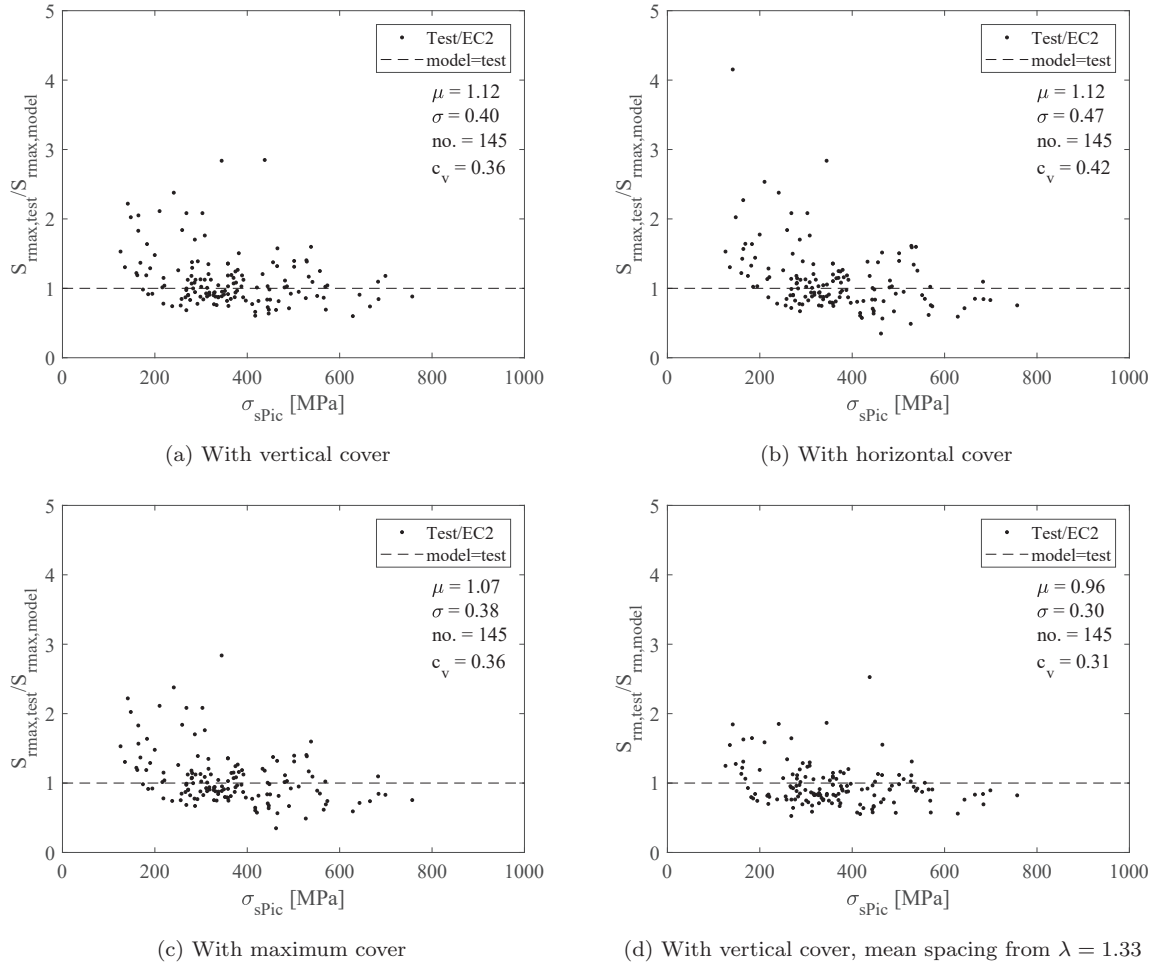


Figure 4.50: Comparison of the Eurocode Model to 145 tests. Relations between test and model as a function of σ_{sPic}

In Fig. 4.51 the same model comparisons are plotted but now as a function of the $\phi_s / \rho_{s,eff,EC2}$ -ratio instead of the stress level. The plots show how the model also estimates the crack spacing inaccurately with respect to variation in the $\phi_s / \rho_{s,eff,EC2}$ -ratio. The estimated crack spacings are too small for low $\phi_s / \rho_{s,eff,EC2}$ -ratios and too large for high $\phi_s / \rho_{s,eff,EC2}$ -ratios. This result was also found for the Eurocode model comparison with the tests of tension members.

In order to investigate the comparisons in a more comprehensive fashion, the beams are split into the groups of laboratory and structural beams once more. Tables 4.32 and 4.33 list the statistics for the comparison of structural and laboratory beams, separately. With respect to the maximum spacing, in both the laboratory and the structural beams, the Eurocode model with the use of the maximum cover gives the best result due to the mean value being closest to 1 and the lowest relative deviation of 39% and 33%, respectively. The mean crack spacing is estimated with better precision than the maximum spacing for both laboratory and structural beams.

Overall, the secondary crack spacing can be estimated with better precision in the structural beams than in laboratory beams, as is indicated by the higher relative deviation from the mean for the laboratory beams.

For laboratory beams, the model with the use of c_{hor} is better than using c_{ver} which must be due to the high correlation between c_{hor} and c_{max} . In structural beams, the opposite is true, due to high correlation between c_{ver} and c_{max} resulting in the model using c_{ver} or c_{max} being the best. The conclusion to this

must be that if the vertical and horizontal cover is not of the same size in a beam, the maximum cover is to be used when estimating the spacing of cracks on the side face at the reinforcement level when applying the Eurocode.

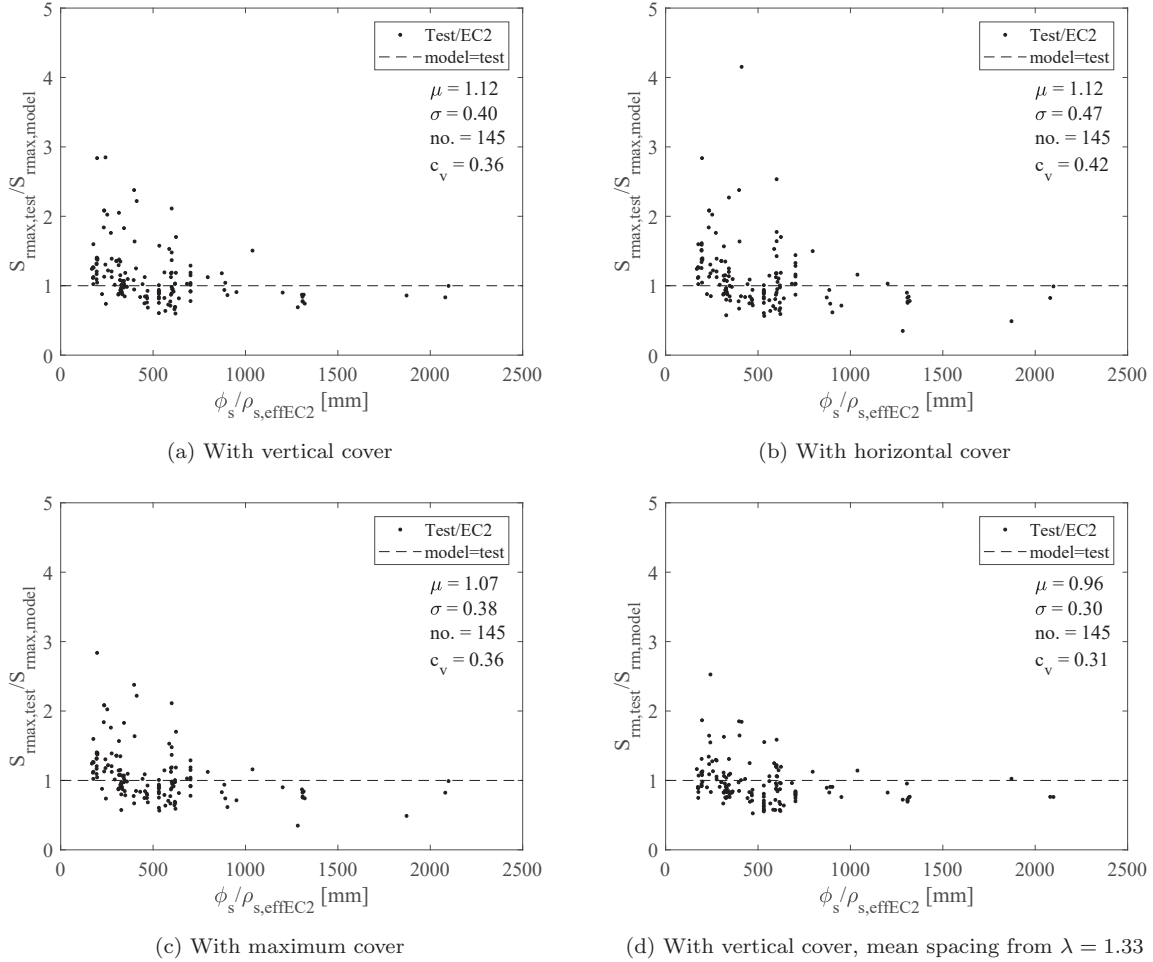


Figure 4.51: Comparison of the Eurocode Model. Relations between test and model against the $\phi_s/\rho_{s,eff,EC}$ -ratio

EC2 Model	no.	σ	μ	c_v
S_{rmax} with c_{ver}	64	0.43	1.14	0.38
S_{rmax} with c_{hor}	64	0.42	1.08	0.39
S_{rmax} with c_{max}	64	0.41	1.04	0.39
S_{rm} with c_{ver}	64	0.30	1.00	0.30

Table 4.32: Comparison of model and tests for beams where $d \leq 300mm$, $\sigma_{sPic} \geq 250MPa$

EC2 Model	no.	σ	μ	c_v
S_{rmax} with c_{ver}	81	0.38	1.11	0.34
S_{rmax} with c_{hor}	81	0.51	1.15	0.44
S_{rmax} with c_{max}	81	0.36	1.09	0.33
S_{rm} with c_{ver}	81	0.29	0.93	0.31

Table 4.33: Comparison of model and tests for beams where $d \geq 300mm$

In Fig. 4.52 the Eurocode model for estimating mean crack spacings is compared to the regression model, for laboratory beams, found earlier, where the ϕ_s/ρ_s -ratio is the only independent variable. When the two plots are compared it can be seen how the constant term in the regression model eliminates the problem of

inaccuracy with respect to variation in the $\phi_s/\rho_{s,eff}$ -ratio. The inclusion of the constant term also results in a smaller deviation from the mean value of 19% compared to 29% for the Eurocode estimates. It can be concluded that there is a large random variation in the secondary crack spacings of the laboratory beams and/or that a parameter, not found here, is missing to describe the total variation in crack spacing.

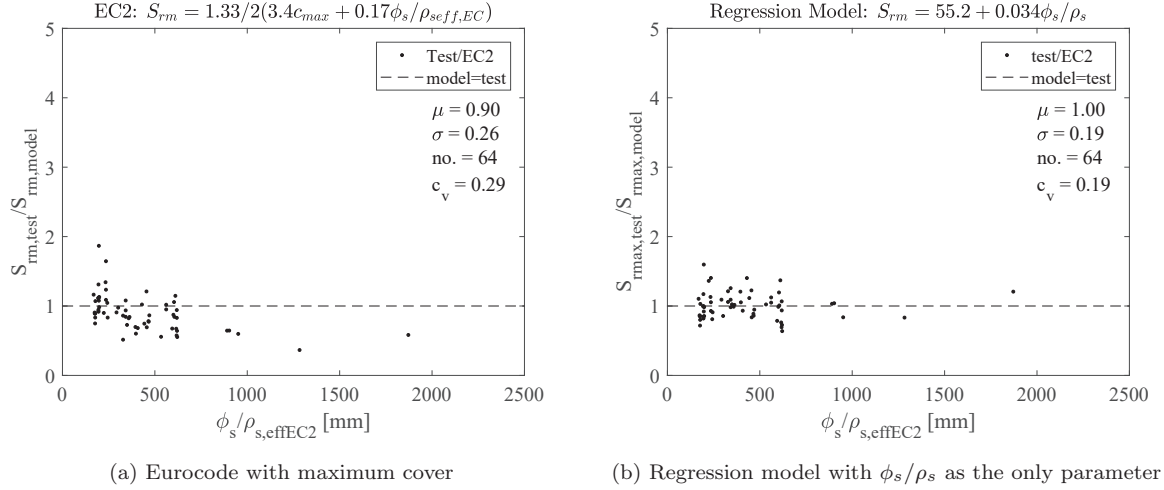


Figure 4.52: Comparison of the Eurocode model and regression models for estimation of mean crack spacing, for $d < 300mm$

In Fig. 4.53 the same comparison as above is made for structural beams with the regression model determined earlier for that data sample. Here, the relative deviation of the data is reduced from 31% to 22%, with the inclusion of the parameter $n_s\phi_s$ which is not included in any existing models but was also seen to have a secondary influence of the crack spacing in the tension members. Another point is that the sensitivity with respect to variation in the $\phi_{s,eff}/\rho_s$ -ratio in the Eurocode model is not seen for the regression model.

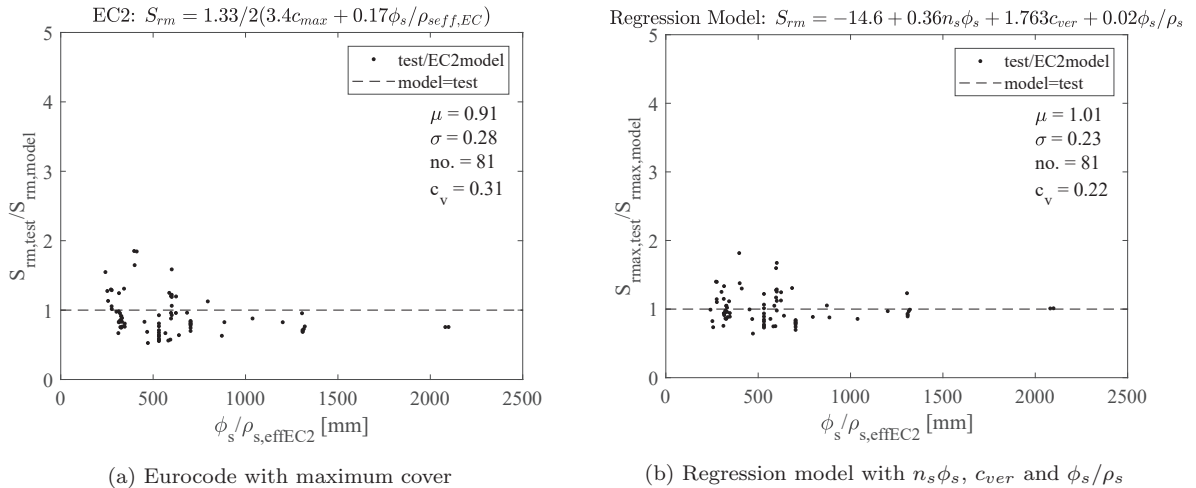


Figure 4.53: Comparison of the Eurocode 2 model and regression models for estimation of mean crack spacing, for $d \geq 300mm$

Other models

In Fig. 4.54 the two bond-slip models (TCMsym and TCMBiga,j) and the no-slip model (Frosch) are compared to the tests. The figures show that none of the models provide an accurate estimation of the

crack spacing. All three models underestimate the crack spacing compared to the test results. In some cases, this is even up to six times lower than the test results.

The inaccuracy with respect to variation in the $\phi/\rho_{s,eff}$ -ratio is also seen for the two bond-slip models on an even larger scale than for the Eurocode Model. As a result, the bond-slip models only provide good results for large $\phi/\rho_{s,eff}$ -ratios, higher than approximately 700mm.

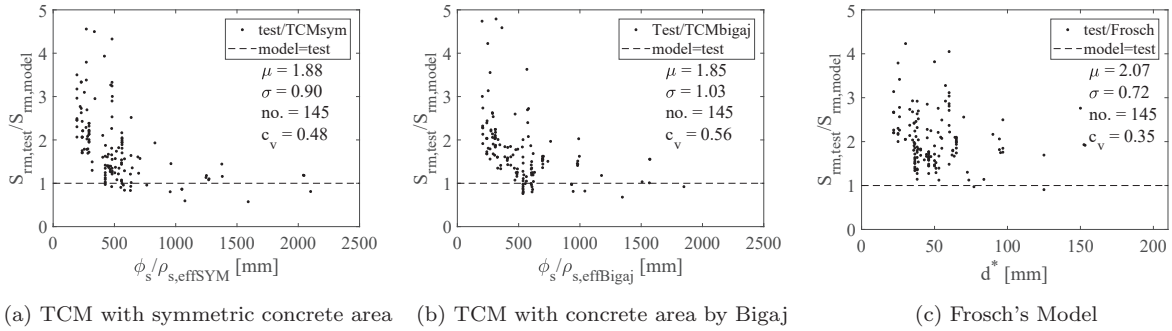


Figure 4.54: Comparison of tests and models for secondary crack spacing

4.5 Investigation of stabilised crack systems

The database of flexural test members includes 82 beams where crack spacings were measured at several different load steps besides at failure. When these were analysed with respect to a stress level to which the crack patterns were stable, i.e. the mean crack spacings were constant with increasing stress, no clear conclusions were found. It is assumed that the main reason for this is that the beams have very different capacities with respect to bending moment and the moment utilisation in the beams was therefore not remotely similar at the time cracking occurred, neither were the stress levels in the reinforcement. Furthermore, from the regression analysis of the laboratory beams, it was found that the stress level still has a minor influence on the secondary and primary crack spacing even though the beams with reinforcement stresses of less than 250MPa were excluded. Thus, a single stress level to which cracking in beams is stabilised does not seem to exist.

In the conducted test, presented in Chapter 3, the development of crack spacing with respect to increasing load was also investigated. The dimensions associated with the beams are given in Table 3.1.

Figs. 4.55a and 4.55b illustrate the result of the mean crack spacings, measured at six different load levels, for the laboratory and the structural beams, respectively. Each figure shows the development of the relative crack spacing S_{rm}/d , for both primary and secondary cracks, with respect to the load utilisation P/P_y . For all beams, the spacing of the primary flexural cracks, $S_{rm,fl}$, is seen to stabilise at load ratios between 40 – 70% of P_y . The stabilisation of the crack spacing at low utilisations is particularly pronounced for the structural beams, where the beams with the large reinforcement ratio stabilised first, at around 40%, while the laboratory beams with the large reinforcement ratio stabilised last, at around 70% of P_y .

In Fig. 4.55a, for the laboratory beams, it is hard to identify a load level at which the secondary crack spacing is stabilised because the crack spacing keeps decreasing with an increase in load. However, in the structural beams it seems that the system of secondary cracks is stabilised at around 60%, whereafter the spacing only decreases slightly. Again, the conclusion that the laboratory beams behave differently than the structural beams is confirmed.

Only a few secondary cracks are observed to develop in the laboratory beams which can be seen from Fig. 4.55a where the secondary cracks spacing, $S_{rm,sec}$, is only slightly lower than the primary crack spacing. In contrast, the spacing of the secondary cracks in the structural beams in Fig. 4.55b indicates a large number of secondary cracks between the primary cracks. This confirms the earlier conclusion that only one system of cracks exists in the laboratory beams.

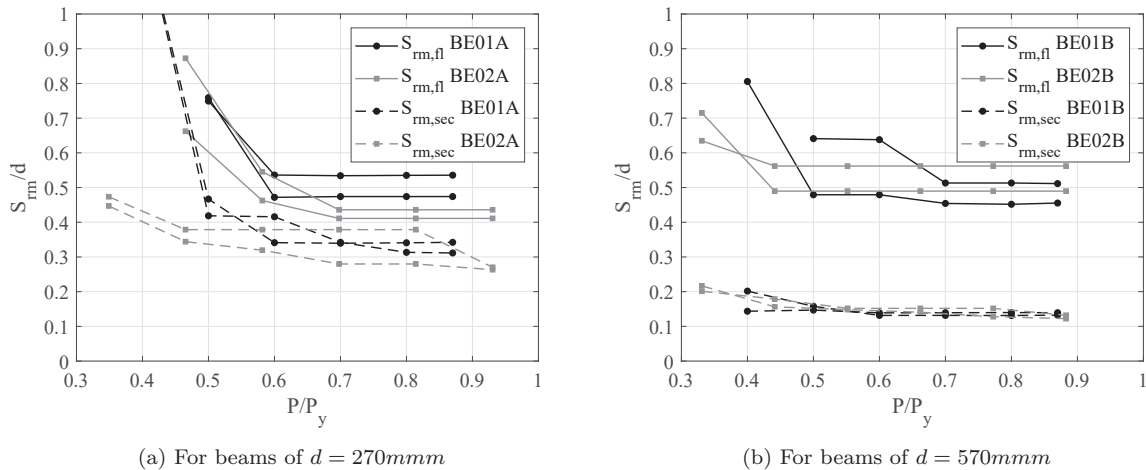


Figure 4.55: Mean relative spacing for primary and secondary crack as a function of load utilisation, reprint from [77]

4.6 Comparison of crack spacings in tensile members and flexural members

In the following section, the mean crack spacings in the tensile members are compared to the mean secondary crack spacings in the flexural members. There are two reasons why this comparison is interesting. Firstly, most models estimating the secondary crack spacing in beams are developed from assumptions of uni-axial tension and observations of tests of tensile members. From that point of view, a comparison of the crack spacings in the two different structural members should show some similarities. Secondly, the Eurocode model has the same basis for tensile and flexural members but with a difference in a coefficient on the ϕ_s/ρ_s -term, which is twice the size for tensile members as it is for flexural members. This basically means that the influence of $\phi_s/\rho_{s,eff}$ -ratio is smaller for flexural members than the ϕ_s/ρ_s -ratio is for tensile members. Therefore, some difference in the behaviour of the crack spacings in the two different structural members should be seen with respect to variation of ϕ_s/ρ_s .

The investigation is carried out for structural beams as these have shown the most clear behaviour in the previous investigations in this chapter. The members included in the investigation are the entire database of 142 tensile tests and the 81 structural beams used in the regression analysis of the secondary cracks. In Fig. 4.56a the mean crack spacings are plotted with respect to the ϕ_s/ρ_s -ratio for tensile members and with respect to the $\phi_s/\rho_{s,eff}$ for flexural members. Fig. 4.56b plots the same mean crack spacings but with respect to the maximum cover.

The plot in 4.56b shows a very clear proportionality between the maximum cover and the crack spacing in both types of member. Furthermore, the data points for tensile members and flexural members form the same slope, meaning that they have what looks to be the same proportionality factor between cover and crack spacing. With respect to variation in the ϕ_s/ρ_s -ratio, the crack spacings of the flexural members are scattered for small $\phi_s/\rho_{s,eff}$ -ratios and the crack spacings in the flexural members looks as though they are slightly larger compared to the tensile members for the same ϕ_s/ρ_s -ratios.

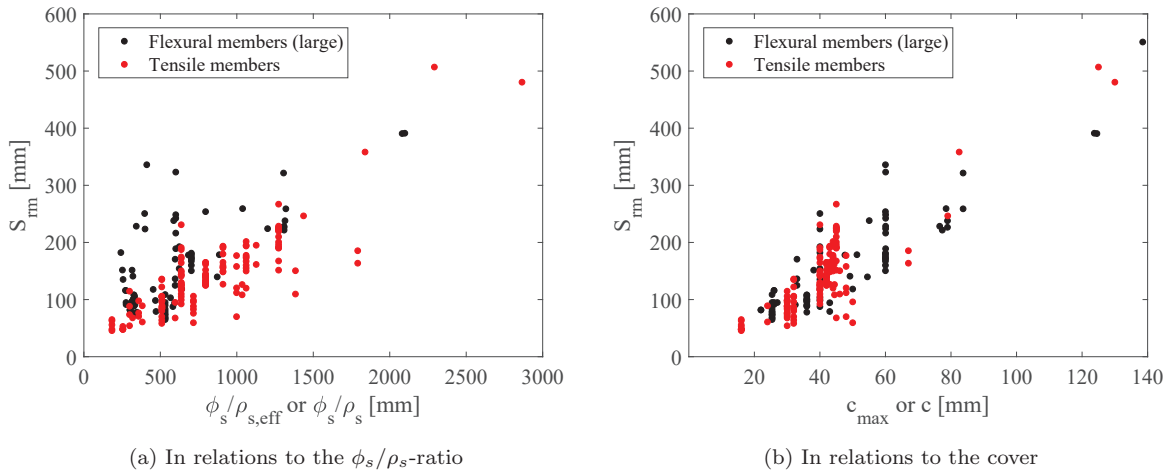


Figure 4.56: Comparison mean crack spacings in tension and flexural members, $300 \leq d \leq 2000$

The Eurocode model specifies that the ϕ_s/ρ_s -ratio should have half the influence on crack spacings in flexural members compared to crack spacings in tensile members:

EC2 for tensile members: $S_{rm} = 2.26c + 0.23\phi_s/\rho_s$

EC2 for flexural members: $S_{rm} = 2.26c_{ver} + 0.11\phi_s/\rho_{s,effEC2}$

The regression models for tensile members and flexural members made from the data in Fig. 4.56 are:

Regression model for tensile members: $S_{rm} = 1.91c + 0.083\phi_s/\rho_s$

Regression model for flexural members: $S_{rm} = 2.65c_{ver} + 0.057\phi_s/\rho_{s,effEC2}$

When the Eurocode models are compared to the regression models it is seen that the influence of the ϕ_s/ρ_s -ratio is smaller for flexural members than for tensile members but the coefficient is not quite half the size. Furthermore, the regression indicates that the coefficient of the cover-term for the flexural members should be larger than for tensile members. The coefficients of the regression models are, in general, smaller than for the Eurocode due to the fact that the Eurocode model is very conservative, as concluded earlier.

4.7 Discussion and conclusions

4.7.1 Tensile members

The aim of the empirical study of the tensile members was to answer the following questions:

1. Which parameters control crack spacing?
2. Which existing models are able to estimate crack spacings most accurately?
3. What is the relation between extreme and mean crack spacings?

From the analysis of the database holding crack spacing measurements of 142 tensile members, the main results and conclusions are:

1. The controlling parameters with respect to estimation of crack spacing in tensile members are the cover c and the ϕ_s/ρ_s -ratio. Furthermore, the diameter, ϕ_s , also has a smaller influence on the variation of the crack spacing. A multi-variable linear regression model which combines two or all three of these parameters describes approximately 70% of the variation in the crack spacing with no need for a constant term.

Linear regression models holding the cover or the ϕ_s/ρ_s -ratio alone, describe around 65% of the variation, making them almost as good as the model where the parameters are combined.

For quadratic tensile members, the parameter ϕ_s/ρ_s can also be expressed as c^2/ϕ_s approximating the same value. Hence, the ϕ_s/ρ_s -ratio is also highly dependent on the cover. This is a sound reason as to why the two parameters (cover and ϕ_s/ρ_s) describe much of the same variation in the crack spacing.

In many cases, the connection between these two parameters will mean that they are highly correlated, which, in turn, will result in a proportionally between both parameters and the crack spacing. Therefore, the crack spacing can be described just as well by one of the parameters instead of both of them. This issue is also discussed in the parameter study of the combined bond-slip and no-slip models in Section 2.2.3 where the ϕ_s/ρ_s -term was seen to approximate a straight line instead of a parabola because a realistic interval for cover is not sufficiently large to provoke a non-linear variation.

The issue discussed above could be the reason that the two rather conflicting approaches; the bond-slip and the no-slip, both still exist and both give good results when validated against smaller test series.

2. Due to the fact that all the reviewed existing models hold either a cover-term or ϕ_s/ρ_s -term, they all agree fairly well with the test results of the database. When appointing the best model it therefore becomes a matter of which model has the most accurate empirical coefficients resulting in a mean value of $S_{rm,test}/S_{rm,model}$ closest to 1 and the smallest relative deviation, rather than which of the parameters are included. This is found to be Beeby's model: $S_{rm,sec} = 1.33(3.05c)$ with $c_v = 0.25$ and $\mu = 0.85$.

The Eurocode and the Model Code also both give good results with respect to a small deviation from the mean, but they greatly overestimate the crack spacing compared to the test results, with means values $S_{rm,test}/S_{rm,model}$ of $\mu = 0.52$ and $\mu = 0.71$.

All the models that contain a bond-slip-term (MPN, MC2010, EC2 and TCM) vary inaccurately with respect to the ϕ_s/ρ_s -ratio. For small ratios, the models overestimate the crack spacing compared to the test result and underestimate slightly for large ϕ_s/ρ_s -ratios. It thus seems as though the models

overestimate the influence of ϕ_s/ρ_s . Accordingly, the coefficient of the ϕ_s/ρ_s -term is too large. When the linear regression model determined in the chapter, with a lower coefficient of the ϕ_s/ρ_s -term, is compared to the test, the weakness with respect to variation in ϕ_s/ρ_s is eliminated. This regression model is: $S_{rm} = 1.98c + 0.075\phi_s/\rho_s$. Meanwhile, the Eurocode expression is: $S_{rm} = 2.26c + 0.23\phi_s/\rho_s$

3. The relations between the extreme and mean crack spacing for the tensile tests are $S_{rm} = 1.51S_{rmin}$ and $S_{rmax} = 2.12S_{rmin}$ which are fairly close to the results from the existing literature of $S_{rm} = 1.33S_{rmin}$ and $S_{rmax} = 2S_{rmin}$.

The minimum crack spacing is observed to deviate more from the mean than the maximum crack spacing for the members in the database. Consequently, the maximum crack spacing appears a better basis for estimating crack widths. From a physical point of view, this makes sense as it is the maximum crack spacing that yields the maximum crack width.

4.7.2 Flexural members

The aim of the empirical study of the flexural members was to answer the following questions:

1. Which parameters control the crack spacing? Furthermore, do the beams, characterised as laboratory beams and structural beams, behave in the same manner or does different behaviour apply?
2. Which existing models are able to estimate crack spacings most accurately?
3. What are the relations between extreme and mean crack spacings?
4. Can a stabilised crack system be identified with respect to a stress level?

The main results and conclusions from the analysis of the database holding crack spacing measurements of 462 beams are summarised below separated into two parts; primary cracks and secondary cracks.

Generally, with respect to the analysis of the flexural members, the results are clearer for the structural beams compared to the laboratory beams.

Primary cracks

1. Parameters of influence:

- Laboratory beams $50mm \leq d < 300mm$

It is observed that the primary cracks did not extend to mid-height in all the beams in the database which results greater scattering and uncertainties for the primary crack spacings in laboratory beams compared to the structural beams.

The crack spacing in the laboratory beams is not proportional to d and therefore the relative crack spacing S_{rm}/d is not normally distributed. Instead, the crack spacing is primarily dependent on the bond-parameter, $\phi_s/\rho_s / \phi_s/\rho_{s,eff}$, as well as the vertical cover having a smaller influence. Taking this finding into consideration and the fact that the beams' effective depths are smaller than $300mm$, it makes sense to assume that the concentrated tensile reinforcement also acts as distributed reinforcement and that cracking in laboratory beams is therefore not affected by lack of distributed reinforcement.

The stress level in the reinforcement also shows significant influence on the crack spacing, although the level of significance decreases when beams with $\sigma_{sPic} \leq 250MPa$ are excluded. However, the parameter does not become totally insignificant.

A model holding the three parameters ϕ_s/ρ_s , σ_{sPic} and c_{ver} is able to describe 62% of the variation in the primary crack spacing in laboratory beams but with a constant term of large significance, indicating a high level of random scatter in the data.

- Structural beams $300mm \leq d \leq 2000mm$

The primary crack spacing in the structural beams shows proportionality to the effective depth, d , and the relative mean crack spacing S_{rm}/d is normally distributed. Parameters of secondary influence are the horizontal cover, c_{hor} and the beam width, b . No physical explanation is found for the influence of these parameters other than the fact that they are needed to describe the distance to the closest reinforcement from a position on the side face of a beam.

A linear regression model holding the parameter d alone describes 85% of the variation in the crack spacing without the need for a constant term; $S_{rm,fl} = 0.42d$

The stress level in the reinforcement is not a parameter of influence on the primary crack spacing in the structural beam as it is in the laboratory beams.

The above conclusions regarding which parameters influence the primary crack spacing in the structural beams also rule out the influence of all the other investigated parameters, which are: $\phi_s, n_s, \rho_s, f_{c,cyl}, \sigma_{sPic}, M_{Pic}/M_y, a, a/d$.

From the above evidence it can be concluded that the laboratory and structural beams do not behave in the same way with respect to development of primary cracks. The main reason for this is that only one type of crack forms in the laboratory beams and these are primarily controlled by the bond-parameter, not the size of the member.

2. Performance of existing models:

- Laboratory beams $50mm \leq d < 300mm$

Because the cracks at mid-height in the laboratory beams are controlled by the same parameters as the secondary cracks, none of the existing models for estimating crack spacing at mid-height agree well with the test.

- Structural beams $300mm \leq d \leq 2000mm$

All four models (Reineck, Hamadi, EC2, and Frosch) give good results when comparing them to the tests. This confirms that the crack spacing is primarily dependent on d , as all the models include this parameter or a parameter related to it. The most simple model, which is Hamadi's: $S_{rm} = 0.5d$, is the model with the most accurate results with respect to the smallest relative deviation from the mean of $S_{rm,test}/S_{rm,model}$ of 23% and a mean value of 0.90, which is slightly conservative. The Eurocode, on the other hand, estimates the crack spacings too conservatively, with a mean value of 0.65 for $S_{rm,test}/S_{rm,model}$.

3. Relations between extreme and mean crack spacings:

- The same results apply for the laboratory and the structural beams:

There is a fairly large variation in the results for the ratios S_{rmax}/S_{rmin} and S_{rm}/S_{rmin} and they are not normally distributed. The maximum spacing S_{rm}/S_{rmax} shows more stable results with smaller variation and the ratio S_{rm}/S_{rmax} is normally distributed.

The mean values of both the S_{rmax}/S_{rmin} and S_{rm}/S_{rmin} are larger than what was expected from the literature review. However, the bins in the distribution plots holding the largest number of tests coincide with the mean values referred to in the existing literature, which is the same as for tensile members; $S_{rmax} = 2S_{rmin}$ and $S_{rm} = 1.33S_{rmin}$. Furthermore, the mean value of S_{rm}/S_{rmax} corresponds to the ratio found in the existing literature. The results therefore indicate that the maximum crack spacing should be used as the basis for estimating crack widths, instead of the minimum spacing.

4. Stabilised crack pattern:

- The results of the single test series presented in Chapter 3 indicate that the primary crack spacing stabilises at stress levels in the reinforcement not much higher than the stress level at first cracking. This result is most pronounced for the structural beams.

Secondary cracks

1. Parameters of influence:

The two parameters, cover and ϕ_s/ρ_s , which, in existing models, are said to be of influence on the secondary crack spacing level, are highly correlated for the data in the database. As for tensile members, this makes it more difficult to interpret the results and it also leaves some uncertainties as to whether both of the parameters really have influence on the crack spacing or if they are more or less always correlated.

- Laboratory beams $50mm \leq d < 300mm$

The two parameters that show statistical significance are the same as for the primary crack spacing in the laboratory beams, namely the ϕ_s/ρ_s -ratio and σ_{sPic} . The regression model found for beams with $\sigma_{sPic} \geq 250MPa$ is; $S_{rm,sec} = 55.2 + 0.034\phi_s/\rho_s$. The model describes 66% of the variation in the crack spacing, which is quite good, but the constant term is of great significance, which means that there is either a large scatter in the result or a parameter is missing to describe the rest of the variation.

None of the reviewed existing models' parameters, which hold the effective reinforcement ratio, are able to describe more of the variation, however, the Eurocode's parameters $\phi_s/\rho_{eff,EC}$ and c_{ver} and Leonhardt's with the same parameters with the inclusion of σ_{sPic} describe the crack spacing variation most accurately.

- Structural beams $300mm \leq d \leq 2000mm$

The parameters that show influence on the crack spacing for the structural beams are ϕ_s/ρ_s , c_{ver} and $n_s\phi_s$ which are the same parameters as for the tensile members. The found regression model is: $S_{rm,sec} = -14.6 + 0.36n_s\phi_s + 1.76c_{ver} + 0.02\phi_s/\rho_s$, which describes 83% of the variation in the crack spacing with an insignificant constant term, making the linear regression model a very good fit with the observed data.

As for the tensile members, the cover and the ϕ_s/ρ_s -ratio describe the variation in the crack spacing. When a regression model is created holding just one of the parameters, almost the same percentage of variation is described due to the correlation between the two parameters.

Referring to the parameter study in the literature review of the Eurocode model in Section 2.3.3, it seems that the variation of the cover-term and the ϕ_s/ρ_s -term is not noticeably different because they are both approximately two straight lines with respect to variation of the cover.

This issue was also introduced for the tensile members and is identified as a possible reason as to why the two conflicting approaches; the bond-slip and the no-slip, both give good results when validated against smaller test series in the existing literature and why a general consensus does not exist with regard to the two theories and the influence of the two parameters, cover and ϕ_s/ρ_s on the crack spacings.

When using the Eurocode parameters to describe the variation in the crack spacing, the most accurate model is using the maximum cover instead of the vertical cover. When this is the case, the $\phi_s/\rho_{s,effEC2}$ -ratio becomes insignificant.

What seems to confuse the above results is that in a notable number of tests in the database the horizontal and vertical cover are not the same, even though one could argue that the two covers should be the same due to that fact that the same durability requirements apply in both directions. A regression analysis is made from the beams where the vertical cover and the horizontal cover are approximately equal, thus $c_{max} = c_{ver} = c_{hor}$. In this case, the cover is the only significant parameter, and is able to describe 79% of the variation in crack spacing for the structural beams. The model is found to be; $S_{rm,sec} = 4.16 + 3.20c$.

2. Performance of existing models:

For both the laboratory and structural beams it applies that the Tension Chord Model, with only a $\phi_s/\rho_{s,eff}$ -term and Frosch's model with only a cover-term, are the most inaccurate estimates for the secondary crack spacing. This leaves the Eurocode and the Model Code which are similar and agree quite well with the test results.

When that maximum cover is used, the Eurocode yields the best estimate both for structural and laboratory beams. It could be argued that in real structural beams, there is no difference between the horizontal and vertical cover and thus which cover to use would not be an issue. Nevertheless, a large proportion of the tests found in the literature had different covers in the two directions.

- Laboratory beams $50mm \leq d < 300mm$

The secondary crack spacing in the laboratory beam is affected by the stress level in the reinforcement. When beams with stress levels less than $250MPa$ are excluded, the Eurocode estimates the maximum crack spacings with good precision. The mean value of $S_{rm,test}/S_{rm,model}$ is 1.04, however, the relative deviation from the mean is quite high; $c_v = 0.39$.

- Structural beams $300mm \leq d \leq 2000mm$

The Eurocode model is a better estimate for the crack spacing in the structural beam than for the laboratory beams. Here, the mean value of $S_{rm,test}/S_{rm,model}$ is the same ($\mu = 1.04$) but the deviation is less; $c_v = 0.33$.

The Eurocode shows weakness with respect to variation of the $\phi_s/\rho_{s,eff}$ -ratio, as it did for the tensile members. For small ratios of $\phi_s/\rho_{s,eff}$, the crack spacing is underestimated and for large ratios it is overestimated. This is eliminated if the regression model, found in the chapter, is applied. In the regression model for the structural beams, the coefficient for the ϕ_s/ρ_s -ratio is smaller than in the Eurocode and a $n_s\phi_s$ -term is added; $S_{rm,sec} = -14.60.36n_s\phi_s + 1.763c_{ver} + 0.020\phi_s/\rho_s$.

3. Relations between extreme and mean crack spacings:

- The same results apply for the laboratory and the structural beams. Neither the mean values nor the largest bins for the distributions of S_{rmax}/S_{rmin} , S_{rm}/S_{rmin} , and S_{rm}/S_{rmax} are consistent with the existing theory when all the beams in the database are included in the investigation. However, if only crack spacings in the constant moment span of the beams are included, the result are more or less the same as for the primary cracks in beams. The mean values of S_{rmax}/S_{rmin} , S_{rm}/S_{rmin} , and S_{rm}/S_{rmax} are larger than those found in the literature, but the bins with largest number of beams are located at values found in the literature. The smallest deviation from the mean value is again found for the maximum spacing, S_{rm}/S_{rmax} .

4. Stabilised crack pattern:

- The results are again from a single test series presented in Chapter 3. The secondary crack spacing has a tendency of to stabilise before yielding, for the structural beams, while new cracks keep forming up until yielding in the laboratory beams.

It has not been possible to establish a stress level regarding which the secondary crack spacing was stable and it is concluded that this might not exist and that instead, a stable crack spacing is dependent on other parameters than just the stress in the reinforcement. The main reason for the conclusion being that the stress level at first cracking depends on the reinforcement ratio.

4.7.3 Tension and flexural members

The investigations show that there is a direct connection between the crack spacing in tensile members and secondary crack spacing in the flexural members because both can be described from the same two parameters; cover and ϕ_s/ρ_s -ratio.

However, the empirical coefficients are slightly different for the two different structural members. The Eurocode suggests that the difference should be a reduction in the coefficient of the ϕ_s/ρ_s -term from tensile members to the $\phi_s/\rho_{s,eff}$ -term for flexural members. This, however, means that a beam with the same cover and $\phi_s/\rho_{s,eff}$ -ratio as a tension bar has a smaller crack spacing than the tension bar, which is not seen in the comparison. Instead it was concluded that while the influence of the $\phi_s/\rho_{s,eff}$ -term should be reduced in flexural members compared to tensile members, the influence of the cover-term should be increased simultaneously. Moreover, from the comparison, there was no indication that the $\phi_s/\rho_{s,eff}$ should be reduced as much as the Eurocode dictates.

5 THE APPROACH FOR ESTIMATION OF CRACK WIDTHS, STIFFNESS, AND DEFLECTION IN FLEXURAL MEMBERS

In the following chapter an approach is proposed to estimate all the important aspects of the serviceability limit state. The approach is developed from one requirement; that all aspects, namely flexural stiffness, deflection and crack widths, can be estimated from coherent physical considerations of how flexural members behave. This requirement resulted in an approach based on knowledge of one single parameter, i.e. the crack spacing. The hypothesis investigated and accepted in the Introduction in Chapter 1 forms the basis for the development of the approach.

The following chapter includes research already published by the author of this thesis with both some paragraphs that are directly reused text and some paragraphs that are re-phrased. Firstly, Sections 5.1–5.3, concerning the approach to estimate crack widths with the use of the crack spacing, are a summary of [48] but with some modifications to the approach. Secondly, Section 5.4, regarding the proposed approach for estimation of the flexural stiffness including tension-stiffening from the knowledge of the crack spacing and crack width, is from [161] and [71] with some rewrites of the model formulations. Lastly, Section 5.6, relating to the use of the flexural stiffness on statically indeterminate beams is from [69].

The approach is exemplified for the case of a simply supported beam subjected to four-point-bending, as illustrated in Fig. 5.1a. It involves five steps: 1) identification of the system of cracks and estimation of crack spacings, 2) estimation of reinforcement strains, 3) prediction of crack widths from summation of reinforcement strains, 4) estimation of the flexural stiffness from crack spacing and crack width, and 5) deflection analysis with the use of the flexural stiffness.

5.1 Identification of the system of cracks

The crack pattern is assumed to be a combination of the two previously described crack systems; the primary flexural cracks and the local secondary cracks. The two different crack systems should be considered whenever the effective depth of the beam is larger than 300mm and when distributed reinforcement is not sufficient to control crack development in the web of the member.

In the empirical study, in Chapter 4, it was found that beams with a smaller depth than 300mm only develop one system of cracks, which is controlled by parameters of secondary cracking, even though they penetrate to the height of the neutral axis. In these beams, called laboratory beams, the crack spacing is thus $S_{fl} = S_{sec}$. An example of the crack pattern for these beams is given in Fig. 5.1a. The figure also shows a numbering of the primary cracks; $n = [1; N_{fl}]$, where N_{fl} is the total number of primary cracks along the span. The primary cracks are assumed to propagate from the surface of the tensile zone to the neutral axis, being vertical from the surface to the location of the longitudinal reinforcement and continuing with a constant inclination, γ . The inclination of the crack located in the constant moment span is zero while, as a simplification, all other cracks are assumed to have an inclination of $\gamma = 30$ deg [162]. This is a simplified assumption because the inclination of the cracks in the shear span would, in reality, vary, and there would be a transition zone from the constant moment span to the shear span with gradually increasing inclination of the cracks instead of an abrupt change, as illustrated in Fig. 5.1a.

In the beams where $d \geq 300\text{mm}$, the spacing of the primary cracks is proportional to the member depth, as also concluded in Chapter 4. Whether or not secondary cracks occur in these beams, called structural beams, depends on the spacing of the primary cracks. If the primary crack spacing is sufficiently large for

From equilibrium considerations in the cracked cross-section, shown in Fig. 5.3, the bending moment can be described from the force in the reinforcement and the inner lever arm:

$$M(x) = A_s \epsilon_{sc} E_s \left(d - \frac{1}{3} x_{cr} \right) \quad (5.2)$$

From this expression for the bending moment, the strain in the reinforcement in the n 'th primary crack can be deduced:

$$\epsilon_{sc,n} = \frac{3M(x_n)}{E_s A_s d (3 - \beta)} \quad (5.3)$$

where $M(x_n)$ is the moment at the location of the n 'th primary crack and the coefficient of the neutral axis is $\beta = \frac{x_{cr}}{d}$.

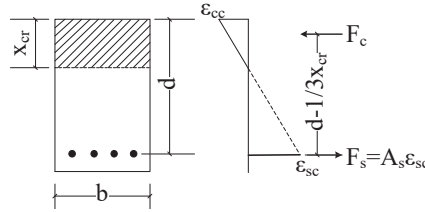


Figure 5.3: Fully cracked reinforced concrete section with elastic strain distribution

The strain in the reinforcement varies both due to the variation in the moment and due to the transfer of stresses from the reinforcement to the concrete between cracks as illustrated in the bottom of Figs. 5.2a and 5.2b. The principal rate of variation in strain, ξ , is determined from the variation of the bending moment between two cracks:

$$\xi = \frac{3\Delta M}{E_s A_s d (3 - \beta)} = \frac{\Delta \epsilon_{sc}}{S_{fl}} = \frac{\epsilon_{sc,n-1} - \epsilon_{sc,n}}{S_{fl}} \quad (5.4)$$

where ΔM and $\Delta \epsilon_{sc}$ are the differences between the moment and the strain, respectively, in one primary crack to the next crack.

The secondary rate of variation in the strain, η , is determined by the strength of the bond. Hence, the rate of change due to constant bond stresses becomes:

$$\eta = \frac{n_s \phi_s \pi \tau_b}{A_s E_s} = \frac{4\tau_b}{\phi_s E_s} \quad (5.5)$$

where the size of the bond stresses in the elastic stage is assumed to be twice the size of the tensile strength of the concrete:

$$\tau_b = 2f_{ct} = 2\sqrt{0.1f_c} \quad (5.6)$$

The tensile strength is estimated from the Eq. (2.3), in Chapter 2, for members subjected to mixed curing conditions.

The estimate for the bond stresses is similar to the expression proposed in the Tension Chord Model in Eq. (2.12). The only difference is that a more conservative estimate for the tensile strength of the concrete is used in the present estimate, while the Tension Chord Model uses the expression in Eq. (2.2) which, in general, yields higher tensile strengths.

The crack spacings are denoted S_{sec} and S_{fl} in Fig. 5.2 without specifying whether it is the minimum, maximum or mean spacing, because the choice depends on what the strain distribution between cracks is used for. This will be elaborated in the following sections; however, in brief, the maximum crack spacing,

$S_{rmax,sec}$ and $S_{rmax,fl}$, are essentially used to estimate the maximum crack width appearing in a member for control of cracking. On the other hand, the mean crack spacing, $S_{rm,sec}$ and $S_{rm,fl}$, will be used to incorporate the effect of cracking on the flexural stiffness and deflection.

5.3 Estimation of crack widths

From the knowledge of the variation of the strain in the reinforcement, the width of cracks can be determined as the sum of slip from both sides of the considered crack. The concrete strains are assumed to be minor and therefore omitted. This assumption is supported by the conclusion to the investigation of the initial hypothesis in Chapter 1, where it was accepted that deformations can be assumed to occur solely in the cracks.

When primary cracks occur alone, their crack width at the level of the reinforcement can be determined from the integration of strains over the length of $1/2S_{fl}$ on both sides of a crack. This corresponds to the sum of the grey shaded areas in Fig. 5.2a:

$$w_{fl,d} = \sum_{i=1}^4 A_n \quad (5.7)$$

When secondary cracks are present, the width of the primary cracks will be decreased at the level of the reinforcement compared to a beam with no secondary cracks. When moving away from the tensile reinforcement, towards the web, the secondary cracks will close and from considerations of compatibility it must be reasonable to assume that the width of the primary cracks will increase accordingly. This was supported with the test results in Chapter 3 where the shape of a primary crack in the beams with $h = 300mm$ were found to be wedge-shaped while the primary cracks in the beams with $h = 600mm$ were fish-shaped due to the appearance of secondary cracks.

In beams where secondary cracks occur, the width of the n 'th primary crack at the level of the reinforcement can still be evaluated using Eq. (5.7). However, the sub-areas $A_1 - A_4$ will now be located as illustrated in Fig. 5.2b.

For the specific case considered in Fig. 5.2b, where two secondary cracks have formed in-between the primary cracks, the maximum primary crack width, occurring in the web, can be estimated as:

$$w_{fl,w} = \sum_{i=1}^{12} A_n \quad (5.8)$$

where the areas A_1 to A_{12} are all the grey shaded areas in Fig. 5.2b.

5.4 Estimation of flexural stiffness

In practical designs of the serviceability limit state, the effect of tension-stiffening is often handled empirically or totally ignored by using the conservative estimate of a fully cracked concrete section. Here, a simple, yet physical, approach is proposed for how to include the tension-stiffening effect in flexural stiffness and deflection estimations.

It is known from the literature review in Chapter 2, that the tension-stiffening has the greatest effect on beams and slabs of small reinforcement ratios. After the approach is presented it will be investigated whether the proposed model can confirm this. Furthermore, the effect of tension-stiffening in statically indeterminate beams is investigated. This investigation seeks to clarify whether the large effect of tension-stiffening on beams with low reinforcement ratios affects the distribution of the moment if the flexural member is reinforced differently in the top and bottom.

5.4.1 The effect of tension-stiffening

The flexural stiffness contribution due to tension-stiffening is assumed to be dependent on the crack spacing, simply because the intact concrete between cracks is the material contributing to a higher stiffness. The crack spacing thus provides information about how much coherent concrete there is between cracks. The further apart the cracks are spaced, the more stress can be transferred from the reinforcement to the concrete, and the more the concrete can contribute to a larger stiffness. An increase in crack spacing will therefore result in an increase in flexural stiffness, resulting in a decrease in the total deformation of a beam.

5.4.2 Flexural stiffness

In the following section, the proposed approach for including tension-stiffening in the flexural stiffness, is described. A similar description is found in [161] and [71] with one difference; that the current approach include the effect of a debonded length adjacent to and on each side of the cracks.

Flexural stiffness excluding tension-stiffening

Firstly, the stiffness of a fully cracked cross-section neglecting tension-stiffening, EI_{cr} , is found from equilibrium based on an elastic stress distribution and the fact that $EI = M\kappa$:

$$EI_{cr} = \frac{1}{3}A_sE_sbd^2(3 - \beta)(1 - \beta) \quad (5.9)$$

With a height of the elastic compression zone expressed by:

$$x_{cr} = \beta d = \alpha\rho_s \left(\sqrt{1 + \frac{2}{\alpha\rho_s}} - 1 \right) \quad (5.10)$$

Flexural stiffness including tension-stiffening

The expression for the flexural stiffness including the effect of tension-stiffening, $EI_{cr,ef}$ is found through the following geometrical relations which were also described in the initial hypothesis in Chapter 1.

At a primary crack, the curvature, κ , can be described from the mean strain in the reinforcement, the crack width at the reinforcement, w , and the secondary crack spacing:

$$\epsilon_{sm} = \frac{w}{S_{rm}} \quad (5.11)$$

$$\kappa = \frac{\epsilon_{sm}}{d - x_{cr}} \quad (5.12)$$

$$\Rightarrow \kappa = \frac{w}{S_{rm}(d - x_{cr})} \quad (5.13)$$

The above relations apply for beams both with and without secondary cracks in-between the primary cracks. The reason why the spacing between the secondary cracks, $S_{rm,sec}$, is used to find the curvature for both situations, is that in the beams without secondary cracks, the primary crack spacing is equal to the secondary crack spacing (if $2S_{rm,sec} > S_{rm,fl} \Rightarrow S_{rm,sec} = S_{rm,fl}$). Furthermore, the above relations should be considered as a smeared description of the deformation. For beams with fish-shaped cracks, the expression for the strain in a crack in Eq. (5.11) holds due to findings in the investigation of the sum of crack widths in Chapter 3, where it was discovered that the sum of cracks for beams both with and without secondary cracks is wedge-shaped with the largest crack width, causing the curvature, at the tensile face or which can be approximated by the location of the reinforcement. Therefore, the following applies for all beams, with respect to Eq. (5.11):

$$\epsilon_{sm} = \frac{\sum w}{L} \Rightarrow \epsilon_{sm} = \frac{w_m}{S_{rm,sec}} \quad (5.14)$$

where L is the total length of the beam, $\sum w$ is sum of cracks over the whole length of the beam and w_m is the mean crack width.

The curvature, found in Eq. (5.13) is proportional to the moment through the following constitutive formulation:

$$\kappa(x) = \frac{M(x)}{EI_{cr,ef}(x)} \quad (5.15)$$

When combining Eq. (5.13) and (5.15), an expression for the stiffness, dependent on the crack width, w , and the size of the moment, is found:

$$EI_{cr,ef}(x) = \frac{M(x)(d - x_{cr})S_{rm,sec}}{w(x)} \quad (5.16)$$

where $w(x)$ is replaced by the crack width at the level of the reinforcement, $w_{fl,d}(x)$ as found earlier in Eq. (5.7):

$$w_{fl,d}(x) = A_1 + A_2 + A_3 + A_4 \quad (5.17)$$

When the principal rate of variation in strain, ξ , is continuous, the size of the areas A_1 to A_4 in Fig. 5.2 becomes independent on ξ and only dependent on the strain in the crack, ϵ_{sc} , and the secondary rate of variation, η . The crack width can thus be expressed by:

$$w_{fl,d}(x) = \epsilon_{sc}(x)S_{rm,sec} - \frac{\tau_b}{\phi_s E_s} (S_{rm,sec} - 2L_{deb})^2 \quad (5.18)$$

where the strain in the crack is found earlier as:

$$\epsilon_{sc}(x) = \frac{3M(x)}{E_s A_s d(3 - \beta)} \quad (5.19)$$

Again, the expression in Eq. (5.18) for the crack width is the same for beams with and without secondary cracking because in the beams with no secondary cracking the following applies; $S_{fl} = S_{sec}$.

The final expression for the flexural stiffness can be deduced by inserting Eqs. (5.19) and (5.18) into Eq. (5.16):

$$EI_{cr,ef}(x) = \frac{M(x)EI_{cr}}{M(x) - k_t} \quad (5.20)$$

where k_t is defined as the tension-stiffening coefficient dependent on the crack spacing:

$$k_t = \frac{1}{3} \tau_b \frac{(S_{rm,sec} - 2L_{deb})^2}{\phi_s S_{rm,sec}} A_s d (3 - \beta) \quad (5.21)$$

Eq. (5.20) is only valid for $k_t \leq M(x) \leq M_y$. For a moment smaller than k_t , the stiffness of an uncracked section applies: EI_{uncr} .

The stiffness estimated from Eq. (5.20) is dependent on the size of the moment, which is dependent on the location, x , in a beam. The stiffness thus varies in the length of a beam depending on the type of loading and static system of a beam.

5.4.3 Smearred flexural stiffness including tension-stiffening

In the following section, it is briefly explained how the variable stiffness, $EI_{cr,ef}(x)$, with respect to $M(x)$, is transformed into a smeared mean stiffness unique for a certain type of loading and static system. The mean stiffness is denoted $EI_{cr,ef}$.

The principle of virtual work is used to find the deflection, by applying a virtual unit load at the location of maximum deflection from the real applied load. The deflection can be found from:

$$u = \int_0^L \frac{M_v(x)M(x)}{EI(x)} dx \quad (5.22)$$

where $M_v(x)$ is the function for the virtual moment and $M(x)$ is the function of the applied moment.

The deflection is found with this method for two different scenarios:

1. A beam with a constant stiffness, $EI_{cr,ef}$
2. A beam with a variable stiffness like in Eq. (5.20), $EI_{cr,ef}(x)$

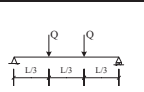
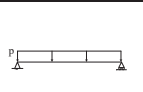
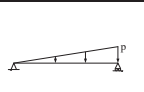
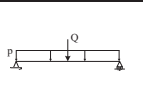
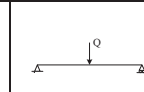
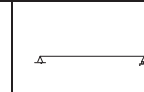
The two expressions from the scenarios are equalled to each other and the mean stiffness $EI_{cr,ef}$ is deduced. An example of the deduction of the smeared stiffness of a beam subjected to four-point-bending is shown in [71].

The table on the following page provides a summary of the different types of loading this procedure is carried out for in [71]. The table lists two different options for the relations between the fully cracked stiffness, EI_{cr} and the stiffness including tension-stiffening, $EI_{cr,ef}$. For the stiffness relations $EI_{cr}/EI_{cr,ef,coarse}$, a coarse assumption is made with respect to the stiffness variation in the beam. It is assumed that when the cracking moment, M_{cr} , is reached at one location in the beam, the whole beam is cracked. This means that the expression for the stiffness including tension-stiffening is used in the whole length of the beam the instant the maximum moment in the beam has reached the cracking moment.

For the other stiffness relations, $EI_{cr}/EI_{cr,ef,fine}$, a more precise assumption is made. Here, the cracked stiffness including tension-stiffening is only applied in the areas of the beam where the moment is larger than M_{cr} , while the stiffness of an uncracked section, EI_{uncr} , is used in the rest of the beam.

In Fig. 5.4 the variation of the stiffness relations $EI_{cr}/EI_{cr,ef}$ with respect to the moment utilisation is illustrated for two different reinforcement ratios and two different static systems. The plot in Fig. 5.4a shows the variation of the stiffness relations for a beam with a low reinforcement ratio of 0.3% for both three- and four-point-bending while 5.4b illustrates the same but for a medium-size reinforcement ratio of 1.2%. The plots demonstrate how, with increasing moment, the stiffness approaches that of a fully cracked member, EI_{cr} . However, in the interval from the cracking moment, M_{cr} , until the reinforcement reaches yielding, the stiffness varies significantly. The following can be observed from the theoretical curves:

- The influence of tension-stiffening decreases with the increase of reinforcement ratio.

Static system							
M_{max}	M_0	$\frac{1}{3}Ql$	$\frac{1}{8}pl^2$	$0.0641pl^2$ ($M_{max} = M_{(0.577l)}$)	$\frac{1}{8}pl^2 + \frac{1}{4}Ql$	$\frac{1}{4}Ql$	M_0
u_{max}	$\frac{1}{8} \frac{M_0 l^2}{EI}$	$\frac{23}{648} \frac{Ql^3}{EI}$	$\frac{5}{384} \frac{pl^4}{EI}$	$0.00652 \frac{pl^4}{EI}$ ($u_{max} = u_{(0.519l)}$)	$\frac{1}{48} \frac{Ql^3}{EI} + \frac{5}{384} \frac{pl^4}{EI}$	$\frac{1}{48} \frac{Ql^3}{EI}$	$\frac{1}{9\sqrt{3}} \frac{M_0 l^2}{EI}$ ($u_{max} = u_{(0.577l)}$)
$\frac{EI_{cr}}{EI_{cr,ef,coarse}}$ (Cracks occur in the whole length)	$1 - \frac{k_t}{M_0}$	$1 - \frac{27k_t}{23M_{max}}$	$1 - \frac{6k_t}{5M_{max}}$	$1 - \frac{1.228k_t}{M_{max}}$	$1 - \frac{k_t(12Q + 6pl)}{M_{max}(8Q + 5pl)}$	$1 - \frac{3k_t}{2M_{max}}$	$1 - \frac{1.902k_t}{M_0}$
$\frac{EI_{cr}}{EI_{cr,ef,fine}}$ (Uncracked areas taken into account)	$1 - \frac{k_t}{M_0}$	$1 - \frac{27k_t}{23M_{max}} - \frac{23M_{max}^3}{8M_{cr}^3} + \frac{8M_{cr}^3 EI_{cr}}{23M_{max}^3 EI_{uncr}} + \frac{12k_t M_{cr}^2}{23M_{max}^3}$				$1 - \frac{3k_t}{2M_{max}} - \frac{M_{cr}^3}{M_{max}^3} + \frac{M_{cr}^3 EI_{cr}}{M_{max}^3 EI_{uncr}} + \frac{3k_t M_{cr}^2}{2M_{max}^3}$	

- The influence of tension-stiffening decreases with the increase in moment due to the fact that: 1) the stiffness including tension-stiffening is dependent on the size of the moment, and 2) with respect to the fine assumption for the stiffness including tension-stiffening, the stiffness decreases as a larger part of the beam becomes cracked with increase in moment.
- The simplest assumption for the estimate of the stiffness; $EI_{cr,ef,coarse}$, deviates considerably from the more complex estimate; $EI_{cr,ef,fine}$, for the small reinforcement ratio in Fig. 5.4a and load levels less than approx. 60% of the moment at yielding, M_y . On the other hand, for the reinforcement ratio of a medium size, $\rho_s = 1.2\%$ in Fig. 5.4b, the difference between the two stiffness estimates is barely visible and for load levels above 40% the two different stiffness estimates are more or less the same. Moreover, they are very close to the stiffness of a fully cracked member, EI_{cr} .
- The tension-stiffening effect is more dominating for the static system of three-point-bending than for four-point-bending. This is because, for the latter, a larger part of the length of the beam is subjected to the maximum moment. The larger the moment is and the larger part of a beam is subjected to a moment greater than M_{cr} , the smaller the tension-stiffening effect is.

In the table, the static systems are listed in the order from the system that is least affected by tension-stiffening (constant moment) to the system most affected (one end moment). Furthermore, the order also reflects the system with least difference between the two stiffness estimates $EI_{cr,ef,fine}$ and $EI_{cr,ef,coarse}$ to the system with the most difference between them.

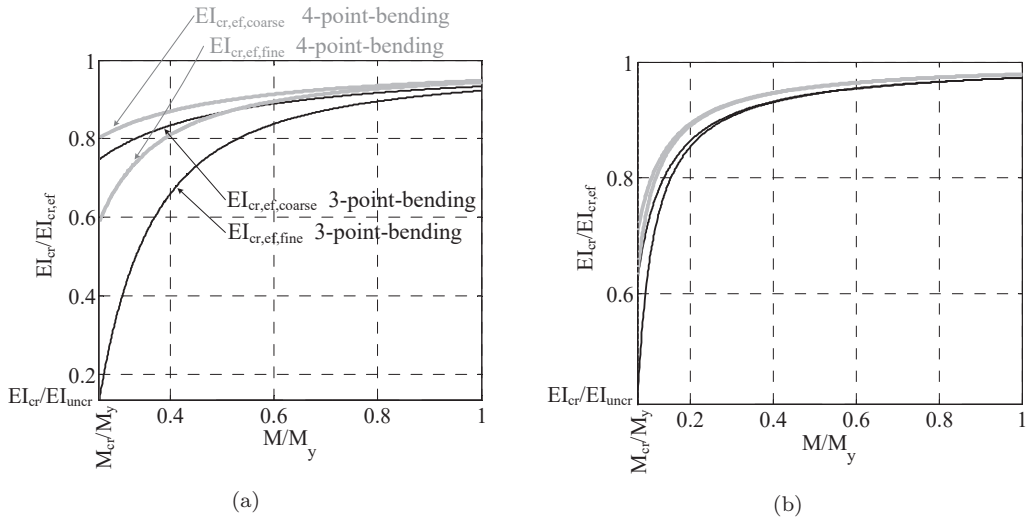


Figure 5.4: Theoretical variation of the stiffness, from cracking (M_{cr}) to yielding (M_y), for four-point-bending and three-point-bending: (a) reinforcement ratio; $\rho_s = 0.3\%$, (b) $\rho_s = 1.2\%$, reprint from [71]

5.5 Deflection analysis on the basis of the flexural stiffness

In this section, a theoretical example from [71] is used to demonstrate the use of the flexural stiffness to estimate the deflection of a beam in four-point-bending. Some characteristics of tension-stiffening effect are also illustrated. The deflection of the beam at a load of 60% of the yield load is estimated for a beam with the properties: effective depth $d = 300\text{mm}$, slenderness ratios of $a/d = 3$, $a/d = 6$, $a/d = 9$ and variable reinforcement ratio. The deflection is estimated from the expression for the stiffness from the table on the previous page and by the use of the Principle of Virtual Work.

In Fig. 5.5a the deflection including tension-stiffening effect, $u_{cr,ef}$, is plotted as a function of the reinforcement ratio with the use of two different estimates for the crack spacing, namely Reineck's estimate for the primary crack spacings and the Tension Chord Model for the secondary crack spacing. As can be seen, the size of the deflection is associated with the size of the crack spacing. As was discovered in Chapter 4, the primary crack spacing is larger than the secondary spacing, therefore the deflection calculated from the primary crack spacing is smaller than when calculated from the secondary crack spacing. Naturally, the deflection also increases with the increase in slenderness.

Fig. 5.5b shows the difference in the estimated deflection with and without the tension-stiffening effect, $u_{cr} - u_{cr,ef}$. The plot illustrates how, for the Tension Chord Model, the tension-stiffening has the largest effect on beams with small reinforcement ratios and large slenderness ratios. Meanwhile, Reineck's estimate is not affected by the reinforcement ratio, only variation of slenderness. This is due to the fact that the primary crack spacing is not dependent on the reinforcement ratio. From previous investigations of tension stiffening, described in the literature review in Chapter 2, it is known that the tension stiffening effect decreases with the increase in reinforcement ratio. Therefore, it is concluded that the secondary crack spacing is to be used when estimating flexural stiffness and deflection with the current proposed approach.

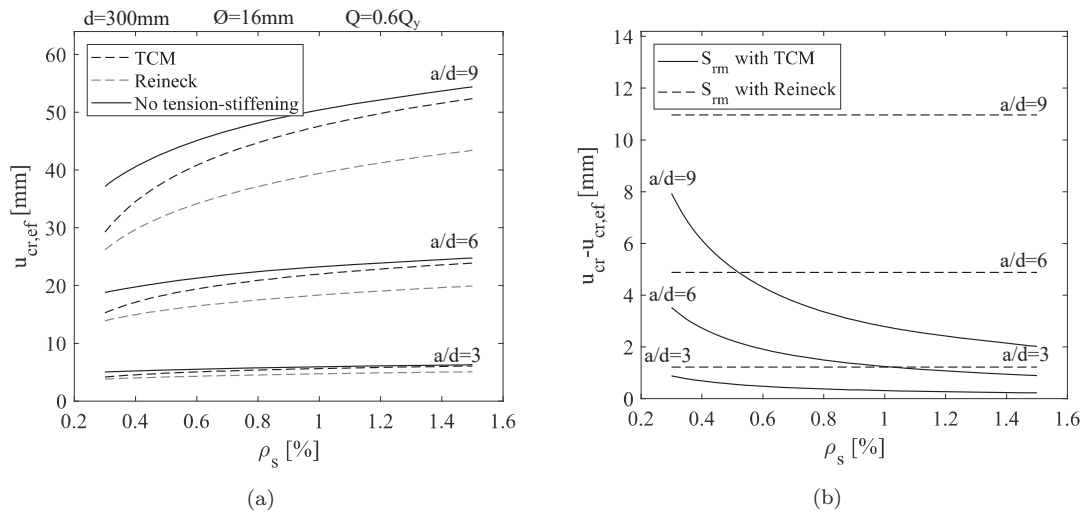


Figure 5.5: (a) Deflection with respect to reinforcement ratio for three different slenderness ratios, (b) difference between deflection with and without tension-stiffening for the TCM and Reineck's estimate, reprint from [71]

5.6 Analysis of statically indeterminate beams on the basis of the flexural stiffness

The model for estimating the flexural stiffness is applied on the statically indeterminate beam illustrated in Fig. 5.6 for determination of the redistribution of moment during service load. The redundant, in this case, the moment at the sub-support, M_B , is determined by applying the Energy Concept referred to in Section 2.4. The total elastic energy in the beam can be expressed by the internal moment times the curvature over the length of the beam. Minimisation of the elastic energy leads to the true state of equilibrium and the solution for the redundant:

$$U = \int_0^L M(x)\kappa dx = \int_0^L \frac{M(x)^2}{EI_{cr,ef}(x)} dx \quad (5.23) \quad \frac{\delta U}{\delta M_B} = 0 \quad (5.24)$$

When applying the expression for the flexural stiffness including tension-stiffening both the moment and the stiffness in the above equation becomes variable with respect to the distance to the support, x .

The above-explained procedure was used to estimate the distribution of bending moment between the moment at mid-span, M_E and the moment at the sub-support, M_B , both with and without taking tension-stiffening into account. In Fig. 5.7a-c the result is compared to tests by M. Alvarez et al. [163]. For more details on the investigation see [69].

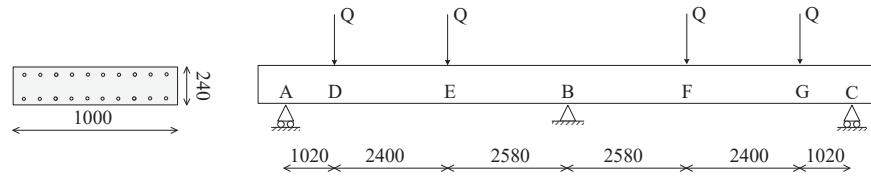


Figure 5.6: Set-up of tests by M. Alvarez et al. [163], reprint from [69]

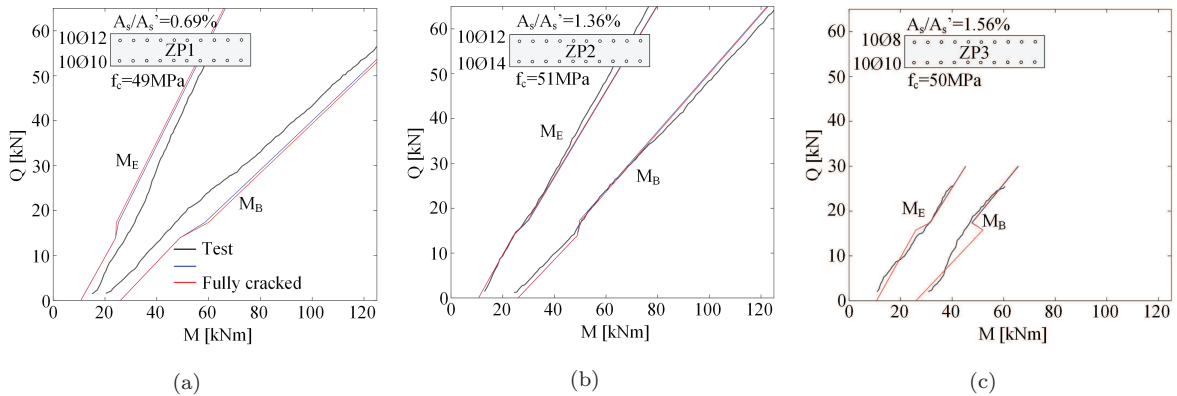


Figure 5.7: Comparison with tests by Alvarez et al. [163]: (a) Relations between applied load, Q , and moment at midspan, M_E and at support, M_B for ZP1, (b) for ZP2, (c) For ZP3, reprint from [69]

The approach for calculating the moment redistribution shows overall good agreement with the selected tests. It can be observed that the difference between the model with and without the effect of tension-stiffening is insignificant because the blue and the red lines, representing the stiffness with and without

tension-stiffening, coincides. A straightforward explanation for this could be that the effect of tension-stiffening for negative and positive moments in the beams is more or less of equal size and the effect therefore cancels out. Based on this, it can be argued that, with respect to redistribution of moment in statically indeterminate beams, the effect of tension-stiffening can, in most cases, be neglected.

A situation where tension-stiffening is of larger influence on the redistribution in the elastic phase, could be for cases where the reinforcement design causes a large difference between the top and bottom reinforcement area, A_s/A'_s . This is even more apparent if one of the reinforcement areas is close to the minimum, $\rho_{s,min}$. Hence, the difference between the effect of tension-stiffening in the top and bottom is the largest possible.

5.7 Conclusions

In this chapter an approach is proposed to estimate crack widths, flexural stiffness and deflection of flexural members in serviceability limit state from the knowledge of the crack spacing. The approach makes it possible to estimate crack widths both at the level of the reinforcement and in the web of beams as well as to estimate every crack width and not only the maximum in a beam. The flexural stiffness found from the crack spacing and crack width can be used to estimate the maximum deflection, the deflection curve and the force-deflection response.

From theoretical investigations of the expression for the flexural stiffness it was concluded that tension-stiffening is an effect that should be taken into account in beams and slabs with low reinforcement ratios and with a type of loading causing a large variation in the moment in the beam. In contrast, for beams with normal to large reinforcement ratios, the stiffness approaches that of a fully cracked section, EI_{cr} , where it is assumed that the concrete carries no tension at any point.

The flexural stiffness expression was evaluated on statically indeterminate beams to estimate the moment redistribution under service load. The method was compared to tests of lightly reinforced concrete slabs. It is concluded that the method gives results that agreed well with the test. However, there is no significant difference in the results when using the stiffness including the tension-stiffening effect and using the fully crack stiffness, EI_{cr} . The interpretation of this is that the tension-stiffening effect in the top and in the bottom of the slabs cancel each other out and that only rather extreme circumstances concerning reinforcement layout could result in a different behaviour.

6 APPLICATION OF APPROACH

This chapter concerns the application of the theory established in the previous chapter. Firstly, an overview of the approach is established where the course of action for designing flexural members in the serviceability limit state is illustrated and both possibilities and restrictions of the approach are outlined. Secondly, the approach is exemplified on a beam subjected to four-point-bending. Lastly, the approach is applied on two different test series and compared to the test results.

6.1 A coherent design of serviceability limit state

The design of flexural members in the serviceability limit state is based on the knowledge of the crack spacing and the assumption that stresses are being transferred with a constant rate from the reinforcement to the concrete between cracks. The fact that all aspects of the serviceability limit state can be estimated from the same assumptions makes this approach coherent.

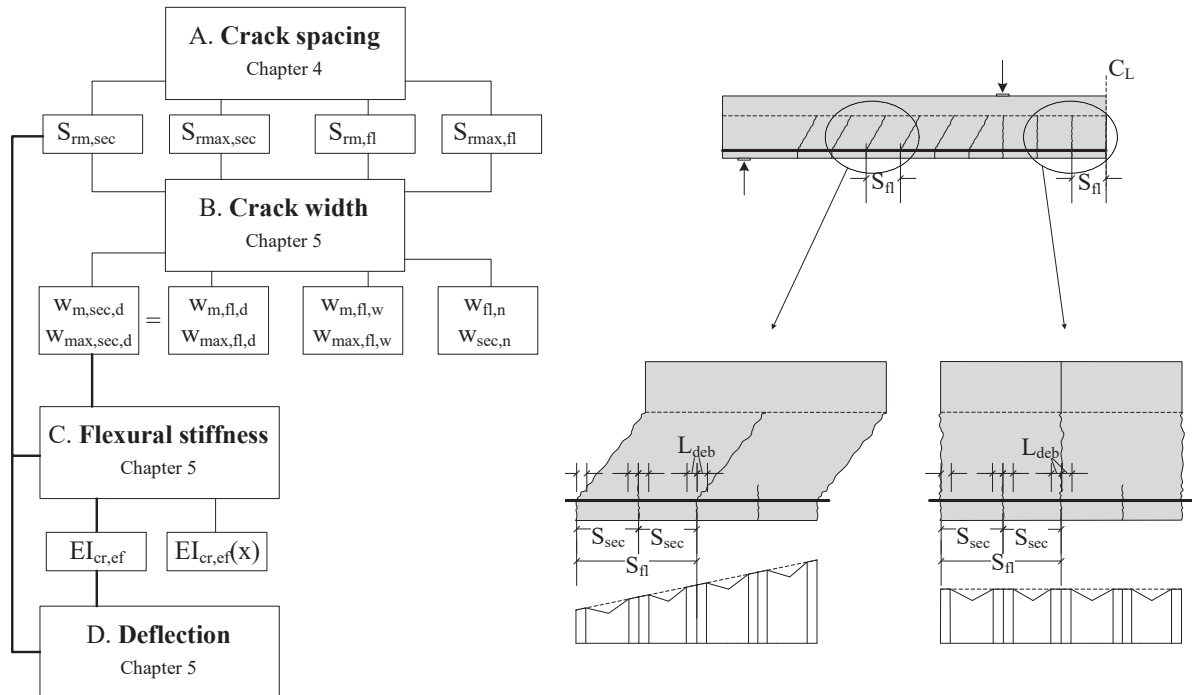


Figure 6.1: Designing flexural members in the serviceability limit state, overview of models deduced from knowledge of the crack spacing

Fig. 6.1 illustrates that, from the crack spacing both crack widths, flexural stiffness and deflection can be determined. The map in this figure encompasses the following four steps:

A: Crack spacings As explained earlier, the foundation for the approach is the crack spacing. The study of the crack spacing in Chapter 4 resulted in formulations describing the mean crack spacing of both the secondary and primary cracks, denoted $S_{rm,sec}$ and $S_{rm,fl}$. Furthermore, the results of the investigations of the relations between mean and maximum crack spacings make it possible to estimate the maximum crack spacing from the mean spacing; $S_{rmax,sec}$ and $S_{rmax,fl}$.

B: Crack widths From the knowledge of the maximum and mean crack spacing, various different crack widths can be determined. The maximum crack width is determined from the largest appearing crack spacing in a beam at the location of the maximum moment. The crack width at the level of the reinforcement is assumed to be the same in the primary and the secondary cracks, hence, $w_{max,sec,d} = w_{max,fl,d}$ and $w_{m,sec,d} = w_{m,fl,d}$. The crack width at the level of the reinforcement is estimated from the crack spacing between secondary cracks.

In the structural beams, the width of the primary cracks in the web, $w_{m,fl,w}$ and $w_{max,fl,w}$, is found from the spacing of the primary cracks. Furthermore, the approach allows us to estimate crack widths at an arbitrary location of the beam. The crack width in the n 'th crack, $w_{fl,n}$ and $w_{sec,n}$, is determined from the same spacing but with the size of the moment at that location of the n 'th crack.

C: Flexural stiffness When the secondary crack spacing, $S_{rm,sec}$, and the width of the crack at the level of the reinforcement, $w_{m,fl,d}$, are known for a particular beam, an expression for the flexural stiffness including tension-stiffening, $EI_{cr,ef}(x)$, can be deduced. Knowing the type of loading and the static system of the beam, a smeared stiffness can also be found, $EI_{cr,ef}$.

D: Deflection Ultimately, from the stiffness, $EI_{cr,ef}$, and the secondary crack spacing, $S_{rm,sec}$, the deflection can be determined.

The crack development and the crack spacings have been studied thoroughly through first the literature review in Chapter 2, secondly the test series of eight beams in Chapter 3, and, finally, the large empirical study in Chapter 4. Through these studies some guidelines can be created for the design:

A For the structural beams ($d \geq 300mm$), the size of the primary and secondary crack spacing, estimated from the regression models found in Chapter 4, settles whether secondary cracks exist. When $2S_{rm,sec} \leq S_{rm,fl}$, secondary cracks form in-between the primary cracks. In the laboratory beams ($d < 300mm$), all cracks penetrate to the web of the beam and thus $S_{rm,fl} = S_{rm,sec}$.

B For the structural beams with no distributed web reinforcement, the maximum crack width is located in the web. When sufficient web reinforcement is applied, the maximum crack width is found, at the concrete surface, at the level of the tensile reinforcement. The literature review indicated that sufficient web reinforcement has an effective reinforcement ratio larger than the well-known minimum reinforcement ratio, $\rho_{s,min}$, to ensure yielding before failure. Furthermore, a limited number of tests in the literature indicate that the spacing of the distributed reinforcement should be a maximum of $200mm$. For the laboratory beams, the maximum crack width is always found at the level of the reinforcement.

For beams with no distributed reinforcement the crack width is the same at the level of the reinforcement in the primary and secondary cracks. This applies for all depths of the beams. The reason for this is that the crack width is estimated from the crack spacing of the secondary cracks regardless. Thus $w_{m,sec,d} = w_{m,fl,d}$ and $w_{max,sec,d} = w_{max,fl,d}$.

C The flexural stiffness is particularly affected by the tension-stiffening when flexural members are lightly reinforced and have small cross-sectional depth. This is due to the fact that the tension-stiffening effect increases with increasing crack spacing and the secondary crack spacing increases with a decrease in the reinforcement ratio. The flexural stiffness is also affected by tension stiffening when there is a large variation in the moment across the length of the member. In members of small depth, with a small reinforcement ratio and a variable moment, it is thus important to include the tension-stiffening in the flexural stiffness estimate, $EI_{cr,ef}$. The further away a beam is from these three restrictions, the more the flexural stiffness approaches the stiffness of a fully cracked member, EI_{cr} .

6.2 Exemplification of approach

The process for estimating the maximum crack width, flexural stiffness and deflection in a beam subjected to four-point-bending, as shown in Fig. 6.2, is elaborated below.

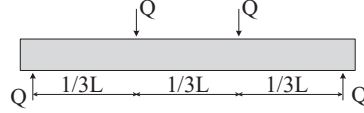


Figure 6.2: Beam in four-point-bending used for exemplification

6.2.1 Essential parameters

The following parameters are initially estimated to be applied in the approach. Their origins are described in Chapter 2 and Chapter 4:

The mean spacing of secondary cracks, Eq. (4.16) and (4.17)

Empirical Model for $d < 300mm$: $S_{rm,sec} = 55.2 + 0.034\phi_s/\rho_s$

Empirical Model for $d \geq 300mm$: $S_{rm,sec} = -14.6 + 0.36n_s\phi_s + 1.76c_{ver} + 0.02\phi_s/\rho_s$

The mean spacing of primary cracks, Eq. (4.14)

For $d < 300mm$: $S_{rm,fl} = S_{rm,sec}$

Empirical Model for $d \geq 300mm$: $S_{rm,fl} = 0.42d$

The relations between mean and maximum crack spacing, Eq. (2.28) and (2.29)

$$S_{rmax} = 1.5S_{rm}$$

The debonded length, Eq. (2.27)

$$L_{deb} = \min\left(\left(\frac{1}{2} + \frac{f_{ct}}{200\rho_{s,effSYM}}\right)\phi_s, 0.67c_{ver}\right)$$

Variation and size of bond stresses, Eq. (5.6)

Constant with respect to x , $\tau_b = 2f_{ct}$

Tensile strength of concrete, Eq. (2.3)

$$f_{ct} = \sqrt{0.1f_c}$$

Flexural tensile strength of concrete, Eq. (2.6) and (2.5)

$$f_{tb} = 1.7s(h)f_{ct} \quad s(h) = \left(\frac{h}{100}\right)^{-0.27}$$

6.2.2 Crack width

To determine a crack width, the area under the reinforcement strain curve is to be found for $1/2$ of a crack spacing to each side of the crack. This can be performed for a arbitrary crack in the beam. Below it is only reviewed for the maximum crack width in a beam in four-point-bending.

The variation in the strain in the constant moment span of a beam in four-point-bending is illustrated to the far right of Fig. 6.1. Assuming that the crack system in the beam consists of both primary and secondary cracks, the maximum crack width could occur in the web of the beam. Therefore, both the crack width at the level of the reinforcement and in the web are estimated. For the maximum crack width at the level of the reinforcement, the area under the strain curve $1/2S_{rmax,sec}$ to each side of a crack should be used. As mentioned, the widths of the primary and secondary cracks are the same at this level:

$$w_{max,d} = 2\epsilon_{sc}L_{deb} - \frac{1}{2}(\epsilon_{sc} + \epsilon_{smin})(S_{rmax,sec} - 2L_{deb}) \quad (6.1)$$

where the strain in the crack is:

$$\epsilon_{sc} = \frac{3M}{E_s A_s d (3 - \beta)} \quad (6.2)$$

while the minimum strain between two cracks is:

$$\epsilon_{smin} = \epsilon_{sc} - \eta \left(\frac{1}{2} S_{rmax,sec} - L_{deb} \right) \quad (6.3)$$

and the secondary rate of variation in the strain is:

$$\eta = \frac{4\tau_b}{\phi_s E_s} \quad (6.4)$$

Assuming that only one secondary crack forms in-between the primary cracks, the maximum crack width in the primary cracks is found from the area under the stain curve one $S_{rmax,sec}$ to each side of the primary crack:

$$w_{max,fl,w} = 4\epsilon_{sc}L_{deb} - (\epsilon_{sc} + \epsilon_{smin})(S_{rmax,sec} - 2L_{deb}) \quad (6.5)$$

$$w_{max,fl,w} = 2w_{max,d} \quad (6.6)$$

6.2.3 Flexural stiffness

The first step to estimating the deflection of a beam is to find the flexural stiffness. When taking the tension-stiffening into account, the flexural stiffness varies with the location in the beam, x . To simplify the flexural stiffness expression, a smeared flexural stiffness is determined. The smeared stiffness is constant and represents an average stiffness taking into account the variable bending moment along the beam's length.

The smeared flexural stiffness is found by the use of the Principle of Virtual Work and is dependent on the static system. For further elaboration see the table in Section 5.4.3. For four-point-bending, taking into account that a part of the beams is not cracked, the flexural stiffness is:

$$EI_{cr,ef,fine} = \frac{EI_{cr}}{1 - \frac{27k_t}{23M_{max}} - \frac{8M_{cr}^3}{23M_{max}^3} + \frac{8M_{cr}^3 EI_{cr}}{23M_{max}^3 EI_{uncr}} + \frac{12k_t M_{cr}^2}{23M_{max}^3}} \quad (6.7)$$

And for a more conservative and simple expression, the smeared stiffness, with the assumption that the beam is cracked in the whole length, is:

$$EI_{cr,ef,coarse} = \frac{EI_{cr}}{1 - \frac{27k_t}{23M_{max}}} \quad (6.8)$$

The parameters in the above expressions are:

The tension-stiffening coefficient:

$$k_t = \frac{1}{3} \tau_b \frac{(S_{rm,sec} - 2L_{deb})^2}{\phi_s S_{rm,sec}} A_s d (3 - \beta) \quad (6.9)$$

The flexural stiffness of a fully cracked section:

$$EI_{cr} = \frac{1}{3} A_s E_s d^2 (3 - \beta) (1 - \beta) \quad (6.10)$$

Coefficient of the neutral axis of a fully cracked section:

$$\beta = \frac{x_{cr}}{d} = \frac{\alpha A_s}{bd} \left(\sqrt{1 + \frac{2bd}{\alpha A_s}} - 1 \right) \quad (6.11)$$

Flexural stiffness of an uncracked section:

$$EI_{uncr} = \frac{1}{12} bh^3 E_c \quad (6.12)$$

Maximum moment in the beam:

$$M_{max} = \frac{1}{3} QL \quad (6.13)$$

Moment of first cracking:

$$M_{cr} = \frac{1}{6} bh^2 f_{tb} - M_{sw} \quad (6.14)$$

where M_{sw} is the moment in the beam from self-weight.

Moment of yielding in the tensile reinforcement:

$$M_y = \frac{1}{3} A_s d (3 - \beta) f_y - M_{sw} \quad (6.15)$$

6.2.4 Deflection

From the flexural stiffness and a chosen load level, Q , the maximum deflection, which is at mid-point of the beam, can be determined. For the stiffness including the tension stiffening effect and the uncracked areas of the beam the expression for the deflection becomes:

$$u_{fine} = \frac{23}{216} \frac{M_{max} L^2}{EI_{cr,ef,fine}} \quad (6.16)$$

For an estimation of the more conservative deflections of the coarse approach of including tension-stiffening or from a fully cracked stiffness, the stiffness in the above equation can be replaced with $EI_{cr,ef,coarse}$ or EI_{cr} .

For comparison, the deflection calculated with the use of the Eurocode model, taking into account tension-stiffening and variable moment, is:

$$u_{EC2} = \frac{23}{216} \frac{M_{max} L^2}{EI_{EC2}} \quad (6.17)$$

where the stiffness for short-term loading is:

$$EI_{EC2} = \frac{EI_{cr}}{1 - \left(1 - \frac{EI_{cr}}{EI_{uncr}} \frac{M_{cr}}{M}\right)^2} \quad (6.18)$$

6.3 Comparison of test and model

In this section the previously explained approach and procedure are applied to eight different flexural members and compared to their test results, which were also used in the introduction of this thesis (Chapter 1). The eight tests are from two different series conducted by Kenel and Marti [1] and Gilbert and Nejadi [2]. The tests were also treated in [69] and [71] with regard to estimation of the deflection. However, in the following sections, a more thorough examination of the tests will be carried out.

6.3.1 Introduction to test

In both test series the members were subjected to four-point-bending, as illustrated in Figs. 6.3 and 6.6, respectively. The tests by Kenel and Marti are one-way spanning slabs with an effective depth of $d = 167\text{mm}$. The only variations between the slabs are the reinforcement ratio and the concrete strength. The tests by Gilbert and Nejadi are beams with an effective depth of $d = 300\text{mm}$. These tests are identical in pairs with the only variation between the two pairs being the cover to the tensile reinforcement. The cross-sectional properties of all eight beams are presented in the force-deflection plots in Fig. 6.5 and 6.7. The black dots on the plots mark the load stages where crack widths were measured. During testing the crack widths were measured with microscopes with magnification in both test series.

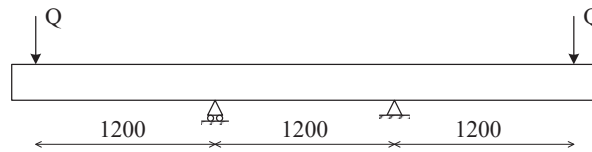
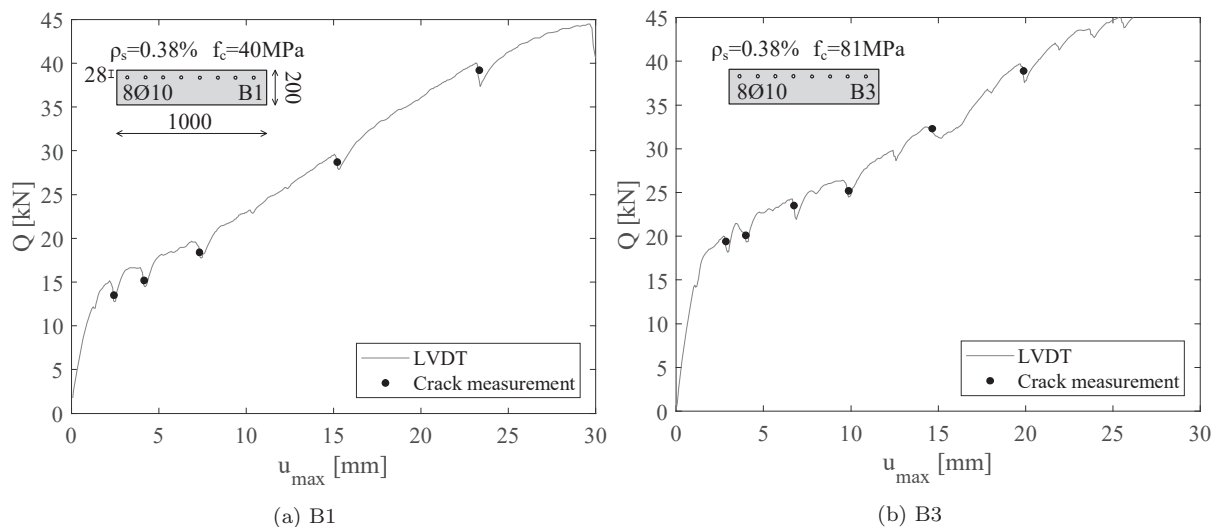


Figure 6.3: Static system of test beams by Kenel and Marti

Kenel and Marti's test series originally consisted of five members but the specimen named B2 was equipped with prestressed tendons. Therefore, only four members are included here; B1, B3, B4, B5, where three of them (B1, B3, B5) have approximately the same reinforcement ratio, $\rho_s \approx 0.38\%$, while B4 is even more lightly reinforced; $\rho_s = 0.19\%$. Three of the beams (B1, B4, B5) had approximately the same concrete strength, $f_c = 36 - 40\text{MPa}$, while B3 are cast with high strength concrete; $f_c = 81\text{MPa}$.



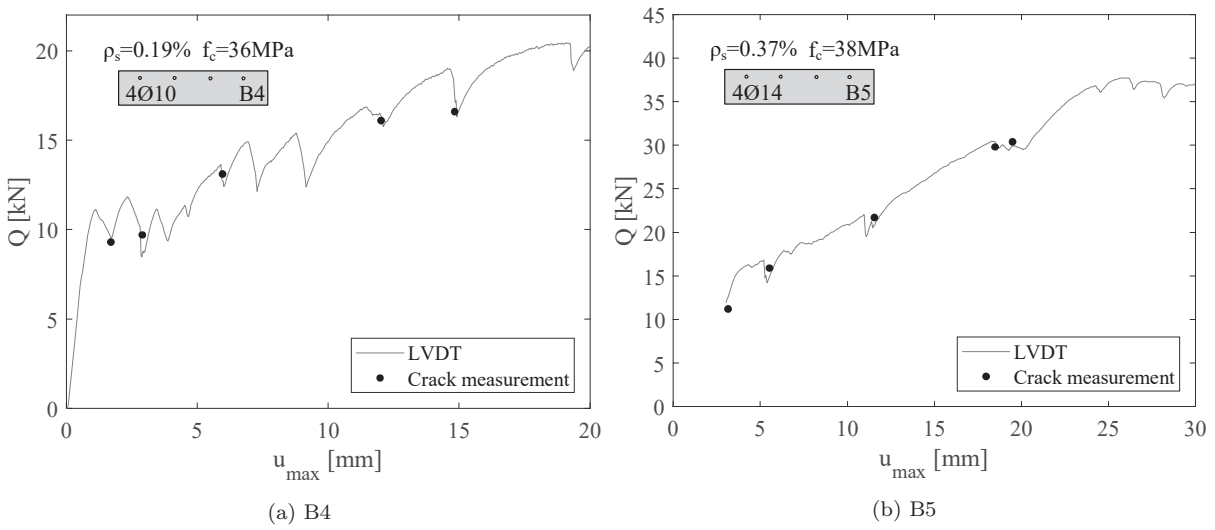


Figure 6.5: Force-deflection response and identification of load levels of crack measurements, test beams by Kenel and Marti

Because Gilbert and Nejadi’s tests are identical in the two pairs; B1a/B1b and B2a/B2b, some of the results are also plotted together as the force-deflection response in Fig. 6.6. As mentioned, the only variable in these tests is the cover, which goes from 40mm in B1a/B1b to 25mm in B2a/B2b. The beams had a fairly low reinforcement ratio of $\rho_s = 0.54\%$ from two bars of the diameter $\phi_s = 16mm$ in all four beams (2O16).

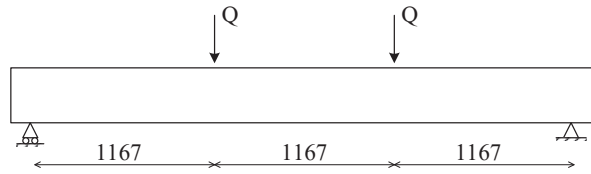


Figure 6.6: Static system of test beams by Gilbert and Nejadi

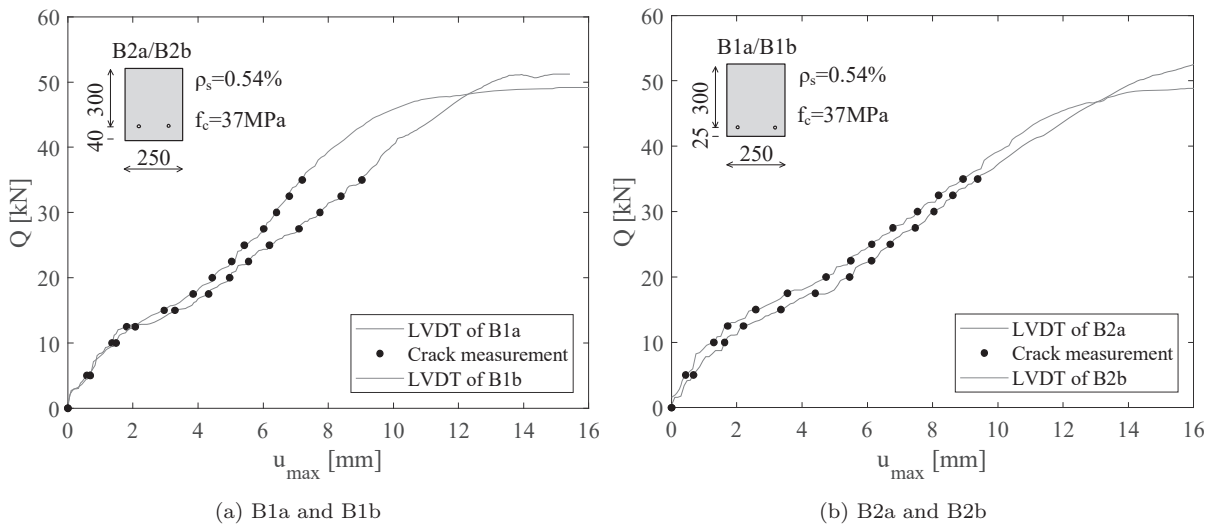


Figure 6.7: Force-deflection response and identification of load levels of crack measurements, test beams by Gilbert and Nejadi

6.3.2 Crack spacings

Table 6.1 lists the measured and estimated crack spacings in the eight members. The measured values are found with the measuring procedure used in the empirical study described in Section 4.4.1. The estimated crack spacings are found from the regression models established in the empirical study and repeated in Section 6.2.1. The table only lists the secondary crack spacings, which is simply because only one system of cracks exists according to the approach. The beams of $d = 167mm$, conducted by Kenel and Marti, are from the category of laboratory beams which in Chapter 3 and Chapter 4 were found to be characterised by the fact that only one type of crack forms in them. The beams tested by Gilbert and Nejadi of $d = 300mm$ are just on the limit of the two categories of beams and could equally have formed both secondary and primary cracks. Nevertheless, the limit $2S_{sec} \leq S_{fl}$ is not met. The estimate for the primary crack spacing; $S_{fl} = 0.42d$, found in Chapter 4, for $d = 300mm$ results in a smaller primary crack spacing; $S_{rm,fl} = 126mm$, than secondary crack spacing; $S_{rm,sec} = 157mm$. Accordingly, both types of crack cannot exist.

	Measured		Estimated		$\frac{Meas.}{Estim.} - 1$	$\frac{Meas.}{Estim.} - 1$
	$S_{rm,sec}$	$S_{rmax,sec}$	$S_{rm,sec}$	$S_{rmax,sec}$	$S_{rm,sec}$	$S_{rmax,sec}$
Specimen	[mm]	[mm]	[mm]	[mm]	[%]	[%]
B1	149	257	146	219	2.1	17
B3	150	215	146	219	2.7	-1.8
B4	282	355	236	354	19	0.3
B5	151	216	183	274	-17	-21
B1a	190	284	157	236	21	20
B1b	178	262	157	236	13	11
B2a	152	258	157	236	-3.2	9.3
B2b	188	262	157	236	20	11

Table 6.1: Measured and estimated secondary crack spacing in tests by Gilbert and Nejadi and Kenel and Marti

With respect to Kenel and Marti's test, the measured mean crack spacings confirm the previously stated theory, namely that the crack spacing increases with the decrease in reinforcement ratio and ϕ_s/ρ_s -ratio. Member B4 has a reinforcement ratio of $\rho_s = 0.19\%$ while the other three members (B1, B3, B5) have a ratio of $\rho_s = 0.38\%$. The difference in the reinforcement ratio is consistent with the measured crack spacing being almost twice the size in B4 than in the remaining three beams.

The difference between Gilbert and Nejadi's B1a/B1b and B2a/B2b was the size of the cover. When comparing the crack spacings of the four members there is no notable difference between the specimens with the small cover (B2a/B2b) and the large cover (B1a/B1b). The slightly larger mean spacing of B1a and B1b compared to B2a and B2b could be due to the larger cover but could also be due to the random variation in the results. The crack spacing variation in these members is thus largely consistent with the characteristics of the laboratory beams found in Chapter 4, where the regression models indicated that the crack spacing is only dependent on the ϕ_s/ρ_s -ratio, which is the same size for all four test members.

The table also lists the difference between the measured and the estimated crack spacings for both mean and maximum values. The crack spacings are all estimated within approximately 20% deviation from the measured spacings and a quarter of the estimates deviate less than 3%. From this, it can be concluded

that the estimates are in good agreement with the tests.

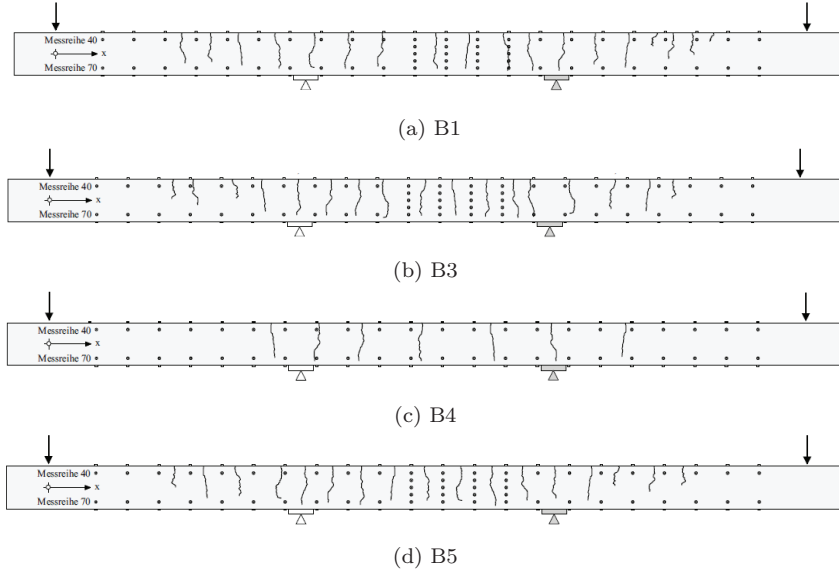


Figure 6.8: Crack patterns in tests by Kenel and Marti, reprint from [1]

When studying the crack patterns from the eight test members in Figs. 6.8 and 6.9 it is also clear that only one type of crack developed as was predicted by the proposed approach. No cracks are seen to be concentrated around the tensile reinforcement in either of the beams. In contrast, all cracks have approximately the same height, which is greater than $2c_{ver}$ being the approximate height of secondary cracks.

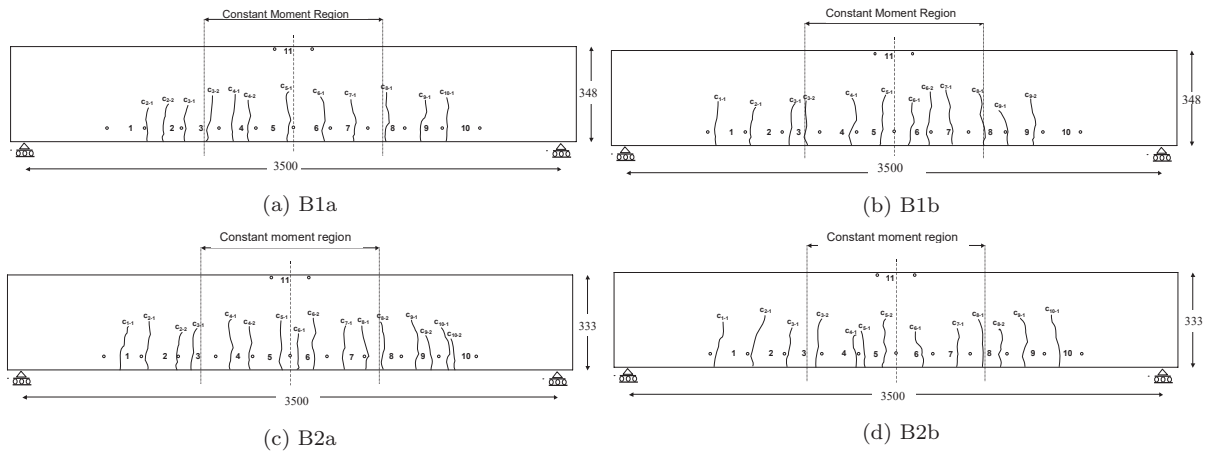


Figure 6.9: Crack patterns in tests by Gilbert and Nejadi, reprint from [2]

6.3.3 Essential parameters

Table 6.2 lists the essential parameters needed to calculate the coming illustrated results of the eight test members; deflection and crack widths.

The bottom of the table lists the difference between the fully cracked stiffness, EI_{cr} , and the stiffness including tension-stiffening taking the uncracked areas into account, $EI_{cr,ef,fine}$. Due to the fact that the stiffness including tension-stiffening decreases with an increase in the load, Q , the stiffnesses are compared

for a single load level chosen to be 60% of the yield load, Q_y . The numbers reveal how the stiffness including tension-stiffening increases with an increase in the concrete strength. This can be seen from comparing B1 and B3, where the only difference is the concrete strength. The difference in stiffness with and without tension-stiffening is 14% for B1 with a concrete compressive strength of 40MPa and 25% for B3 with a strength of 81MPa. This result is due to the difference in the size of the moment at first cracking, M_{cr} . All other parameters are more or less the same size for the two members. Cracks will form later in beam B3 than in B1 due to the larger cracking moment, which is beneficial with respect to the stiffness. This also means that if the stiffness, including tension-stiffening, estimated with the coarse assumption, $EI_{cr,ef,coarse}$, it would be approximately of equal size for B1 and B3 because the uncracked areas are not taken into account.

	Specimen	B1	B3	B4	B5	B1a/B1b	B2a/B2b
f_c	[MPa]	40	81	36	38	37	37
f_t	[MPa]	2.0	2.8	1.9	2.0	1.9	1.9
f_{tb}	[MPa]	2.8	4.0	2.7	2.8	2.3	2.3
τ_b	[MPa]	4.0	5.7	3.8	3.9	3.8	3.8
ϕ_s/ρ_s	10^3 [mm]	2.7	2.7	5.3	3.8	3.0	3.0
L_{deb}	[mm]	11	15	21	16	10	7.8
M_{cr}	[kNm]	13	21	12	12	8.5	7.8
M_y	[kNm]	49	50	22	42	57.6	57.8
k_t	[kNm]	2.8	2.7	1.9	2.0	2.4	2.8
EI_{uncr}	10^{13} [MPamm ⁴]	2.3	2.7	2.2	2.3	2.4	2.1
EI_{cr}	10^{13} [MPamm ⁴]	0.28	0.28	0.15	0.26	0.52	0.52
$EI_{cr,ef,fine}(0.6M_y)$	10^{13} [MPamm ⁴]	0.32	0.35	0.23	0.29	0.57	0.58
$\frac{EI_{cr,ef,fine}(0.6M_y)}{EI_{cr}} - 1$	[%]	14	25	53	12	10	12

Table 6.2: Essential parameters for design of serviceability limit state

All the following modelled results are estimated solely from the estimated parameters listed in Tables 6.1 and 6.2 and the expressions given in Section 6.2.1. Hence, in order to be able to objectively assess the proposed model, no test results are used to predict how the tests behave, for example the estimated crack spacings are used and not the crack spacings measured from the photos of the test members.

6.3.4 Force-deflection response

The approach for estimating the deflection from the crack spacing is applied and compared to the experimental results. Fig. 6.10 shows the comparison with the tests conducted by Kenel and Marti while Fig. 6.11 illustrates the comparison with Gilbert and Nejadi's test beams. The test responses are compared with the modelled responses with the use of: 1) the Eurocode expression for the stiffness, EI_{EC2} , 2) the fully cracked stiffness, EI_{cr} , 3) the coarse approach for including tension-stiffening, $EI_{cr,ef,coarse}$, and 4) the fine approach for including tension-stiffening, $EI_{cr,ef,fine}$.

Gilbert and Nejadi beams were cured under moist conditions for 28 days, by covering the members with wet Hessian, to avoid shrinkage effects on the force-deflection response. This is assumed to be the most

ideal when the tests are used for comparison with an approach for estimating the short-term response, which is the case here. The test members by Kenel and Marti were covered with wet cloths for the first five days of curing.

An overall good agreement is found when comparing the theoretical approach with the experimental results of the load-deflection response with the use of either $EI_{cr,ef,fine}$, $EI_{cr,ef,coarse}$ or the Eurocode expression. The tests as well as the modelled responses confirm that the tension-stiffening is more pronounced for the small reinforcement ratios because the tension-stiffening effect increases with the increase in crack spacing at level of the reinforcement. For test member B4, in Fig. 6.10c, the difference between the test and the response estimated with the fully crack stiffness is greater than in the other tests because this member has the smallest reinforcement ratio. The difference between the modelled response using $EI_{cr,ef,fine}$ and $EI_{cr,ef,coarse}$ is also greatest here. For the beams with the largest reinforcement ratios, which are B1a/B1b and B2a/B2b in Fig. 6.11a and 6.11b, the tension-stiffening effect is negligible for all load levels. In all cases, the flexural stiffness assuming a fully crack beam EI_{cr} , is a conservative estimate which yields larger deflections than indicated by the test.

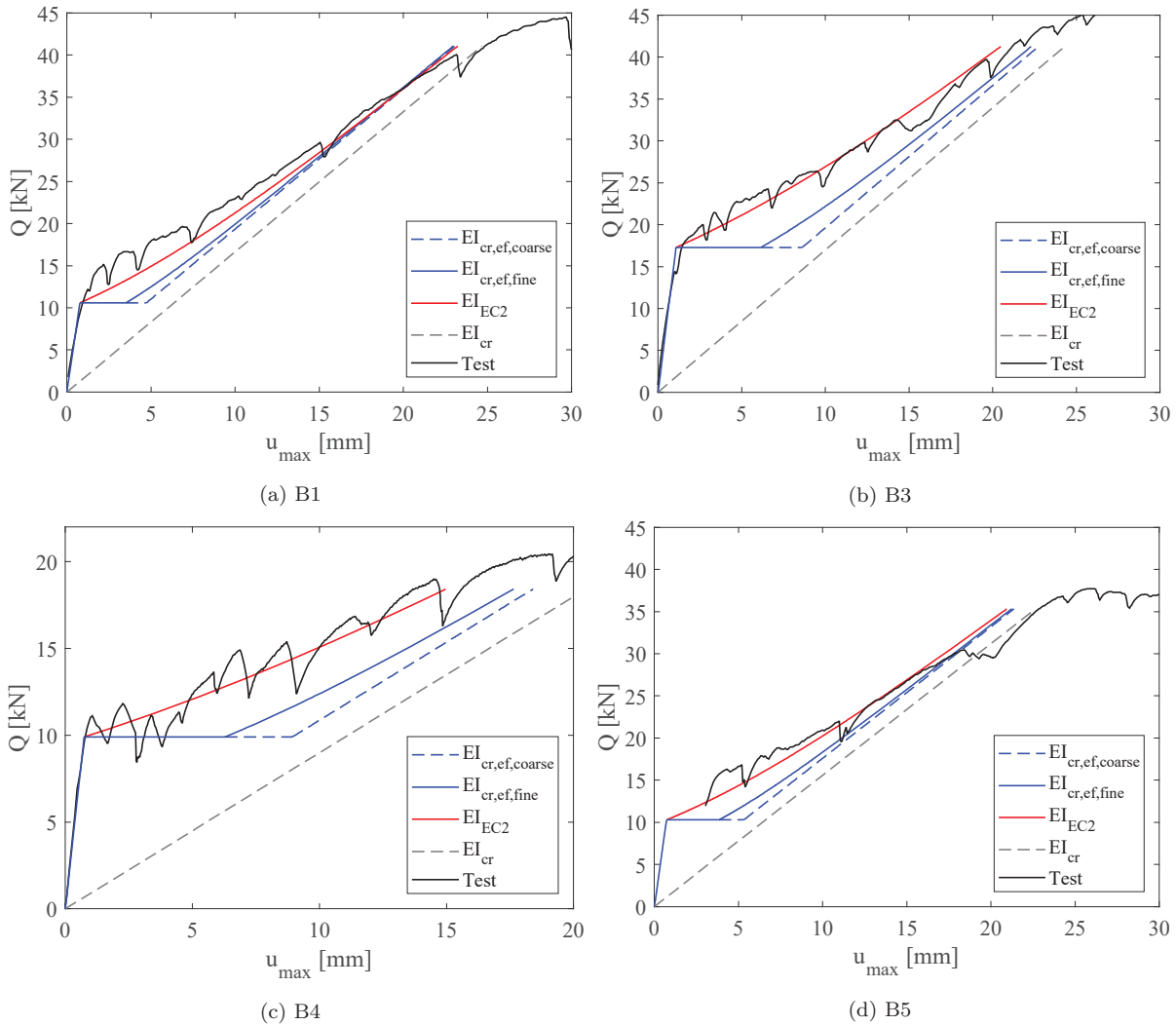


Figure 6.10: Force-deflection relations for test beams by Kenel and Marti.

When comparing the proposed approach to the Eurocode model with the use of EI_{EC2} , the Eurocode seems to slightly underestimate the deflection for small reinforcement ratios. For all the slabs in Fig. 6.10,

the response of the Eurocode model, indicated by the red line, exhibits a moderately larger stiffness than the test response especially for load levels close to yielding for B3 and B4. For the beams with higher reinforcement ratio, by Gilbert and Nejadi, the response estimated by the Eurocode yields more or less the same result as the proposed approach because the tension-stiffening effect is less pronounced.

The Eurocode and the proposed model show different behaviour at load levels just after cracking has initiated. The response with the use of the Eurocode model is continuous because the stiffness gradually decreases from the stiffness of an uncracked section, EI_{un-cr} , towards the stiffness of a fully cracked section, EI_{cr} . The extrapolation of the stiffness from the uncracked stiffness and the fully cracked stiffness, used in the Eurocode, has no apparent connection to the process of cracking and how this reduces the stiffness. In contrast to the Eurocode model, assumptions are made for the proposed approach as to how the beam cracks and how this affects the stiffness. It is assumed that the concrete strength is entirely constant in the whole member, which leads to the assumption that all cracks form at exactly the same load, namely Q_{cr} . This results in a horizontal shift in the deflection at the load level of cracking, Q_{cr} , because the member is subjected to four-point-bending and the whole constant moment span thus cracks at the same load level. For the fine approach, $EI_{cr,ef,fine}$, the stiffness gradually decreases as an increasing area of the beam reaches the cracking load. For the coarse approach, $EI_{cr,ef,coarse}$, the whole beam is cracked the instant the cracking moment is reached in one location of the beam, which is the reason for the larger horizontal shift in this response.

If the proposed approach was applied on a beam in three-point-bending or a beam subjected to uniformly distributed loading, the force-deflection response would not shift at Q_{cr} but would look more like the response estimated by the Eurocode for load levels close to cracking.

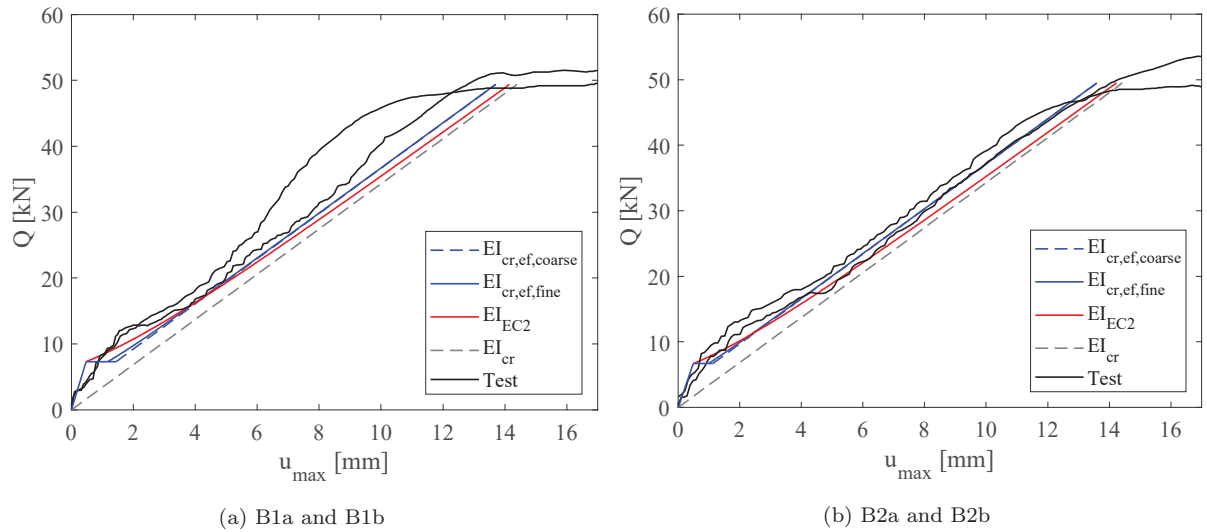


Figure 6.11: Force deflection relations for test beams by Gilbert and Nejadi

From the comparison of the test and estimated force-deflection response, it can be concluded that the proposed model for estimating the deflection under short-term loading, from knowledge of the crack spacing, agrees well with tests.

It is also concluded that the proposed approach performs just as accurately as the Eurocode model. The Eurocode model and the proposed approach are very similar for the beams with reinforcement ratios of $\rho_s = 0.54\%$, whereas they exhibit quite different behaviour for the beams/slabs with lower reinforcement ratios. With respect to members with low reinforcement ratios the Eurocode is observed to be more sensitive to tension-stiffening, resulting in a slight overestimation of the stiffness. Even though this only results in a small underestimation of the deflection it can be argued that the proposed approach is more

accurate due to the fact that the tests used for the comparison in this section only represent the response of first time loading. If the modelled responses were compared to beams subjected to multiple reloading, which must represent reality, the Eurocode would overestimate the stiffness even more.

6.3.5 Investigation of the location of maximum crack width

The approach proposed in Chapter 5 to estimate the maximum crack width in a member presumes that the maximum crack width is found in the crack that has the largest distances to the other cracks. Accordingly, the maximum crack width is estimated from the strains over half a maximum crack spacing to each side of a crack. Whether this assumption can be accepted with reason, in the current tests, is investigated in Fig. 6.12. The two graphs plot all of the measured crack widths in the constant moment span relative to the measured distance to the adjacent cracks, S_r , for the two test series, respectively. The plots thus only show measured data whereas no estimated results are shown here. The distance S_r is found from half the distance to the adjacent crack on the left side plus half the distance to the crack on the right side from the crack patterns in Fig 6.8 and 6.9.

If the assumption that the maximum crack width is related to the maximum crack spacings is true, the data points should form something that resembles a straight line with a positive slope. The tests by Kenel and Marti, in Fig. 6.12a display this tendency. When looking at each of the beams separately, the data point with the largest crack spacing is also the point with the largest crack width.

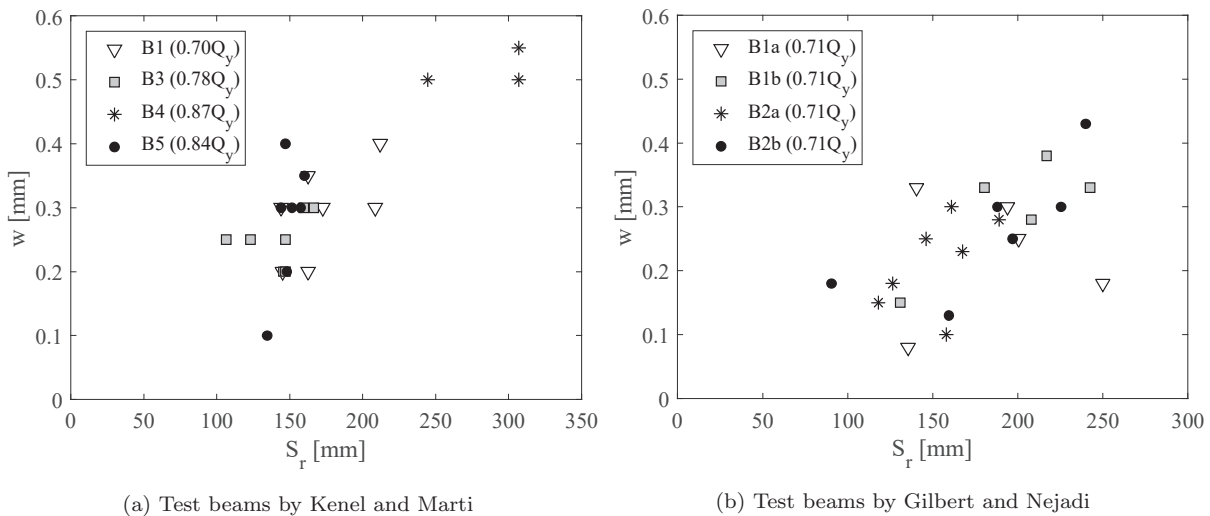


Figure 6.12: Crack width in relations to crack spacing of every single crack in the constant moment span

The results are somewhat more scattered for the test by Gilbert and Nejadi in Fig. 6.12b. When studying each of the four beams separately, it is observed that only for one of the beams the results are the opposite of what is assumed. In beam B1a, with triangular marks, the maximum crack width is found in the crack with the second smallest spacing. In the other three beams (B1b, B2a and B2b), the maximum crack width is located at the largest spacing or at a spacing that is very close to the same size as the largest. With regard to the fact that the results of Kenel and Marti's tests in Fig. 6.12a are not all from the same relative load level, it is concluded that this does not have any influence on the matter investigated here. The results plotted in the figure, for all four beams, are from load levels where all cracks have developed, hence a stabilised crack system has been reached. Therefore, the crack that has the largest crack spacing associated to it, is the same crack as for a higher load level.

Even though one of the eight beams had contradicting results, it is concluded that the investigation strongly indicates that the maximum crack widths are located at the crack with the maximum crack spacings.

6.3.6 Development of crack width with increasing deflection

In Figs. 6.13 and 6.14 the relations between the crack width and the deflection are investigated. The approach proposed in Chapter 5 to design the serviceability limit state of flexural members, assumes that all deformation takes place in the cracks, thus the deformation of the concrete can be neglected. Furthermore, it is assumed that the height of the concrete compression zone, x_{cr} , is constant both with respect to location in the beam and to load level within the service load range. The height of the compression zone is estimated from the consideration of an elastic stress distribution in the cross-section and it is used to define the height of the primary cracks in the stabilised crack system. The crack height is subsequently used to define the crack width and the flexural stiffness. Whether the assumption of constant compression zone holds can be investigated through the relations between the crack width and the deflection, which should be linear.

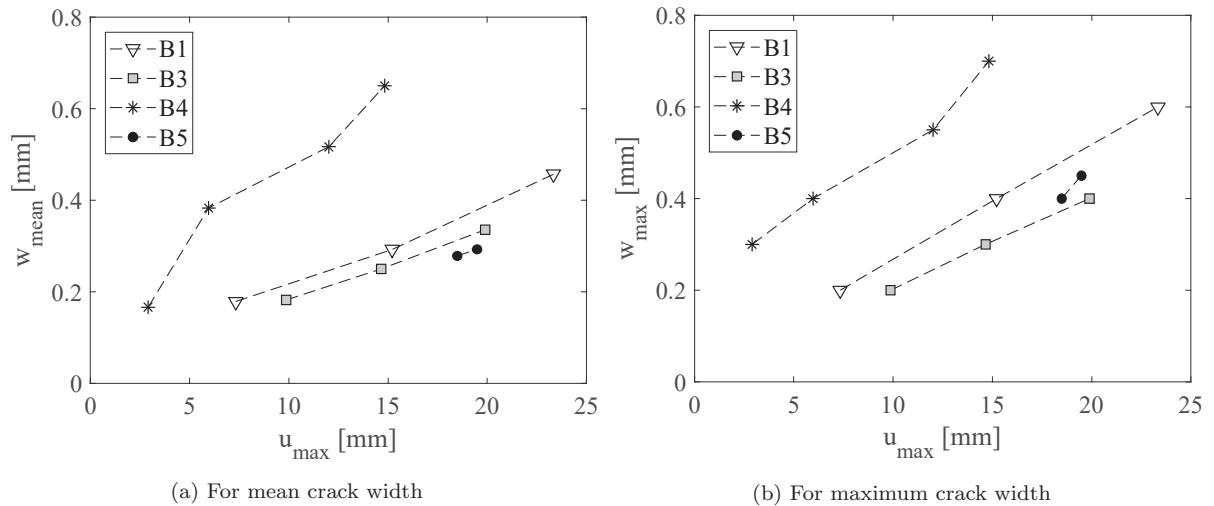


Figure 6.13: Development of crack width with respect to deflection at mid-point of beams from Kenel and Marti's tests

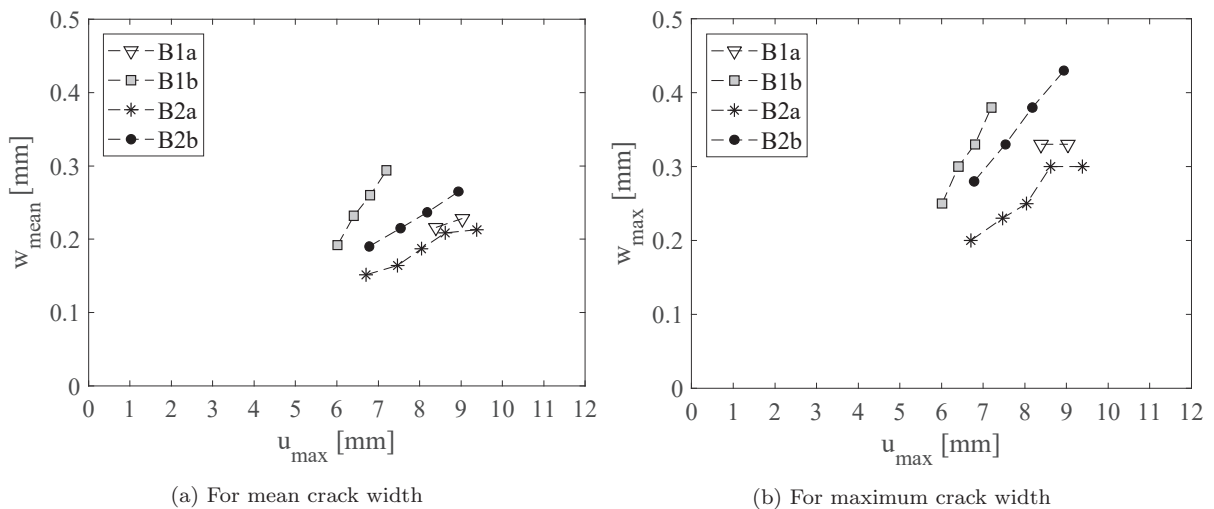


Figure 6.14: Development of crack width with respect to deflection at mid-point of beams from Gilbert and Nejadi's tests

For both test series the relations between the crack width and the corresponding maximum deflection are plotted for the load steps where the crack system is stabilised. A stabilised crack system is, in these tests,

defined by the load step where all the measured cracks in the constant moment span have a crack width of a size that was measurable with the microscope. In Figs. 6.13a and 6.13b the relations are illustrated for Kenel and Marti's four tests, for the mean crack width and the maximum crack width in the constant moment span, respectively. The same are illustrated for Gilbert and Nejadi's four tests in Figs. 6.14a and 6.14b.

From studying the figures, it is concluded that the crack width and the deflection can be assumed to be linearly proportional, because, for a majority of the beams, the relations are clearly linear for both the maximum and the mean crack width. Additionally, the linear relation is related to the fact that the crack spacing is constant for the plotted load levels. Only for the beam named B4 from Kenel and Marti's tests does this not apply, while, for the beams named B1b and B2a from Gilbert and Nejadi's tests, the deflection increases without an increase in the maximum crack width for high load levels. The reason for the latter could be that another crack in the constant moment span increases for that load interval.

The other assumption, that all deformation takes place in the cracks, was investigated in the Introduction in Chapter 1, for the same two test series, which formed the basis for the proposed model due to the agreeable results.

6.3.7 Force-crack width response

Having concluded that the assumptions made in order to estimated crack widths in flexural members can be accepted, the crack widths will now be estimated. Figs. 6.15 and 6.16 illustrate the comparison of the estimated and the measured maximum crack widths in the constant moment span, where the crack widths are plotted in relations to the applied load. Each plot represents one test beam where two different assumptions are used to estimated the crack width. The first assumption; $\tau_b = 2f_t$, is the original approach, as described in Chapter 5, with a stress transfer between reinforcement and concrete, outside the debonded zones, of twice the concrete tensile strength. The second assumption; $\tau_b = 0$, represents a conservative estimate of a fully cracked beam where there is no transfer of stresses to the concrete between cracks. In other words, the reinforcement is debonded from the concrete in the whole beam.

The measured crack widths are plotted for all the load levels where the information was given in the experimental reports. However, some of these load levels are prior to the stabilised crack phase. In Figs. 6.15 and 6.16 the crack widths measured at load levels from the unstable crack system are marked in red while the measured crack widths from a stable crack system are marked in green.

Theoretically, the model does not apply for the load levels prior to stabilisation of the crack system because not all cracks will have formed and the maximum crack spacing can thus be larger than predicted by the model, which results in larger crack widths. Nevertheless, the results are included in the plot in order to also gain a sense of how the model performs for these load levels.

With respect to the model comparison with Kenel and Marti's tests in Fig. 6.15, in two of the four beams, the estimates of the crack width are in very good agreement with the tests, which is for members B3 and B5. For the beam with the smallest reinforcement ratio, B4, the measured crack width at the highest load level is greater than that estimated by both models. This load level is fairly close to the theoretically estimated yield load. Judging from the force-deflection response back in Fig. 6.5a, yielding can already have been initiated and may be an explanation to why the crack width increases significantly for only a small increase in load.

For beam B1 the measured crack widths in the two highest load levels are larger than estimated by the model. In Table 6.1 it is seen that this is the slab where the measured maximum crack spacing was 17% larger than estimated. When this is the case, it makes sense that the model underestimates the crack width because the length over which the area under the strain curve is found, is too small.

With respect to the load levels where the crack system is not yet stabilised, the model also provides reasonably good estimates. In none of the beams were crack widths of the unstable crack system estimated

to be significantly smaller than the test results.

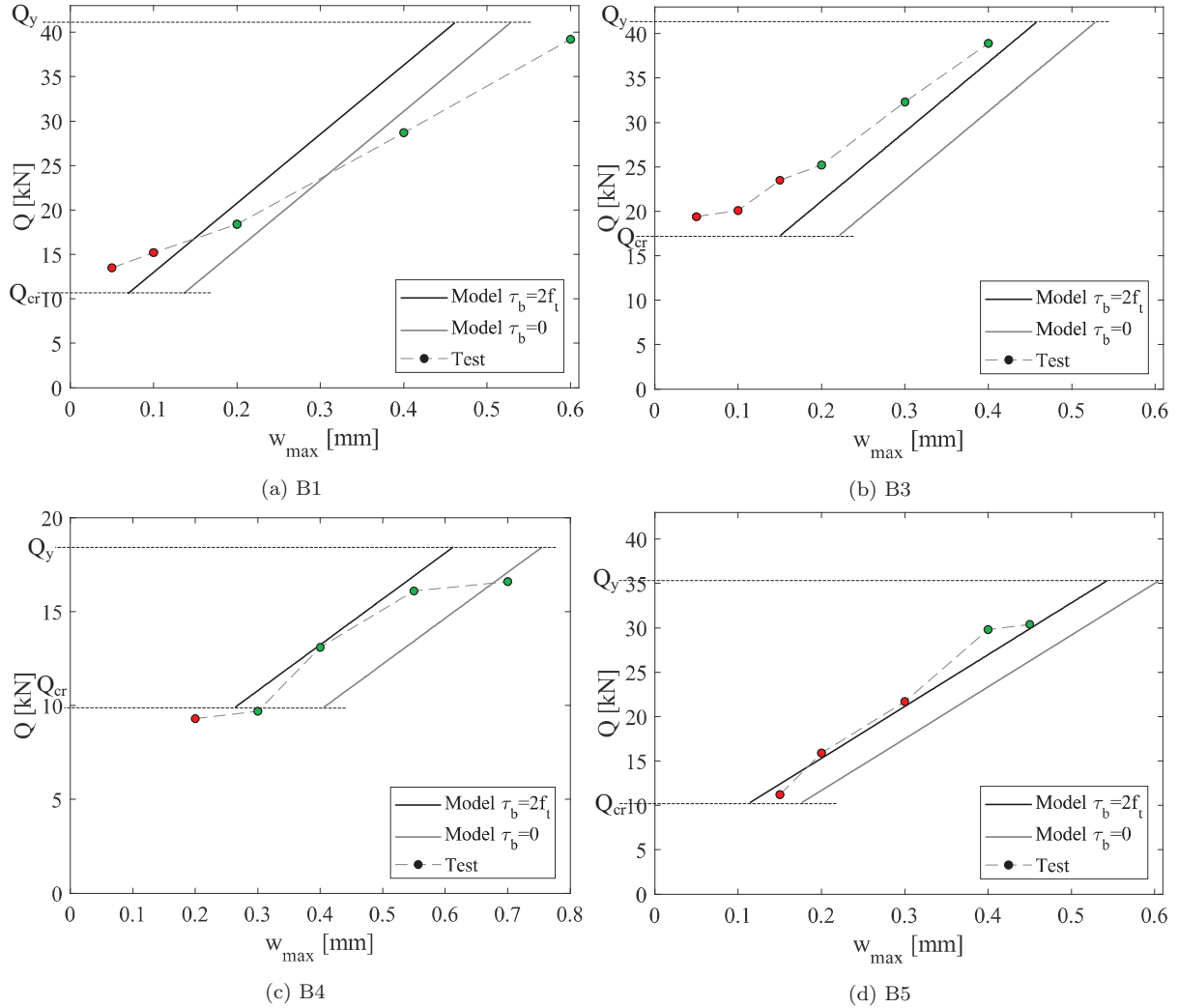


Figure 6.15: Development of maximum crack width with increase in load, Q , for the tests by Kenel and Marti

Overall good agreement is also found from the comparison between the results of model and the test results by Gilbert and Nejadi, in Fig. 6.16. Here, all of the estimated crack spacings in Table 6.1 were 10 – 20% smaller than those measured, which could be the reason why the crack widths at some load levels are underestimated slightly compared to the measured crack widths. This is, for example, the case for beam B2b where the measured crack widths are even higher than the conservative estimate of $\tau_b = 0$. Again, the crack widths, estimated for the load levels of an unstable crack system where the model actually does not apply, also agree well with the model.

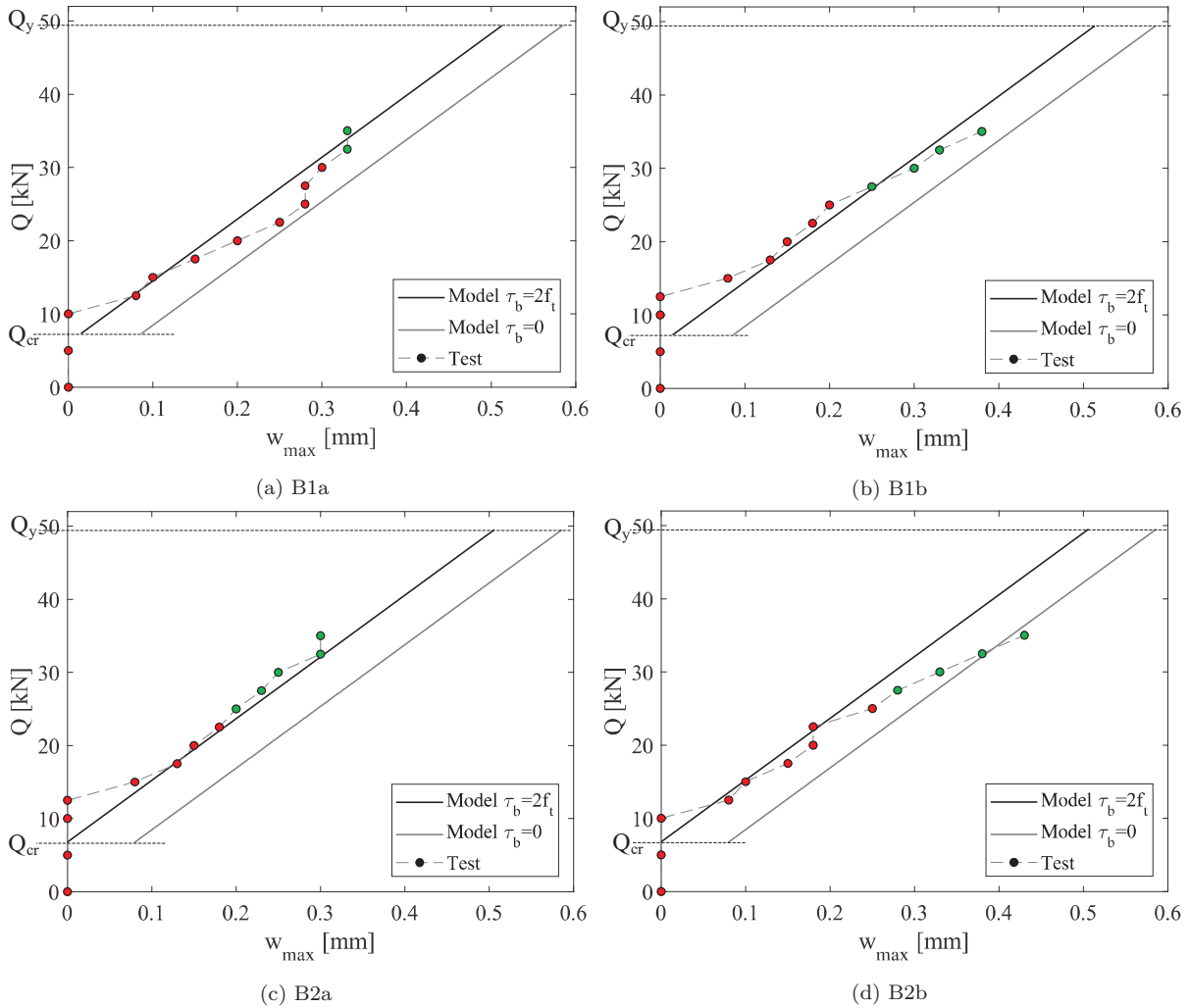


Figure 6.16: Development of maximum crack width with increase in load, Q , for the tests by Gilbert and Nejadi

From the comparison of the models to the force-crack width response, it can be concluded that the approach for estimating crack widths, proposed in Chapter 5, yields good results when compared to flexural members subjected to four-point-bending. The approach has no safety embedded, which means that some of the results are not conservative but rather estimated a slightly lower crack width than those measured. It should thus be considered to incorporate a safety into the approach. The safety could be integrated by adjusting the factor describing the difference between the mean and the maximum crack spacing. In the investigation of the relations between mean and extreme crack spacings in Section 4.4 the relations: $1.5S_{r_{m,sec}} = S_{r_{max,sec}}$ were found to be reasonable, with the factor 1.5 representing the mean value of $S_{r_{max,sec}}/S_{r_{m,sec}}$. By increasing the factor, the beams with a larger maximum crack spacing, and thus a larger maximum crack width, would be taken into account. In the investigation in Section 4.4, the relative standard deviation of the relations $S_{r_{max,sec}}/S_{r_{m,sec}}$ was found to be 19%. This means that, on average, the factor varies from 1.2–1.8. Using a slightly higher factor of, for example, 1.8 instead of 1.5 would therefore be more conservative and still be consistent with empirical results.

7 CONCLUSION

In this thesis an approach was proposed for designing flexural members in the serviceability state resting on the knowledge of the crack spacing.

An initial hypothesis stating that deformation of beams can be assumed to take place solely in the cracks and that the crack widths are related to the mean reinforcement strain and the spacing of the cracks has been proven to be a sound basis for modelling of the serviceability limit state, yielding estimates that agree well with experimental results.

The approach is based on simple, yet physical, assumptions of the behaviour of cracked reinforced concrete beams under service loads. From knowledge of the mean crack spacing and from assuming a constant transfer of stresses from the reinforcement to the concrete between cracks, both the crack width, the flexural stiffness including the tension-stiffening effect and the deflection of beams can be estimated. The approach thus meets the objective of the current research of creating a coherent and physically transparent way of designing all the main aspects of the serviceability limit state with the use of the same assumptions. The approach can potentially form the basis for a connection between the serviceability limit state and the ultimate limit state where models for both states rest on coherent and physical assumptions.

The empirical study of the crack spacing

Due to the fact that the crack spacing is the foundation for the whole approach of designing flexural members in the serviceability limit state, this parameter has been investigated through a comprehensive empirical study of a database of measured crack spacings from tests of 142 tensile members and 462 flexural members found in the existing literature. From the ambition of establishing a database of comparable data resting on the same basis, all crack spacings have been collected in the same manner, by measuring them from photos of the tests members' crack patterns available in the experimental reports. With this method it was possible to avoid subjectivity and to exclude some uncertainties otherwise connected to measuring of crack spacings.

From knowledge gained in the literature review as well as from observations of tests conducted as part of the present research project, the beams in the database are grouped into two categories with respect to their effective depth because they are observed to behave differently. The two categories are the laboratory beams of $d < 300mm$ and the structural beams of $d \geq 300mm$, where their application is indicated by the name of the category. The results of the empirical study justify the division of the beams as the two groups of beams show fundamentally different behaviour with respect to the developed crack system and crack spacings.

Through statistical investigations of the crack spacing with the use of the database, the aim was to assess the following for both tensile and flexural members: 1) which parameters control the crack spacing, 2) what are the relations between the mean and the extreme crack spacings, and 3) which of the reviewed existing models estimate the crack spacing most accurately. For flexural members alone, the aim was also to use the database to investigate whether a stabilised crack system can be identified with respect to a stress level in the reinforcement. The conclusions drawn from the empirical study are summarised below.

Both the laboratory and the structural beams are analysed with respect to two different types of cracks, namely the secondary cracks and the primary cracks. The secondary cracks are characterised by being local and concentrated around the tensile reinforcement and their crack spacing is thus measured at the level of the reinforcement. The primary cracks extend to approximately the location of the neutral axis

and their individual crack spacing is measured at mid-height, being a distance of $d/2$ from the compression face of the member.

Generally, the results of the analysis of the crack spacings in the laboratory beams are associated with more uncertainty and randomness than the results of the structural beams where clearer conclusions can be made from the data analysis. Furthermore, the crack spacings in the laboratory show sensitivity with respect to the stress level in the reinforcement, where, in particular, stress levels below approximately 250MPa increase the crack spacing. This sensitivity towards the stress level is not seen in the structural beams.

Overall, the multi-variable regression analysis of the databases revealed that:

Laboratory beams $50\text{mm} \leq d < 300\text{mm}$ The crack spacing at the level of the reinforcement and at mid-height of the laboratory beams are seen to be controlled by the same parameters. This suggests that only one type of crack develops in laboratory beams, which is found to be primarily controlled by the bond-parameter; ϕ_s/ρ_s . This is also one of two parameters that has the largest statistical significance on the crack spacing in tensile members as well as on the secondary crack spacing in structural beams – the other parameter being the cover. These findings indicate that the concentrated tensile reinforcement in laboratory beams also acts as distributed reinforcement and that cracking in these beams is thus not affected by a lack thereof.

The Eurocode model is generally found to be the best estimate for the crack spacing in the laboratory beams, of the reviewed existing models. The mean value of the ratio $S_{rm,test}/S_{rm,model}$ is found to be 1.04, being very close to the desired value of 1. However, there is a large variation in the results with a relative deviation from the mean of 39%. The other reviewed models are the Tension Chord Model, and models proposed by Leonhardt, Nielsen and Frosch.

Structural beams $300\text{mm} \leq d \leq 2000\text{mm}$ The analysis of the primary cracks in the structural beams supports that a linear proportionality to the effective depth of the member exists. The parameter d can solely describe 85% of the variation in the crack spacing with the relations; $S_{rm} = 0.42d$.

The reviewed existing models from the literature for describing the crack spacing in the web of flexural members, all hold a parameter related to the effective depth of the member and are therefore all fairly good estimates when compared to the measured crack spacings in the database. However, the choice of coefficient is important for the precision of the models. Due to a large empirical coefficient, the Eurocode, in general, overestimates the primary crack spacings. The other reviewed models are proposed by Frosch, Reineck and Hamadi.

The parameters that show significant influence on the secondary crack spacing in structural beams are; ϕ_s/ρ_s , c_{ver} and $n_s\phi_s$, which are the same parameters that have influence on the variation of the crack spacing in tensile members, where the parameter of $n_s\phi_s$ is only of minor influence. A regression model holding all three parameters can describe 83% of the variation in the crack spacing without the need of a constant term. There is no indication that the use of the effective reinforcement ratio, $\phi_s/\rho_{s,eff}$, instead of ϕ_s/ρ_s , results in a better estimate with respect to the values of the $adjR^2$ and the $RMSE$, which is probably because the two ratios are highly correlated.

It should be emphasised that a regression model only holding either the c_{ver} or the ϕ_s/ρ_s -ratio estimates the variation in the crack spacing with almost the same precision as a model holding all three parameters. The reason for this is most likely that these two parameters are highly correlated for the beams in the database and therefore describe almost the same variation in the crack spacing. This discovery could be an explanation as to why the two conflicting approaches from the literature, namely the bond-slip and the no-slip approach, resting in the $\phi_s/\rho_{s,eff}$ -ratio and the cover, respectively, both yield good results when different researchers in the past have validated them against tests. The

cover and the $\phi_s/\rho_{s,eff}$ -ratio are related/correlated because the cover is inherent in the effective reinforcement ratio. This suggests that there will most likely always be a high correlation between the two parameters, which means that, in most cases, both the bond-slip approach and the no-slip approach will give estimates in good agreement with tests.

From the investigation of which of the reviewed models performs best when compared to the database, the Eurocode model gives the best result for the secondary crack spacing in structural beams. The relative deviation from the mean value of $S_{rm,test}/S_{rm,model}$ is 33%, which is smaller than for the comparison of the Eurocode model with the crack spacing in the laboratory beams.

The database holds a large number of beams where the cover is of different sizes in horizontal and vertical directions. This raises the question of which of the two covers should be used in the Eurocode model as this is not specified. An investigation of the matter suggests that the model agrees best with the tests in the database if the maximum of the two covers is used, resulting in a mean value of 1.09 for $S_{rm,test}/S_{rm,model}$. It could be argued the the horizontal cover should be used in the Eurocode model as the crack spacings in all the tests in the database are measured on the side face of the beams. The horizontal cover is thus the smallest distance to the reinforcement, which was the distance Beeby proposed to use. However, when applying this to the Eurocode model it results in a mean value of 1.15 and a relative deviation from the mean of 44% which is significantly higher than when using the maximum cover.

The Eurocode model as well as the Tension Chord Model show inaccuracy with respect to variation in the $\phi_s/\rho_{s,eff}$ -ratio. The crack spacings estimated by the models are underestimated for low $\phi_s/\rho_{s,eff}$ -ratios and, on the other hand, overestimated for high $\phi_s/\rho_{s,eff}$ -ratios. This is also seen to be the case for the analysis of crack spacing in the tensile members and indicates that the influence of the $\phi_s/\rho_{s,eff}$ -ratio is overestimated with a too large coefficient on the $\phi_s/\rho_{s,eff}$ -term. This is confirmed by the regression model, estimated from the database, for the secondary crack spacing in the structural beams. In this model, the coefficient on the ϕ_s/ρ_s -term is smaller than the coefficient on the $\phi_s/\rho_{s,eff}$ -term in the Eurocode model and the regression model is not sensitive to variation in the ϕ_s/ρ_s -ratio.

With respect to establishing a stress level to which the system of cracks is stable with a constant crack spacing, it is concluded that this was not possible from the data in the database and might not be possible at all. As mentioned earlier, the crack spacing in the laboratory beams is less noticeably affected by the stress level beyond $\sigma_{sPic} = 250MPa$ but not totally unaffected. On the other hand, the regression analysis of the structural beams shows that neither the primary nor the secondary crack are significantly affected by the stress level.

The results suggest that parameters other than merely the stress level have an influence on when a crack system is stable. This could, for example, be the reinforcement ratio or the yield stress of the reinforcement. At least for beams with small reinforcement ratios, close to the minimum ratio, cracking will occur at stress levels close to yielding and will thus not necessarily be stable at $250MPa$.

In general, the study of the relations between mean and extreme crack spacings, for both secondary and primary cracks in flexural members as well as in the tensile members, confirms the relations stated in the existing literature, which is $S_{rmax} = 2S_{rmin}$ and $S_{rm} = 1.33S_{rmin}$. However, for the secondary cracks this only holds for spacings in the constant moment span. Moreover, the mean values of the relations S_{rmax}/S_{rmin} , S_{rm}/S_{rmin} , and S_{rm}/S_{rmax} are inconsistent with the relations in the literature but the largest amount of data has the relations dictated by the existing literature. Lastly, it should also be mentioned that the relations S_{rm}/S_{rmax} have a smaller relative deviation from the mean than S_{rm}/S_{rmin} . This indicates that the maximum crack spacing is connected to less random variation and therefore a more

solid basis for estimation of crack widths than the minimum spacing, which is also quite convenient as it is most often the maximum crack width that is sought to be determined, which is found from the maximum crack spacing.

When comparing crack spacings in tensile and flexural members a direct connection is found between the parameters that control cracking in tensile members and the secondary cracks in the flexural members, which are the cover to the reinforcement and the ϕ_s/ρ_s -ratio or $\phi_s/\rho_{s,eff}$ -ratio.

The Eurocode model suggests that there should be a difference in the formulation for the two structural members with a reduction in the coefficient on the $\phi_s/\rho_{s,eff}$ -term from tensile members to flexural members. This, however, means that a beam with the same cover and $\phi_s/\rho_{s,eff}$ -ratio as a tension bar, has a smaller crack spacing than the tension bar, which is not seen in the comparison. Instead it was concluded that, while the influence of the $\phi_s/\rho_{s,eff}$ -term should be reduced for flexural members, the influence of the cover-term should simultaneously be increased.

Analysis of experimental behaviour

Through analysis of experimental results of eight beams in four-point-bending from the literature and eight beams conducted as part of the present research project, the main assumptions of the proposed approach are confirmed. From the aforementioned tests, it is observed that the maximum crack width is located in the cracks with the largest distance to the adjacent cracks on both sides. This indicates that the crack width is related to the crack spacing. Furthermore, the height of the compression zone, which defines the crack height and is related to the crack width and the flexural stiffness, is in the proposed approach assumed to be constant with respect to both location and load level within the service load range. From observation of the tests, it was concluded that the deflection and the crack width is linearly proportional, when a stabilised crack system is reached. Hence, this indicates that the assumption of a constant compression zone is reasonable.

In addition to the fact that two different crack types only develop in structural beams, the tests conducted as part of the present research project revealed several differences with respect to how laboratory beams and structural beams behave. For one, the primary cracks are observed to propagate differently with respect to increase in load. While the cracks in the laboratory beams grew slowly towards the neutral axis with a load increase, the primary cracks in the structural beams immediately after forming, reached a height close to the final crack height without any notable load increase. This difference can possibly be described through tensile-softening where equilibrium in a cracked section can potentially be established with a lower crack height in the laboratory beams compared to the structural beams.

The tests also reveal that the crack width varies differently with respect to the beam height, which is due to the fact that secondary cracks only develop in the structural beams. In the laboratory beams there are more or less the same number of cracks in the web and at the level of the reinforcement. The largest crack width is therefore located at the outermost tensile fibres, because the largest deformation takes place there, resulting in wedge-shaped cracks. In the structural beams, there is a significantly larger number of cracks at the level of the reinforcement than in the web. From considerations of compatibility, this means that a larger crack width occurs in the web than at the level reinforcement, resulting in fish-shaped primary cracks. Even though the crack width of a single crack in the laboratory and the structural beams are very different, the sum of all cracks are observed to be wedge-shaped in both types of beams. The latter finding enhanced the understanding that all deformation can, with good approximation, be assumed to take place in the cracks.

Application of approach and comparison with tests

From the comparison of the proposed approach with the tests of beams in four-point-bending from the literature, the approach is found to estimate crack spacings within a margin of 20%, which is concluded to be reasonable in the light of the large randomness associated with cracking in concrete. Furthermore, the estimated force-deflection response agrees well with the test response. The present approach also shows itself to be just as good an estimate as the Eurocode model, which is a model that carries no apparent physical explanation to it as well as the fact that it is not related to the modelling of the other aspects of the serviceability limit state. In that sense, the proposed approach is thus a better estimate, holding a sound physical interpretation of the behaviour.

It is confirmed, by the proposed approach as well as the tests, that tension-stiffening only has a significant influence on the stiffness, and therefore also on the deflection, for beams/slabs with small reinforcement ratios. In this case, the present approach shows itself to be a slightly better estimate than the Eurocode model due to the fact that the Eurocode is very sensitive to tension-stiffening and does not necessarily take into account the occurrence of multiple unloading and reloading, which will occur in most real structures. Lastly, from comparison of the estimated force-crack width response to the test response, it is concluded that the agreement is good and that even for load levels prior to stabilisation of the crack system, the crack width estimates agreed well with the tests.

7.1 Further application and future studies

The comparison of the approach to test results is, in the current study, limited to tests of fairly small effective depths. In fact, one of the two test series is from the group characterised as beams for laboratory use only, with $d = 167mm$, while the other test series is just on the limit of the requirement for structural beams with $d = 300mm$. The main reason for this limitation is the lack of tests in the literature of members with larger effective depths, where the main focus of the experimental work is to thoroughly measure deflections and crack widths prior to yielding of the reinforcement. Even though the literature holds a significant number of tests of larger beams, the behaviour in the serviceability limit state has not been reported to a satisfying extent. This is a very important issue for future research and it is therefore recommended that more tests are carried out where the main focus is monitoring and measuring the behaviour in the serviceability limit state with respect to crack pattern, crack spacings, crack widths and deflections.

The issue of a lack of test results stated above, is also the main reason why the proposed approach is not validated against tests for estimation of crack widths at other locations in the beam than at maximum moment even though the procedure is described in the current thesis. Further work and additional testing is therefore required to investigate whether the approach also applies for estimating crack widths in arbitrary locations of beams.

The comparison of the approach to tests is also limited to members subjected to first time loading as well as short-term loads. The effects of sustained loading and multiple reloading are thus not considered. However, it is believed that creep and shrinkage are long-term effects that can be included in the proposed approach by alteration of the modulus of elasticity to match the long-term properties of the material affected by creep as well as adding a contribution to the instantaneous deflection and crack width from the shrinkage effects. Furthermore, it should be evaluated whether the bond stresses will be reduced over time due to relaxation. The general physical behaviour of flexural members in the serviceability with respect to cracking and stiffness, which is described by the approach, is therefore assumed to be the same when adding the effects of creep and shrinkage. This assumption has not been validated against test results due to the limitations of the current research. However, it is regarded as being of importance for further development of the approach. Nevertheless, only a few tests exist of members that have been subjected to sustained loading while both deflections and crack widths have been monitored thoroughly.

In the present research, the hypothesis established in the Introduction was limited to application on flexural members. However, some potential is seen for using the same fundamental assumptions for modelling other aspects of the behaviour of reinforced concrete structures. For further application, it should be investigated whether the same assumptions could be implemented in the development of an approach for evaluation of torsional resistance of cracked reinforced concrete beams. Furthermore, other aspects of the ultimate limit state also require knowledge of the crack widths as well as the crack location, among other things; assessment of the shear capacity of members without transverse reinforcement or rotational capacity of plastic hinges.

Another issue that has not been subject to much research is the presence and the extension of the debonded length. The main reason for the lack of experimental evidence of the phenomenon is probably that such tests are not straightforward to perform. Several tests in the literature confirm that a debonded zone exists, which was presented in the literature review, although no experimental work was found of establishment of the actual length of debonding. The researchers proposing an approach to estimate L_{deb} have only validated their model describing the crack spacing where the debonded length is included, but L_{deb} is not validated alone, namely due to the lack of experimental measurements of the length. The experimental

procedure for retrieving results of L_{deb} requires that internal cracking can be monitored either during loading or after loading. Furthermore, due to the very small width of the conical cracks, causing debonding, it might be difficult to observe them without the use of microscopes or digital image correlation equipment. Future studies could conduct investigations into how the presence and actual length of the debonded zone could be experimentally quantified.

The database of measurement for crack spacings established in the current research has been shown to be a useful tool to investigate a parameter associated with a fairly large level of randomness. It is therefore found relevant to establish a database of measured crack widths to be able to gain even more knowledge concerning the variation of crack widths in connection to the crack spacing. However, for the time being, there are several complications related to the establishment of such a database. The crack width cannot be measured from photos of test members in the same manner as the crack spacing. The existence of a database of crack widths therefore relies on the fact that crack widths are measured thoroughly and stated in the experimental reports, or, even better, that a digital image correlation tool has been used throughout the whole load history. Currently, this is only the case for a very limited amount of tests in the existing literature.

REFERENCES

- [1] Kenel A, Marti P. Faseroptische Dehnungsmessungen an einbetonierten Bewehrungsstäben. vol. 271. vdf Hochschulverlag AG; 2002.
- [2] Gilbert RI, Nejadi S. An experimental study of flexural cracking in reinforced concrete members under short term loads. School of Civil and Environmental Engineering, University of New South Wales, Australia; 2004.
- [3] Van Mier JG. Fracture processes of concrete. vol. 12. CRC press; 1996.
- [4] Neville AM. Properties of concrete. Pearson Education India; 1963.
- [5] Hsu TT, Slate FO, Sturman GM, Winter G. Microcracking of plain concrete and the shape of the stress-strain curve. *ACI Journal Proceedings*. 1963;60(2):209–224.
- [6] Hordijk DA. Tensile and tensile fatigue behaviour of concrete; experiments, modelling and analyses. *Heron*. 1992;37(1).
- [7] Nielsen MP. Beton 1-del 1, 2. udgave. Technical University of Denmark, Lyngby; 2005.
- [8] Cornelissen H, Hordijk D, Reinhardt H. Experimental determination of crack softening characteristics of normalweight and lightweight concrete. *Heron*. 1986;31(2).
- [9] Hillerborg A, Modéer M, Petersson PE. Analysis of crack formation and crack growth in concrete by means of fracture mechanics and finite elements. *Cement and Concrete Research*. 1976;6(6):773–781.
- [10] EN 1992-1-1. Eurocode 2: Design of concrete structures: Part 1-1: General rules and rules for buildings. CEN European Committee for Standardization. Brussels, Belgium; 2004.
- [11] fib Model Code for Concrete Structures 2010, Fédération Internationale du Béton (fib). Ernst & Sohn; 2013.
- [12] Broms BB, Lutz LA. Effects of arrangement of reinforcement on crack width and spacing of reinforced concrete members. *ACI Journal Proceedings*. 1965;62(11):1395–1410.
- [13] Illston J, Stevens R. Internal Cracking. *Concrete (London)*. 1972;6(7):28–31.
- [14] Leonhardt F. Crack control in concrete structures. *IABSE Surveys*. 1977;S-4.
- [15] Goto Y. Cracks formed in concrete around deformed tension bars. *ACI Journal Proceedings*. 1971;68(4):244–251.
- [16] Masukawa J. Degradation of shear performance of beams due to bond deterioration and longitudinal bar cutoffs. University of Toronto, Canada; 2012.
- [17] Scott R, Gill P. Techniques in experimental stress analysis for reinforced concrete structures. In: *Experimental Stress Analysis*. Springer; 1986. p. 87–96.
- [18] Fellmann W, Menn C. Zugversuche an Stahlbetonscheiben. Birkhäuser Verlag, ETH Zürich; 1981.
- [19] Scott R, Gill P. Short-term distributions of strain and bond stress along tension reinforcement. *The Structural Engineer*. 1987;65(2):39–43.

-
- [20] Kankam CK. Relationship of bond stress, steel stress, and slip in reinforced concrete. *Journal of Structural Engineering*. 1997;123(1):79–85.
- [21] Forth JP, Beeby AW. Study of composite behavior of reinforcement and concrete in tension. *ACI Structural Journal*. 2014;111(2):397–406.
- [22] Tammo K, Thelandersson S. Crack behavior near reinforcing bars in concrete structures. *ACI Structural Journal*. 2009;106(3):259–267.
- [23] Borosnyói A, Snóbli I. Crack width variation within the concrete cover of reinforced concrete members. *Építőanyag*. 2010;62(3):70–74.
- [24] Yannopoulos P. Variation of concrete crack widths through the concrete cover to reinforcement. *Magazine of Concrete Research*. 1989;41(147):63–68.
- [25] Saliger R. High grade steel in reinforced concrete. In: *Preliminary Publication, 2nd Congress of IABSE*. Berlin-Munich: IABSE Publications; 1936. p. 293–315.
- [26] Watstein D, Parsons D. Width and spacing of tensile cracks in axially reinforced concrete cylinders. *Journal of Research*. 1943;31:1–24.
- [27] Broms BB. Crack width and crack spacing in reinforced concrete members. *ACI Journal Proceedings*. 1965;62(11):1237–1256.
- [28] Beeby AW. *The prediction of cracking in reinforced concrete members*. University of London, United Kingdom; 1971.
- [29] Marti P, Alvarez M, Kaufmann W, Sigrist V. Tension chord model for structural concrete. *Structural Engineering International*. 1998;8(4):287–298.
- [30] Olsen DH, Nielsen MP. Ny teori til bestemmelse af revneafstande og revnevidder i betonkonstruktioner. Department of structural Engineering, Technical University of Denmark, Technical Report. 1990;R-254.
- [31] Ruiz MF, Muttoni A, Gambarova P. Analytical modeling of the pre-and postyield behavior of bond in reinforced concrete. *Journal of Structural Engineering*. 2007;133(10):1364–1372.
- [32] Shima H, Chou LL, Okamura H. Micro and macro models for bond in reinforced concrete. *Journal of the Faculty of Engineering*. 1987;39(2):133–194.
- [33] Gambarova P, Plizzari G, Balazs G, Cairns J, et al. Bond of reinforcement in concrete. *fib Bulletin*. 2000;10:1–98.
- [34] Ciampi V, Eligehausen R, Bertero VV, Popov EP. Analytical model for deformed bar bond under generalized excitations. In: *Proceedings of the IABSE Colloquium on Advanced Mechanics of Reinforced concrete*; 1981. p. 53–67.
- [35] Kaklauskas G, Ramanauskas R, Jakubovskis R. Mean crack spacing modelling for RC tension elements. *Engineering Structures*. 2017;150:843–851.
- [36] de Saint-Venant M. *Mémoire sur la torsion des prismes: avec des considérations sur leur flexion ainsi que sur l'équilibre intérieur des solides élastiques en général: et des formules pratiques pour le calcul de leur résistance à divers efforts s'exerçant simultanément*. Imprimerie nationale; 1856.
- [37] Park R, Paulay T. *Reinforced concrete structures*. John Wiley & Sons; 1975.

REFERENCES

- [38] Tan R, Hendriks MA, Kanstad T. Evaluation of Current Crack Width Calculation Methods According to Eurocode 2 and fib Model Code 2010. In: High Tech Concrete: Where Technology and Engineering Meet. Springer; 2018. p. 1610–1618.
- [39] Base GD, Read JB, Beeby A, Taylor H. An investigation of the crack control characteristics of various types of bar in reinforced concrete beams. Cement and Concrete Association, Research Report 18; 1966.
- [40] Broms BB. Stress distribution in reinforced concrete members with tension cracks. ACI Journal Proceedings. 1965;62(9):1095–1108.
- [41] Beeby A, Scott R. Cracking and deformation of axially reinforced members subjected to pure tension. Magazine of Concrete Research. 2005;57(10):611–621.
- [42] Beeby AW. The influence of the parameter ϕ/ρ_{eff} on crack widths. Structural Concrete. 2004;5(2):71–83.
- [43] Jokela J. Dimensioning of strain or deformation-controlled reinforced concrete beams. Espoo, Publications 33, Technical Research Centre of Finland; 1986.
- [44] Nielsen MP. Beton 1-del 3, 2. udgave. Technical University of Denmark, Lyngby; 2005.
- [45] Bigaj AJ. Structural dependence of rotations capacity of plastic hinges in RC beams and slabs. TU Delft, Delft University of Technology, The Netherlands; 1999.
- [46] Borges JF. Cracking and deformability of reinforced concrete beams. Laboratório Nacional de Engenharia Civil; 1965.
- [47] Base G. Bond, and control of cracking in reinforced concrete. In: Proceedings, International Conference on Bond in Concrete, London; 1982. p. 331–341.
- [48] Rasmussen AB, Fisker J, Hagsten LG. Cracking in flexural reinforced concrete members. Procedia Engineering. 2017;172:922–929.
- [49] Sherwood EG. One-way shear behaviour of large, lightly-reinforced concrete beams and slabs. Department of Civil Engineering, University of Toronto, Canada; 2008.
- [50] Jin-Keun K, Yon-Dong P. Shear strength of reinforced high strength concrete beam without web reinforcement. Magazine of Concrete Research. 1994;46(166):7–16.
- [51] Kani G. How safe are our large reinforced concrete beams? ACI Journal Proceedings. 1967;64(3):128–141.
- [52] Taylor HP. Shear strength of large beams. Journal of the Structural Division. 1972;98(Proc. Paper 9329):2473–2490.
- [53] Braam CR. Control of crack width in deep reinforced concrete beams. Heron. 1990;35(4).
- [54] Cavagnis F, Ruiz MF, Muttoni A. Shear failures in reinforced concrete members without transverse reinforcement: An analysis of the critical shear crack development on the basis of test results. Engineering Structures. 2015;103:157–173.
- [55] Feddersen B, Nielsen MP. Revneteorier for enaksede spaendingstilstande. Department of structural Engineering, Technical University of Denmark, Technical Report. 1983;R-163.

-
- [56] Leonhardt F, Walther R. The Stuttgart shear tests. Cement and Concrete Association Library. 1961;111:49–54.
- [57] Attisha HP, et al. High tensile steel as normal reinforcement in concrete. University of Salford, United Kingdom; 1972.
- [58] Pérez AC, Peiretti HC, Iribarren JP, Soto AG. Cracking of RC members revisited: influence of cover, $\phi/\rho_{s,ef}$ and stirrup spacing—an experimental and theoretical study. Structural Concrete. 2013;14(1):69–78.
- [59] Beeby A. An Investigation of Cracking in Slabs Spanning One Way. Cement and Concrete Association. Technical Report No. TRA 433, London; 1970.
- [60] Kaklauskas G, Ramanauskas R. A new approach in predicting the mean crack spacing of flexural reinforced concrete elements. In: fib Symposium. Performance-based approaches for concrete structures, Cape Town, South Africa; 2016. .
- [61] Frantz GC, Breen JE. Control of cracking on the side faces of large reinforced concrete beams. Center for highway research, University of Texas, Austin. No. 198-1F; 1978.
- [62] Beeby A. An investigation of cracking on the side faces of beams. Cement and Concrete Association; 1971.
- [63] Pedersen JG, Eriksen JO. Behaviour of shear-critical reinforced concrete beams without transverse reinforcement: Experimental report. Master Thesis, Department of Engineering, Aarhus University, Denmark; 2014.
- [64] Borosnyói A, Balázs G. Models for flexural cracking in concrete: the state of the art. Structural Concrete. 2005;6(2):53–62.
- [65] Burns C. Serviceability analysis of reinforced concrete based in the tension chord model. ETH Zurich; 2011.
- [66] Reineck KH. Ein mechanisches Modell für den Querkraftbereich von Stahlbetonbauteilen. Universität Stuttgart, Institut für Tragwerksentwurf und-konstruktion; 1990.
- [67] Frosch RJ. Modeling and control of side face beam cracking. ACI Structural Journal. 2002;99(3):376–385.
- [68] Hamadi YD. Force transfer across cracks in concrete structures. University of Central London Westminster, United Kingdom; 1976.
- [69] Rasmussen AB. Progress report, Modelling of reinforced concrete in the serviceability limit state. Department of Engineering, Aarhus University, Denmark; 2016.
- [70] Gilbert R. Revisiting the tension stiffening effect in reinforced concrete slabs. Australian Journal of Structural Engineering. 2008;8(3):189–196.
- [71] Rasmussen AB, Hagsten LG. Investigation of reinforced concrete beams in serviceability limit state. In: The 11th fib International PhD Symposium in Civil Engineering. Federation internationale du beton (fib); 2016. p. 157–164.
- [72] Bischoff PH. Rational model for calculating deflection of reinforced concrete beams and slabs. Canadian Journal of Civil Engineering. 2007;34(8):992–1002.

REFERENCES

- [73] Gilbert R. The serviceability limit states in reinforced concrete design. *Procedia Engineering*. 2011;14:385–395.
- [74] Gilbert RI. Closure to “Tension Stiffening in Lightly Reinforced Concrete Slabs” by R. Ian Gilbert. *Journal of Structural Engineering*. 2008;134(7):1264–1265.
- [75] Christiansen M. Serviceability limit state analysis of reinforced concrete. Report No. R-69, Technical University of Denmark, Lyngby, Denmark; 2000.
- [76] Timoshenko S, Goodier J. *Theory of Elasticity*. Third Edition, McGraw-Hill; 1970.
- [77] Rasmussen AB, Sørensen BW, Skov M, Rasmussen PK, Hagsten LG. An experimental study of crack development in flexural reinforced concrete members. In: *IABSE Symposium Report*. vol. 109, No. 11. International Association for Bridge and Structural Engineering; 2017. p. 3092–3099.
- [78] D’Agostino RB. *Goodness-of-fit-techniques*. vol. 68. CRC press; 1986.
- [79] D’agostino RB, Belanger A, D’Agostino Jr RB. A suggestion for using powerful and informative tests of normality. *The American Statistician*. 1990;44(4):316–321.
- [80] Ross SM. *Introduction to probability and statistics for engineers and scientists*. Academic Press; 2014.
- [81] Thangaratnam N, Østrup TM. *Cracking in Reinforced Tension Bars*, Experimental report. Bachelor Thesis, Department of Engineering, Aarhus University, Denmark; 2018.
- [82] Rimkus A, Gribniak V. Experimental investigation of cracking and deformations of concrete ties reinforced with multiple bars. *Construction and Building Materials*. 2017;148:49–61.
- [83] Baah P. *Cracking behavior of structural slab bridge decks*. University of Akron, Ohio; 2014.
- [84] Kharal Z. *Tension Stiffening and Cracking Behaviour of GFRP Reinforced Concrete*. University of Toronto, Canada; 2014.
- [85] Wenkenbach I. *Tension stiffening in reinforced concrete members with large diameter reinforcement*. Durham University, United Kingdom; 2011.
- [86] Wu H, Gilbert R. An experimental study of tension stiffening in reinforced concrete members under short-term and long-term loads. The University of New South Wales, UNICIV Report no R-449; 2008.
- [87] Bischoff PH. Tension stiffening and cracking of steel fiber-reinforced concrete. *Journal of Materials in Civil Engineering*. 2003;15(2):174–182.
- [88] Arduini M, Russo SI. *Bond in RC Members Ties with Composite and Stainless Steel Bars*. Report of RILEM. 2001;TC 147-FMB.
- [89] Biagj A, Uijl J. *Cracking behaviour of RC tensile members simulated with confinement based bond model*. Report of RILEM. 2001;TC 147-FMB.
- [90] Eligehausen R, Bigaj A, Mayer U, Sanchez FJ. *Report of RILEM TC 147-FMB: Round-Robin Analysis and Test on Bond*. Report of RILEM. 2001;TC 147-FMB.
- [91] Hikosaka H, Liu Y, Saito S. *Round-Robin Analysis on Bond*. Report of RILEM. 2001;TC 147-FMB.
- [92] Al-Fayadh S. *Cracking behaviour of reinforced concrete tensile members*. Chalmers University of Technology, Sweden; 1997.

-
- [93] Lorrain M, Maurel O, Seffo M. Cracking behavior of reinforced high-strength concrete tension ties. *ACI Structural Journal*. 1998;95(5):626–635.
- [94] Farra B, Jaccoud JP. Influence du béton et de l'armature sur la fissuration des structures en béton: rapport des essais de tirants sous déformation imposée de courte durée. *École Polytechnique Fédérale de Lusianne*, No. 185152.; 1994.
- [95] van der Veen C. Cryogenic bond stress-slip relationship. TU Delft, Civil Engineering and Geosciences, The Netherlands; 1992.
- [96] Belbachir A, Alam SY, Matallah M, Loukili A. Size Effect on Behaviour of Critical Shear Crack in Reinforced Concrete Beam Using Digital Image Correlation. 9th International Conference on Fracture Mechanics of Concrete and Concrete Structures. 2016;FraMCos-9.
- [97] Gribniak V, Caldentey AP, Kaklauskas G, Rimkus A, Sokolov A. Effect of arrangement of tensile reinforcement on flexural stiffness and cracking. *Engineering Structures*. 2016;124:418–428.
- [98] Høegh R, Jørgensen L. Formation of Cracks in Reinforced Concrete Beams Subjected to Bending Moment - Experimental Report. Bachelor Thesis, Department of Engineering, Aarhus University, Denmark; 2016.
- [99] Daluga DR. The Effect of Maximum Aggregate Size on the Shear Strength of Geometrically Scaled Reinforced Concrete Beams. Purdue University, Indiana; 2015.
- [100] Mohammadyan-Yasouj S, Marsono A, Abdullah R, Moghadasi M. Wide Beam Shear Behavior with Diverse Types of Reinforcement. *ACI Structural Journal*. 2015;112(2):199–208.
- [101] Campana S, Ruiz MF, Muttoni A. Shear strength of arch-shaped members without transverse reinforcement. *ACI Structural Journal*. 2014;111(3):573–582.
- [102] Korol E, Tejchman-Konarzewski A. Experimental and numerical investigations of size effects in reinforced concrete beams with steel or basalt bars. 8th International Conference on Fracture Mechanics of Concrete and Concrete Structures. 2013;FraMCos-8.
- [103] Mihaylov BI, Bentz EC, Collins MP. Behavior of Deep Beams with Large Headed Bars. *ACI Structural Journal*. 2013;110(6):1013–1021.
- [104] Møller KH, Rasmussen AK. Experimental Report - Shear in Reinforced Concrete Members without Transverse Reinforcement. Master Thesis, Department of Engineering, Aarhus University, Denmark; 2013.
- [105] Perera S, Mutsuyoshi H. Shear capacity of reinforced high-strength concrete beams without web reinforcement. In: *Proceedings of the Thirteenth East Asia-Pacific Conference on Structural Engineering and Construction (EASEC-13)*; 2013. p. B–6.
- [106] Yu L, Che Y, Song Y. Shear Behavior of Large Reinforced Concrete Beams without Web Reinforcement. *Advances in Structural Engineering*. 2013;16(4):653–665.
- [107] McCain KA. The effect of scale on the resistance of reinforced concrete beams to shear. Purdue University, Indiana; 2012.
- [108] Słowik M, Nowicki T. The analysis of diagonal crack propagation in concrete beams. *Computational Materials Science*. 2012;52(1):261–267.
-

REFERENCES

- [109] Słowik M, Smarzewski P. Study of the scale effect on diagonal crack propagation in concrete beams. *Computational Materials Science*. 2012;64:216–220.
- [110] Birgisson SR. Shear resistance of reinforced concrete beams without stirrups. School of Science and Engineering, Reykjavik; 2011.
- [111] Gedik YH. Experimental and numerical study on shear failure mechanism of RC deep beams. Nagoya University, Japan; 2011.
- [112] Nghiep VH. Shear design of straight and haunched concrete beams without stirrups. Technische Universität Hamburg, Germany; 2011.
- [113] Sagaseta J, Vollum R. Influence of beam cross-section, loading arrangement and aggregate type on shear strength. *Magazine of Concrete Research*. 2011;63(2):139–155.
- [114] Thamrin R, Samad AA, YE CD, Hamid NA. Experimental study on diagonal shear cracks of concrete beams without stirrups longitudinally reinforced with GFRP bars. In: *Proceedings of fib Symposium, Prague*. Federation internationale du beton (fib); 2011. .
- [115] Mihaylov BI, Bentz EC, Collins MP. Behavior of Large Deep Beams Subjected to Monotonic and Reversed Cyclic Shear. *ACI Structural Journal*. 2010;107(6):726–734.
- [116] Murray MR. An investigation of the unit shear strength of geometrically scaled reinforced concrete beams. Purdue University, Indiana; 2010.
- [117] Anastasi A. Essais d'effort tranchant sur poutres en béton armé sans ou avec une faible armature transversale - Rapport technique. Master Thesis, École Polytechnique Fédérale de Lausanne (EPFL); 2009.
- [118] Hassan A, Hossain K, Lachemi M. Behavior of full-scale self-consolidating concrete beams in shear. *Cement and Concrete Composites*. 2008;30(7):588–596.
- [119] Hassan TK, Seliem HM, Dwairi H, Rizkalla SH, Zia P. Shear behavior of large concrete beams reinforced with high-strength steel. *ACI Structural Journal*. 2008;105(2):173–179.
- [120] Sneed LH. Influence of member depth on the shear strength of concrete beams. Purdue University, Indiana; 2007.
- [121] Zhang N, Tan KH. Size effect in RC deep beams: Experimental investigation and STM verification. *Engineering Structures*. 2007;29(12):3241–3254.
- [122] Guadagnini M, Pilakoutas K, Waldron P. Shear resistance of FRP RC beams: Experimental study. *Journal of Composites for Construction*. 2006;10(6):464–473.
- [123] Lubell AS. Shear in wide reinforced concrete members. Department of Civil Engineering, University of Toronto, Canada; 2006.
- [124] Bentz EC, Buckley S. Repeating a classic set of experiments on size effect in shear of members without stirrups. *ACI structural journal*. 2005;102(6):832–838.
- [125] Tan K, Cheng G, Cheong H. Size effect in shear strength of large beams—Behaviour and finite element modelling. *Magazine of Concrete Research*. 2005;57(8):497–509.
- [126] Minelli F. Plain and Fiber Reinforced Concrete Beams under Shear Loading: Structural Behavior and Design Applications. University of Brescia, Italy; 2005.

-
- [127] Vecchio F, Shim W. Experimental and analytical reexamination of classic concrete beam tests. *Journal of Structural Engineering*. 2004;130(3):460–469.
- [128] Yang KH, Chung HS, Lee ET, Eun HC. Shear characteristics of high-strength concrete deep beams without shear reinforcements. *Engineering structures*. 2003;25(10):1343–1352.
- [129] Hibino K, Kojima T, Takagi N. FEM study on the shear behavior of RC beam by the use of discrete model. In: *Finite Elements in Civil Engineering Applications: Proceedings of the Third Diana World Conference, Tokyo, Japan, 9-11 October 2002*. CRC Press; 2002. .
- [130] Kwak YK, Eberhard MO, Kim WS, Kim J. Shear strength of steel fiber-reinforced concrete beams without stirrups. *ACI Structural Journal*. 2002;99(4):530–538.
- [131] Tompos EJ, Frosch RJ. Influence of beam size, longitudinal reinforcement, and stirrup effectiveness on concrete shear strength. *ACI Structural Journal*. 2002;99(5):559–567.
- [132] Cao S. Size effect and the influence of longitudinal reinforcement on the shear response of large reinforced concrete members. University of Toronto, Canada; 2001.
- [133] Oh JK, Shin SW. Shear strength of reinforced high-strength concrete deep beams. *ACI Structural Journal*. 2001;98(2):164–173.
- [134] Tureyen AK. Influence of longitudinal reinforcement type on the shear strength of reinforced concrete beams without transverse reinforcement. Purdue University, Indiana; 2001.
- [135] Yoshida Y. Shear reinforcement for large lightly reinforced concrete members. Master Thesis, Department of Civil Engineering, University of Toronto, Canada. 2000;.
- [136] Angelakos D. The influence of concrete strength and longitudinal reinforcement ratio on the shear strength of large-size reinforced concrete beams with, and without, transverse reinforcement. Department of Civil Engineering, University of Toronto, Canada; 1999.
- [137] Tan K, Lu H. Shear behavior of large reinforced concrete deep beams and code comparisons. *ACI Structural Journal*. 1999;96(5):836–846.
- [138] Kulkarni SM, Shah SP. Response of reinforced concrete beams at high strain rates. *ACI Structural Journal*. 1998;95(6):705–715.
- [139] Podgorniak-Stanik BA. The influence of concrete strength, distribution of longitudinal reinforcement, amount of transverse reinforcement and member size on shear strength of reinforced concrete members. Master Thesis, Department of Civil Engineering, University of Toronto, Canada; 1998.
- [140] Yoon YS, Cook WD, Mitchell D. Minimum shear reinforcement in normal, medium, and high-strength concrete beams. *ACI Structural Journal*. 1996;93(5):576–584.
- [141] Abrishami HH. Studies on bond and cracking of structural concrete. Department of Civil Engineering and Applied Mechanics, McGill University Libraries, Montreal, Canada; 1994.
- [142] Khorasgany MG. Size effect in the shear failure of normal and high strength reinforced concrete beams. University of Missouri, Columbia; 1994.
- [143] Walravena J, Lehwalter N. Size effects in short beams loaded in shear. *ACI Structural Journal*. 1994;91(5):585–593.
- [144] Johnson MK, Ramirez JA. Minimum shear reinforcement in beams with higher strength concrete. *ACI Structural Journal*. 1989;86(4):376–382.
-

REFERENCES

- [145] Kim W. Shear-critical cracks in reinforced concrete beams without web reinforcement: their initiation and propagation. Cornell University, United Kingdom; 1987.
- [146] Niwa J, Yamada K, Yokozawa K, Okamura H. Revaluation of the equation for shear strength of reinforced concrete beams without web reinforcement (Translation from Proceedings of JSCE No. 372/V-5 1986-8). Concrete library of JSCE. 1987;9:65–84.
- [147] Iguro M, Shioya T, Nojiri Y, Akiyama H. Experimental studies on shear strength of large reinforced concrete beams under uniformly distributed load (Translation from Proceedings of JSCE No. 345/V-1 1984). Concrete Library of JSCE. 1985;5:137.
- [148] Mphonde AG. Shear strength of high strength concrete beams. The University of Connecticut; 1984.
- [149] Smith K, Vantsiotis A. Shear strength of deep beams. ACI Journal Proceedings. 1982;79(3):201–213.
- [150] Cederwall K, Hedman O, Loeberg A. Shear strength of partially prestressed beams with pretensioned reinforcement of high grade deformed bars. ACI Special Publication. 1974;42:215–230.
- [151] Manuel RF, Slight BW, Suter GT. Deep beam behavior affected by length and shear span variations. ACI Journal Proceedings. 1971;68(12):954–958.
- [152] Bhal NS. Über den Einfluss der Balkenhöhe auf die Schubtragfähigkeit von einfeldrigen Stahlbetonbalken mit und ohne Schubbewehrung. Otto-Graf-Institut, Amtliche Forschungs- und Materialprüfungsanstalt für das Bauwesen, Universität Stuttgart, Schriftenreihe Heft Nr. 35; 1968.
- [153] Taylor HP. Shear stresses in reinforced concrete beams without shear reinforcement. Cement and Concrete Association, Technical Report No. TRA 407, London; 1968.
- [154] Kani G. Basic facts concerning shear failure. ACI Journal Proceedings. 1966;63(6):675–692.
- [155] Kani G. The riddle of shear failure and its solution. ACI Journal Proceedings. 1964;61(4):441–468.
- [156] Bresler B, Scordelis AC. Shear strength of reinforced concrete beams. ACI Journal Proceedings. 1963;60(1):51–74.
- [157] Taylor R, Brewer R. The effect of the type of aggregate on the diagonal cracking of reinforced concrete beams. Magazine of Concrete Research. 1963;15(44):87–92.
- [158] Leonhardt F, Walther R. Schubversuche an einfeldrigen Stahlbetonbalken mit und ohne Schubbewehrung zur Ermittlung der Schubtragfähigkeit und der oberen Schubspannungsgrenze. Ernst; 1962.
- [159] Taylor R. Some shear tests on reinforced concrete beams without shear reinforcement. Magazine of Concrete Research. 1960;12(36):145–154.
- [160] Rasmussen PK, Skov M, Sørensen BW. Flexural cracks in reinforced concrete beams. Master Thesis, Department of Engineering, Aarhus University, Denmark; 2017.
- [161] Rasmussen AB. Analytical and numerical modelling of reinforced concrete in serviceability limit state. Master Thesis, Department of Engineering, Aarhus University, Denmark; 2012.
- [162] Fisker J, Hagsten LG. Mechanical model for the shear capacity of R/C beams without stirrups: A proposal based on limit analysis. Engineering Structures. 2016;115:220–231.
- [163] Alvarez M, Koppel S, Marti P. Rotation capacity of reinforced concrete slabs. Structural Journal. 2000;97(2):235–242.

Appendices

A NOTATIONS

Notations

Greek charaters

α	Ratio of Young's modulus for reinforcement to concrete $\frac{E_s}{E_c}$ / Deformation parameter in Eurocode model
α_I	Deformation parameter for uncracked state
α_{II}	Deformation parameter for cracked state
β	Coefficient of the neutral axis from $\frac{x_{cr}}{d}$ / Influence of the duration of loading in Eurocode model
δ	Slip between reinforcement and concrete
ϵ_c	Concrete strain
ϵ_s	Reinforcement strain
ϵ_{bu}	Bond ultimate strain
ϵ_{sc}	Reinforcement strain in a crack
ϵ_{smin}	Minimum strain in the reinforcement between two cracks
ϵ_{sm}	Mean strain in the reinforcement
ϵ_y	Yield strain of the reinforcement
η	Secondary rate of variation in the reinforcement strain
γ	Inclination of a crack
κ	Curvature
λ	Ratio of mean crack spacing to minimum crack spacing
μ	Mean value
ϕ_s	Diameter of reinforcement bar
$\rho_{s,effSYM}$	Effective reinforcement ratio with an effective concrete area placed symmetrically around the reinforcement
$\rho_{s,eff}$	Effective reinforcement ratio from $\frac{A_s}{A_{c,eff}}$
$\rho_{s,min}$	Minimum reinforcement ratio
ρ_s	Reinforcement ratio from $\frac{A_s}{A_c}$
σ	Stress / Standard deviation
σ_c	Concrete stress
σ_s	Reinforcement stress
$\sigma_{s,cr,TC}$	Stress in reinforcement in fictitious tension bar

NOTATIONS

$\sigma_{s,cr}$	Stress in reinforcement in elastic cracked cross-section
$\sigma_{s,r}$	Stress in the reinforcement at forming of a crack
σ_{sPic}	Stress in the reinforcement at measurements of crack spacings
τ_b	Bond stress
ξ	Principal rate of variation in the reinforcement strain
ζ	Distribution coefficient for tension-stiffening in Eurocode model

Latin charaters

a	Height of reinforcement ribs / Length of shear span
A_c	Concrete area
A_s	Area of reinforcement
a_v	Vertical distance between layers of reinforcement
$A_{c,eff}$	Effective concrete area around tensile reinforcement in a beam
b	Width
b_2	Descriptive statistics of kurtosis
c	cover
c_v	Coefficient of variation (relative deviation)
c_{hor}	Horizontal concrete cover
c_{max}	Maximum concrete cover
C_{rein}	Circumference of a reinforcement bar
c_{ver}	Vertical concrete cover
d	Effective depth
d^*	Smallest distance to the reinforcement in Frosch's model
d_{max}	Maximum aggregate size
E_c	Young's modulus of concrete
E_s	Young's modulus of reinforcement
E_h	Hardening modulus of the reinforcement from Fernandez's Root Mean Square model
EI	Flexural stiffness
$EI_{cr,ef,coarse}$	Flexural stiffness with coarse assumption for including tension-stiffening
$EI_{cr,ef,fine}$	Flexural stiffness with fine assumption for including tension-stiffening
$EI_{cr,ef}$	Flexural stiffness including the effect of tension-stiffening
EI_{cr}	Flexural stiffness of fully cracked member

EI_{EC2}	Flexural stiffness with the use of the Eurocode model
EI_{uncr}	Flexural stiffness of an uncracked cross-section
f_c	Compressive strength of concrete
$f_{c,cyl}$	Measured cylinder compressive strength of concrete
f_{ct}	Tensile strength of concrete
f_{tb}	Flexural tensile strength of concrete
f_{ts}	Spitting tensile strength of concrete
g, k	Arbitrary constants
G_c	Crack energy
h	Height
h_r	Crack height
$h_{c,ef}$	Effective height of the concrete
I_{cr}	Second moment of area for a cracked cross-section
I_{uncr}	Second moment of area for an uncracked cross-section
k_0	Constant term in multi-variable regression model
k_n	Coefficients of independent variables in multi-variable linear regression model
k_t	Tension-stiffening coefficient
L	Length of tensile or flexural member
l_p	Length of plastic zone
L_{deb}	Debonded length
M	Bending moment
M_y	Moment at theoretical yielding of the reinforcement
M_{cr}	Cracking moment
M_{max}	Maximum moment in beam
M_{Pic}	Moment that provoked the measured crack spacing
M_y	Theoretical moment at yielding of the reinforcement
n_s	Number of reinforcement bars
n_{cr}	Total number of cracks in a member
P	Point load
P_y	Point load at theoretical yielding of the reinforcement
Q	Point load

NOTATIONS

Q_y	Point load at theoretical yielding of the reinforcement
Q_{cr}	Point load at first cracking in a beam
r	Correlation coefficient
$s(h)$	Factor accounting for the size effect of f_{tb}
S_0	Transfer length
S_r	Crack spacing
$S_{r,fl}$	Spacing of primary cracks
$S_{r,sec}$	Spacing of secondary cracks
$S_{rm,model}$	Mean crack spacing estimated from model
$S_{rm,test}$	Measured mean crack spacing from test
S_{rmax}	Maximum crack spacing
S_{rmin}	Minimum crack spacing
S_{rm}	Mean crack spacing
U	Elastic energy
u	Deflection of flexural member
u_{model}	Deflection estimated by model
u_{test}	Deflection measured in test
w	Crack width
w_0	Crack width limit for tensile-softening
$w_{fl,d}$	Crack width of primary crack at the level of the reinforcement
$w_{fl,w}$	Crack width of primary crack in the web
w_{max}	Maximum crack width
w_m	Mean crack width
$w_{sec,d}$	Crack width of secondary crack at the level of the reinforcement
W_{unscr}	Moment of resistance of uncracked reinforced concrete cross-section
x	Location in tensile or flexural member
X_i	Redundant in statically indeterminate beam
x_n	Independent variables of multi-variable linear regression model
x_{cr}	Height of compression zone in a cracked elastic cross-section
x_{unscr}	Height of compression zone in an uncracked cross-section

Abbreviations and other symbols

\bar{x}	Mean value of sample x_i
$\sqrt{b_1}$	Descriptive statistics of skewness
$\sum w$	Sum of all crack widths in a member
a/d	Slenderness ratio of beam
$adjR^2$	The R^2 adjusted for the number of independent variables
K^2	Test statistics of the D'Agostino & Pearson Test
<i>N.A.</i>	Neutral axis
<i>no.</i>	Number of observations in a data sample
R^2	The ratio of the variance of a dependent variable which is described by the regression model
<i>RMSE</i>	Root mean square error
<i>SSE</i>	Sum of squared errors
<i>TSS</i>	Total sum of squares
EC2	The Eurocode model
LEO	Leonhardt's model for the effective concrete area
MC2010	The model from the fib Model Code 2010
SLS	Serviceability limit state
TCM	The Tension Chord model
ULS	Ultimate limit state